

UNIVERSITÄT
BAYREUTH



Reusable Earth-Abundant Metal Catalysts for Selective Organic Syntheses

Dissertation

zur Erlangung des akademischen Grades
eines Doktors der Naturwissenschaften (Dr. rer. nat.)
im Fach Chemie der Fakultät Biologie, Chemie und Geowissenschaften
der Universität Bayreuth

vorgelegt von

M. Sc. Tobias Schwob

geboren in Aschaffenburg

Bayreuth, 2019

Die vorliegende Arbeit wurde in der Zeit von Januar 2016 bis März 2019 in Bayreuth am Lehrstuhl Anorganische Chemie II unter Betreuung von Herrn Professor Dr. Rhett Kempe angefertigt.

Vollständiger Abdruck der von der Fakultät für Biologie, Chemie und Geowissenschaften der Universität Bayreuth genehmigten Dissertation zur Erlangung des akademischen Grades eines Doktors der Naturwissenschaften (Dr. rer. nat.).

Dissertation eingereicht am: 08.03.2019

Zulassung durch die Promotionskommission: 20.03.2019

Wissenschaftliches Kolloquium: 12.12.2019

Amtierender Dekan: Prof. Dr. Matthias Breuning

Prüfungsausschuss:

Prof. Dr. Rhett Kempe (Gutachter)

Dr. habil. Günter Motz (Gutachter)

Prof. Dr. Rainer Schobert (Vorsitz)

Prof. Dr. Seema Agarwal

Meiner Familie in Dankbarkeit gewidmet

Table of contents

Abbreviations.....	9
1 Summary	11
2 Zusammenfassung	15
3 Introduction.....	19
3.1 Polymer-derived ceramics as catalyst support materials	19
3.2 Heterobimetallic complexes	20
3.3 Selective hydrogenation of nitroarenes	21
3.4 Deoxygenation of alcohols and carbonyl compounds	22
4 Overview of thesis results.....	27
4.1 Synopsis.....	27
4.2 Individual contribution to joint publications	39
5 A Reusable Co Catalyst for the Selective Hydrogenation of Functionalized Nitroarenes and the Direct Synthesis of Imines and Benzimidazoles From Nitroarenes and Aldehydes.....	41
5.1 Introduction	41
5.2 Results and Discussion	42
5.3 Acknowledgements	48
5.4 References	48
5.5 Supplementary Information	51
6 A Co catalyst permits the direct hydrogenative synthesis of 1<i>H</i>-perimidines from a dinitroarene and an aldehyde	101
6.1 Introduction	101
6.2 Results and Discussion	102
6.3 Acknowledgements	107
6.4 References	107
6.5 Supplementary Information	110

7 General and selective deoxygenation by hydrogen employing a reusable earth-abundant metal catalyst.....	143
7.1 Introduction	144
7.2 Results and Discussion	145
7.3 Supplementary Materials	152
7.4 References	152
7.5 Supplementary Materials	156
8 List of publications	197
9 Acknowledgements	199
10 Declaration / Erklärung	201

Abbreviations

Ar	argon
BET	Brunauer-Emmett-Teller
DCP	dicumylperoxide
DFT	density functional theory
NLDFT	non-linear density functional theory
EDX	energy dispersive X-ray spectroscopy
Et	ethyl
GC	gas chromatography
GC-MS	gas chromatography coupled with mass spectroscopy
HAADF	high-angle annular dark-field
HTT-1800	commercially available polysilazane precursor
HRMS	high-resolution mass spectrometry
ICP-OES	inductively coupled plasma optical emission spectrometry
<i>i</i> -Pr	<i>iso</i> -propyl
M@SiCN	silicon carbonitride supported metal
Me	methyl
<i>n</i> -Bu	<i>n</i> -butyl
NMR	nuclear magnetic resonance
OMe	methoxy
OAc	acetate
PDC	polymer-derived ceramic
Ph	phenyl
ppm	parts per million

Ref.	reference
RT	room temperature
SEM	scanning electron microscopy
SI	supporting information
SiCN	silicon carbonitride
SM	supplementary materials
TEM	transmission electron microscopy
TPD	temperature programmed desorption
TPR	temperature programmed reduction
wt. %	weight-%
XPS	X-ray photoelectron spectroscopy

1 Summary

The primary aim of this thesis was the synthesis and complete characterization of novel, heterogeneous catalysts based on earth-abundant metals, and their application in selective organic syntheses. Consequently, different metal complexes were prepared and applied in the development of novel catalyst systems. An overview of the methods and applications is shown in Figure 1.

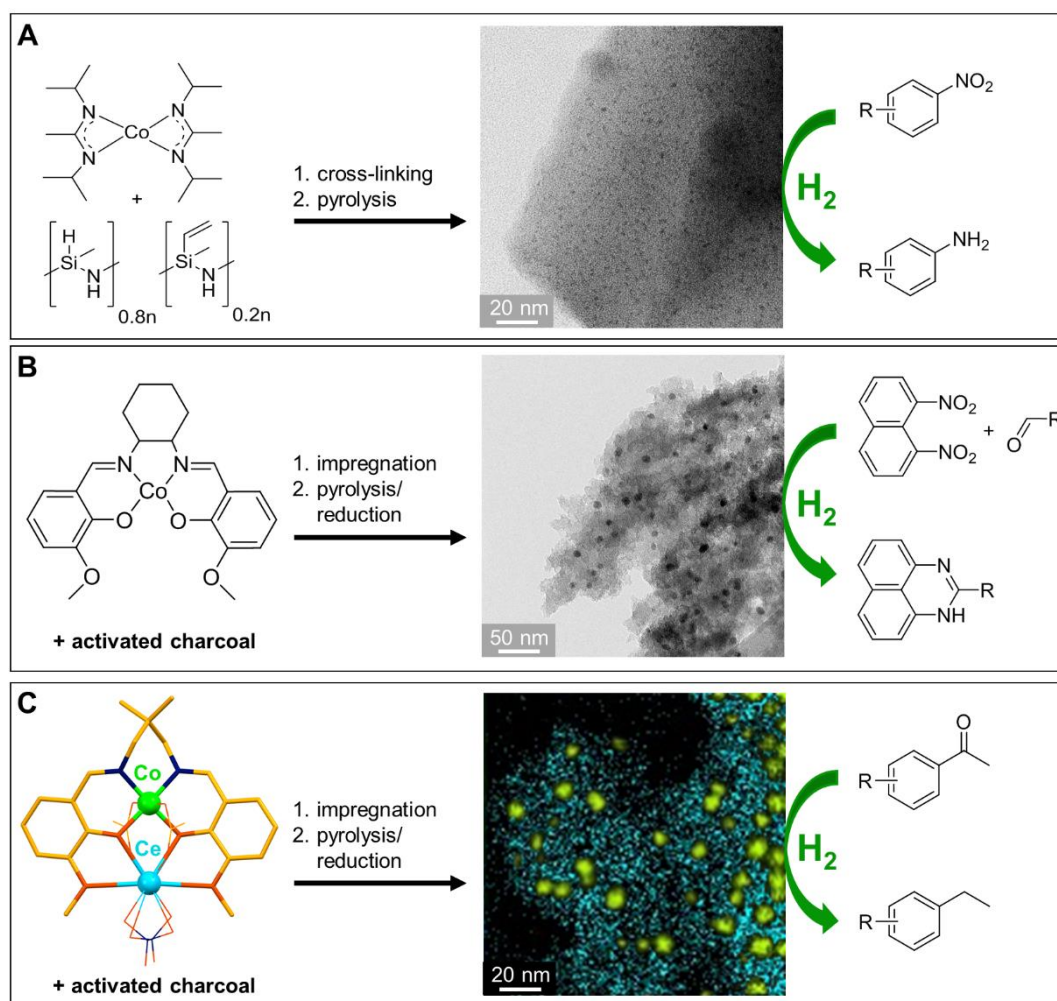


Figure 1: Overview of the different catalyst systems and the corresponding catalytic applications.

In the first part, the development of a porous Co-SiCN catalyst and its application in the selective hydrogenation of nitro derivatives is described. A suitable cobalt complex was combined with the ceramic precursor HTT-1800, followed by cross-linking and pyrolysis at 750 °C (Figure 1A). Magnetic measurements showed a change from paramagnetic behavior of the cross-linked polysilazane containing cobalt to superparamagnetic properties of the nanocomposite after pyrolysis. This is in agreement with the presence of isolated Co^{2+} ions after

cross-linking and their reduction to small metallic Co nanoparticles during pyrolysis. TEM analysis provided evidence of the generation of homogeneously distributed metal nanoparticles with a mean diameter of 1.6 nm. The novel Co-SiCN nanocomposite emerged as a suitable catalyst for the reduction of nitroarenes applying molecular hydrogen. This transformation is one of the most important reactions in the chemical industry, since it is the method of choice regarding the production of aniline and its derivatives. Furthermore, two new protocols for the synthesis of imines and benzimidazoles from nitroarenes and aldehydes were developed. The general applicability was confirmed by the hydrogenation of 17 nitro derivatives and the synthesis of 18 imines and 8 benzimidazoles. An extraordinary tolerance towards hydrogenation-sensitive functional groups was demonstrated in all cases.

Due to the importance of the reaction type, we were interested in further organic transformations, which include a nitroarene hydrogenation step. The direct usage of compounds containing two nitro functionalities is especially highly interesting, since this would allow the synthesis of a further class of *N*-heterocycles. However, the Co-SiCN nanocomposite was not able to mediate this reaction. The challenges of this transformation are shown in Figure 2.

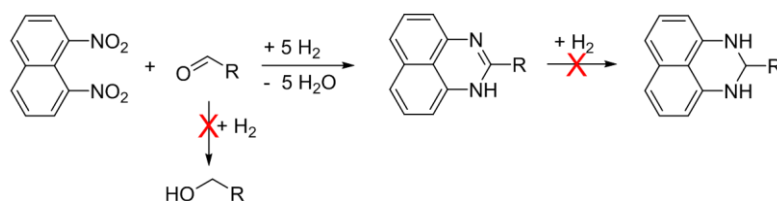


Figure 2: Challenges regarding the direct synthesis of 1*H*-perimidines from 1,8-dinitronaphthalene and aldehydes.

While the hydrogenation of the challenging 1,8-dinitronaphthalene must proceed smoothly and selectively, the aldehyde has to remain unaffected, even at the higher temperatures, needed for the condensation step. In addition, the hydrogenation of the 1*H*-perimidine desired must be suppressed, to prevent the formation of unwanted 2,3-dihydroperimidine side products. Such a direct synthesis route has not been described in the literature to date. The synthesis of a suitable catalyst is shown in Figure 1B. Commercially available activated charcoal was impregnated with a specific cobalt salen complex, followed by pyrolysis and reduction. TEM analysis of the catalyst verified the presence of small, homogeneously distributed metal nanoparticles with a mean diameter of 7.3 nm. XPS measurements proved the coexistence of metallic cobalt species besides cobalt oxides or hydroxides. The general applicability of the novel protocol was demonstrated by the synthesis of 20 examples. 1,8-dinitronaphthalene could be used in a technical grade, which is highly important for a possible industrial application. A remarkable tolerance towards a variety of hydrogenation-sensitive functional groups was observed in all

cases and six new products were synthesized. These 1*H*-perimidines are known as common starting materials for the preparation of azapyrenes, which are promising materials for the manufacture of organic semiconductor devices.

The class of salen ligands is capable of complexing several metal ions. This property was used in the third part of the thesis for the preparation of a bimetallic Co-Ce complex, which was fully characterized by X-ray crystallography (Figure 1C). Regarding the synthesis of the active catalyst, commercially available activated charcoal was impregnated with the heterobimetallic complex, followed by pyrolysis and reduction. The composition of the surface was analyzed by a combination of HAADF-STEM and EDX measurements. The analysis indicated the presence of two types of nanosized species: Co nanoparticles with a mean diameter of 6.8 nm and small Ce agglomerates (~1 nm) which were homogeneously embedded in the matrix. The hydrogenation of acetophenone was chosen for the first investigation of the catalytic properties. The introduction of a second metal species led to a significant change in the catalytic behavior. While the catalyst, which was synthesized from a monometallic cobalt salen complex, was very selective towards aldehydes, the bimetallic catalyst showed a high activity in the hydrodeoxygenation of carbonyls and alcohols. This cleavage of C-O bonds is a highly interesting type of reaction, since it offers the possibility of a modification of functionality-laden fine chemicals, natural products or pharmaceuticals, and it is crucial for the economic upgrading of biomass-derived molecules into fuels and chemicals. After optimization of the reaction conditions, the general applicability was demonstrated by hydrodeoxygenation of 56 examples. A tolerance towards a variety of functional groups was observed and the concept could be applied to aromatic and aliphatic substrates.

2 Zusammenfassung

Das primäre Ziel dieser Arbeit war die Synthese und vollständige Charakterisierung neuer, heterogener Katalysatoren auf Basis unedler Metalle, sowie deren Anwendung in der selektiven organischen Synthese. Hierzu wurden zunächst unterschiedliche Metallkomplexe hergestellt und über geeignete Verfahren auf die entsprechenden Trägermaterialien aufgebracht. Die verschiedenen Varianten sind in Abbildung 1 dargestellt.

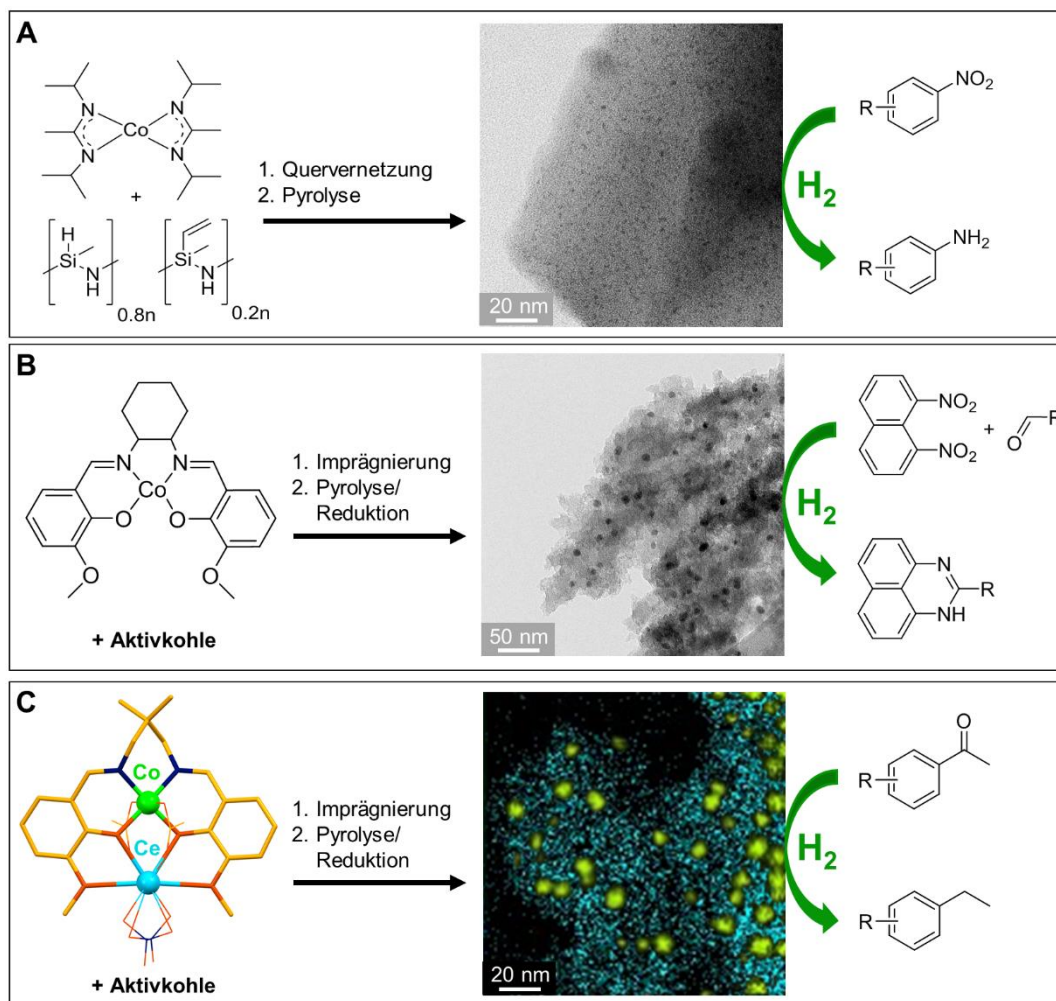


Abbildung 1: Überblick über die in dieser Arbeit vorgestellten Katalysatorsysteme mit den entsprechenden katalytischen Anwendungen.

Zunächst erfolgte die Entwicklung eines porösen Co-SiCN Katalysators und dessen Anwendung in der selektiven Hydrierung von Nitroderivaten. Durch Kombination eines geeigneten Cobalt-Komplexes mit dem keramischen Präkursor HTT-1800 wurde über Transmetallierung des Metalls auf den Präkursor und nachfolgende Quervernetzung der metallhaltige Grünkörper erzeugt. Eine Pyrolyse bei 750 °C unter Inertgas führte zu der

Bildung von sehr kleinen Nanopartikeln mit einem mittleren Durchmesser von 1.6 nm (Abbildung 1A). Der Übergang vom paramagnetischen Verhalten des Grünkörpers hin zu superparamagnetischen Eigenschaften des Nanokomposits konnte anhand von magnetischen Messungen bestätigt werden. Dies steht im Einklang mit dem Vorhandensein von isolierten Co^{2+} -Ionen nach der Quervernetzung und der Bildung von kleinen metallischen Nanopartikeln während der Pyrolyse. Der Katalysator zeigte eine außerordentliche Aktivität in der selektiven Hydrierung von Nitroderivaten, einer der wichtigsten katalytischen Transformationen in der chemischen Industrie. Weiterhin konnten auf Basis der gezeigten Selektivitäten zwei neue Syntheseprotokolle zur Darstellung von Iminen und Benzimidazolen entwickelt werden. Die generelle Anwendbarkeit wurde anhand der Hydrierung von 17 Nitroderivaten, sowie der Synthese von 18 Iminen und 8 Benzimidazolen bestätigt. In allen Fällen konnte eine außerordentliche Toleranz gegenüber weiteren hydrierempfindlichen funktionellen Gruppen nachgewiesen werden.

Aufgrund der Bedeutung der beschriebenen Reaktion erfolgte im zweiten Teil der Arbeit die Entwicklung eines Synthesekonzepts für die direkte Darstellung von 1*H*-Perimidinen aus 1,8-Dinitronaphthalen und Aldehyden. Die industriell bedeutsame Reduktion von Substraten mit mehreren Nitro-Gruppen konnte unter Verwendung des beschriebenen Co-SiCN Nanokomposits nicht vermittelt werden. In Abbildung 2 sind die Anforderungen an das entsprechende Katalysatorsystem dargestellt.

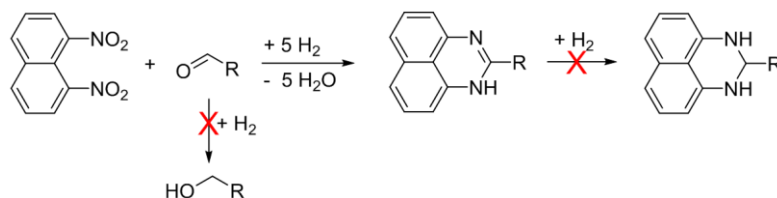


Abbildung 2: Anforderungen an den Katalysator zur direkten Synthese von 1*H*-Perimidinen ausgehend von 1,8-Dinitronaphthalen und verschiedenen Aldehyden.

Das anspruchsvolle Substrat 1,8-Dinitronaphthalen muss vollständig und selektiv hydriert werden, während die Reduktion des Aldehyds zum entsprechenden Alkohol zu unterdrücken ist. Weiterhin ist es notwendig, dass die Reaktion auf der Stufe des 1*H*-Perimidins stoppt, um die Bildung von unerwünschten Nebenprodukten zu verhindern. Eine solche direkte Syntheseroute wurde bisher nicht in der Literatur beschrieben. Die Darstellung des geeigneten Katalysators ist in Abbildung 1B dargestellt. Zunächst erfolgte die Synthese eines Cobalt-Komplexes auf Basis einer Schiff'schen Base (Salen-Typ-Komplex). Im Anschluss wurde kommerziell erhältliche Aktivkohle mit dem Salen-Komplex imprägniert, gefolgt von Pyrolyse

und Reduktion. TEM-Aufnahmen bestätigten die Bildung von homogen verteilten Nanopartikeln mit einem mittleren Durchmesser von 7.3 nm. Mittels XPS-Analyse konnte das Vorhandensein von metallischen und oxidischen Cobalt-Spezies auf der Katalysatoroberfläche nachgewiesen werden. Die generelle Anwendbarkeit des neuen Syntheseprotokolls wurde anhand von 20 Beispielen gezeigt, wobei 1,8-Dinitronaphthalen mit einem technischen Reinheitsgrad verwendet werden konnte. Auch in diesem Fall war eine bemerkenswerte Toleranz gegenüber einer Vielzahl an hydrierempfindlichen funktionellen Gruppen zu verzeichnen und es konnten sechs neue Produkte synthetisiert werden. Diese 1*H*-Perimidine werden in der Literatur beispielsweise als Ausgangsverbindungen zur Darstellung von Azapyrenen verwendet, für welche ein breites Anwendungsspektrum im Bereich der Halbleitertechnik diskutiert wird.

Die beschriebene Klasse der Salen-Liganden ist in der Lage mehrere Metallionen zu komplexieren. Im dritten Teil der Arbeit wurde diese Eigenschaft genutzt, um einen bimetalischen Co-Ce-Komplex zu synthetisieren, welcher mittels Röntgenstrukturanalyse vollständig charakterisiert wurde (Abbildung 1C). Der Komplex wurde ebenfalls mittels Nassimprägnierung auf kommerziell erhältliche Aktivkohle aufgebracht, gefolgt von Pyrolyse und Reduktion. Anhand einer Kombination aus HAADF-STEM und EDX-Analyse konnte die Bildung von Cobalt-Nanopartikeln mit einem mittleren Durchmesser von 6.8 nm nachgewiesen werden. Weiterhin konnte die homogene Verteilung der zweiten Metallspezies (Ce) in Form von sehr kleinen Agglomeraten (~1 nm) belegt werden (Abbildung 1C). Dies führte zu einer signifikanten Änderung der katalytischen Eigenschaften. Während sich das Katalysatorsystem, welches unter Verwendung des monometallischen Co-Salen-Komplexes synthetisiert wurde, durch eine außerordentliche Toleranz gegenüber Aldehyden auszeichnete, zeigte der bimetalische Co-Ce-Katalysator eine hohe Aktivität in der Hydrodeoxygenierung von Carbonylen und Alkoholen. Nach Optimierung der Reaktionsbedingungen konnte die Anwendbarkeit anhand von 56 Beispielen demonstriert werden. Es wurde eine Toleranz gegenüber einer Vielzahl von funktionellen Gruppen beobachtet und das Konzept konnte sowohl auf aromatische als auch auf aliphatische Substrate angewendet werden.

3 Introduction

3.1 Polymer-derived ceramics as catalyst support materials

The so-called polymer-derived ceramics have attracted increasing attention in recent decades due to their excellent material properties, such as stability against corrosion and oxidation, as well as their thermal and chemical robustness.^[1] Common preceramic polymers for the preparation of such PDCs are polysilanes, polycarbosilanes, polysiloxanes, polysilazanes and polysilylcarbodiimids. Depending on the ceramic precursor, there is a differentiation between oxidic and non-oxidic ceramics.^[2] In the field of non-oxidic ceramics, silicon carbonitrides have proven to be excellent support materials in heterogeneous catalysis. A general synthesis route for this class of materials is shown in Figure 1.

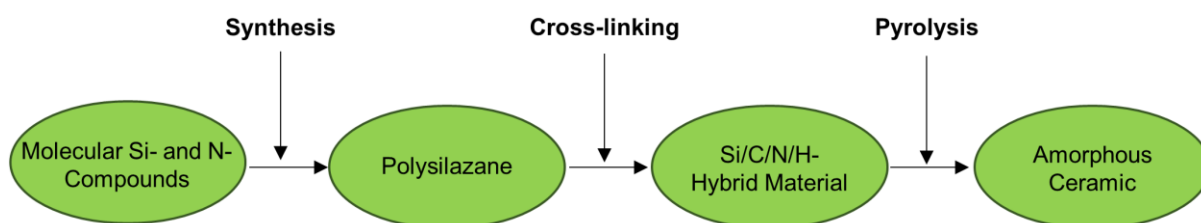


Figure 1: Flow chart for the molecular synthesis of polymer-derived SiCN materials.

Starting from molecular Si- and N-compounds, the corresponding polysilazane is synthesized. Cross-linking leads to the formation of a Si/C/N/H-hybrid material, which is converted into an amorphous SiCN ceramic by subsequent pyrolysis.^[3] The properties of the final ceramic material can be adjusted by the type and molecular structure of the preceramic polymer. This molecular synthesis route offers the possibility of a modification of the precursor polymers, by applying coordination compounds, such as metal complexes. Our group established a molecular approach for the transfer of transition metals from suitable aminopyridinato complexes to the commercially available polysilazane HTT-1800.^[4] Applying this novel synthesis concept, a variety of heterogeneous catalysts for different catalytic applications were introduced. *Glatz et al.* developed a Cu@SiCN material, which was applied in the oxidation of cycloalkanes.^[5] In addition, Pd₂Si particles incorporated in an SiCN matrix led to an appropriate system for the hydrogenation of ketones and aldehydes to the corresponding alcohols.^[6] The combination of further noble metals with the SiCN support emerged as a suitable method for the generation of catalysts for more complex organic transformations. It was shown that an Ir@SiCN catalyst can mediate the synthesis of pyrroles from secondary alcohols and 1,2-amino alcohols.^[7] Furthermore, a bimetallic Pd₂Ru@SiCN catalyst for the reversible hydrogen storage^[8] and a

more complex system consisting of three different catalysts (Ru@SiCN, Ir@SiCN, Pd@SiCN) for the synthesis of carbazoles, quinolines and acridines were introduced.^[9] The combination of earth-abundant metals with PDCs as catalyst support materials seems to be an interesting area of research, as this substitution could contribute to more sustainable chemistry regarding the conservation of rare noble metal resources.

3.2 Heterobimetallic complexes

Metal complexes containing an early and late transition metal are an interesting class of chemical compounds, as their catalytic properties may differ from those of bimetallic complexes with identical or closely related metals.^[10] Ligands based on compartmental Schiff bases are capable of complexing several metal ions. A general synthesis route is shown in Figure 2.

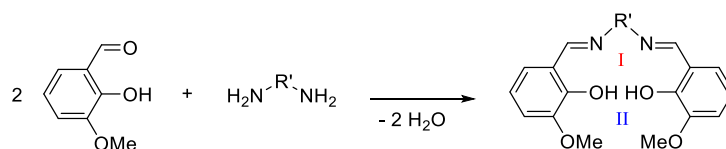


Figure 2: General synthesis of a Schiff base ligand containing two different coordination spheres (H₂-Salen).

There are a lot of different coordination compounds described in the literature containing a transition and a rare-earth metal, based on different types of salen ligands. The transition metal is generally located in coordination sphere **I** (N₂O₂) and the rare-earth metal in coordination sphere **II** (O₂O₂).^[11] *Elias et al.* introduced a synthetic route towards phase-pure, monodisperse transition-metal-substituted ceria nanoparticles applying a solution-based pyrolysis of a series of such heterobimetallic Schiff base complexes. Monodisperse crystallites with the composition M_{0.1}Ce_{0.9}O_{2-x} (M = Mn, Fe, Co, Ni, Cu) and a mean diameter of 3 nm were obtained. The catalyst synthesized from a Cu-Ce-salen complex (Cu_{0.1}Ce_{0.9}O_{2-x}) showed a high activity in the catalytic oxidation of carbon monoxide.^[12] The development of novel synthesis concepts for heterogeneous catalysts applying heterobimetallic complexes seems to be an interesting field of research. Their combination with commercially available catalyst support materials may lead to unobserved catalytic activities.

3.3 Selective hydrogenation of nitroarenes

The hydrogenation of nitroarenes is one of the most important reactions in the chemical industry because it is the method of choice for the production of aniline and its derivatives.^[13] Due to this importance, a huge effort has been invested in the development of highly efficient and selective catalysts for this transformation in recent years. *Haber* proposed a complex reaction network for the electrochemical reduction of nitro compounds more than 100 years ago, which is now generally accepted as a basis to describe how the catalytic hydrogenation proceeds.^[14]

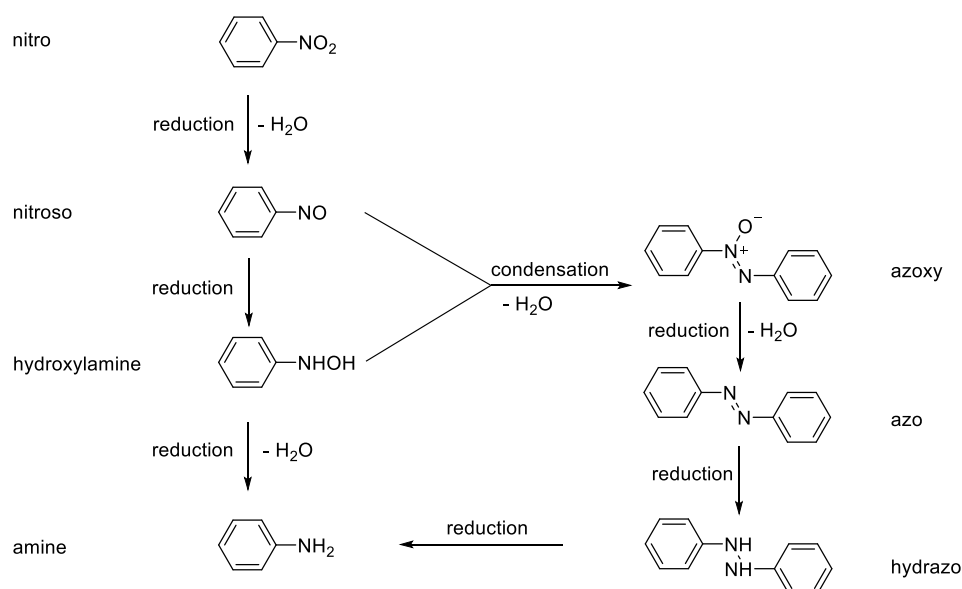


Figure 3: Reaction network proposed by Haber for the (electrochemical) reduction of a nitroarene.

The key challenges of the catalytic transformation are demonstrated in Figure 3. An accumulation of the hydroxylamine intermediate must be suppressed, to prevent the formation of azo compounds as side products. This condensation does not usually occur, however, it was observed for slow reactions and low temperatures.^[15] Until 1998, the field of research was dominated mainly by modified commercial systems based on noble metals. In this context, a 5 wt% Pt/C catalyst modified with H_3PO_2 and promoted with vanadium compounds proved to be very effective and a tolerance towards a variety of functional groups, such as halides and nitriles as well as C-C double and triple bonds was observed.^[16] *Corma and coworkers* reported a breakthrough regarding the tolerance of functional groups in 2006. They applied gold catalysts and observed a selectivity of over 95 % for the hydrogenation of the nitro group in 3-nitrostyrene, 4-nitrobenzaldehyde, 4-nitrobenzotrile and 4-nitrobenzamide.^[17] In 2013, *Beller and coworkers* showed that reusable catalysts based on abundantly available transition metals, such as iron^[18] and cobalt^[19], can also mediate the highly chemoselective hydrogenation of

nitroarenes. The development of reusable, earth-abundant metal catalysts is an important area of research, as their industrial application could contribute to greater sustainability in terms of conserving precious metal resources. The substitution of these precious metals is especially attractive if novel selectivity patterns are observed, which allow the design of innovative synthesis concepts. The direct use of nitro derivatives in more complex and selective organic syntheses has so far been rarely disclosed. In this case, the use of molecular hydrogen as a reducing agent is especially attractive due to the high atom and cost efficiency.

3.4 Deoxygenation of alcohols and carbonyl compounds

Reductive deoxygenation of alcohols and carbonyl compounds is of wide interest, since this transformation is connected with the synthesis of fine chemicals^[20] and the production of biofuels^[21]. There are several classic methods, such as the Barton-McCombie^[22], Clemmensen^[23], or Wolff-Kishner^[24] reduction, however, all these methodologies suffer from harsh reaction conditions, the use of stoichiometric amounts of toxic reagents and a poor functional group tolerance. *Volkov et al.* introduced a heterogenous Pd/C catalyst and applied polymethylhydrosiloxane as the hydride source. They demonstrated the deoxygenation of aromatic ketones and aldehydes in the presence of functional groups, such as halides, amides and esters. The deoxygenation proceeded under relatively mild conditions, however, the scope was limited to benzylic carbonyl functionalities. In addition, three equivalents of the silane regarding the substrate were applied as a reducing agent, leading to high amounts of waste.^[25] *Li and coworkers* showed the highly selective deoxygenation of primary alcohols by a combination of oxidative dehydrogenation and Wolff-Kishner reduction. They applied homogenous Ru and Ir catalysts and were able to deoxygenate benzylic and aliphatic primary alcohols in the presence of reducible moieties, such as C-C double and triple bonds and further secondary alcohol functionalities. The concept could also be extended to the selective deoxygenation of complex steroid molecules. Despite the outstanding substrate scope and functional group tolerance, this protocol bears one major disadvantage: The deoxygenation proceeds with an excess of very toxic hydrazine monohydrate and nearly stoichiometric amounts of base.^[26] The use of atom-efficient and easily available molecular hydrogen as a reducing agent is highly attractive from an economic and environmental point of view. *Yi and coworkers* applied cationic ruthenium-hydride complexes and demonstrated the chemoselective hydrodeoxygenation of carbonyl compounds applying 2.0 MPa hydrogen pressure and reaction temperatures around 130 °C. A broad substrate scope and tolerance towards a variety of hydrogenation-sensitive functional groups was observed. In addition, the concept was extended

to the hydrodeoxygenation of biologically active molecules.^[27] Current synthetic pathways for the hydrodeoxygenation of carbonyl compounds and alcohols based on the application of reusable, earth-abundant metal catalysts cannot fulfill the requirements of a broad substrate scope and an adequate functional group tolerance.^[28] The development of novel catalyst systems mediating this reaction type is highly interesting, since these catalysts could contribute to sustainable and cost-efficient deoxygenation under industrially viable conditions.

-
- [1] P. Colombo, R. Riedel, G. D. Soraru, H.-J. Kleebe in *Polymer Derived Ceramics: From Nano-Structure to Applications*, DEStech Publications, Pennsylvania, **2010**.
- [2] E. Ionescu, H.-J. Kleebe, R. Riedel, *Chem. Soc. Rev.* **2012**, *41*, 5032.
- [3] E. Kroke, Y.-L. Li, C. Konetschny, E. Lecomte, C. Fasel, R. Riedel, *Mater. Sci. Eng. R Rep.* **2000**, *26*, 97.
- [4] M. Zaheer, T. Schmalz, G. Motz, R. Kempe, *Chem. Soc. Rev.* **2012**, *41*, 5102.
- [5] G. Glatz, T. Schmalz, T. Kraus, F. Haarmann, G. Motz, R. Kempe, *Chem. Eur. J.* **2010**, *16*, 4231.
- [6] M. Zaheer, G. Motz, R. Kempe, *J. Mater. Chem.* **2011**, *21*, 18825.
- [7] D. Forberg, J. Obenauf, M. Friedrich, S.-M. Hühne, W. Mader, G. Motz, R. Kempe, *Catal. Sci. Technol.* **2014**, *4*, 4188.
- [8] D. Forberg, T. Schwob, M. Zaheer, M. Friedrich, N. Miyajima, R. Kempe, *Nat. Commun.* **2016**, *7*, 13201.
- [9] D. Forberg, T. Schwob, R. Kempe, *Nat. Commun.* **2018**, *9*, 1751.
- [10] D. W. Stephan, *Coord. Chem. Rev.* **1989**, *95*, 41.
- [11] P. A. Vigato, S. Tampurini, *Coord. Chem. Rev.* **2008**, *252*, 1871.
- [12] J. S. Elias, M. Risch, L. Giordano, A. N. Mansour, Y. Shao-Horn, *J. Am. Chem. Soc.* **2014**, *136*, 17193.
- [13] K. Eller, E. Henkes, R. Rossbacher, H. Höke in *Ullmann's Encyclopedia of Industrial Chemistry*, Wiley-VCH, Weinheim, Germany, **2012**, p. 654.

- [14] a) F. Haber, *Z. Elektrotech. Elektrochem.* **1889**, *4*, 506; b) F. Haber, *Angew. Chem.* **1900**, *13*, 433.
- [15] H.-U. Blaser, H. Steiner, M. Studer, *ChemCatChem* **2009**, *1*, 2010.
- [16] a) P. Baumeister, H.-U. Blaser, U. Siegrist, M. Studer, *Chem. Ind.* **1998**, *75*, 207; b) H.-U. Blaser, U. Siegrist, H. Steiner, M. Studer in *Fine Chemicals through Heterogeneous Catalysis*, Eds.: R. A. Sheldon, H. van Bekkum, Wiley-VCH, Weinheim, **2001**, p. 389.
- [17] A. Corma, P. Serna, *Science* **2006**, *313*, 332.
- [18] a) R. V. Jagadeesh, A.-E. Surkus, H. Junge, M.-M. Pohl, J. Radnik, J. Rabeah, H. Huan, V. Schünemann, A. Brückner, M. Beller, *Science* **2013**, *342*, 1073; b) R. V. Jagadeesh, T. Stemmler, A.-E. Surkus, H. Junge, K. Junge, M. Beller, *Nat. Protoc.* **2015**, *10*, 548.
- [19] F. A. Westerhaus, R. V. Jagadeesh, G. Wienhofer, M.-M. Pohl, J. Radnik, A.-E. Surkus, J. Rabeah, K. Junge, H. Junge, M. Nielsen, A. Brückner, M. Beller, *Nat. Chem.* **2013**, *5*, 537.
- [20] a) R. O. Hutchins, M. K. Hutchins in *Comprehensive Organic Synthesis*, Ed.: I. Fleming, Elsevier, Oxford, **1991**, p. 327; b) J. M. Herrmann, B. König, *Eur. J. Org. Chem.* **2013**, *2013*, 7017.
- [21] J. N. Chheda, G. W. Huber, J. A. Dumesic, *Angew. Chem. Int. Ed.* **2007**, *46*, 7164; R. A. Sheldon, *Green Chem.* **2014**, *16*, 950.
- [22] D. L. J. Clive, J. Wang, *J. Org. Chem.* **2002**, *67*, 1192.
- [23] a) E. Clemmensen, *Ber. Dtsch. Chem. Ges.* **1914**, *47*, 681; b) E. Vedejs, *Org. React.* **1975**, *22*, 401.
- [24] a) J. J. Kishner, *Russ. Phys. Chem. Soc.* **1911**, *43*, 582; b) C. Wolff, *Justus Liebigs Ann.* **1912**, *394*, 86; c) D. Todd, *Org. React.* **1948**, *4*, 378; d) H. Minlon, *J. Am. Chem. Soc.* **1949**, *71*, 3301.
- [25] A. Volkov, K. P. J. Gustafson, C.-W. Tai, O. Verho, J.-E. Bäckvall, H. Adolfsson, *Angew. Chem. Int. Ed.* **2015**, *54*, 5122.
- [26] X.-J. Dai, C.-J. Li, *J. Am. Chem. Soc.* **2016**, *138*, 5433.

- [27] N. Kalutharage, C. S. Yi, *J. Am. Chem. Soc.* **2015**, *137*, 11105.
- [28] For selected examples, please see: a) V. Kogan, Z. Aizenshtat, R. Neumann, *Angew. Chem. Int. Ed.* **1999**, *38*, 3331; b) F. Zaccheria, N. Ravasio, M. Ercoli, P. Allegrini, *Tetrahedron Lett.* **2005**, *46*, 7743; c) S. Liu, X. Fan, X. Yan, X. Du, L. Chen, *Appl. Catal., A* **2011**, *400*, 99; d) J. Ma, S. Liu, X. Kong, X. Fan, X. Yan, L. Chen, *Res. Chem. Intermed.* **2012**, *38*, 1341; e) X. Kong, L. Chen, *Catal. Commun.* **2014**, *57*, 45; f) L. Petitjean, R. Gagne, E. S. Beach, D. Xiao, P. T. Anastas, *Green Chem.* **2016**, *18*, 150.

4 Overview of thesis results

This thesis contains three publications, which are presented in chapter 5-7. In chapter 4.1 the results are summarized and in chapter 4.2 the individual contributions are pointed out in detail.

4.1 Synopsis

During the past few years, the Kempe group has focused on the synthesis of novel heterogeneous catalysts for complex organic syntheses, applying PDCs as catalyst support materials and noble metals as the active species. It was shown that an Ir@SiCN catalyst can mediate the synthesis of pyrroles from secondary alcohols and 1,2-amino alcohols. Furthermore, a bimetallic Pd₂Ru@SiCN for the reversible hydrogen storage and a more complex system consisting of three different catalysts (Ru@SiCN, Ir@SiCN, Pd@SiCN) for the synthesis of carbazoles, quinolines and acridines were introduced. In further studies, *Rößler et al.* showed that homogeneous catalysts based on the earth-abundant metal cobalt are suitable for the hydrogenation of carbonyl groups and the alkylation of aromatic amines with alcohols. The development of such earth-abundant metal catalysts is an important area of research, as their industrial application could contribute to a greater sustainability in terms of conserving precious metal resources. The substitution of these precious metals is especially attractive if novel selectivity patterns are observed which allow the design of innovative synthesis concepts. The aim of this thesis was the development of novel catalysts, which combine the advantages of earth-abundant metals as an active species (low cost and selectivity) with the benefits of a heterogeneous catalyst system (reusability and easy separation from the reaction product) and their application in selective organic syntheses.

The first part of the thesis describes the development of an SiCN-based cobalt catalyst. The synthesis route is shown in Figure 1A. In the first step, an amidinato cobalt(II) complex and the commercially available polysilazane HTT-1800 were dissolved in tetrahydrofuran, followed by cross-linking using dicumylperoxide as a radical initiator. After removal of the solvent *in vacuo*, the green body was pyrolyzed under a constant nitrogen flow at 750 °C. It was shown that higher temperatures led to an agglomeration of the nanoparticles, which is generally detrimental for the catalytic activity of a heterogeneous catalyst.

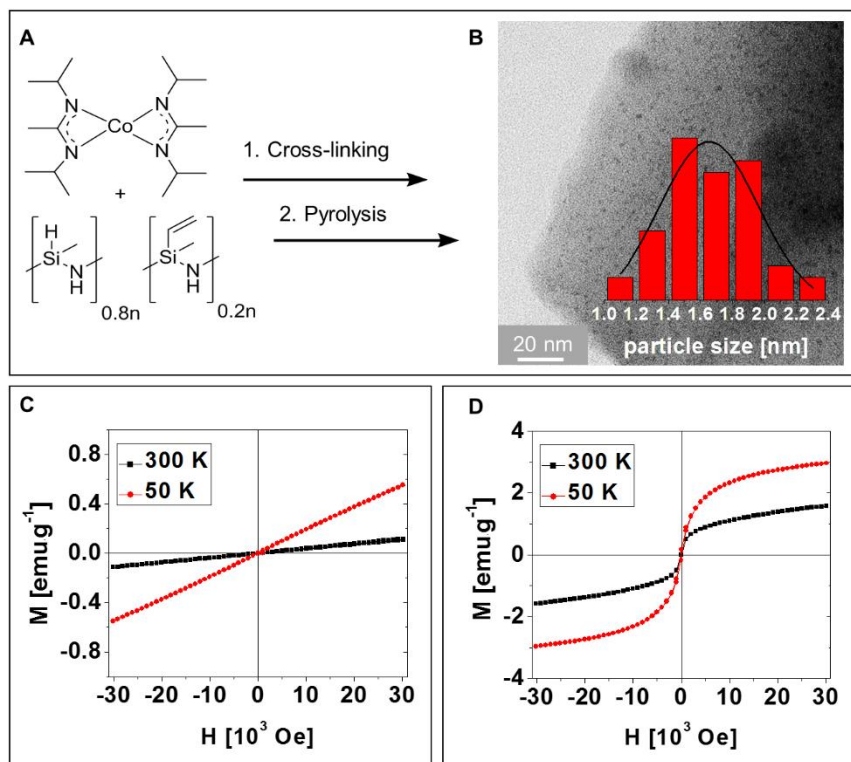


Figure 1: Synthesis and characterization of the Co-SiCN nanocomposite. A) Combination of a suitable metal complex with the ceramic precursor HTT-1800, followed by pyrolysis under a nitrogen atmosphere. B) TEM analysis and the corresponding particle size distribution provided evidence of small homogeneously distributed nanoparticles. C, D) Magnetic measurements verified the transition from para- to superparamagnetic properties.

Magnetic measurements showed a change from the paramagnetic behavior of the cross-linked polysilazane containing cobalt to superparamagnetic properties of the nanocomposite after pyrolysis (Figure 1C, D). This is in agreement with the presence of isolated Co^{2+} ions after cross-linking and their reduction to small metallic Co nanoparticles during pyrolysis. TEM analysis provided evidence of the generation of small homogeneously distributed metal nanoparticles with a mean diameter of 1.6 nm (Figure 1B). The novel Co-SiCN nanocomposite emerged as a suitable catalyst for the reduction of nitroarenes applying cheap and easily available molecular hydrogen. This transformation is one of the most important reactions in the chemical industry, since it is the method of choice regarding the production of aniline and its derivatives. After the optimization of different reaction conditions, we were able to hydrogenate aromatic nitroarenes in a highly selective fashion. A variety of different functional groups, such as halides (including reactive iodides), amides, nitriles, ketones, aldehydes and nitriles, as well as C-C double bonds were well tolerated under reductive reaction conditions (Figure 2).

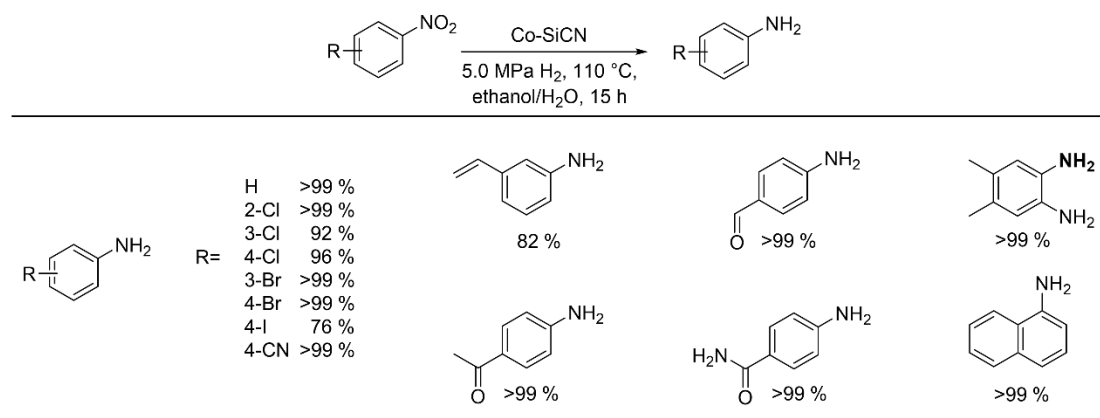


Figure 2: Representative substrate scope for the selective hydrogenation of nitroarenes. Reaction conditions: 110 °C, 5.0 MPa hydrogen pressure, 35 mg catalyst (4.8 mol% Co), 2 mL ethanol, 0.5 mL H₂O, 15 h. Yields were determined by GC and GC-MS using *n*-dodecane as an internal standard.

The tolerance towards aldehydes and ketones is especially attractive, since it allows the design of innovative synthesis concepts. We were able to demonstrate the first highly selective synthesis of imines and benzimidazoles from nitro derivatives and aldehydes. After an adjustment of the reaction conditions, the general applicability of this reductive coupling was proved by the synthesis of 26 different examples (Figure 3).

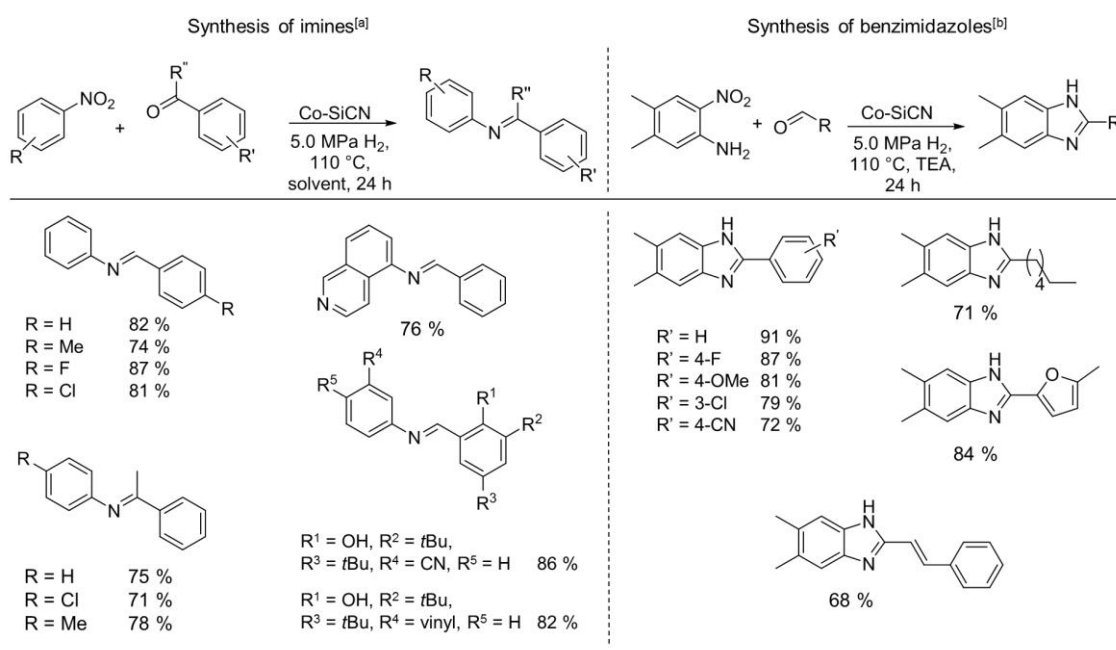


Figure 3: Representative substrate scope for the selective synthesis of imines and benzimidazoles. [a] Reaction conditions: R''=H: 110 °C, 5.0 MPa H₂, 1.5 mmol nitroarene, 3.0 mmol aldehyde, 110 mg catalyst (5.0 mol% Co), 4 mL triethylamine, 24 h. R''=Me: 115 °C, 5.0 MPa H₂, 1.5 mmol nitroarene, 3.0 mmol ketone, 175 mg catalyst (8.0 mol% Co), 10 mg Amberlyst® 15, molsieves, 4 mL toluene, 48 h. [b] Reaction conditions: 110 °C, 5.0 MPa H₂, 1.5 mmol nitroarene, 3.0 mmol aldehyde, 110 mg catalyst (5.0 mol% Co), 4 mL triethylamine, 24 h; yields of isolated products.

Inspired by these results and due to the importance of the reaction type, we were interested in further complex organic transformations, which include a nitroarene hydrogenation step. The direct usage of compounds containing two nitro functionalities is especially highly interesting, since this would allow the synthesis of a further class of *N*-heterocycles. We decided to investigate the application of a technical grade 1,8-dinitronaphthalene for the direct synthesis of 1*H*-perimidines. The challenges of this reaction are shown in Figure 4.

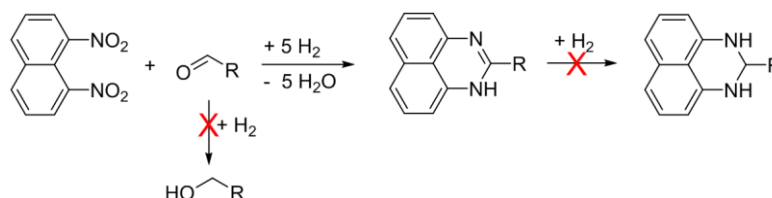


Figure 4: Challenges of the synthesis concept. The hydrogenation of 1,8-dinitronaphthalene must proceed smoothly and selectively, while the aldehyde and the 1*H*-perimidine desired must remain unaffected.

While the hydrogenation of the challenging 1,8-dinitronaphthalene must proceed smoothly and selectively, the aldehyde has to remain unaffected even at the higher temperatures needed for the condensation step. In addition, the hydrogenation of the 1*H*-perimidine desired must be suppressed to prevent the formation of 2,3-dihydroperimidine side products. We started our investigations applying the Co-SiCN nanocomposite described above, however, the catalyst emerged as unsuitable for the hydrogenation of compounds bearing two nitro functionalities. The fact that this reaction type has not been described in the literature to date and the broad applicability of this class of substances, for example, as starting materials for the synthesis of azapyrenes, which are promising materials for the manufacture of organic semiconductor devices, motivated us to investigate the development of a novel catalyst system. Regarding the generation of the active catalyst, commercially available activated charcoal was impregnated with a specific cobalt salen complex, followed by pyrolysis and reduction. The general synthesis concept is shown in Figure 5. The activated charcoal was added to a solution of complex I in acetonitrile and the mixture was stirred at 95 °C. After evaporation of the solvent, the sample was pyrolyzed under a nitrogen atmosphere at 700 °C, followed by reduction at 550 °C using forming gas (N₂/H₂ 90/10). A homogeneous distribution of the metal species over the entire catalyst surface, which is particularly important when synthesizing a catalyst by wet impregnation, was confirmed by EDX analysis. No phase separation could be detected, indicating a clean and smooth impregnation process. TEM analysis of the catalyst verified the presence of small, homogeneously distributed metal nanoparticles with a mean diameter of 7.3 nm (Figure 5B). XPS measurements were accomplished to get a deeper insight into the

composition of the surface. An analysis of the Co $2p_{3/2}$ region indicated the coexistence of metallic cobalt species in addition to cobalt oxides or hydroxides, which cannot be distinguished definitely (Figure 5C).

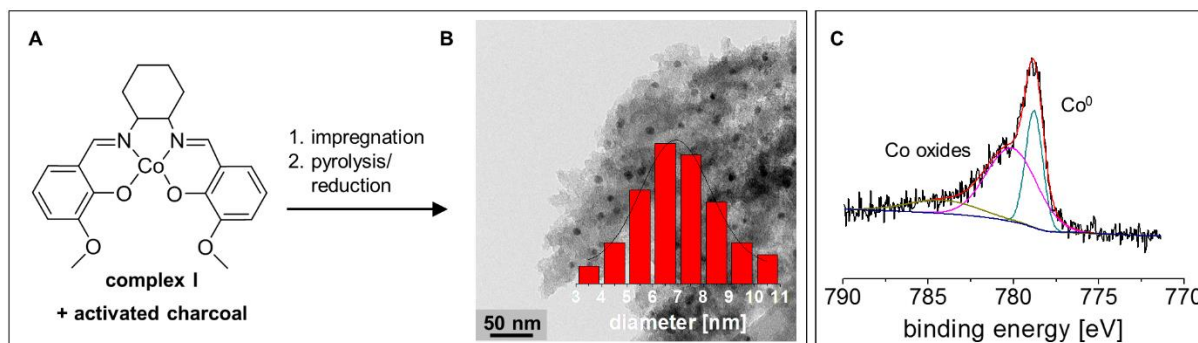
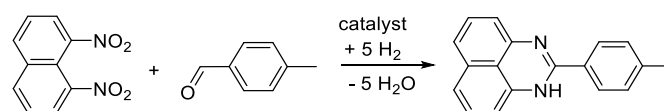


Figure 5: Synthesis and characterization of the novel cobalt catalyst. A) Wet impregnation of commercially available charcoal with complex I, followed by pyrolysis and reduction. B) TEM analysis in combination with the corresponding particle size distribution proved evidence of homogeneously distributed metal nanoparticles with a mean diameter of 7.3 nm. C) XPS analysis of the Co $2p_{3/2}$ region confirmed the presence of metallic cobalt and different oxides or perhaps hydroxides.

At the beginning of our catalytic studies, the influence of the support material and the pyrolysis temperature during the preparation of the catalyst were investigated. The reductive coupling of 1,8-dinitronaphthalene and 4-methylbenzaldehyde was chosen as a model reaction. The nitro derivative was used in a technical grade around 90 % (determined by GC and GC-MS). This limits the isolated yields. However, it is very important to ensure the general applicability of the novel reaction sequence. The results are summarized in Table 1.

Table 1: Screening of reaction parameters – catalyst screening.

Entry	Metal source	Pyrolysis temperature [°C]	Support	Yield [%]
1	Complex I	600	Activated charcoal	41
2	Complex I	700	Activated charcoal	72
3	Complex I	800	Activated charcoal	61
4	Complex I	700	TiO ₂	31
5	Complex I	700	CeO ₂	18
6	Complex I	700	γ-Al ₂ O ₃	54
7	Co(OAc) ₂ * 4 H ₂ O	700	Activated charcoal	15
8 [§]	Complex I	700	Activated charcoal	87

Reaction conditions: 0.5 mmol nitro derivative, 1.1 eq aldehyde, 35 mg catalyst (4 mol% Co), 120 °C, 6.0 MPa H₂, 3 mL toluene, 20 h; [§]130 °C reaction temperature; Yields were determined by GC and GC-MS using *n*-dodecane as an internal standard.

The use of metal oxides as support materials led to a decrease in product yield in all cases (Table 1, entries 4-6). A significant amount of aldehyde hydrogenation, even at incomplete conversion of the nitroarene derivative, was observed. A replacement of complex I by the common metal salt cobalt acetate led to a distinct drop in catalytic activity, indicating the superiority of the synthesis concept based on the application of the cobalt salen complex in catalyst synthesis (Table 1, entry 7). In summary, the synthesis of 2-(*p*-tolyl)-1*H*-perimidine proceeded well with a catalyst synthesized from complex I in combination with commercially available activated charcoal at 130 °C reaction temperature, 6.0 MPa hydrogen pressure, applying toluene as the solvent. With the optimized reaction conditions in hand, the synthesis protocol was applied to several substrates. A representative substrate scope is shown in Figure 6. The reductive coupling of 1,8-dinitronaphthalene with aromatic and aliphatic aldehydes proceeded smoothly and an extraordinary tolerance towards various hydrogenation-sensitive functional groups was observed. The synthesis concept tolerates halides, ethers, thioethers, boronic esters, amides, hydroxy functionalities, as well as heterocycles, nitriles, and C-C double and triple bonds. An up-scaling of the reaction was demonstrated, and the catalyst showed stability over several consecutive runs without a remarkable decrease in catalytic activity. It is noteworthy to mention that we were able to synthesize six new products with this direct synthesis of 1*H*-perimidines. These compounds are generally known as common starting materials for the synthesis of 6,8-disubstituted 1,3-diazapyrenes or 7-bromo-1,3-diazapyrenes,

which are promising materials for the manufacture of organic semiconductor devices, such as light-emitting diodes, field-effect transistors and photovoltaic elements for solar cells.

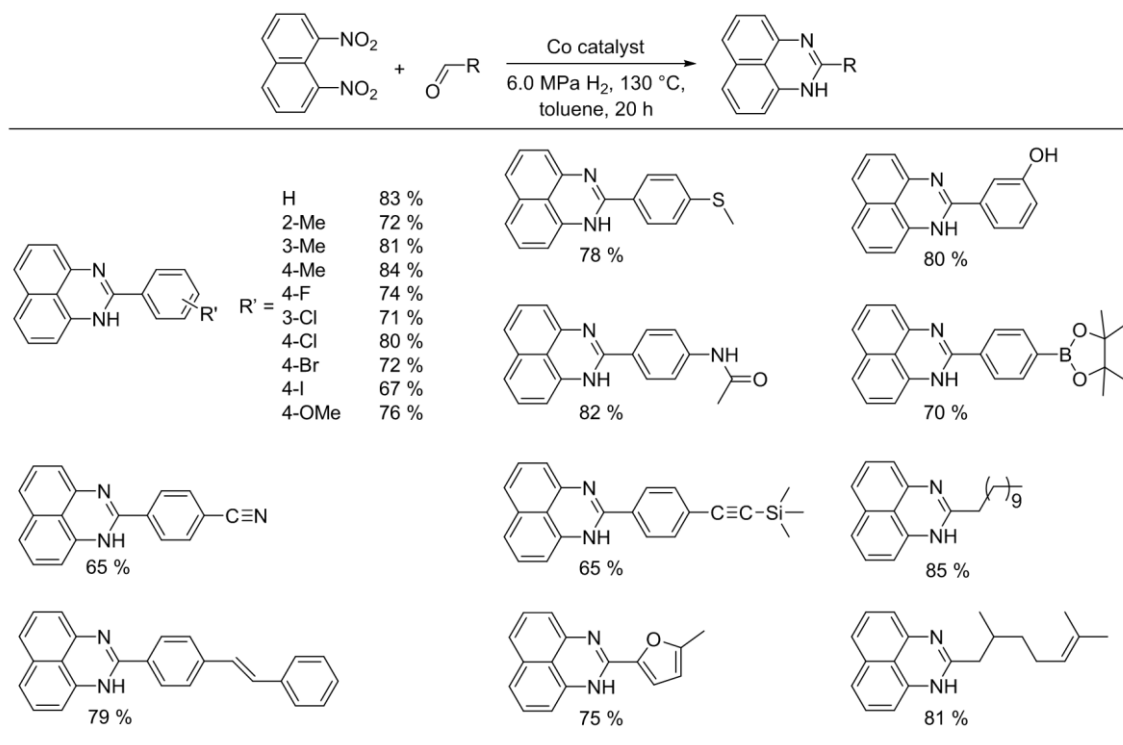


Figure 6: Selective synthesis of 1*H*-perimidines from 1,8-dinitronaphthalene and various aldehydes. Reaction conditions: 1.5 mmol nitro derivative, 1.1 eq aldehyde, 120 mg catalyst (4.7 mol% Co), 130 °C, 6.0 MPa H₂, 3 mL toluene, 20 h; yields of isolated products.

As described previously, salen-type ligands offer the possibility of the synthesis of stable heterobimetallic complexes due to the presence of two different coordination spheres. The impregnation of activated charcoal with a monometallic cobalt salen complex led to a highly active catalyst for the selective hydrogenation of nitroarenes. The third part of this thesis deals with the generation of a bimetallic catalyst system based on the impregnation of commercially available support materials with a heterobimetallic complex and the resulting changes in the catalytic properties. Consequently, a bimetallic Co-Ce salen complex was synthesized and characterized by X-ray crystallography (Figure 7A).

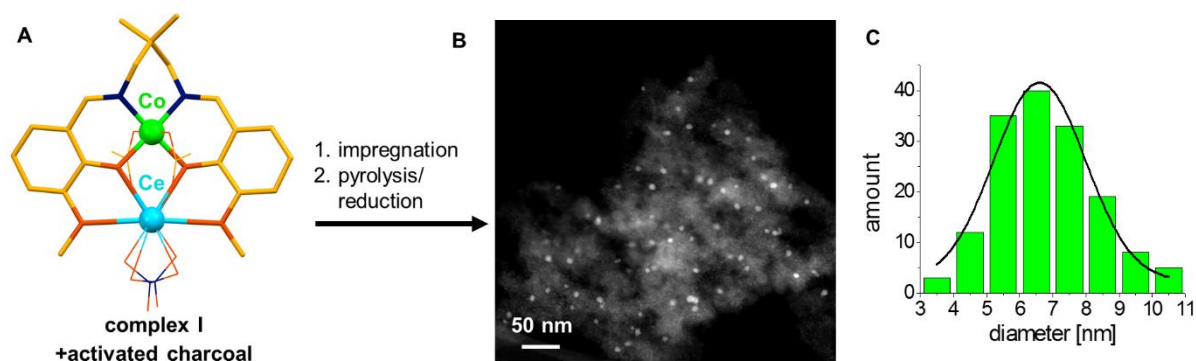


Figure 7: Synthesis of the catalyst in combination with HAADF-STEM analysis. A) Wet impregnation of commercially available charcoal with the bimetallic precursor complex I, followed by pyrolysis and reduction. B) HAADF-STEM analysis in combination with the corresponding particle size distribution (C) verified the presence of homogeneously distributed metal nanoparticles.

Regarding the synthesis of the active catalyst, commercially available activated charcoal was impregnated with the bimetallic Co-Ce complex, followed by pyrolysis at 700 °C under a nitrogen atmosphere and reduction at 550 °C under forming gas (N₂/H₂ 90/10). HAADF-STEM in combination with the corresponding particle size distribution verified the presence of a homogeneously distributed metal species over the entire catalyst sample analyzed (Figure 7B, C). The composition of the surface was analyzed by a combination of HAADF-STEM analysis and EDX measurements (Figure 8).

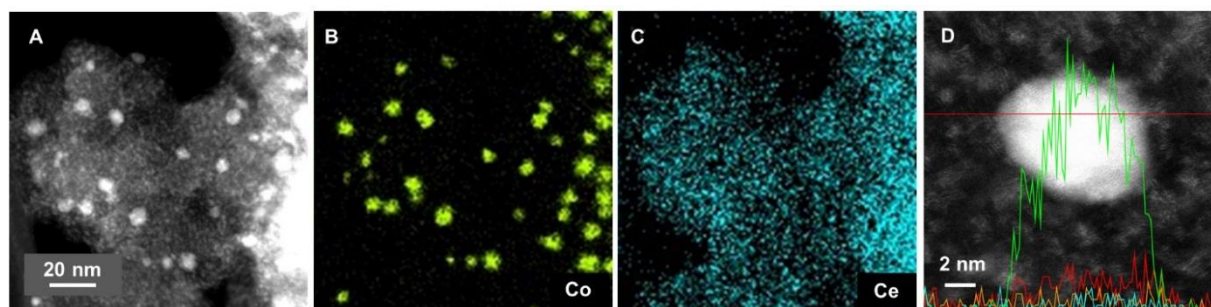


Figure 8: Characterization of the bimetallic catalyst system. A detailed HAADF-STEM of the catalyst (A) and the corresponding EDX based element maps (B, C, D) indicate that Co forms the nanoparticles while Ce is distributed over the whole carbon support (Co: green; Ce: blue; O: red; P: orange).

Detailed HAADF-STEM provided evidence of the presence of two types of nanosized species embedded in the matrix: Nanoparticles with a mean diameter of 6.8 nm and smaller (~1 nm) structures (Figure 8A). HAADF-STEM in combination with EDX-mapping revealed that Co forms the larger particles, while Ce is distributed in the matrix in the form of very small agglomerates (Figure 8B, C, D). The presence of oxygen and phosphorous can be reduced to

the use of a chemically activated carbon support. An analysis of the oxidation states of both metals was carried out by XPS analysis (Figure 9).

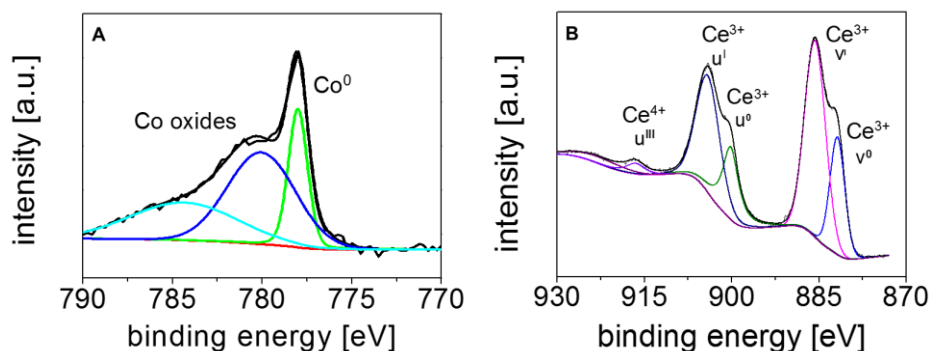
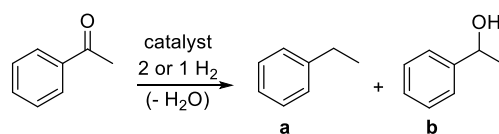


Figure 9: XPS analysis of the Co 2p_{3/2} (A) and the Ce 3d_{5/2} (B) region indicated the presence of different oxidation states for both metal species.

Analysis of the Co 2p_{3/2} region confirmed the presence of metallic cobalt species (~20 %) and oxides/hydroxides (~80 %), which cannot be distinguished definitely (Figure 9A). Cerium is present as an oxide of predominantly Ce³⁺ (~90 %) and small amounts of Ce⁴⁺ (~10 %), concluded from an analysis of the Ce 3d_{5/2} region (Figure 9B).

The hydrogenation of acetophenone was chosen for a first investigation of the catalytic properties of the bimetallic catalyst system. The introduction of a second metal species led to a significant change in the catalytic behavior. While the catalyst, which was synthesized from a monometallic cobalt salen complex, was very selective towards carbonyl compounds, the bimetallic catalyst showed a high activity in the hydrodeoxygenation of acetophenone. This cleavage of C-O bonds is a highly interesting type of reaction, since it offers the possibility of a modification of functionality-laden fine chemicals, natural products or pharmaceuticals and it is crucial for the economic upgrading of biomass-derived molecules into fuels and chemicals. The influence of the catalyst support material and different metal sources was investigated first. The results are summarized in Table 2.

Table 2: Screening of reaction parameters – catalyst screening.

Entry	Metal source	Support	Yield [%]	
			a	b
1	Bimetallic complex I	TiO ₂	62	27
2	Bimetallic complex I	CeO ₂	15	69
3	Bimetallic complex I	γ-Al ₂ O ₃	6	21
4	Bimetallic complex I	Activated charcoal	81	16
5 [§]	Bimetallic complex I	Activated charcoal	98	-
6	Co(NO ₃) ₂ + Ce(NO ₃) ₃	Activated charcoal	-	18
7 [‡]	Monometallic complex II	Activated charcoal	-	10
8 [§]	Monometallic complex III	Activated charcoal	-	-
9	Monometallic complex II + III	Activated charcoal	32	51

Reaction conditions: 0.5 mmol substrate, 15 mg catalyst (1.8 mol% Co, 1.6 mol% Ce), 100 °C, 4.0 MPa H₂, 3 mL methylcyclohexane, 20 h; [§]110 °C reaction temperature; [‡]1.8 mol% Co without Ce; [§]1.6 mol% Ce without Co; Yields were determined by GC and GC-MS using *n*-dodecane as an internal standard.

Only the combination of TiO₂ with the bimetallic complex I gave moderate yields of the product desired, while poor yields were achieved using CeO₂ and Al₂O₃ as a support (Table 2, entries 1-4). When complex I was replaced by the common metal salts Co(NO₃)₂ and Ce(NO₃)₃, no ethylbenzene formation could be detected (Table 2, entry 6). The monometallic Co complex II (essentially complex I without Ce) and the monometallic Ce complex III (essentially complex I without Co) were used for the catalyst synthesis to ensure a necessity of the bimetallic complex I. Neither the use of complex II or III nor a combination of both led to comparable hydrodeoxygenation activities (Table 2, entries 7-9). After a further optimization of the reaction conditions, the substrate scope of the hydrodeoxygenation protocol was investigated.

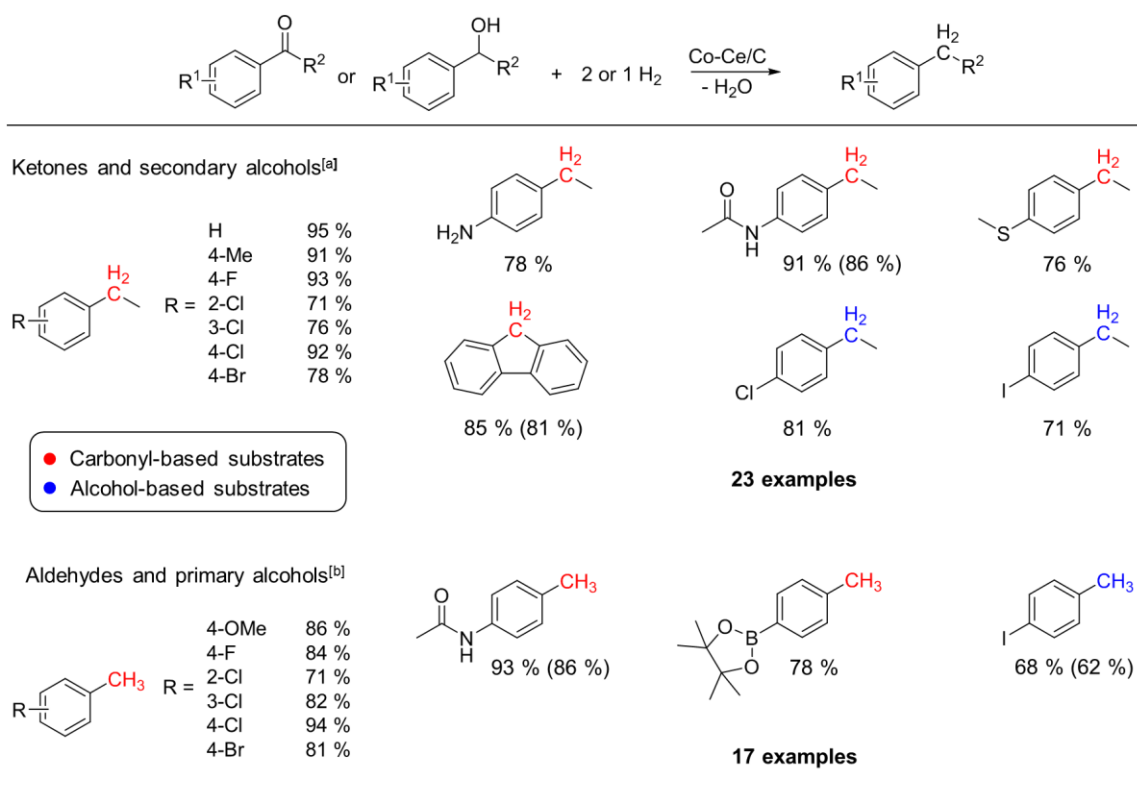


Figure 10: Representative substrate scope for the selective hydrodeoxygenation of alcohols and carbonyl compounds I. [a] Reaction conditions: 0.5 mmol substrate, 15 or 35 mg catalyst (1.8 mol% Co and 1.6 mol% Ce or 4.2 mol% Co and 3.7 mol% Ce, respectively), 110-130 °C, 5.0 MPa H₂, 3 mL methylcyclohexane, 20 h, (10 mg Amberlyst® 15 for halogenated substrates). [b] Reaction conditions: 0.5 mmol substrate, 50 mg catalyst (6.1 mol% Co, 5.2 mol% Ce), 130 °C, 6.0 MPa H₂, 3 mL methylcyclohexane, 20 h, (5 mol% Zn(OTf)₂ for halogenated substrates). Yields were determined by GC and GC-MS using *n*-dodecane as an internal standard; isolated yields in parentheses.

The hydrodeoxygenation of aromatic ketones, secondary alcohols, aldehydes and primary alcohols proceeded highly chemoselectively and functional groups, easily reduced by hydrogen in the presence of conventional catalysts, remained unaffected. Halides (including reactive iodides), ethers (including thio- and benzylethers), esters (including boronic esters), amides, phenols and *N*-heterocycles were tolerated under reaction conditions (Figure 10). The protocol could be extended by an adjustment of the reaction conditions and the hydrodeoxygenation of aliphatic and more complex substrates was accomplished. The selective removal of aromatic carbonyl and alcohol functionalities in the presence of an aliphatic alcohol group was demonstrated. The hydrodeoxygenation of complex natural products, pharmaceuticals and biomass-derived platform molecules was performed to ensure a general applicability and good to excellent yields were achieved (Figure 11).

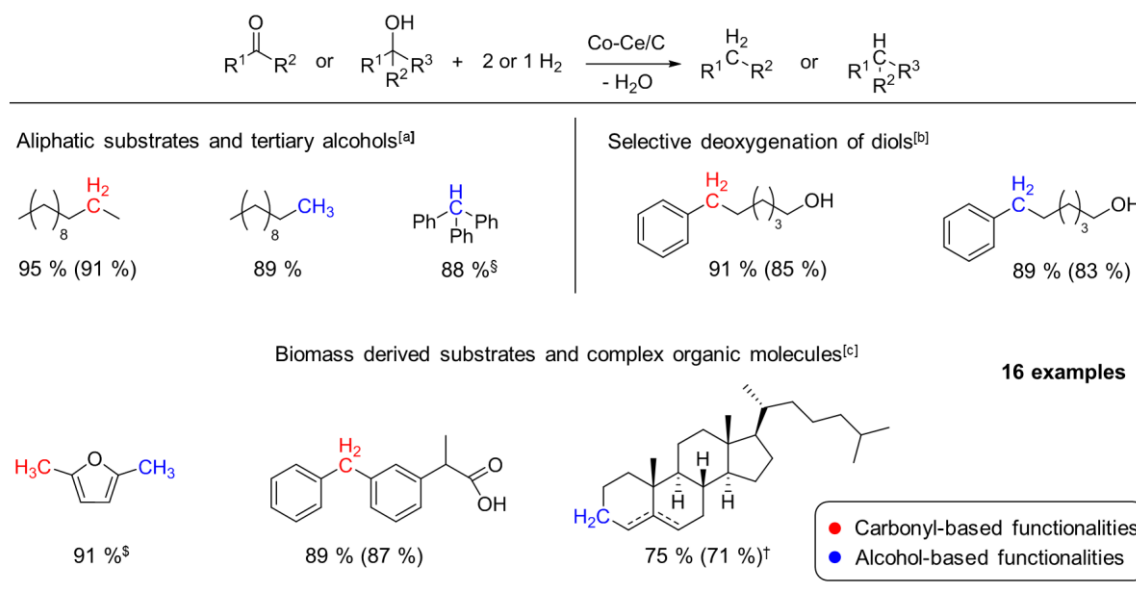


Figure 11: Representative substrate scope for the selective hydrodeoxygenation of alcohols and carbonyl compounds II. [a] Reaction conditions: 1.0 mmol substrate, 100 mg catalyst (6.1 mol% Co, 5.2 mol% Ce), 160 °C, 6.0 MPa H₂, 6 mL methylcyclohexane, 20 mg Amberlyst® 15, 20 h; §1 mmol substrate, 30 mg catalyst (1.8 mol% Co, 1.6 mol% Ce), 110 °C, 4.0 MPa H₂, 6 mL methylcyclohexane, 20 h, no additive. [b] Reaction conditions: 1.0 mmol substrate, 70 mg catalyst (4.2 mol% Co, 3.7 mol% Ce), 130 °C, 5.0 MPa H₂, 6 mL ethanol, 20 h. [c] Reaction conditions: 1.0 mmol substrate, 100 mg catalyst (6.1 mol% Co, 5.2 mol% Ce), 160 °C, 6.0 MPa H₂, 6 mL methylcyclohexane, 20 h; §diglyme was used as the solvent; †5 mol% Zn(OTf)₂ as the additive. Yields were determined by GC and GC-MS using *n*-dodecane as an internal standard. Isolated yields are given in parentheses.

Up-scaling reactions and recycling studies were carried out to prove the potential of this hydrodeoxygenation protocol. An extension of the reaction batch by a factor of 20 showed no negative influence on the product yields. Furthermore, the catalyst could be reused in five consecutive runs without a remarkable decrease in catalytic activity, which demonstrates the stability of the bimetallic system clearly.

4.2 Individual contribution to joint publications

The results presented in this thesis were obtained in collaboration with others and are published or submitted as indicated below. The contributions of all the co-authors to the respective publications are specified in the following. The corresponding author is denoted by an asterisk (*).

Chapter 5

This work is published in *Angewandte Chemie International Edition (Angew. Chem. Int. Ed.* **2016**, *55*, 15175.) with the title

“A Reusable Co Catalyst for the Selective Hydrogenation of Functionalized Nitroarenes and the Direct Synthesis of Imines and Benzimidazoles from Nitroarenes and Aldehydes”

Authors: Tobias Schwob, Rhett Kempe*

I synthesized and characterized the catalyst and carried out the catalytic reactions and the related analytics. Prof. Kempe and I designed the experiments and co-wrote the manuscript. In addition, Prof. Kempe was involved in the scientific discussions and supervised the work presented in this paper.

Chapter 6

This work is submitted to *ChemSusChem* and out for review with the title

“A Co catalyst permits the direct hydrogenative synthesis of 1*H*-perimidines from a dinitroarene and an aldehyde”

Authors: Tobias Schwob, Mirco Ade, Rhett Kempe*

I synthesized and characterized the catalyst and carried out the catalytic reactions and the related analytics. M. Ade contributed to this topic during his bachelor thesis. Prof. Kempe and I designed the experiments and co-wrote the manuscript. In addition, Prof. Kempe was involved in the scientific discussions and supervised the work presented in this paper.

Now published as:

T. Schwob, M. Ade, R. Kempe, *ChemSusChem* **2019**, *12*, 3013.

5.2 Chapter 7

This work is submitted to Science Advances and out for review with the title

“General and selective deoxygenation by hydrogen employing a reusable earth-abundant metal catalyst”

Authors: Tobias Schwob, Peter Kunnas, Niels de Jonge, Christian Papp, Hans-Peter Steinrück, Rhett Kempe*

I synthesized and characterized the catalyst and carried out the catalytic reactions and the related analytics. R. Kempe and I designed the experiments and co-wrote the manuscript. P. Kunnas and N. de Jonge performed the HAADF-STEM, EDX and EELS analyses. C. Papp and H.-P. Steinrück accomplished the XPS studies. All authors were involved in the scientific discussions. R. Kempe supervised the work and was responsible for the correction of the manuscript.

Now published as:

T. Schwob, P. Kunnas, N. de Jonge, C. Papp, H.-P. Steinrück, *Sci. Adv.* **2019**, *5*, eaav3680.

5 A Reusable Co Catalyst for the Selective Hydrogenation of Functionalized Nitroarenes and the Direct Synthesis of Imines and Benzimidazoles From Nitroarenes and Aldehydes

Tobias Schwob,^[a] and Rhett Kempe*^[a]

[a] Anorganische Chemie II, Universität Bayreuth, 95440, Bayreuth.

Published in *Angew. Chem. Int. Ed.* **2016**, *55*, 15175.

Abstract: The employment of abundantly available transition metals in reactions, which have been preferentially mediated by rare noble metals such as hydrogenations, is a desirable aim in catalysis and an attractive element conservation strategy. The observation of novel selectivity patterns with such inexpensive metal catalysts is especially appealing. Herein, we report on a novel, robust and reusable cobalt catalyst, which permits the selective hydrogenation of nitroarenes in the presence of highly hydrogenation-sensitive functional groups, as well as the direct synthesis of imines from nitroarenes and aldehydes or ketones in the presence of such substituents. Furthermore, we introduce the first base metal-mediated direct synthesis of benzimidazoles from nitroarenes and aldehydes. Functional groups that are easy to hydrogenate are again well tolerated.

5.1 Introduction

Hydrogenation reactions are of very high and continuing interest for the chemical industry and academic research.^[1] The hydrogenation of aromatic nitro compounds with reusable catalysts is the method of choice for the production of aniline derivatives, an extremely important class of compounds.^[2] Corma and coworkers reported a breakthrough with regard to the tolerance of functional groups in 2006.^[3] They applied gold catalysts and observed a selectivity of over 95 % for the hydrogenation of the nitro group in 3-nitrostyrene, 4-nitrobenzaldehyde, 4-nitrobenzotrile and 4-nitrobenzamide. Beller and coworkers have recently shown that heterogeneous catalysts based on abundantly available transition metals, such as iron^[4] and cobalt^[5] (3d-metals or base metals), can also mediate the highly selective hydrogenation of nitroarenes. The replacement of expensive and rare noble metals by base metals is a key to a

sustainable future, since it helps to preserve our element resources. The use of such abundantly available metals is especially attractive if novel selectivity patterns are observed. Herein, we report on a novel reusable and robust Co catalyst, which permits the selective hydrogenation of nitroarenes in the presence of iodo, olefin, aldehyde, ketone and nitrile functional groups. More importantly, we describe the first application of a base metal catalyst for the direct synthesis of imines from nitroarenes and aldehydes or ketones, tolerating functional groups regarded as highly hydrogenation-sensitive, such as olefins, nitriles and ketones. Furthermore, we introduce the first base metal-mediated direct synthesis of benzimidazoles from nitroarenes and aldehydes. Imines and their derivatives are an important class of compounds. They have been used extensively as ligands^[6] and because of their diverse reactivity for the synthesis of materials,^[7] fragrances, fungicides, pharmaceuticals and agricultural chemicals.^[8] Thus, the development of novel imine synthesis protocols is of high interest.^[9,10] Benzimidazoles and the development of efficient protocols permitting their synthesis are similarly important.^[11] We have recently introduced a variety of SiCN (silicon carbonitride) metal nanocomposite catalysts^[12] and have, very recently, introduced highly active homogenous 3d-metal or base metal catalysts for reactions classically mediated by expensive noble metals.^[13]

5.2 Results and Discussion

Our novel cobalt nanocomposite catalyst was synthesized in a two-step procedure. In the first step, an amidinato cobalt(II) complex (Figure 1, top left) and a commercially available polysilazane were dissolved in tetrahydrofuran (THF), followed by crosslinking using dicumylperoxide (DCP). After removal of the solvent under vacuum, the sample was pyrolyzed under a constant nitrogen flow at 750 °C. Inductively coupled plasma optical emission spectrometry (ICP-OES) measurements revealed 3.8 wt% cobalt in the pyrolyzed sample. The change from a paramagnetic behavior of the Co containing crosslinked polysilazane to superparamagnetic properties of the nanocomposite was confirmed by magnetic measurements (Figure 1, middle). This is in agreement with the presence of isolated Co²⁺ ions after crosslinking and their reduction to small metallic Co nanoparticles (NPs) during pyrolysis. The presence of small metal NPs, homogeneously distributed, was additionally verified via transmission electron microscopy (TEM; Figure 1, top right). The mean Co particle size, measured by TEM, is 1.7 nm. The Co particle size distribution is shown in Figure 1 (top right). After washing the as-synthesized Co-SiCN nanocomposite material with an aqueous basic

solution, a specific surface area of $320 \text{ m}^2\text{g}^{-1}$ (Brunauer-Emmet-Teller) was observed (Figure S1). Pore-size distribution calculations revealed a hierarchically structured Co catalyst containing micro- and mesopores. Temperature-programmed reduction (TPR) of the Co catalyst was performed next (Figure 1, bottom left). The samples were heated under a reductive atmosphere (95 % N_2 , 5 % H_2 , 5 K/min) up to $550 \text{ }^\circ\text{C}$ and held for 1 h.

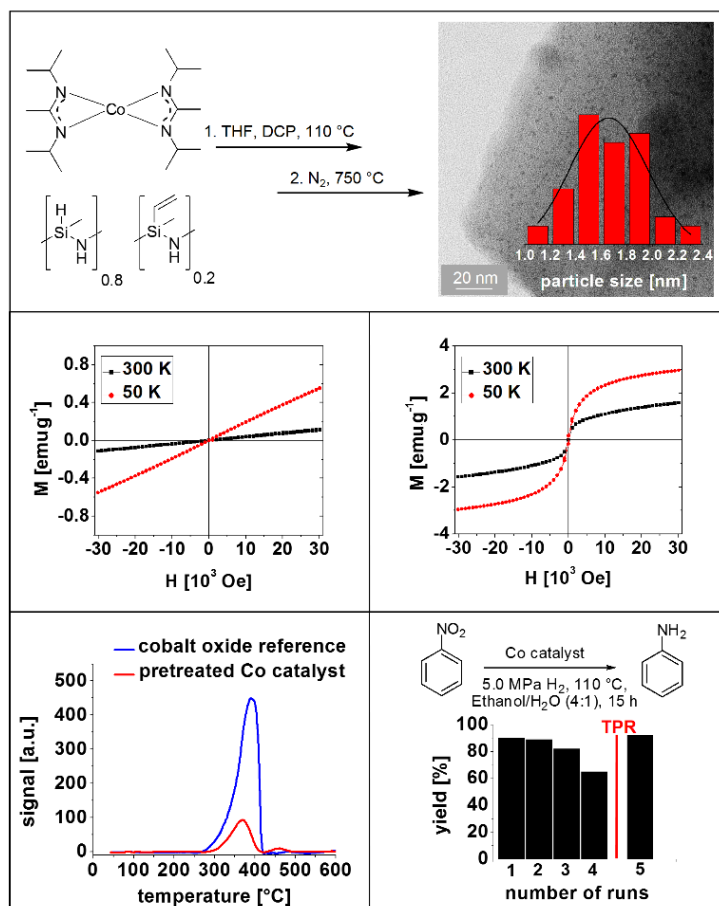


Figure 1: **Top:** Synthesis of the novel Co nanocomposite. The bisamidinato cobalt(II) complex and the commercially available polysilazane HTT 1800 were dissolved in THF, followed by crosslinking with DCP as a radical initiator at $110 \text{ }^\circ\text{C}$. Pyrolysis at $750 \text{ }^\circ\text{C}$ led to an amorphous silicon carbonitride nanocomposite. At the pyrolysis temperature of $750 \text{ }^\circ\text{C}$, the polysilazane precursor is not fully converted into a SiCN material. The presence of small cobalt nanoparticles with a homogenous particle size distribution centered at 1.7 nm was verified by TEM analysis (top right). **Middle:** Magnetic measurements confirmed the change from paramagnetic behavior of the green body (left) to superparamagnetic properties of the as-synthesized nanocomposite (right). The magnetic data are in agreement with a transition from Co^{2+} to metallic Co NP. **Bottom left:** High-temperature hydrogen treatment [temperature-programmed reduction (TPR)] was accomplished before application in catalysis; Co nanocomposite (red), cobalt oxide reference (blue). H_2 uptake between 300 and $400 \text{ }^\circ\text{C}$ indicates partial oxidation of the NP during the washing procedure. **Bottom right:** Recycling of the Co catalyst. Activity could easily be regained by TPR treatment.

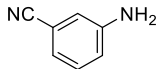
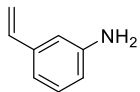
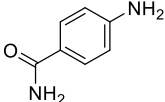
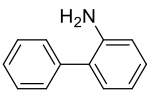
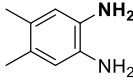
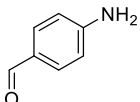
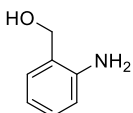
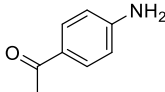
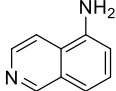
Comparison to a cobalt oxide reference sample indicates the presence of reducible cobalt oxide species in the Co catalyst. The as-synthesized Co-SiCN nanocomposite showed no TPR signal

in this region, indicating a partial oxidation of the Co NP during the washing procedure. X-ray photoelectron spectroscopy (XPS) data are in accordance with this observation (Figure S6). The hydrogenation of nitrobenzene was chosen as a test reaction to optimize the performance of our Co catalyst in the reduction of nitroarenes and to demonstrate its reusability. The following reaction conditions were found to be optimal: a 4:1 ethanol/water mixture under 5.0 MPa hydrogen pressure at 110 °C. Our cobalt catalyst showed a slight decrease in the catalytic activity up to the third run and a significant decline in the fourth run (Figure 1, bottom right). However, leaching experiments demonstrated that only 0.05 % of the total amount of Co leached out during catalysis. To our delight, catalytic activity could easily be regained by TPR treatment (Figure 1, bottom left). This method also indicates complete reduction of the Co oxide species. The Co catalyst was reactivated up to five times without any remarkable decrease in catalytic activity and with only a slight increase of the Co particle size (Figure S14). With the optimized conditions in hand, we were interested in the nitroarene hydrogenation substrate scope of our novel catalyst. Halogenated substrates, such as chlorides and bromides, were smoothly converted into the corresponding anilines (Table 1; Entry 2-7), only 1-iodo-4-nitrobenzene (Table 1; Entry 8) showed traces of dehalogenated product. In addition, different reducible functional groups, for example, nitrile, keto, aldehyde, amide and even vinyl groups were successfully tolerated (Table 1; Entry 9-11, 14, 16). The tolerance towards the aldehyde group is especially interesting in light of the many known Co catalysts able to hydrogenate C=O bonds.^[13a,14] The hydrogenation of sterically demanding nitroarenes (Table 1; Entry 12, 13) required a slight increase in the catalyst loading to ensure high conversions under the optimized conditions.

Table 1: Chemoselective hydrogenation of substituted nitroarenes: substrate scope.^[a]

Entry	Product	Yield ^[b] [%]
1	R = H	>99
2	R = 2-Cl	92
3	R = 3-Cl	96
4	R = 4-Cl	>99
5	R = 2-Br	90
6	R = 3-Br	>99
7	R = 4-Br	>99
8	R = 4-I	76

Table 1: Continued

9		>99
10		82
11		>99
12		84 ^[c]
13		87 ^[c]
14		>99
15		91
16		>99
17		>99

[a] Reaction conditions: 110 °C, 5.0 MPa H₂, 4.8 mol% catalyst (1.4 mg Co, 0.024 mmol, 35 mg), 2 mL ethanol, 0.5 mL H₂O, 15 h. [b] Yields were determined by GC using *n*-dodecane as an internal standard. [c] 6 mol% catalyst.

Next, we were interested in catalytic transformations that include a nitroarene hydrogenation step and identified the direct synthesis of imines from nitroarenes and aldehydes or ketones as an interesting application. The reductive coupling of nitrobenzene with benzaldehyde was chosen as the benchmark reaction to find the optimal reaction conditions. Interestingly, the hydrogenation of benzaldehyde (alone) under our reaction conditions gave about 14 % conversion. If nitrobenzene is added, no aldehyde hydrogenation product could be detected (Figure S12). The reductive coupling of various aromatic aldehydes and nitroarenes was investigated to demonstrate the general applicability. Halogenated substrates (Table 2; Entry 1c, 1d; 3a-c) gave the corresponding imines with 71-87 % isolated yields. The use of sterically more demanding aldehydes had no negative effect on the catalytic results (Table 2; Entry 2a,

2b, 3e). 5-nitroisochinoline was coupled with benzaldehyde in 76 % yield for the generation of an N-heterocyclic imine (Table 2; Entry 4).

Table 2: Selective synthesis of substituted imines: substrate scope.^[a]

Entry	Product	Yield ^[b] [%]
1	1a: R = H	82
	1b: R = Me	74
	1c: R = F	87
	1d: R = Cl	81
2	2a: R ¹ = OH, R ² = OMe, R ³ = H	86
	2b: R ¹ = OH, R ² = <i>t</i> Bu, R ³ = <i>t</i> Bu	91
3	3a: R = 3-Cl	71
	3b: R = 4-Cl	82
	3c: R = 4-Br	86
	3d: R = 3-CN	70
3e: R = 2-Ph	74	
4		76
5	5a: R ¹ = OH, R ² = <i>t</i> Bu, R ³ = <i>t</i> Bu, R ⁴ = CN, R ⁵ = H	86
	5b: R ¹ = OH, R ² = <i>t</i> Bu, R ³ = <i>t</i> Bu, R ⁴ = vinyl, R ⁵ = H	82
6		79
7	7a: R ¹ / R ² = H	75
	7b: R ¹ = H, R ² = Cl	71
	7c: R ¹ / R ² = Me	78
8	8a: R ¹ = Br, R ² = H	67
	8b: R ¹ = H, R ² = Me	72

[a] Reaction conditions: R''=H: 110 °C, 5.0 MPa H₂, 1.5 mmol nitroarene, 3.0 mmol aldehyde, 5.0 mol% catalyst (4.4 mg Co, 0.075 mmol, 110 mg), 4 mL triethylamine, 24 h. R''=Me: 115 °C, 5.0 MPa H₂, 1.5 mmol nitroarene, 3.0 mmol ketone, 8.0 mol% catalyst (7.0 mg Co, 0.119 mmol, 175 mg), 10 mg Amberlyst[®] 15, molsieves, 4 mL toluene, 48 h. [b] Overall yields of isolated products.

Keto, nitrile and even vinyl functionalities were tolerated and the corresponding products were obtained in 70-86 % isolated yields (Table 2; 3d, 5a, 5b, 6). Imine formation with ketones proceeds well under slightly harsher conditions (Table 2, Entry: 7a-c, 8a,b). Finally, we investigated the direct synthesis of benzimidazoles from nitroarenes and aldehydes. 4,5-dimethyl-2-nitro-aniline was coupled with benzaldehyde as the test reaction. The product 5,6-dimethyl-2-phenyl-1*H*-benzo[d]imidazole was obtained in excellent isolated yield under optimized reaction conditions (Table 3; Entry 1a). The introduction of halide substituents (Table 3; Entry 1b, 1d) or a heterocyclic aldehyde (Table 3; Entry 2) gave similarly good outcomes. Reductive coupling using aliphatic aldehyde compounds is more challenging, however, the use of n-heptanal gave the desired product in 68 % yield. Benzimidazoles containing functional groups, such as double bonds or nitrile groups could also be synthesized (Table 3; Entry 1e, 4).

Table 3. Synthesis of benzimidazoles – substrate scope ^[a]

Entry	Product	Yield ^[b] [%]
1	1a: R' = H 1b: R' = 4-F 1c: R' = 4-OMe 1d: R' = 3-Cl 1e: R' = 4-CN	91 87 81 79 72
2		84
3		71
4		68

[a] Reaction conditions: 110 °C, 5.0 MPa H₂, 1.5 mmol nitroarene, 3.0 mmol aldehyde, 5.0 mol% catalyst (4.4 mg Co, 0.075 mmol, 110 mg), 4 mL triethylamine, 24 h. [b] Overall yields of isolated products.

In conclusion, we developed a novel Co nanocomposite catalyst for the highly selective hydrogenation of functionalized nitroarenes. The catalyst is easy to synthesize in a two-step procedure, can be handled and stored under air and its hydrogenation activity can be regained via hydrogen treatment at around 400 °C. The catalyst mediates the selective direct synthesis of imines from nitroarenes and aldehydes or ketones through hydrogenation. This is the first such reaction in which functional groups that are easy to hydrogenate are tolerated, and also the

first base-metal catalyst that can successfully be applied to the direct synthesis of benzimidazoles from aromatic nitro compounds and aldehydes. We expect a broad applicability for reusable and robust base or 3d metal catalysts as introduced here in direct reductive syntheses, based on the tolerance towards hydrogenation-sensitive functional groups.

5.3 Acknowledgements

We thank the Deutsche Forschungsgemeinschaft, SFB 840, project B1, for financial support, Katja Dankhoff and Prof. Dr Birgit Weber for magnetic measurements and Max Männel for XPS analysis.

Keywords: benzimidazoles • catalysis • cobalt • hydrogenation • nitroarenes • imines

5.4 References

- [1] B. Cornils, W. A. Hermann, R. Schlögle, C.H. Wong (Eds.), *Catalysis from A to Z* 2nd edition, Wiley-VCH, Weinheim, **2002**.
- [2] H.-U. Blaser, H. Steiner, M. Studer, *ChemCatChem*. **2009**, *1*, 210-221.
- [3] a) A. Corma, P. Serna, P. Concepcion, J. J. Calvino, *J. Am. Chem. Soc.* **2008**, *130*, 8748-8753; b) A. Corma, P. Serna, *Science* **2006**, *313*, 332-334.
- [4] a) R. V. Jagadeesh, A.-E. Surkus, H. Junge, M.-M. Pohl, J. Radnik, J. Rabeah, H. Huan, V. Schunemann, A. Bruckner, M. Beller, *Science* **2013**, *342*, 1073-1076; b) R. V. Jagadeesh, T. Stemmler, A.-E. Surkus, H. Junge, K. Junge, M. Beller, *Nat. Protoc.* **2015**, *10*, 548-557; For a recent example of the reduction using hydrazine, please see: a) Y. Li, Y.-X. Zhou, X. Ma, H.-L. Jiang, *Chem. Commun.* **2016**, *52*, 4199-4202.
- [5] a) F. A. Westerhaus, R. V. Jagadeesh, G. Wienhofer, M.-M. Pohl, J. Radnik, A.-E. Surkus, J. Rabeah, K. Junge, H. Junge, M. Nielsen, A. Brückner, M. Beller, *Nat. Chem.* **2013**, *5*, 537-543; b) R. V. Jagadeesh, T. Stemmler, A.-E. Surkus, M. Bauer, M.-M. Pohl, J. Radnik, K. Junge, H. Junge, A. Bruckner, M. Beller, *Nat. Protoc.* **2015**, *10*, 916-926; For further examples of highly selective Co nitroarene hydrogenation catalysts, please see: c) Z. Wei, J. Wang, S. Mao, D. Su, H. Jin, Y. Wang, F. Xu, H. Li, Y. Wang,

- ACS Catal.* **2015**, *5*, 4783-4789; d) L. Liu, P. Concepción, A. Corma, *J. Catal.* **2016**, *340*, 1-9; e) B. Chen, F. Li, Z. Huang, G. Yuan, *ChemCatChem.* **2016**, *8*, 1132-1138.
- [6] V. C. Gibson, S. K. Spitzmesser, *Chem. Rev.* **2003**, *103*, 283-315.
- [7] A. W. Bosman, H. M. Janssen, E. W. Meijer, *Chem. Rev.* **1999**, *99*, 1665-1688.
- [8] D. J. Hadjipavlou-Litina, A. A. Geronikaki, *Drug Des. Discov.* **1998**, *15*, 199-206.
- [9] For selected examples of catalytic imine syntheses, please see: (oxidation of amines) a) H. Yuan, W.-J. Yoo, H. Miyamura, S. Kobayashi, *J. Am. Chem. Soc.* **2012**, *134*, 13970-13973; b) T. Sonobe, K. Oisaki, M. Kanai, *Chem. Sci.* **2012**, *3*, 3249-3255. (self-condensation of primary amines upon oxidation) a) B. Chen, L. Wang, S. Gao, *ACS Catal.* **2015**, *5*, 5851-5876; b) B. Chen, L. Wang, W. Dai, S. Shang, Y. Lv, S. Gao, *ACS Catal.* **2015**, *5*, 2788-2794; c) F. Su, S. C. Mathew, L. Mohlmann, M. Antonietti, X. Wang, S. Blechert, *Angew. Chem. Int. Ed.* **2011**, *50*, 657-660. (oxidative coupling of alcohols and amines) a) M. Tamura, K. Tomishige, *Angew. Chem. Int. Ed.* **2015**, *54*, 864-867. (acceptorless dehydrogenative coupling of alcohols and amines) a) A. Mukherjee, A. Nerush, G. Leitus, L. J. W. Shimon, Y. Ben David, N. A. Espinosa Jalapa, D. Milstein, *J. Am. Chem. Soc.* **2016**, *138*, 4298-4301; b) M. Mastalir, M. Glatz, N. Gorgas, B. Stoger, E. Pittenauer, G. Allmaier, L. Veiros, K. Kirchner, *Chem. Eur. J.* **2016**, *22*, 12316-12320; c) J. Bain, P. Cho, A. Voutchkova-Kostal, *Green Chem.* **2015**, *17*, 2271-2280; d) S. Ruch, T. Irrgang, R. Kempe, *Chem. Eur. J.* **2014**, *20*, 13279-13285; e) B. Gnanaprakasam, J. Zhang, D. Milstein, *Angew. Chem. Int. Ed.* **2010**, *122*, 1510-1513.
- [10] For selected examples for the reductive synthesis of imines from nitroarenes and aldehydes, please see: a) Y.-Z. Chen, Y.-X. Zhou, H. Wang, J. Lu, T. Uchida, Q. Xu, S.-H. Yu, H.-L. Jiang, *ACS Catal.* **2015**, *5*, 2062-2069; b) F. G. Cirujano, A. Leyva-Pérez, A. Corma, F. X. Llabrés i Xamena, *ChemCatChem.* **2013**, *5*, 538-549; c) L. L. Santos, P. Serna, A. Corma, *Chem. Eur. J.* **2009**, *15*, 8196-8203; d) Y. Zheng, K. Ma, H. Li, J. Li, J. He, X. Sun, R. Li, J. Ma, *Catal. Lett.* **2009**, *128*, 465-474.
- [11] Selected examples of recent publications reporting catalytic syntheses of benzimidazoles: a) D. Mahesh, P. Sadhu, T. Punniyamurthy, *J. Org. Chem.* **2016**, *81*, 3227-3234; b) C. Xu, Z.-Q. Xiao, H.-M. Li, X. Han, Z.-Q. Wang, W.-J. Fu, B.-M. Ji, X.-Q. Hao, M.-P. Song, *Eur. J. Org. Chem.* **2015**, *2015*, 7427-7432; c) C. Chaudhari, S. H. Siddiki, K.-i. Shimizu, *Tetrahedron Lett.* **2015**, *56*, 4885-4888; d) Z. Sun, G.

- Bottari, K. Barta, *Green Chem.* **2015**, *17*, 5172-5181; e) T. Hille, T. Irrgang, R. Kempe, *Chem. Eur. J.* **2014**, *20*, 5569-5572; f) N. T. Jui, S. L. Buchwald, *Angew. Chem. Int. Ed.* **2013**, *52*, 11624-11627; g) K. Bahrami, M. M. Khodaei, A. Nejati, *Green Chem.* **2013**, *12*, 1237-1241; h) T. B. Nguyen, L. Ermolenko, A. Al-Mourabit, *J. Am. Chem. Soc.* **2013**, *135*, 118-121.
- [12] a) D. Forberg, T. Schwob, M. Zaheer, M. Friedrich, N. Miyajima, R. Kempe, *Nature Commun.* **2016**, DOI: 10.1038/ncomms13201. b) S. Sachau, M. Zaheer, A. Lale, M. Friedrich, C. Denner, U. B. Demirci, S. Bernard, G. Motz, R. Kempe, *Chem. Eur. J.* **2016**, *43*, 15508-15512; c) G. Hahn, J.-K. Ewert, C. Denner, D. Tilgner, R. Kempe, *ChemCatChem* **2016**, *8*, 2461-2465; d) J.-K. Ewert, D. Weingarh, C. Denner, M. Friedrich, M. Zeiger, A. Schreiber, N. Jäckel, V. Presser, R. Kempe, *J. Mater. Chem. A* **2015**, *3*, 18906-18912; e) M. Zaheer, J. Hermannsdörfer, W. P. Kretschmer, G. Motz, R. Kempe, *ChemCatChem* **2014**, *6*, 91-95; f) D. Forberg, J. Obenauf, M. Friedrich, S.-M. Hühne, W. Mader, G. Motz, R. Kempe, *Catal. Sci. Technol.* **2014**, *4*, 4188-4192; g) M. Zaheer, T. Schmalz, G. Motz, R. Kempe, *Chem. Soc. Rev.* **2012**, *41*, 5102-5116.
- [13] a) S. Rösler, J. Obenauf, R. Kempe, *J. Am. Chem. Soc.* **2015**, *137*, 7998-8001; b) S. Rösler, M. Ertl, T. Irrgang, R. Kempe, *Angew. Chem. Int. Ed.* **2015**, *54*, 15046-15050; *Angew. Chem.* **2015**, *127*, 15260-15264 c) F. Kallmeier, T. Irrgang, T. Dietel, R. Kempe, *Angew. Chem. Int. Ed.* **2016**, *55*, 11806-11809; *Angew. Chem.* **2016**, *128*, 11984-11989; d) N. Deibl, R. Kempe, *J. Am. Chem. Soc.* **2016**, *138*, 10786-10789.
- [14] Selected examples of homogenous catalysts: D. Srimani, A. Mukherjee, A. F. G. Goldberg, G. Leitius, Y. Diskin-Posner, L. J. W. Shimon, Y. Ben David, D. Milstein, *Angew. Chem. Int. Ed.* **2015**, *54*, 12357-12360; b) T. J. Korstanje, J. I. van der Vlugt, C. J. Elsevier, B. de Bruin, *Science* **2015**, *350*, 298-302; c) D. Gärtner, A. Welther, B. R. Rad, R. Wolf, A. Jacobi von Wangelin, *Angew. Chem. Int. Ed.* **2014**, *53*, 3722-3726; d) G. Zhang, K. V. Vasudevan, B. L. Scott, S. K. Hanson, *J. Am. Chem. Soc.* **2013**, *135*, 8668-8681; e) G. Zhang, B. L. Scott, S. K. Hanson, *Angew. Chem. Int. Ed.* **2012**, *124*, 12268-12272. Selected examples of heterogeneous catalysts: F. Chen, C. Topf, J. Radnik, C. Kreyenschulte, H. Lund, M. Schneider, A.-E. Surkus, L. He, K. Junge, M. Beller, *J. Am. Chem. Soc.* **2016**, *138*, 8781-8788; b) C. Ando, H. Kurokawa, H. Miura, *Appl. Catal. A* **1999**, *185*, L181-L183; c) Y. Nitta, K. Ueno, T. Imanaka, *Appl. Catal.* **1989**, *56*, 9-22.

5.5 Supplementary Information

General Considerations

Air- and moisture sensitive reactions were carried out under dry argon or nitrogen atmosphere using standard Schlenk or glove box techniques. Dry solvents were obtained from a solvent purification system (activated alumina cartridges) or purchased from Acros. Chemicals were purchased from commercial sources with purity over 95 % and used without further purification. Polysilazane “KiON HTT 1800” was purchased from Clariant Advanced Materials GmbH, Frankfurt (Germany) and used without further purification. NMR spectra were received using a Varian INOVA 300 (300 MHz for ^1H , 75 MHz for ^{13}C) at 296 K. Chemical shifts are reported in ppm relative to the residual solvent signal (CDCl_3 : 7.26 ppm (^1H), 77.16 ppm (^{13}C); DMSO-d_6 : 2.50 ppm (^1H), 39.51 ppm (^{13}C)), coupling constants (J) are reported in Hz. Elemental analysis was performed on an Elementar Vario El *III*. GC analyses were carried out on an Agilent 6890N Network GC system equipped with a HP-5 column (30 m x 0.32 mm x 0.25 μm). GC-MS analyses were carried out on an Agilent 7890A GC system equipped with a HP-5MS column (30 m x 0.32 mm x 0.25 μm) and a 5975C inert MSD detector. High resolution mass spectra (HRMS) were obtained from a Thermo Fisher Scientific Q-Exactive (Orbitrap) instrument in ESI+ mode. Ceramization was carried out under nitrogen atmosphere in a high temperature furnace (Gero, Berlin, Germany). Transmission electron microscopy (TEM) was carried out by using a LEO 922o (200 kV) instrument. The sample was suspended in chloroform and sonicated for 5 min. Subsequently a drop of the suspended sample was placed on a CF200-Cu grid and allowed to dry. Energy dispersive X-ray spectroscopy (EDX) measurements were carried out by using a LEO 1530 GEMINI. The acceleration voltage was 1-5 kV. ICP-OES measurements were carried out by using a Vista-pro radical model from Varian. N_2 sorption measurements were carried out using a Nova2000e (Quantachrome). The specific surface areas were calculated using p/p_0 values from 0.05-0.31 (BET). The pore width and average pore volume were calculated by DFT calculations [calculation model: N_2 at -196.15 $^\circ\text{C}$ on carbon (slit pore, NLDFE equilibrium model)]. Hydrogen chemisorption measurements were carried out by using a ChemBET Pulsar TPR/TPD instrument from Quantachrome. Magnetic measurements of the compounds were carried out using a SQUID MPMS-XL5 from Quantum Design with the field range of -3 to 3 T in hysteresis mode. The sample was prepared in a gelatine capsule held in a plastic straw under protective atmosphere. The raw data were corrected for the diamagnetic part of the sample holder. X-ray photoelectron spectroscopy (XPS) studies were carried out by means of an Axis Ultra photoelectron spectrometer (Kratos

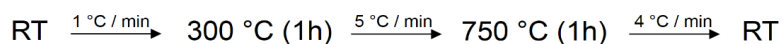
Analytical, Manchester, UK). The spectrometer was equipped with a monochromatic Al K α (h ν = 1486.6 eV) X-ray source of 300 W at 15 kV. The kinetic energy of photoelectrons was determined with hemispheric analyzer set to pass energy of 160 eV for wide-scan spectra and 20 eV for high-resolution spectra. During all measurements, electrostatic charging of the sample was avoided by means of a low-energy electron source working in combination with a magnetic immersion lens. Milling of the catalyst was performed in a ball mill "Pulverisette 0" (Fritsch, Germany) for 15 min.

Synthesis and characterization of the Co nanocomposite catalyst

The bisamidinato cobalt (II) complex was synthesized according to a known literature procedure^[1].

Ceramization

Under vigorous stirring 0.243 g (280 μ L) HTT 1800 was added drop wise to a solution of 64 mg (0.188 mmol) bisamidinato cobalt(II) complex and 12 mg dicumylperoxide (5 wt.-% HTT 1800) in 1 mL tetrahydrofuran. The sample was cross-linked at 110 °C for 24 h. After removal of the solvent, the brown-black solid was pyrolyzed under N₂ atmosphere with the following heating program:



The ceramic yield was 75 %. After ball milling for 15 minutes, 300 mg catalyst were washed by stirring in an aqueous solution of 5 mL NaOH (c = 1 mol/l) and 1 mL MeOH at 60 °C for 12 h under aerobic conditions.

ICP-OES Analysis

25 mg of the sample were solved in 1.5 mL HNO₃ (65 %, distilled), 4.5 mL HCl (32 %, p.a.) and 1 mL HF (40 %) and heated in the microwave at 170 °C for 7 min (80 % power), at 180 °C for 7 min (85 % power) and at 195 °C for 20 min (90 % power).

Results:

as synthesized: 3.8 wt% Co

after washing procedure: 4.0 wt% Co

Leaching experiment: A mixture of 35 mg Co catalyst, 2 mL ethanol and 0.5 mL H₂O were stirred at 110 °C and 50 bar H₂ pressure for 20 hours. The catalyst was removed and the resulting solution was analyzed by ICP-OES. 0.05 % of the total Co amount were found.

N₂ sorption

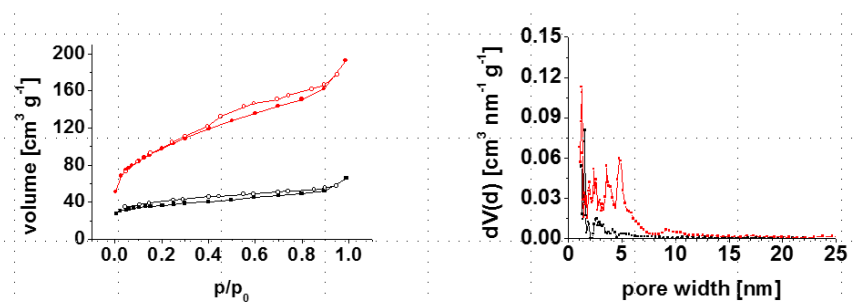


Figure S1: Nitrogen sorption measurements of the Co nanocomposite before (black) and after (red) the washing process. Pore characterization (calculation model: N₂ at 77 K on carbon; slit pore, NLDFT equilibrium model) indicates an increase of the surface area in combination with a growth of the average pore width.

The BET surface area was calculated to be 115 m² for the as synthesized Co nanocomposite and 320 m² after pretreatment in basic solution.

TEM analysis

Figure S2 shows the homogeneous distribution of the Co nanoparticles in the amorphous SiCN matrix.

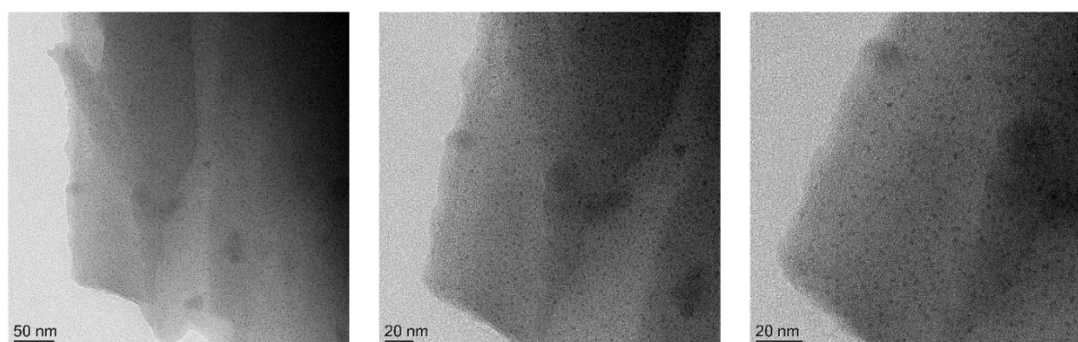


Figure S2: TEM analysis of the cobalt nanocomposite catalyst pyrolyzed at 750 °C.

The size of the cobalt nanoparticles was determined with the program “ImageJ”. The mean particle diameter is 1.6 nm (Figure S3).

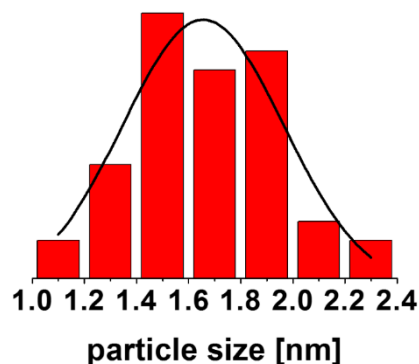


Figure S3: Histogram of the measured cobalt nanoparticles.

Energy dispersive X-ray analysis

To get an insight in the chemical composition of the catalyst surface, EDX analysis was accomplished. Besides the elements silicon, carbon and nitrogen, which can be assigned so the ceramic precursor, cobalt and oxygen could also be identified. The amount of oxygen is presumably reduced to the radical initiator (DCP) used for the cross-linking process.

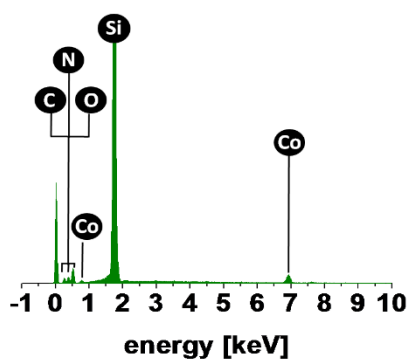


Figure S4: Energy dispersive X-ray analysis of the catalyst surface.

Temperature programmed reduction

TPR analysis was performed, after washing of the catalyst with aqueous basic solution. The sample was heated up to 550 °C with 5 K/min under reductive atmosphere (95 % N₂, 5 % H₂). Afterwards, the sample was cooled to room temperature (20 K/min) and the procedure was accomplished again.

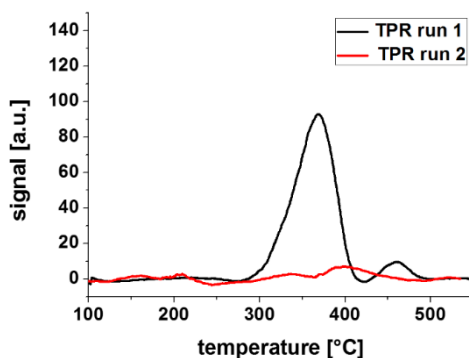


Figure S5: Temperature programmed reduction of the washed Co nanocomposite.

When temperature programmed reduction is accomplished for the first time, the broad signal between 300 and 400 °C indicates the presence of reducible cobalt species on the catalyst surface (black curve). When the procedure is carried out again (red curve) after cooling down without air contact, no signal is observed, indicating the complete reduction of cobalt oxide species on the catalyst surface.

X-ray photoelectron spectroscopy

Figure S6 shows the XPS spectra the Co 2p region of the washed catalyst.

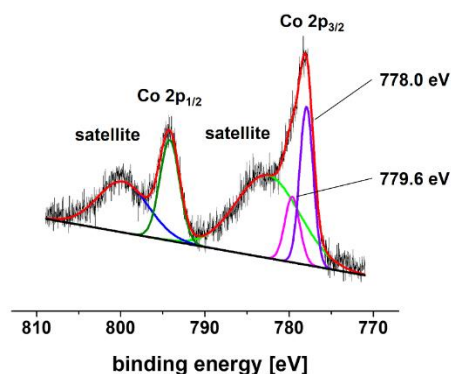


Figure S6: XPS spectra of the washed Co nanocomposite catalyst.

The Co 2p_{3/2} signal can be divided in two minor signals with binding energies of 778.0 and 779.6 eV. In combination with the broad satellite at 783.0 eV, this indicates the presence of elemental cobalt and Co²⁺ species. This is in good agreement with the TPR analysis, where a reduction peak at 360 °C could be identified (Figure S5).

Variation of the pyrolysis temperature

900 °C

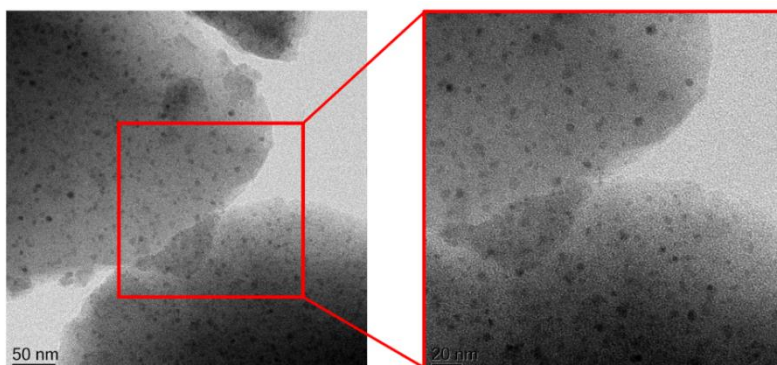


Figure S7: TEM analysis of the cobalt nanocomposite catalyst pyrolyzed at 900 °C.

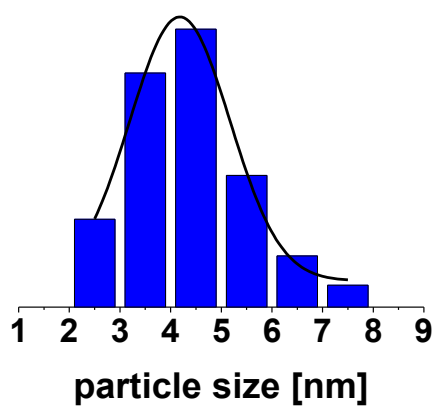


Figure S8: Histogram of the measured cobalt nanoparticles of the 900 °C material.

1000°C

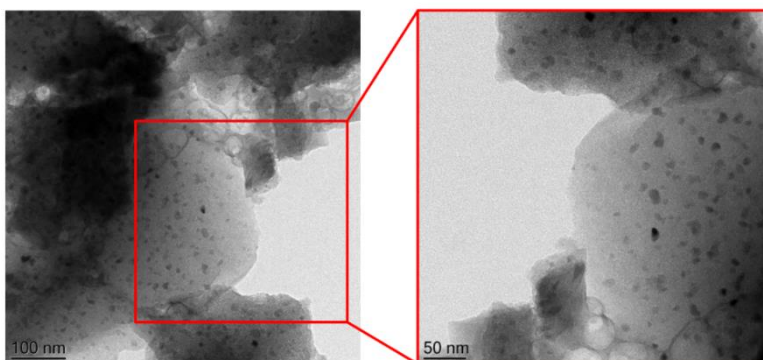


Figure S9: TEM analysis of the cobalt nanocomposite catalyst pyrolyzed at 1000 °C.

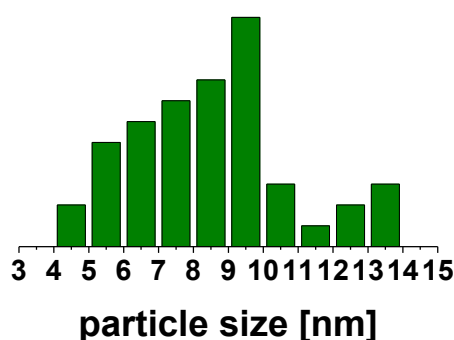


Figure S10: Histogram of the measured cobalt nanoparticles of the 1000 °C material.

Higher pyrolysis temperatures led to an increase in the mean particle size and a significant decrease in the specific surface area, which is conterminous with poorer catalytic results.

Catalytic studies

Screening experiments

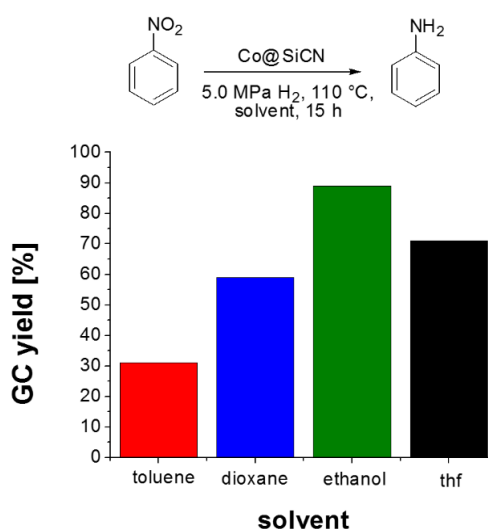


Figure S11: Selective hydrogenation of nitroarenes – solvent screening. Reaction conditions: 110 °C, 5.0 MPa H₂, 4.8 mol% catalyst (1.4 mg Co, 0.024 mmol, 35 mg), 2 mL solvent, 15 h.

Table S3: Selective hydrogenation of nitroarenes – optimization of reaction conditions.

Entry	catalyst loading [mol%]	temperature [°C]	pressure [bar]	GC yield [%]
1	5	110	50	>99
2	4	110	50	83

3	5	100	50	88
4	5	90	50	60
5	5	110	40	86

The novel cobalt nanocomposite catalyst showed a significant better performance in polar solvents. The addition of small amounts of water led to a slight increase in the catalytic performance. 5.0 MPa hydrogen pressure, 110 °C, 4.8 mol% cobalt, 0.5 mmol substrate and a solvent mixture of ethanol/water (4:1) was found to be optimal. For the reductive imination of nitroarenes, hydrogen pressure and temperature remained unchanged, while triethylamine (TEA) was used as the solvent. Furthermore, the reaction time was prolonged to 24 hours. Reductive coupling with ketones instead of aldehydes proceeded well, using toluene as the solvent with addition of molecular sieves and Amberlyst® 15. To overcome the lower activity in nonpolar solvents, the reaction conditions were adjusted (8.0 mol% catalyst, 115 °C, 48 h).

Benzaldehyde hydrogenation

The novel Co nanocomposite catalyst was tested in the hydrogenation of benzaldehyde. A 5 mL reaction vial was charged with a magnetic stirring bar, 0.5 mmol benzaldehyde, 35 mg catalyst (1.4 mg Co, 0.024 mmol, 4.8 mol%), 2 mL ethanol and 0.5 mL H₂O. The vial was placed in a high-pressure autoclave (Parr Instruments) and the autoclave was flushed three times with 20 bar of hydrogen. The autoclave was pressured with 50 bar of hydrogen and the reaction was stirred for 24 h at 110 °C. In a second experiment the temperature was increased to 120 °C. After 24 h the autoclave was cooled to room temperature and the hydrogen pressure was released. Yields were determined by GC and GC-MS using *n*-dodecane as an internal standard.

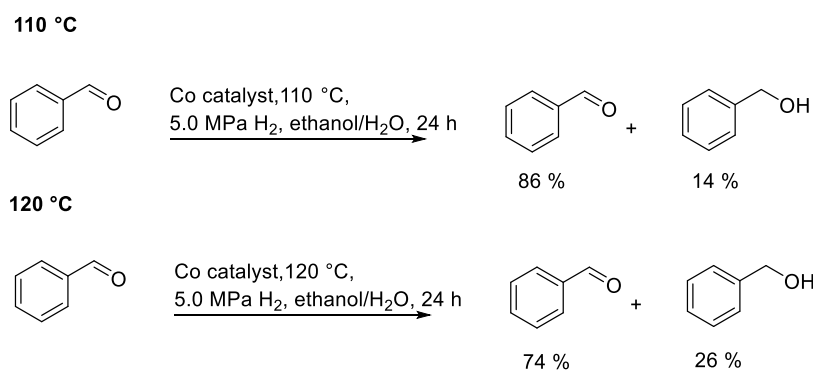


Figure S12: Product distribution for the hydrogenation of sole benzaldehyde.

In both cases, hydrogenation of benzaldehyde took place. While 14 % of benzyl alcohol could be detected at a reaction temperature of 110 °C, the amount of the hydrogenation product increased to 26 % when the reaction is performed at 120 °C. To investigate the influence of the nitro compound, further studies were accomplished. The reactions were repeated as described above, but in this case 0.5 mmol nitrobenzene were added to the reaction mixture.

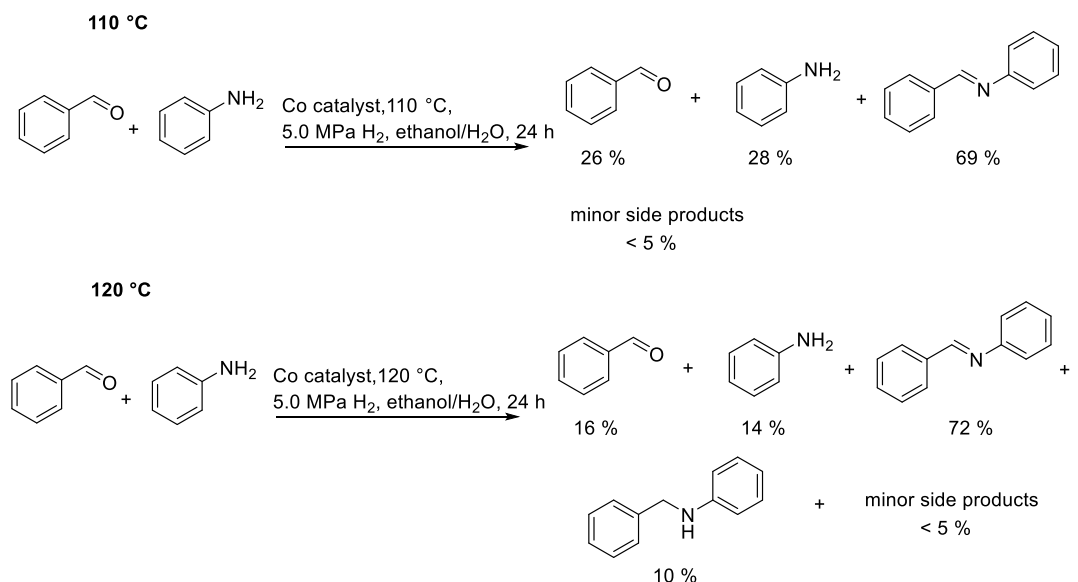


Figure S13: Product distribution for the hydrogenation of a mixture consisting of benzaldehyde and nitrobenzene.

At both temperatures, no benzaldehyde hydrogenation product was observed, not even in a minor side reaction. This is especially interesting in comparison to the 120 °C sample of sole benzaldehyde, where nearly 30 % of benzyl alcohol could be detected. In both cases N-benzylideneaniline was identified as the main product. However, when the temperature is increased to 120 °C small amounts of N-benzylaniline were observed, too. This indicates that coordination and consequently the hydrogenation of the substrates with nitrogen functionalities is highly favored under the selected reaction conditions. This could be the basis of the imine and benzimidazole syntheses from nitroarenes and aldehydes or ketones.

Catalyst recycling

The hydrogenation of nitrobenzene was chosen to investigate the recyclability of the novel cobalt nanocomposite catalyst. A 5 mL reaction vial was charged with a magnetic stirring bar, 0.5 mmol nitrobenzene, 2 mL ethanol, 0.5 mL H₂O and 25 mg Co nanocomposite catalyst (1.0 mg Co, 0.017 mmol, 3.4 mol%). The vial was placed in a high-pressure autoclave (Parr Instruments) and the autoclave was flushed three times with 20 bar of hydrogen. The autoclave was pressured with 50 bar of hydrogen and the reaction was stirred for 20 h at 110 °C. After

20 h the autoclave was cooled to room temperature and the hydrogen pressure was released. The yield of aniline was determined by GC using *n*-dodecane as an internal standard. The catalyst was centrifuged, dried, treated by temperature programmed reduction (5 K/min, 550 °C) and used again. In addition, the recycled catalyst was analyzed by TEM measurements after the fifth run (Figure S14).

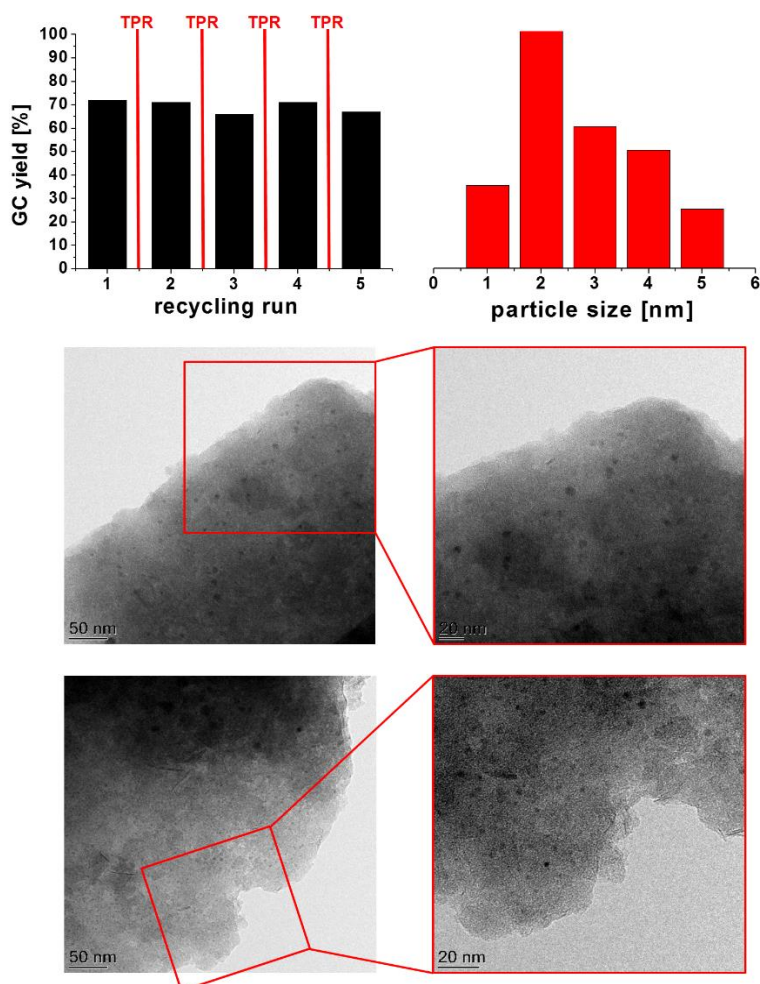


Figure S14: Results of the catalyst recycling experiment. Top left: The catalyst showed no significant decrease in catalytic activity until the fifth run, indicating a complete reactivation by TPR treatment. Top right: The particle size distribution after four times TPR treatment verifies an increase in the mean particle size. Middle/bottom: TEM analysis of the recycled catalyst at different positions.

The catalyst showed no significant decrease in catalytic activity after four times high temperature hydrogen treatment, indicating a complete reactivation of the catalyst (top left). The mean particle size of the four times recycled catalyst is 3.3 nm. The particles are still homogeneously dispersed, however, some larger aggregates could be detected.

General procedures

Selective hydrogenation of nitro derivatives – general procedure

A 5 mL reaction vial was charged with a magnetic stirring bar, 0.5 mmol nitro derivative, 2 mL ethanol, 0.5 mL H₂O and 35 mg Co nanocomposite catalyst (1.4 mg Co, 0.024 mmol, 4.8 mol%). The vial was placed in a high-pressure autoclave (Parr Instruments) and the autoclave was flushed three times with 20 bar of hydrogen. The autoclave was pressured with 50 bar of hydrogen and the reaction was stirred for 20 h at 110 °C. After 20 h the autoclave was cooled to room temperature and the hydrogen pressure was released. Yields were determined by GC and GC-MS using *n*-dodecane as an internal standard.

Selective synthesis of substituted aldimines – general procedure

A 5 mL reaction vial was charged with a magnetic stirring bar, 1.5 mmol nitro derivative, 3 mmol aldehyde, 4 mL triethylamine and 110 mg Co nanocomposite catalyst (4.4 mg Co, 0.075 mmol, 5.0 mol%). The vial was placed in a high-pressure autoclave (Parr Instruments) and the autoclave was flushed three times with 20 bar of hydrogen. The autoclave was pressured with 50 bar of hydrogen and the reaction was stirred for 24 h at 110 °C. After 24 h the autoclave was cooled to room temperature and the hydrogen pressure was released. The catalyst was removed by centrifugation and washed several times with acetone or ethyl acetate. The organic layers were combined and the solvent was removed under reduced pressure. Purification by column chromatography, crystallization or sublimation resulted in the pure products. The products were analyzed by NMR spectroscopy. For new compounds, elemental analysis or high-resolution mass spectrometry were accomplished.

Selective synthesis of substituted ketimines – general procedure

A 5 mL reaction vial was charged with a magnetic stirring bar, 1.5 mmol nitro derivative, 3 mmol ketone, 10 mg Amberlyst[®] 15, molecular sieves, 4 mL toluene and 175 mg Co nanocomposite catalyst (7.0 mg Co, 0.119 mmol, 8.0 mol%). The vial was placed in a high-pressure autoclave (Parr Instruments) and the autoclave was flushed three times with 20 bar of hydrogen. The autoclave was pressured with 50 bar of hydrogen and the reaction was stirred for 48 h at 115 °C. After 48 h the autoclave was cooled to room temperature and the hydrogen pressure was released. The catalyst was removed by centrifugation and washed several times with acetone or ethyl acetate. The residual Amberlyst[®] 15 and molsieves were removed by sieving. The organic layers were combined and the solvent was removed under reduced pressure. Purification by column chromatography, crystallization or sublimation resulted in the

pure products. The products were analyzed by NMR spectroscopy. For new compounds, elemental analysis or high-resolution mass spectrometry were accomplished.

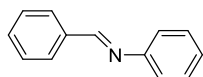
Selective synthesis of substituted benzimidazoles – general procedure

A 5 mL reaction vial is charged with a magnetic stirring bar, 1.5 mmol 4,5-dimethyl-2-nitroaniline, 3 mmol aldehyde, 4 mL triethylamine and 110 mg Co nanocomposite catalyst (4.4 mg Co, 0.075 mmol, 5.0 mol%). The vial was placed in a high-pressure autoclave (Parr Instruments) and the autoclave was flushed three times with 20 bar of hydrogen. The autoclave was pressured with 50 bar of hydrogen and the reaction was stirred for 24 h at 110 °C. After 24 h the autoclave was cooled to room temperature and the hydrogen pressure was released. The catalyst was removed by centrifugation and washed several times with acetone or ethyl acetate. The organic layers were combined and the solvent was removed under reduced pressure. Purification by column chromatography, or recrystallization led to the pure products. The products were analyzed by NMR spectroscopy. For new compounds, elemental analysis or high-resolution mass spectrometry were accomplished.

Characterization of isolated products

Imines

1a:

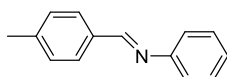


N-benzylideneaniline

¹H NMR (300 MHz, CDCl₃, 296 K): δ = 8.50 (s, 1H), 8.00-7.92 (m, 2H), 7.55-7.50 (m, 3H), 7.50-7.40 (m, 2H), 7.34-7.25 (m, 3H) ppm.

¹³C NMR (75 MHz, CDCl₃, 296 K): δ = 160.45, 152.12, 136.27, 131.45, 129.22, 128.87, 128.84, 126.00, 120.95 ppm. MS (EI, m/z): 180.1 (M⁺).

1b:

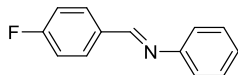


N-(4-methylbenzylidene)aniline

¹H NMR (300 MHz, CDCl₃, 296 K): δ = 8.47 (s, 1H), 7.86-7.83 (d, 2H), 7.47-7.41 (m, 2H), 7.34-7.24 (m, 5H) ppm.

^{13}C NMR (75 MHz, CDCl_3 , 296 K): $\delta = 160.39, 152.28, 141.88, 133.68, 129.53, 129.13, 128.82, 125.76, 120.89, 21.67$ ppm. MS (EI, m/z): 194.1 (M^+).

1c:

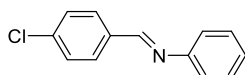


N-(4-fluorobenzylidene)aniline

^1H NMR (300 MHz, CDCl_3 , 296 K): $\delta = 8.44$ (s, 1H), 7.95-7.90 (m, 2H), 7.45-7.39 (m, 2H), 7.28-7.14 (m, 5H) ppm.

^{13}C NMR (75 MHz, CDCl_3 , 296 K): $\delta = 166.37, 163.03, 158.84, 151.85, 130.85, 129.20, 126.03, 120.84, 116.10, 115.81$ ppm. MS (EI, m/z): 198.1 (M^+).

1d:

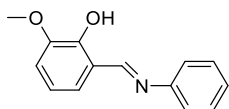


N-(4-chlorobenzylidene)aniline

^1H NMR (300 MHz, CDCl_3 , 296 K): $\delta = 8.44$ (s, 1H), 7.88-7.85 (m, 2H), 7.48-7.40 (m, 4H), 7.29-7.22 (m, 3H) ppm.

^{13}C NMR (75 MHz, CDCl_3 , 296 K): $\delta = 158.85, 151.66, 137.37, 134.70, 129.97, 129.22, 129.10, 126.21, 120.87$ ppm. MS (EI, m/z): 214.1 (M^+).

2a:

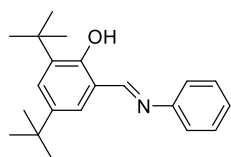


2-methoxy-6-((phenylimino)methyl)phenol

^1H NMR (300 MHz, CDCl_3 , 296 K): $\delta = 13.70$ (s, 1H), 8.64 (s, 1H), 7.47-7.41 (m, 2H), 7.31-7.27 (m, 3H), 7.05-7.00 (m, 2H), 6.92-6.87 (m, 1H), 3.95 (s, 3H) ppm.

^{13}C NMR (75 MHz, CDCl_3 , 296 K): $\delta = 162.62, 151.50, 148.51, 148.19, 129.42, 126.99, 123.79, 121.16, 119.12, 118.52, 114.80, 58.21$ ppm. MS (EI, m/z): 227.1 (M^+).

2b:

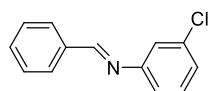


2,4-di-tert-butyl-6-((phenylimino)methyl)phenol

^1H NMR (300 MHz, CDCl_3 , 296 K): δ = 13.71 (s, 1H), 8.65 (s, 1H), 7.48-7.40 (m, 3H), 7.31-7.23 (m, 4H), 1.50 (s, 9H), 1.35 (s, 9H) ppm.

^{13}C NMR (75 MHz, CDCl_3 , 296 K): δ = 163.81, 158.26, 148.75, 140.56, 136.99, 129.33, 128.00, 126.79, 126.52, 121.16, 118.30, 35.11, 34.19, 31.48, 29.43 ppm. MS (EI, m/z): 308.1 (M^+).

3a:

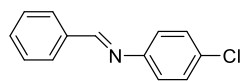


N-benzylidene-3-chloroaniline

^1H NMR (300 MHz, CDCl_3 , 296 K): δ = 8.43 (s, 1H), 7.95-7.92 (m, 2H), 7.54-7.47 (m, 3H), 7.37-7.31 (m, 1H), 7.26-7.23 (m, 2H), 7.15-7.11 (m, 1H) ppm.

^{13}C NMR (75 MHz, CDCl_3 , 296 K): δ = 161.29, 153.40, 135.90, 134.76, 131.80, 130.21, 129.04, 128.87, 125.86, 120.98, 119.49 ppm. MS (EI, m/z): 214.1 (M^+).

3b:

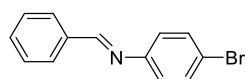


N-benzylidene-4-chloroaniline

^1H NMR (300 MHz, CDCl_3 , 296 K): δ = 8.44 (s, 1H), 7.94-7.91 (m, 2H), 7.52-7.49 (m, 3H), 7.39-7.36 (m, 2H), 7.19-7.16 (m, 2H) ppm.

^{13}C NMR (75 MHz, CDCl_3 , 296 K): δ = 160.68, 150.54, 135.99, 131.65, 131.48, 129.27, 128.92, 128.85, 122.25 ppm. MS (EI, m/z): 214.1 (M^+).

3c:

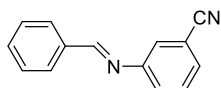


N-benzylidene-4-bromoaniline

^1H NMR (300 MHz, CDCl_3 , 296 K): δ = 8.43 (s, 1H), 7.93-7.90 (m, 2H), 7.54-7.48 (m, 5H), 7.13- 7.08 (m, 2H) ppm.

^{13}C NMR (75 MHz, CDCl_3 , 296 K): δ = 160.73, 151.02, 135.98, 132.23, 131.68, 128.93, 128.85, 122.64, 119.35 ppm. MS (EI, m/z): 259.1 (M^+).

3d:

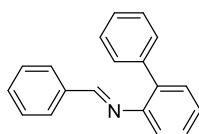


3-(benzylideneamino)benzonitrile

^1H NMR (300 MHz, CDCl_3 , 296 K): δ = 8.43 (s, 1H), 7.93-7.90 (m, 2H), 7.55-7.41 (m, 7H) ppm.

^{13}C NMR (75 MHz, CDCl_3 , 296 K): δ = 162.31, 152.76, 135.52, 132.17, 130.11, 129.24, 129.14, 128.95, 125.65, 124.26, 118.65, 113.12 ppm. MS (EI, m/z): 205.1 (M^+).

3e:

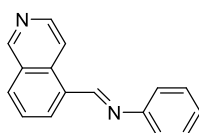


N-benzylidenebiphenyl-2-amine

^1H NMR (300 MHz, CDCl_3 , 296 K): δ = 8.55 (s, 1H), 7.91-7.88 (m, 2H), 7.64-7.57 (m, 3H), 7.52-7.37 (m, 8H), 7.19-7.16 (m, 1H) ppm.

^{13}C NMR (75 MHz, CDCl_3 , 296 K): δ = 149.80, 139.63, 136.56, 135.46, 131.30, 130.46, 130.35, 128.96, 128.79, 128.49, 127.80, 126.67, 126.12 ppm. MS (EI, m/z): 257.1 (M^+).

4:

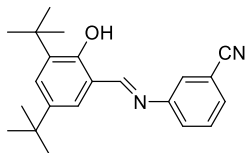


N-benzylideneisoquinolin-5-amine

^1H NMR (300 MHz, CDCl_3 , 296 K): δ = 9.27 (s, 1H), 8.58-8.56 (m, 2H), 8.14-8.12 (m, 1H), 8.05-8.01 (m, 2H), 7.85-7.82 (d, 1H), 7.62-7.52 (m, 4H), 7.29-7.27 (m, 1H) ppm.

^{13}C NMR (75 MHz, CDCl_3 , 296 K): $\delta = 161.38, 152.14, 148.20, 143.11, 136.04, 131.88, 131.66, 129.11, 128.92, 127.48, 125.07, 116.80, 116.62$ ppm. MS (EI, m/z): 231.1 (M^+).

5a:

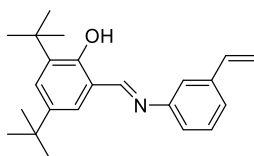


3-((3,5-di-tert-butyl-2-hydroxybenzylidene)amino)benzonitrile

^1H NMR (300 MHz, CDCl_3 , 296 K): $\delta = 13.17$ (s, 1H), 8.65 (s, 1H), 7.57-7.52 (m, 5H), 7.27-7.26 (m, 1H), 1.50 (s, 9H), 1.36 (s, 9H) ppm.

^{13}C NMR (75 MHz, CDCl_3 , 296 K): $\delta = 165.79, 158.38, 149.68, 141.06, 137.28, 130.32, 129.77, 129.08, 127.27, 125.99, 124.51, 118.34, 117.93, 113.50$ ppm. MS (EI, m/z): 333.1 (M^+).

5b:



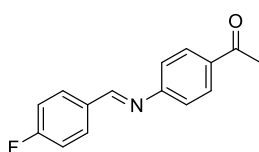
2,4-di-tert-butyl-6-((3-vinylphenylimino)methyl)phenol

^1H NMR (300 MHz, CDCl_3 , 296 K): $\delta = 13.70$ (s, 1H), 8.68 (s, 1H), 7.49-7.48 (m, 1H), 7.42-7.32 (m, 3H), 7.26-7.25 (m, 1H), 7.22-7.18 (m, 1H), 6.82-6.72 (m, 1H), 5.86-5.81 (m, 1H), 5.35-5.31 (m, 1H) 1.51 (s, 9H), 1.36 (s, 9H) ppm.

^{13}C NMR (75 MHz, CDCl_3 , 296 K): $\delta = 163.92, 158.29, 149.03, 140.59, 138.86, 137.02, 136.38, 129.45, 128.08, 126.84, 124.46, 120.36, 119.06, 118.28, 114.71, 35.11, 34.21, 31.39, 29.45$ ppm. MS (EI, m/z): 335.1 (M^+).

HRMS (ESI): calc. for $\text{C}_{23}\text{H}_{29}\text{NO}$ [$\text{M}+\text{H}$] $^+$: 336.23218; found: 336.23219

6:

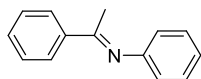


1-(4-((4-fluorobenzylidene)amino)phenyl)ethan-1-one

^1H NMR (300 MHz, CDCl_3 , 296 K): δ = 8.40 (s, 1H), 8.01-7.99 (m, 2H), 7.94-7.91 (m, 2H), 7.23-7.16 (m, 4H), 2.61 (s, 3H) ppm.

^{13}C NMR (75 MHz, CDCl_3 , 296 K): δ = 196.93, 165.72, 163.70, 159.86, 155.65, 134.29, 130.91, 130.84, 129.45, 120.53, 115.87, 115.70, 26.27 ppm. MS (EI, m/z): 240.1 (M^+).

7a:

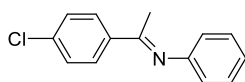


N-(1-phenylethylidene)aniline

^1H NMR (300 MHz, CDCl_3 , 296 K): δ = 8.04-8.01 (m, 2H), 7.50-7.48 (m, 3H), 7.42-7.27 (m, 2H), 7.16-7.11 (m, 1H), 6.86-6.84 (m, 2H), 2.27 (s, 3H) ppm.

^{13}C NMR (75 MHz, CDCl_3 , 296 K): δ = 165.49, 151.76, 139.52, 130.52, 129.01, 128.41, 127.22, 123.25, 119.42, 17.42 ppm. MS (EI, m/z): 195.1 (M^+).

7b:

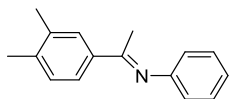


N-(1-(4-chlorophenyl)ethylidene)aniline

^1H NMR (300 MHz, CDCl_3 , 296 K): δ = 7.95-7.92 (m, 2H), 7.44-7.35 (m, 4H), 7.14-7.09 (m, 1H), 6.81-6.79 (m, 2H), 2.23 (s, 3H) ppm.

^{13}C NMR (75 MHz, CDCl_3 , 296 K): δ = 164.25, 151.37, 137.89, 136.62, 129.01, 128.56, 123.42, 119.32, 17.26 ppm. MS (EI, m/z): 229.1 (M^+).

7c:

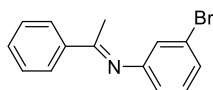


N-(1-(3,4-dimethylphenyl)ethylidene)aniline

^1H NMR (300 MHz, CDCl_3 , 296 K): δ = 7.83 (s, 1H), 7.71-7.68 (m, 1H), 7.40-7.35 (m, 2H), 7.27-7.22 (m, 1H), 7.13-7.08 (m, 1H), 6.84-6.81 (m, 2H), 2.36-2.35 (m, 6H), 2.24 (s, 3H) ppm.

^{13}C NMR (75 MHz, CDCl_3 , 296 K): δ = 165.52, 151.91, 139.44, 137.20, 136.64, 129.60, 128.93, 128.23, 124.80, 123.07, 119.50, 19.88, 19.77, 17.36 ppm. MS (EI, m/z): 223.1 (M^+).

8a:

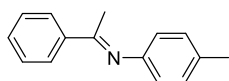


3-bromo-N-(1-phenylethylidene)aniline

^1H NMR (300 MHz, CDCl_3 , 296 K): δ = 7.99-7.96 (m, 2H), 7.53-7.44 (m, 3H), 7.24-7.22 (m, 2H), 7.00 (s, 1H), 6.76-6.73 (m, 1H), 2.26 (s, 3H) ppm.

^{13}C NMR (75 MHz, CDCl_3 , 296 K): δ = 166.32, 153.08, 138.96, 130.75, 130.33, 128.40, 127.20, 126.09, 122.65, 122.30, 118.11, 17.55 ppm. MS (EI, m/z): 273.1 (M^+).

8a:



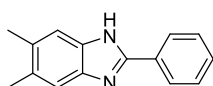
4-methyl-N-(1-phenylethylidene)aniline

^1H NMR (300 MHz, CDCl_3 , 296 K): δ = 8.02-7.99 (m, 2H), 7.49-7.45 (m, 3H), 7.21-7.18 (m, 2H), 6.76-6.73 (m, 2H), 2.39 (s, 3H) 2.27 (s, 3H) ppm.

^{13}C NMR (75 MHz, CDCl_3 , 296 K): δ = 165.39, 149.02, 139.60, 132.51, 130.28, 129.44, 128.27, 127.08, 119.33, 20.82, 17.23 ppm. MS (EI, m/z): 209.1 (M^+).

Benzimidazoles

1a:

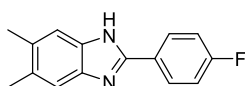


5,6-dimethyl-2-phenyl-1H-benzimidazole

^1H NMR (300 MHz, CDCl_3 , 296 K): δ = 12.66 (s, 1H), 8.18-8.16 (d, 2H), 7.55-7.31 (m, 5H), 2.32 (s, 6H) ppm.

^{13}C NMR (75 MHz, CDCl_3 , 296 K): δ = 150.81, 143.03, 134.01, 131.57, 130.96, 130.36, 129.88, 129.30, 126.67, 119.42, 111.80, 20.49 ppm. MS (EI, m/z): 221.1 (M^+).

1b:

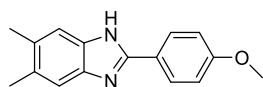


2-(4-fluorophenyl)-5,6-dimethyl-1H-benzimidazole

^1H NMR (300 MHz, CDCl_3 , 296 K): δ = 8.20-8.15 (m, 2H), 7.40-7.34 (m, 4H), 2.32 (s, 6H) ppm.

^{13}C NMR (75 MHz, CDCl_3 , 296 K): δ = 164.92, 161.64, 149.96, 131.01, 128.95, 127.54, 116.48, 116.19, 20.46 ppm. MS (EI, m/z): 240.1 (M^+).

1c:

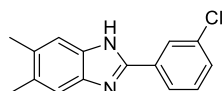


2-(4-methoxyphenyl)-5,6-dimethyl-1H-benzo[d]imidazole

^1H NMR (300 MHz, CDCl_3 , 296 K): δ = 12.47 (s, 1H), 8.09-8.06 (m, 2H), 7.38 (s, 1H), 7.25 (s, 1H), 7.10-7.07 (m, 2H), 3.83 (s, 3H), 2.30 (s, 6H) ppm.

^{13}C NMR (75 MHz, CDCl_3 , 296 K): δ = 160.78, 150.92, 143.01, 133.93, 131.02, 130.01, 128.20, 123.48, 119.09, 114.71, 111.57, 55.74, 20.48 ppm. MS (EI, m/z): 252.1 (M^+).

1d:

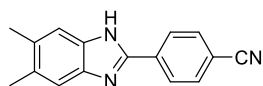


2-(3-chlorophenyl)-5,6-dimethyl-1H-benzo[d]imidazole

^1H NMR (300 MHz, CDCl_3 , 296 K): δ = 12.76 (s, 1H), 8.18 (s, 1H), 8.12-8.09 (m, 1H), 7.58-7.31 (m, 4H), 2.32 (s, 6H) ppm.

^{13}C NMR (75 MHz, CDCl_3 , 296 K): δ = 149.24, 142.80, 134.15, 132.93, 131.30, 129.59, 126.18, 125.21, 119.52, 111.90, 20.49 ppm. MS (EI, m/z): 256.1 (M^+).

1e:

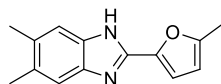


4-(5,6-dimethyl-1H-benzo[d]imidazol-2-yl)benzonitrile

^1H NMR (300 MHz, CDCl_3 , 296 K): δ = 8.30-8.27 (d, 2H), 8.00-7.97 (d, 2H), 7.40 (s, 2H), 2.32 (s, 6H) ppm.

^{13}C NMR (75 MHz, CDCl_3 , 296 K): δ = 148.87, 134.97, 133.36, 132.00, 127.13, 119.17, 111.86, 20.52 ppm. MS (EI, m/z): 247.1 (M^+).

2:

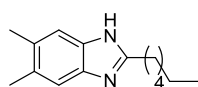


5,6-dimethyl-2-(5-methylfuran-2-yl)-1H-benzo[d]imidazole

^1H NMR (300 MHz, CDCl_3 , 296 K): δ = 12.54 (s, 1H), 7.34-7.24 (m, 2H), 7.01-7.00 (d, 1H), 6.31-6.30 (d, 1H), 2.39 (s, 3H), 2.30 (s, 6H) ppm.

^{13}C NMR (75 MHz, CDCl_3 , 296 K): δ = 153.69, 144.75, 143.49, 133.14, 131.40, 130.38, 119.07, 111.70, 111.25, 108.87, 20.43, 13.90 ppm. MS (EI, m/z): 226.1 (M^+).

3:

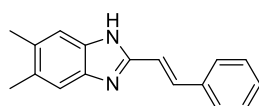


2-hexyl-5,6-dimethyl-1H-benzo[d]imidazole

^1H NMR (300 MHz, CDCl_3 , 296 K): δ = 11.87 (s, 1H), 7.26 (s, 1H), 7.15 (s, 1H), 2.76-2.71 (t, 2H), 2.27-2.26 (m, 6H), 1.77-1.67 (q, 2H), 1.32-1.23 (m, 6H), 0.87-0.83 (m, 3H) ppm.

^{13}C NMR (75 MHz, CDCl_3 , 296 K): δ = 154.56, 142.42, 133.19, 129.92, 129.05, 118.68, 111.23, 31.35, 28.99, 28.82, 28.09, 22.48, 20.38 ppm. MS (EI, m/z): 230.2 (M^+).

4:



5,6-dimethyl-2-styryl-1H-benzo[d]imidazole

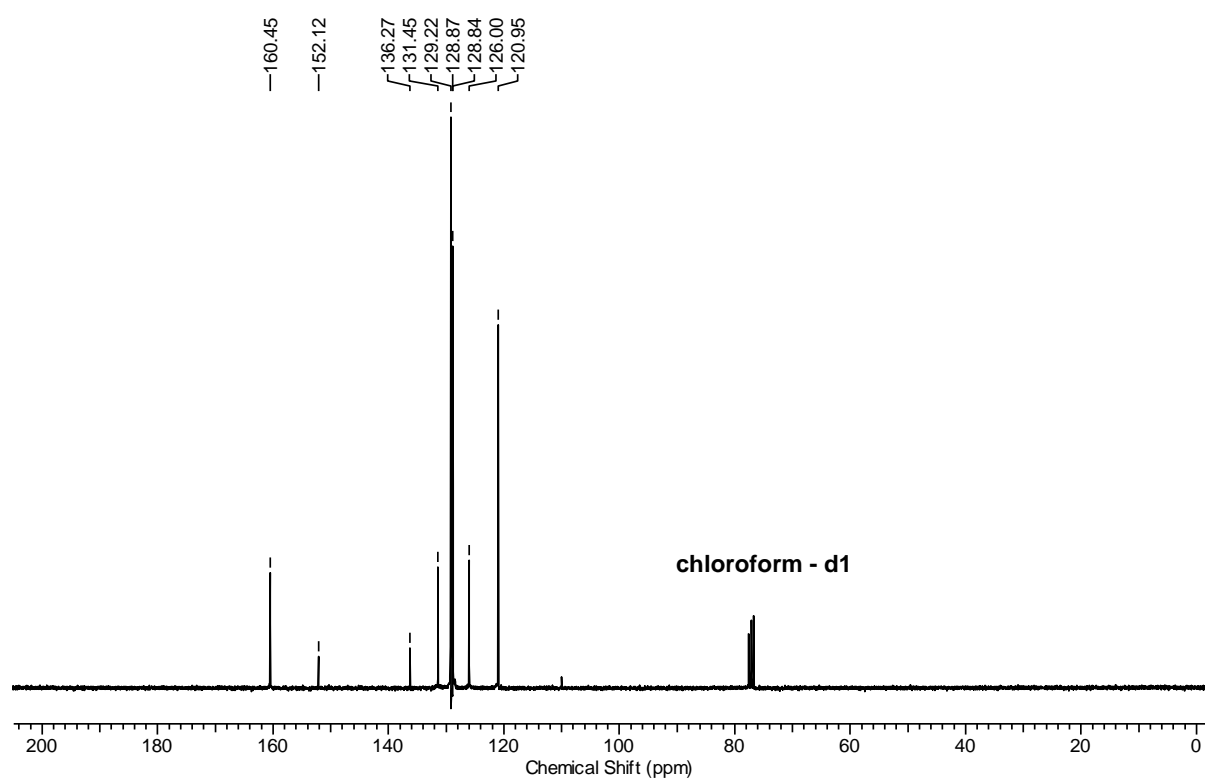
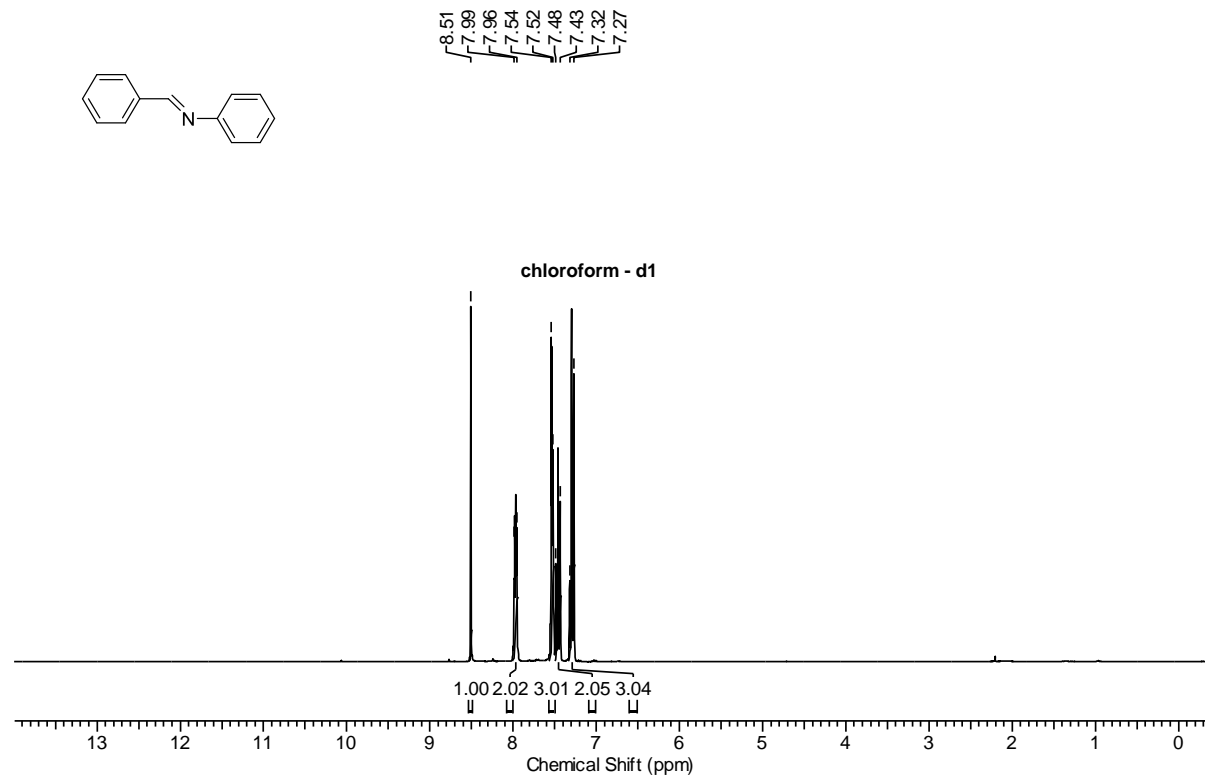
^1H NMR (300 MHz, CDCl_3 , 296 K): δ = 12.43 (s, 1H), 7.66-7.59 (m, 3H), 7.42-7.18 (m, 6H), 2.31 (s, 6H) ppm.

^{13}C NMR (75 MHz, CDCl_3 , 296 K): δ = 150.54, 143.15, 136.41, 133.74, 131.75, 130.49, 129.39, 129.05, 127.31, 119.23, 118.46, 111.58, 20.48 ppm. MS (EI, m/z): 247.1 (M^+).

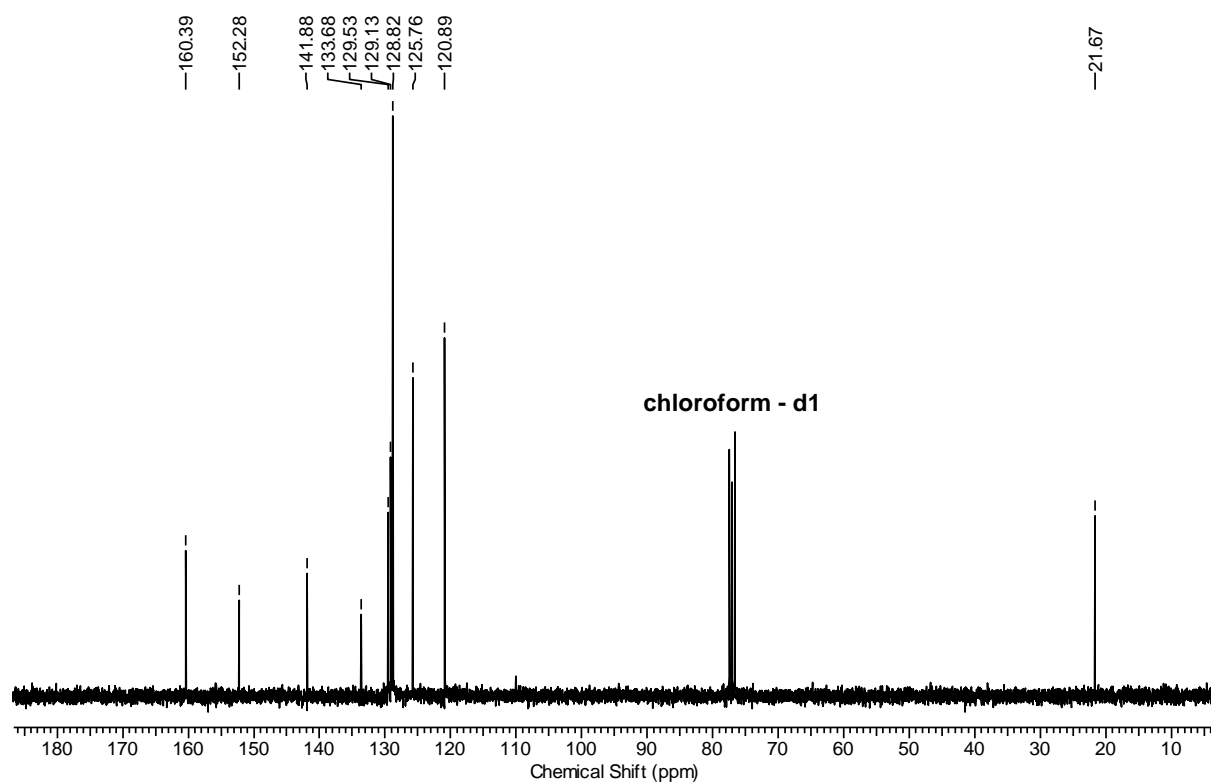
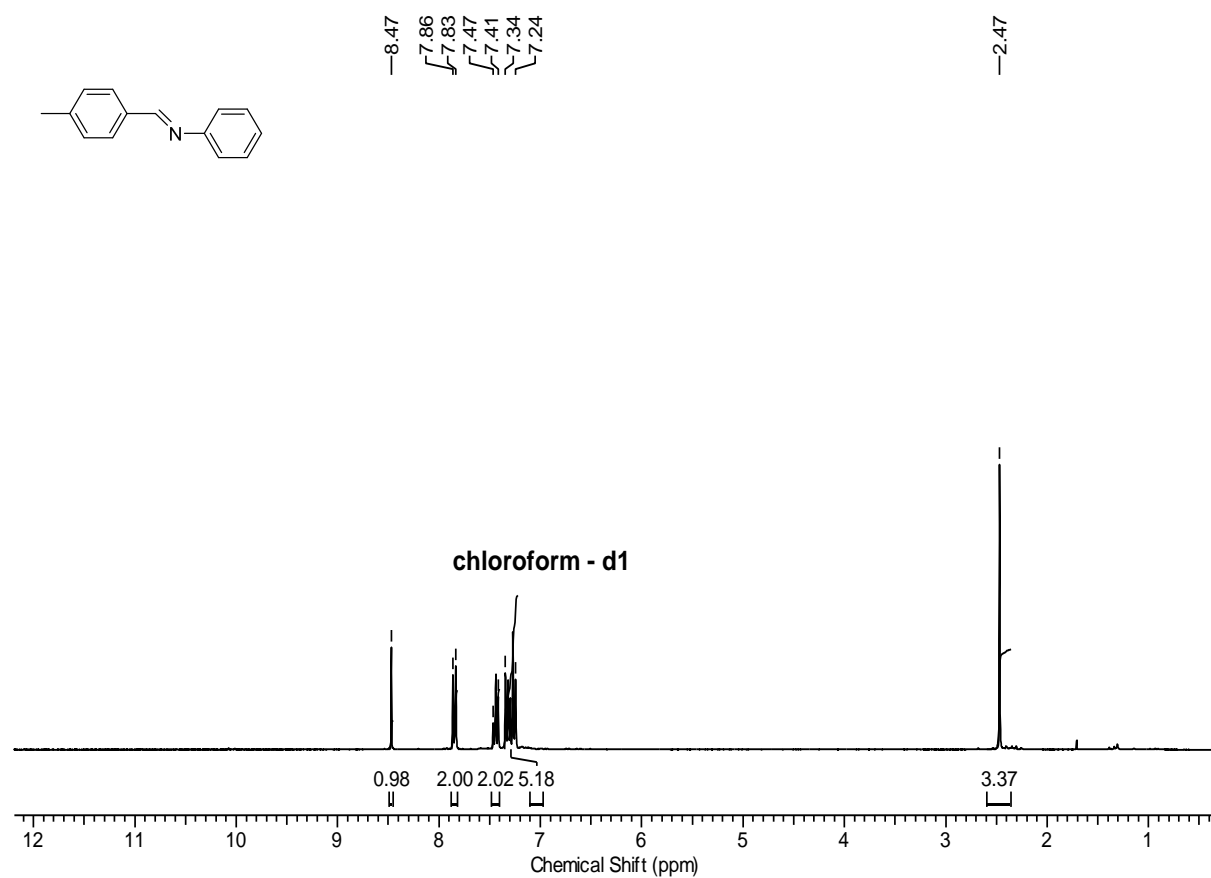
NMR Spectra

Imines

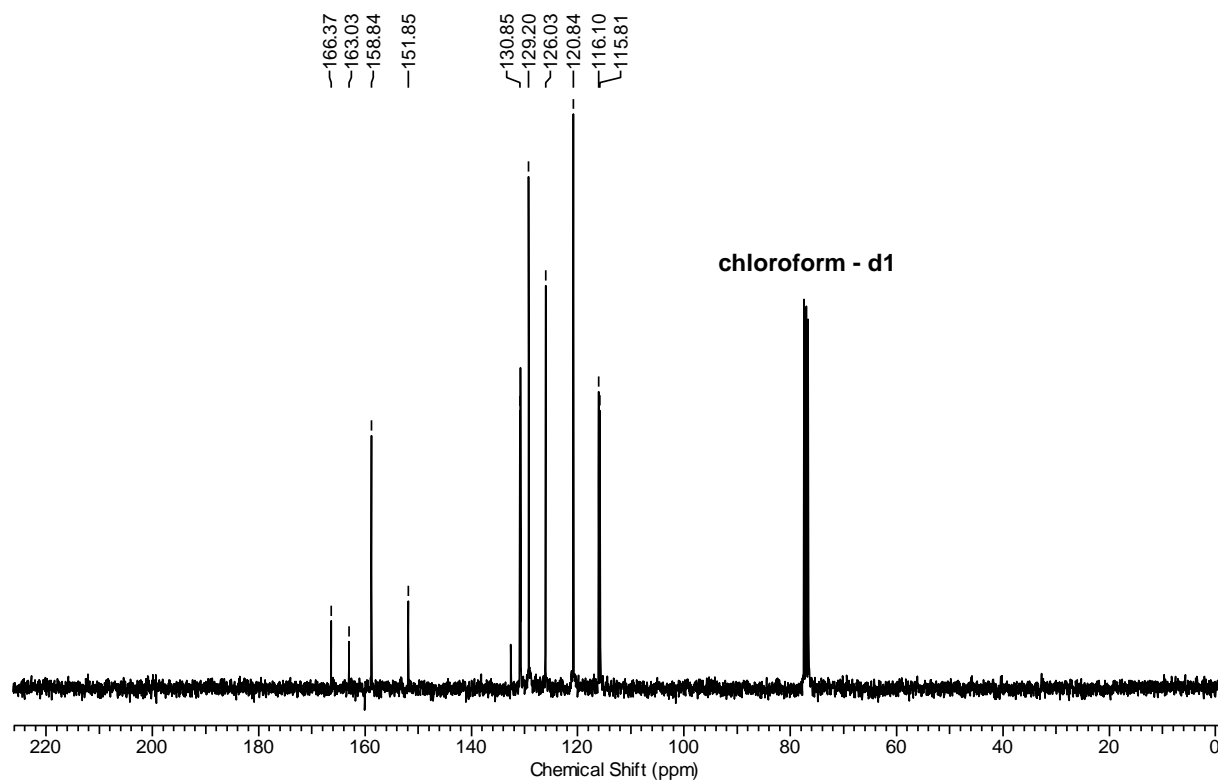
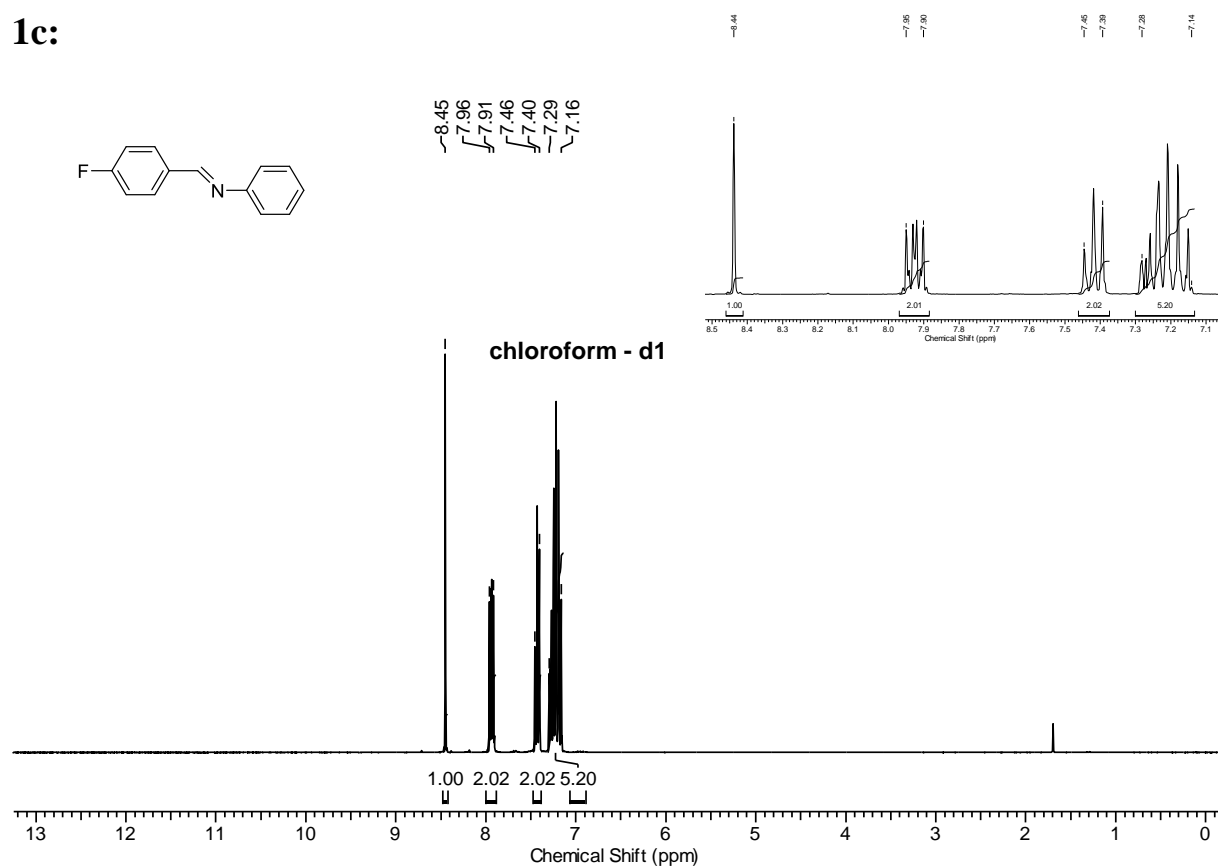
1a:



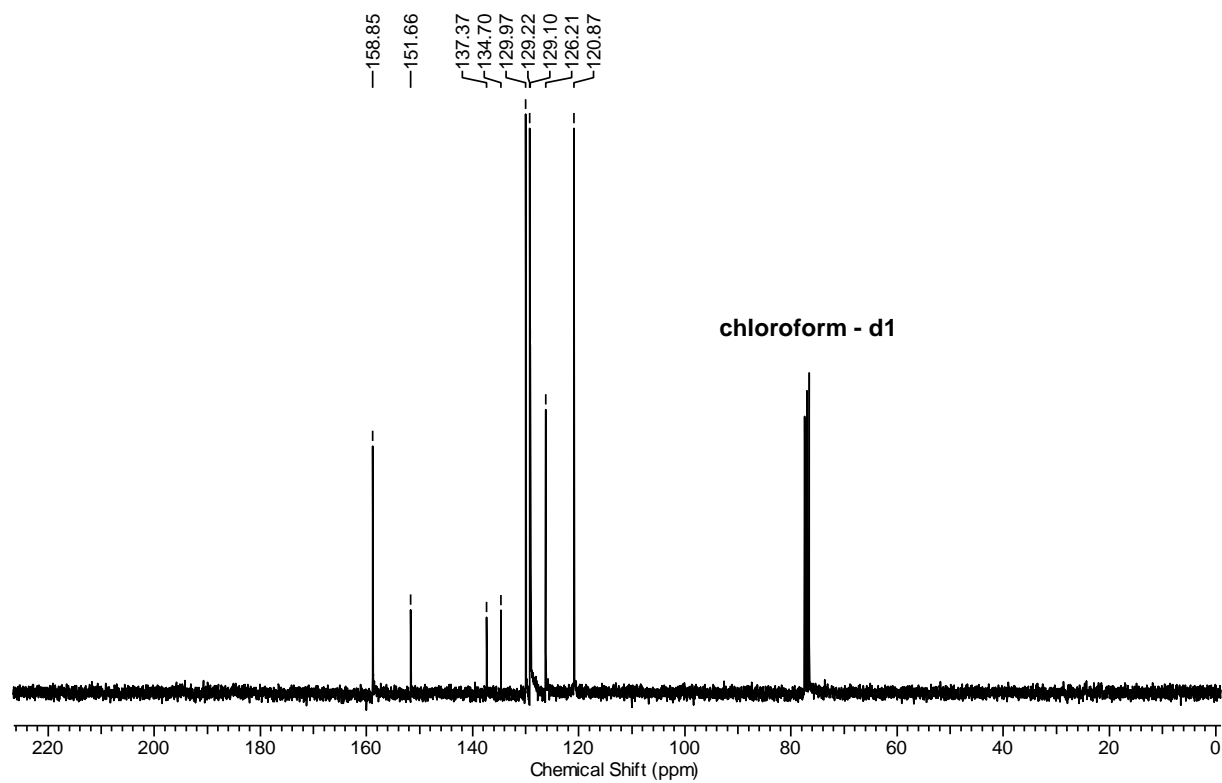
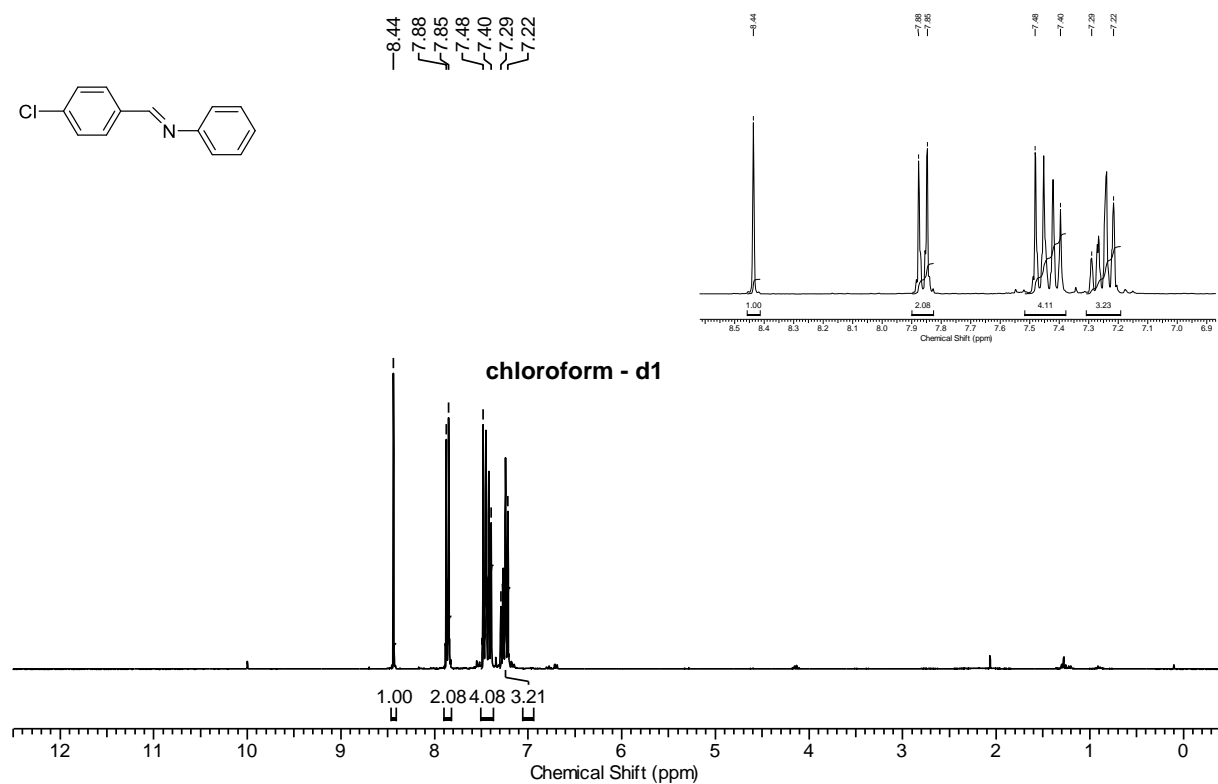
1b:



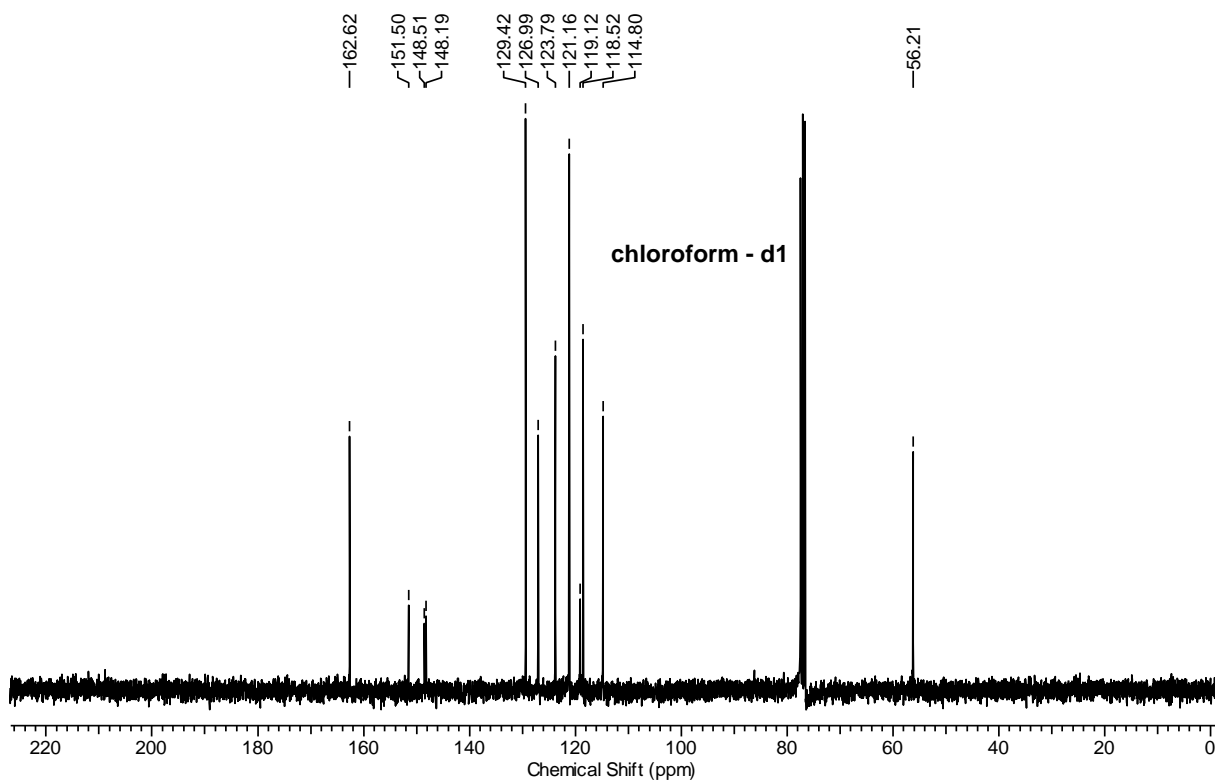
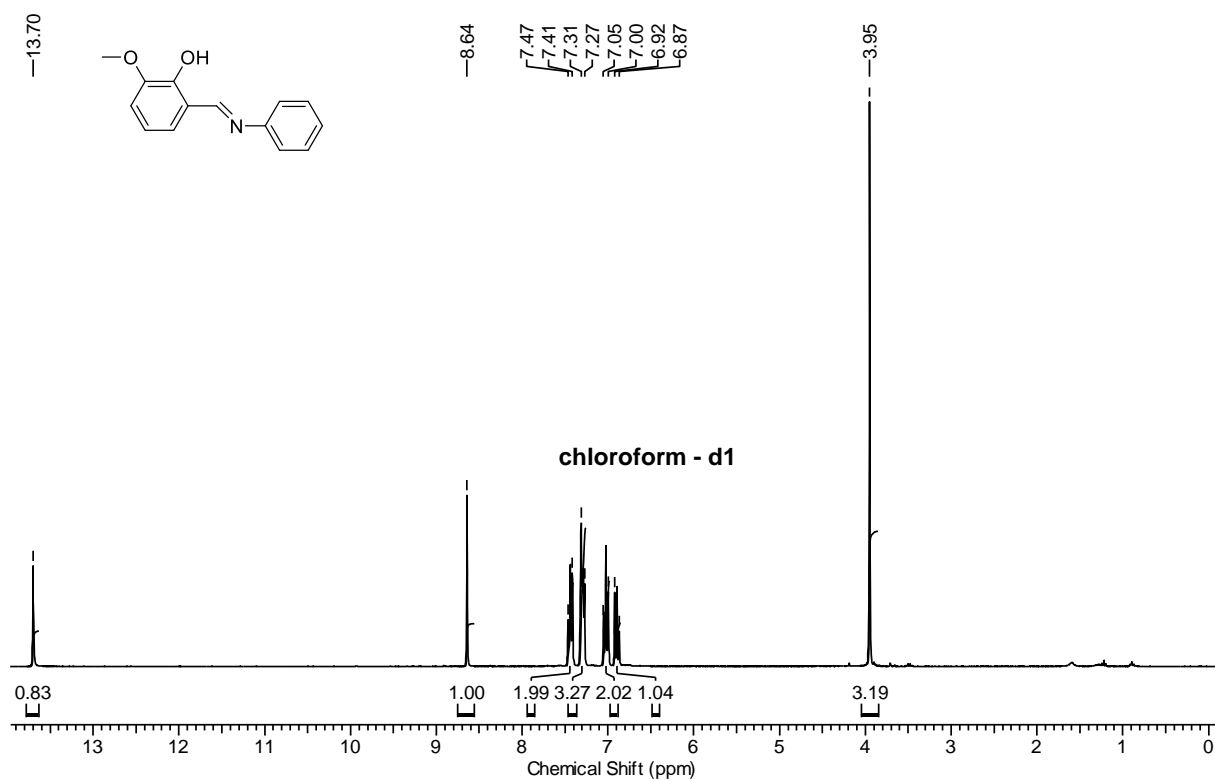
1c:



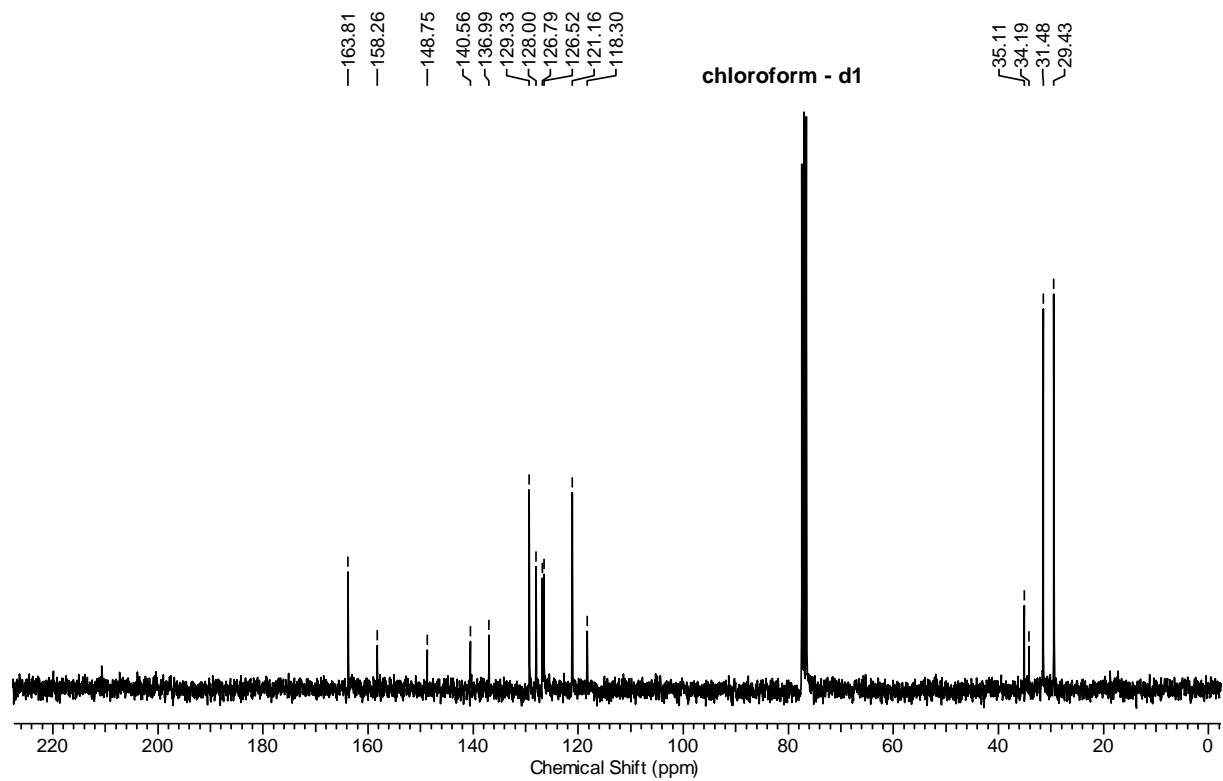
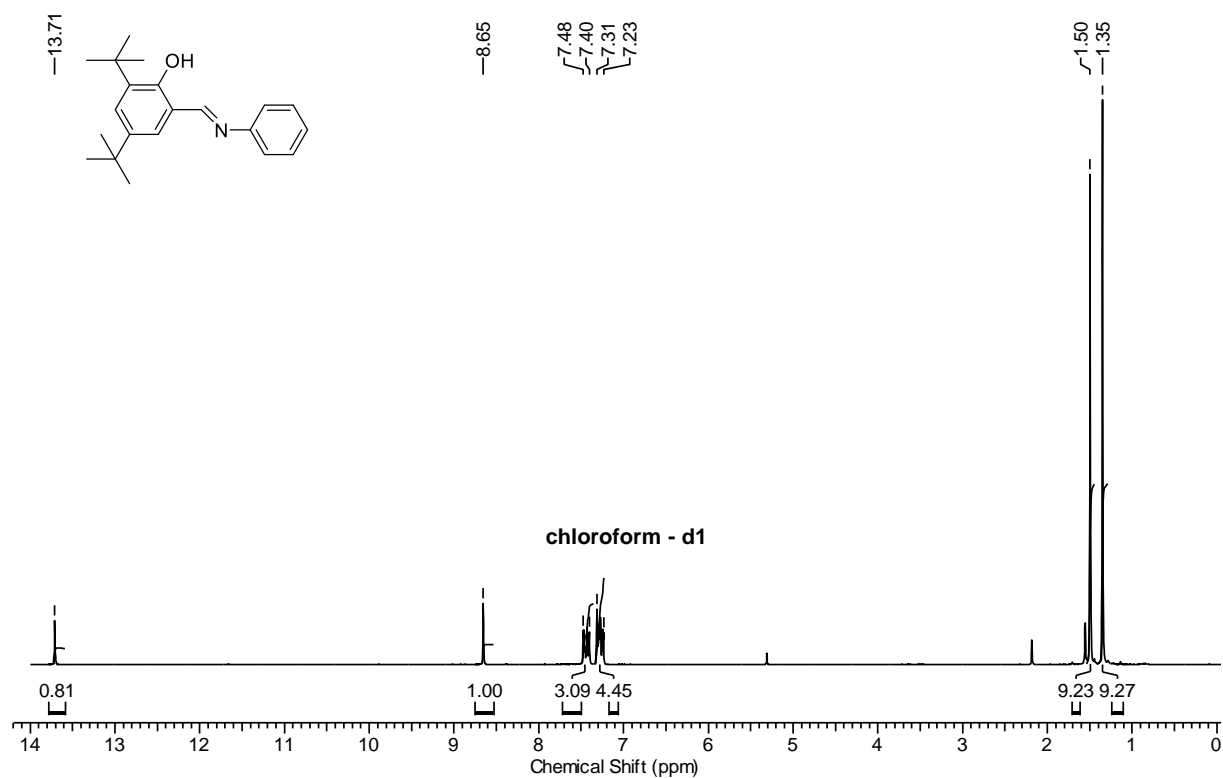
1d:



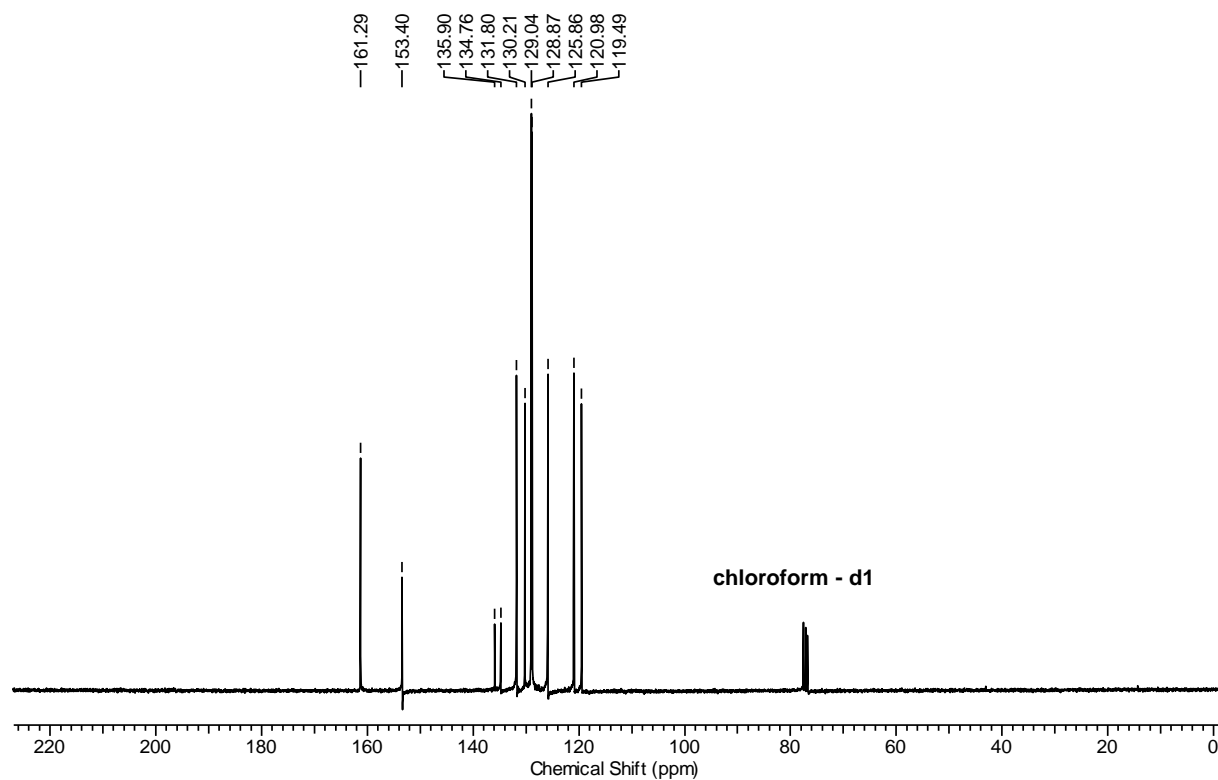
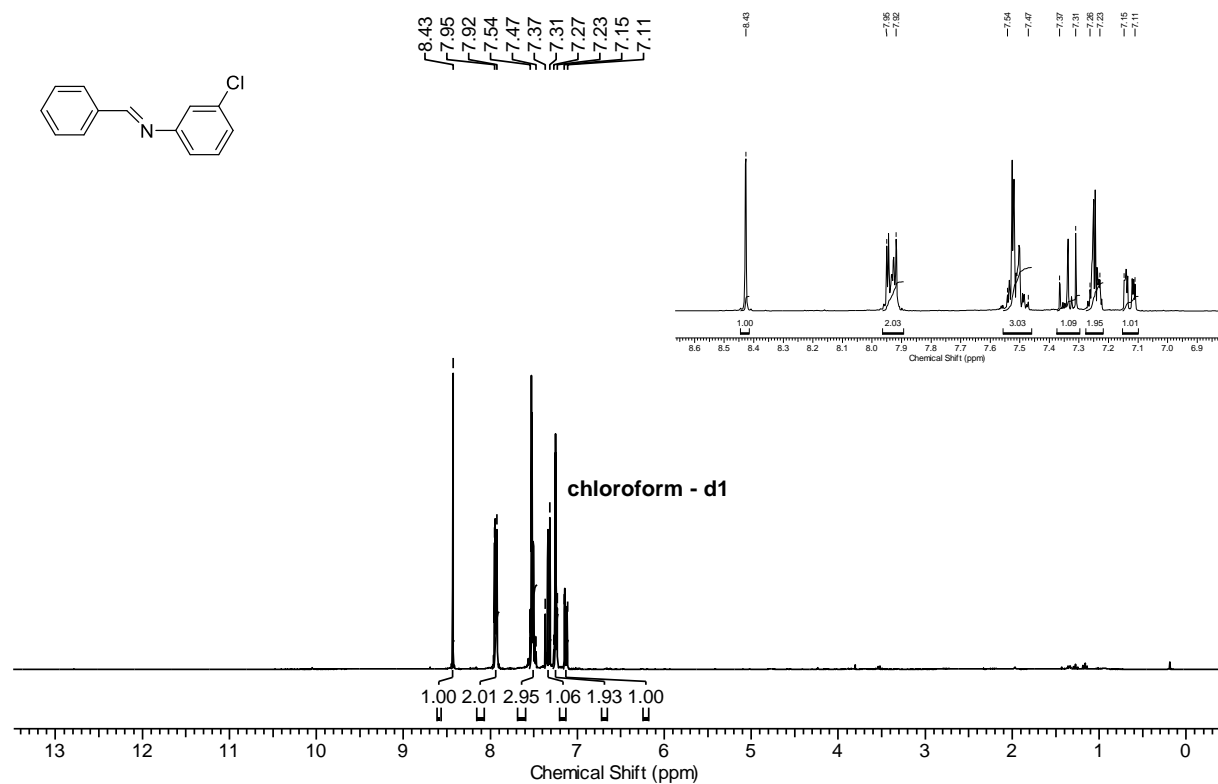
2a:



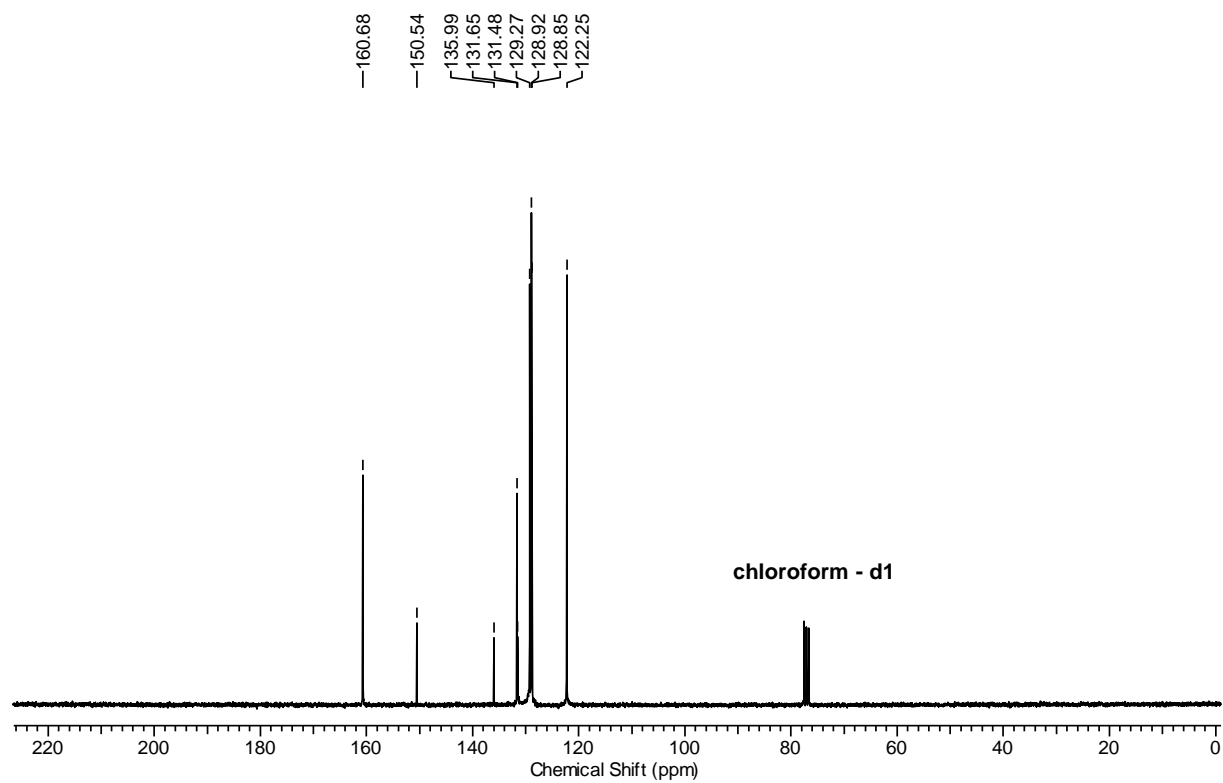
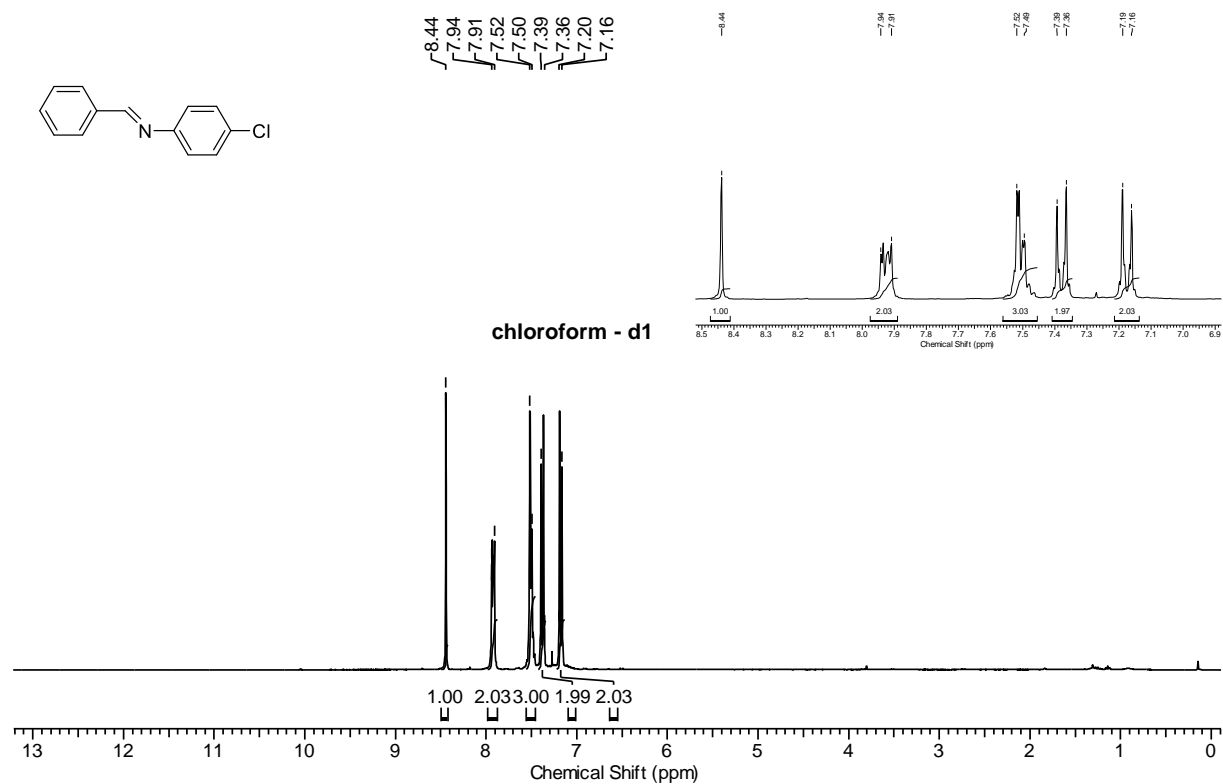
2b:



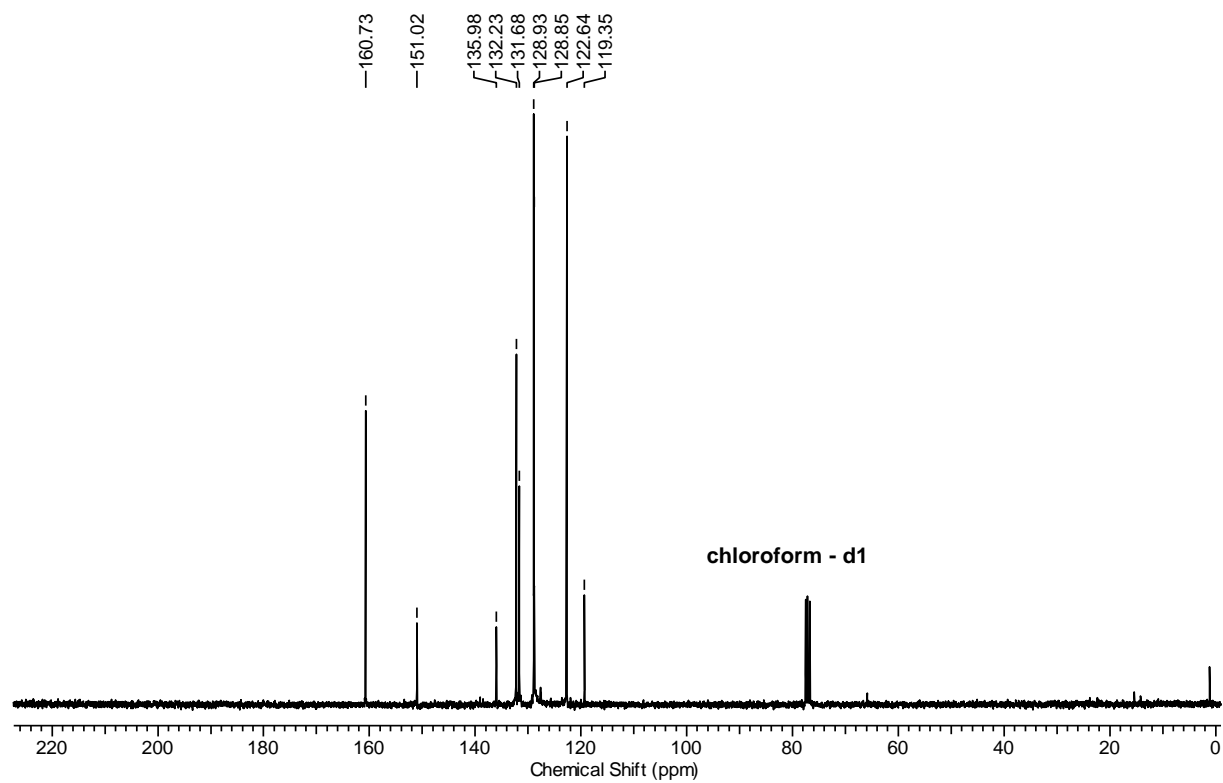
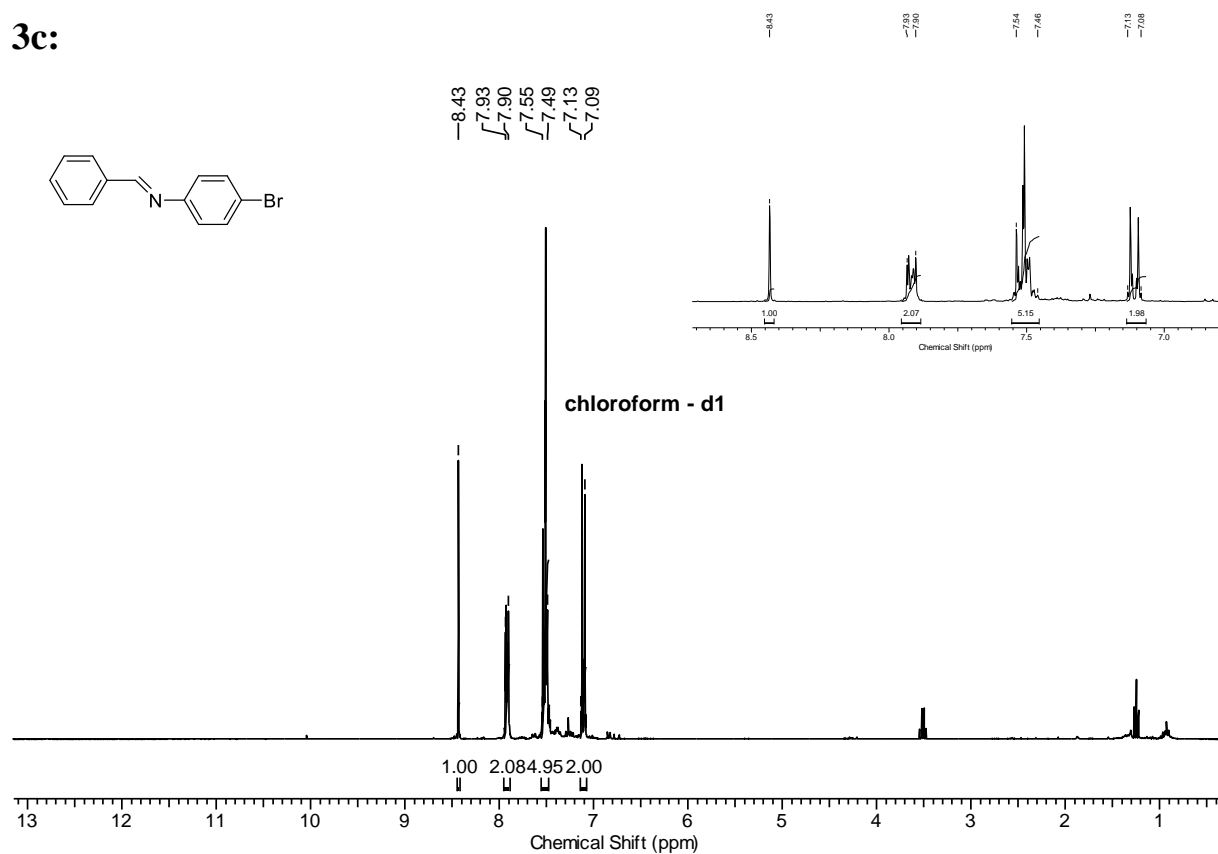
3a:



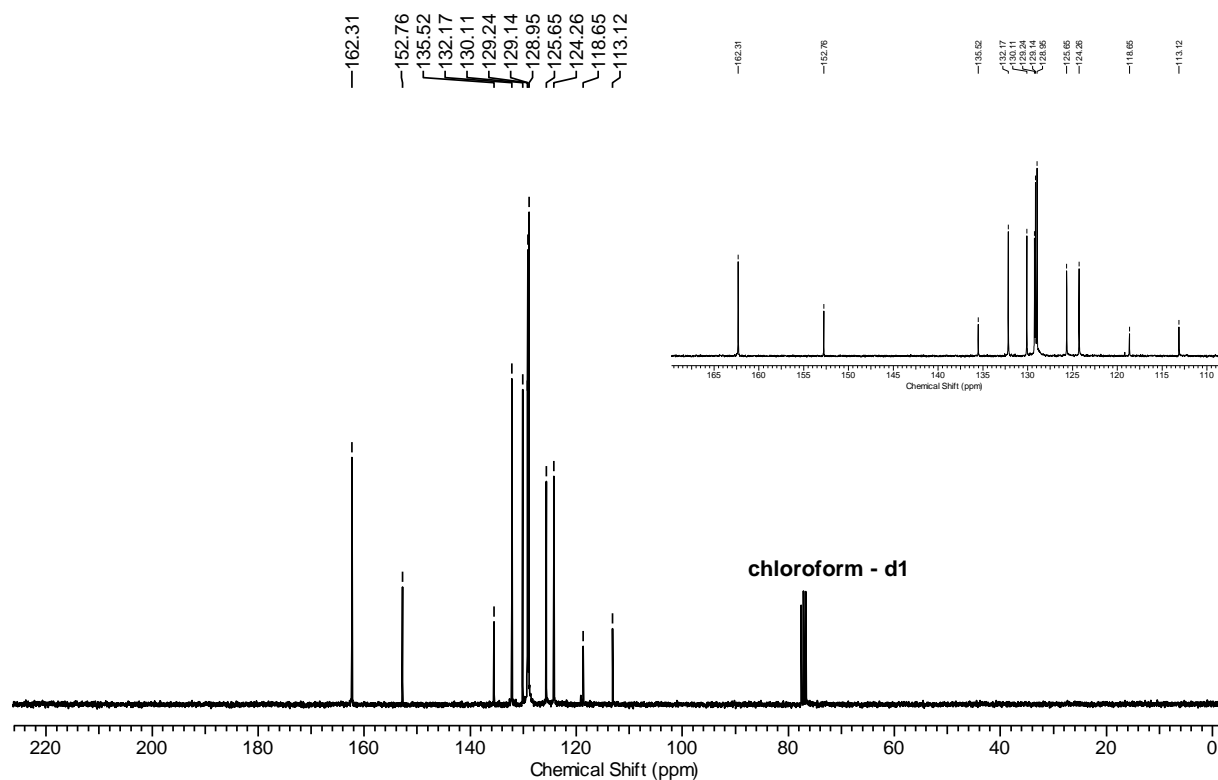
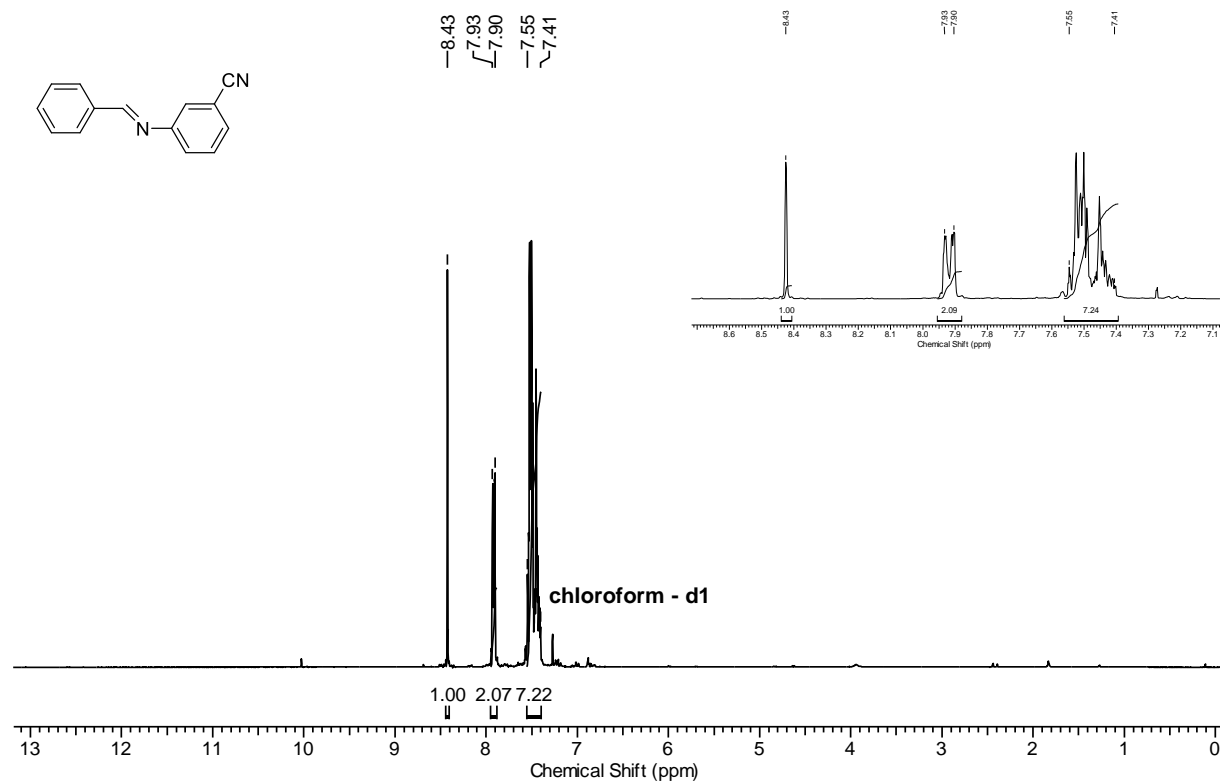
3b:



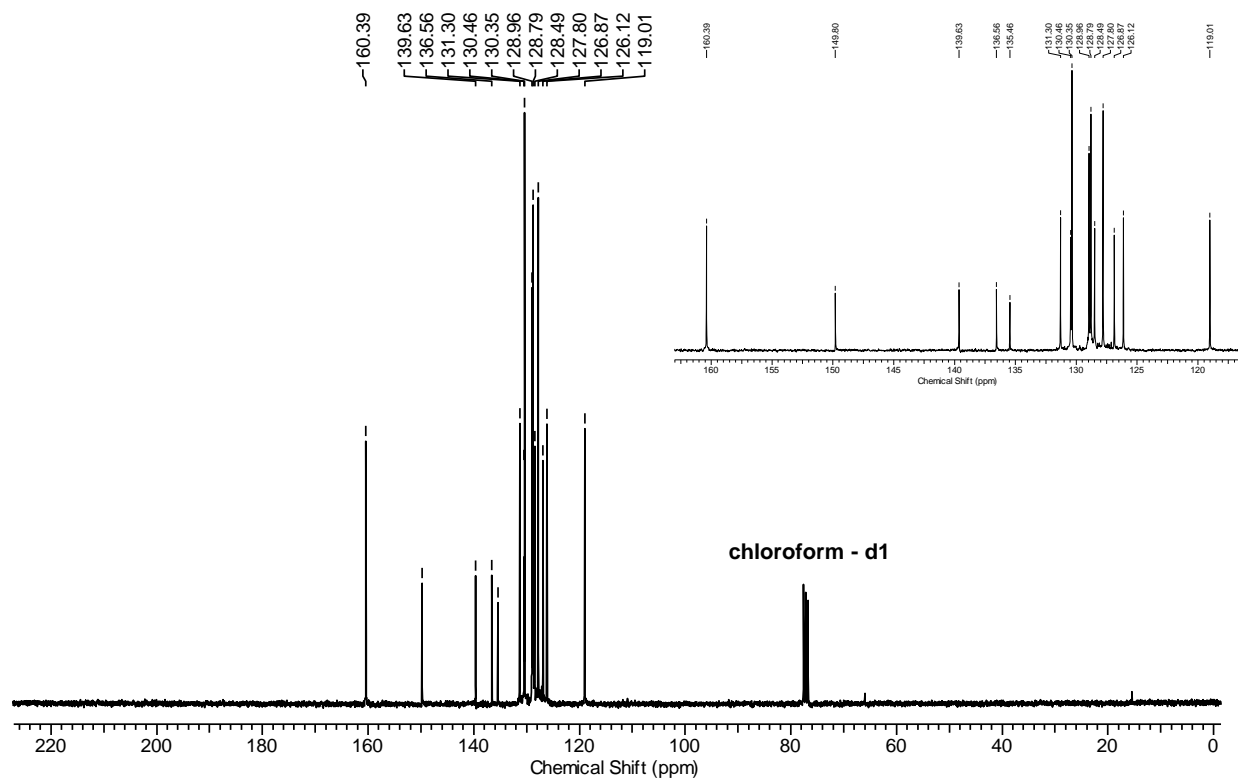
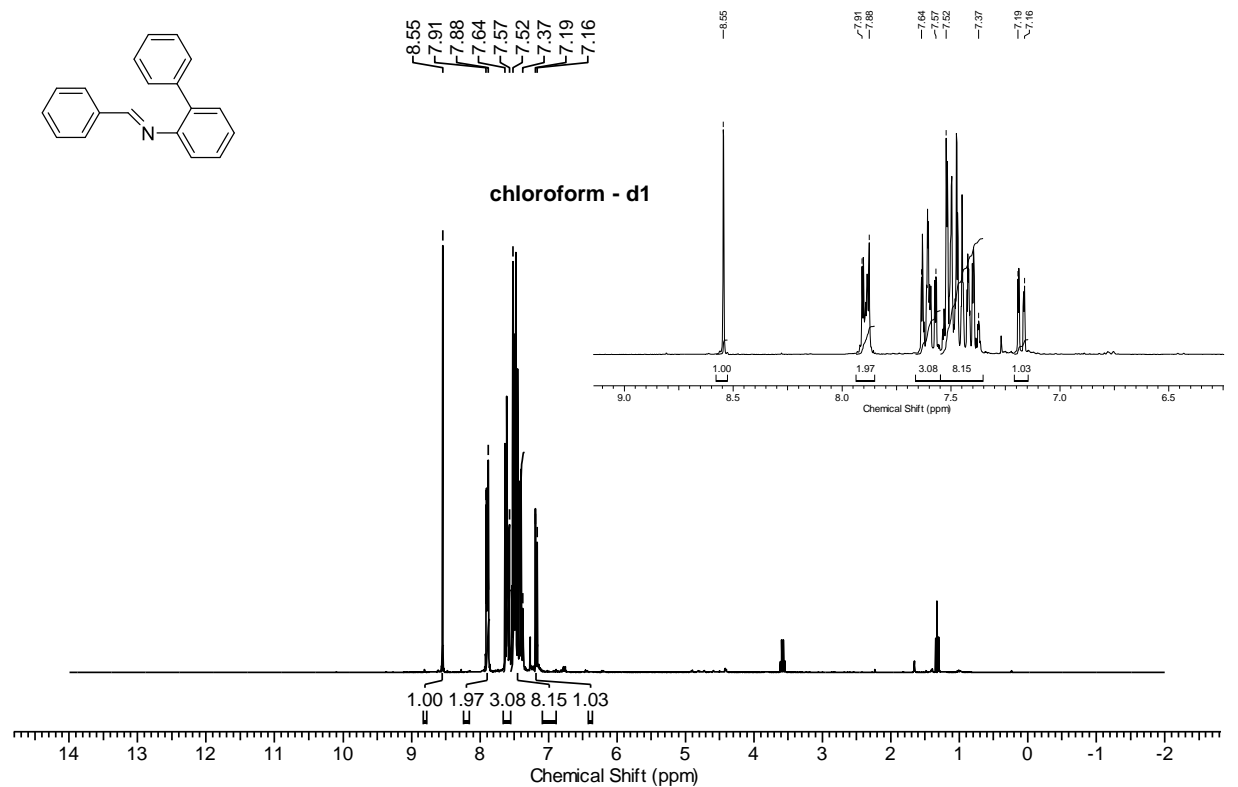
3c:



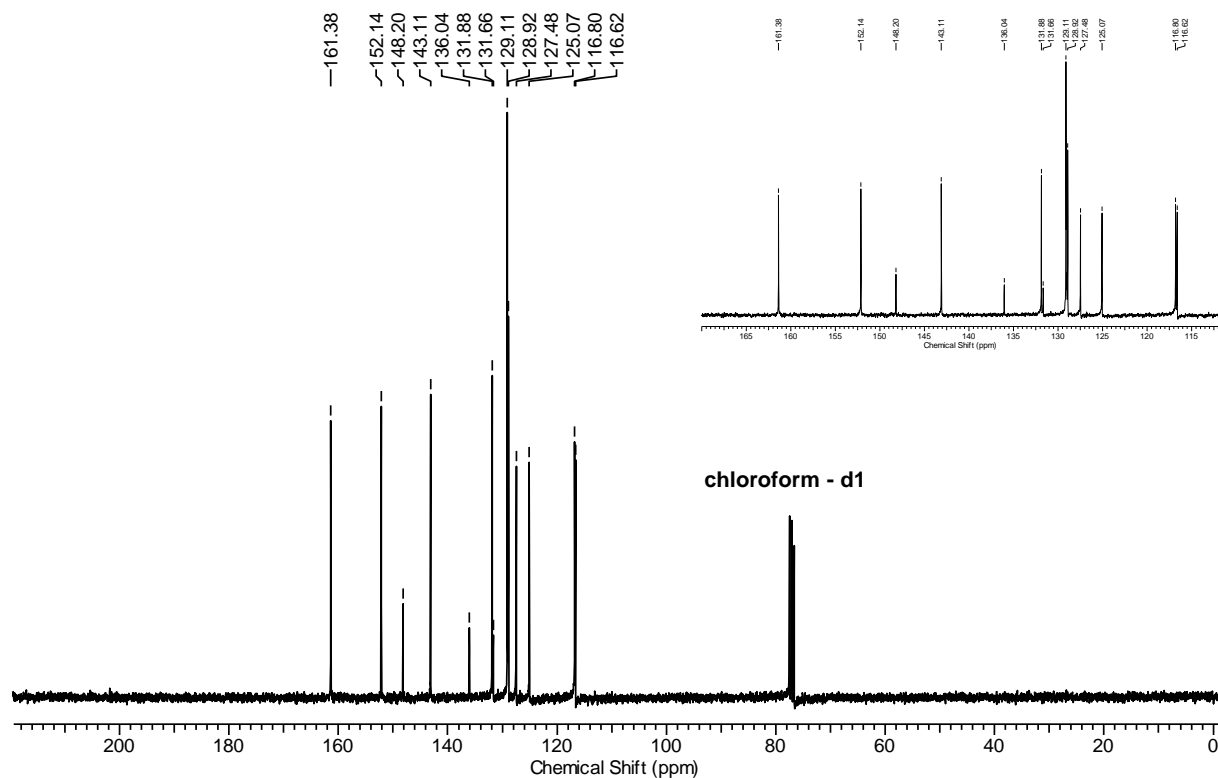
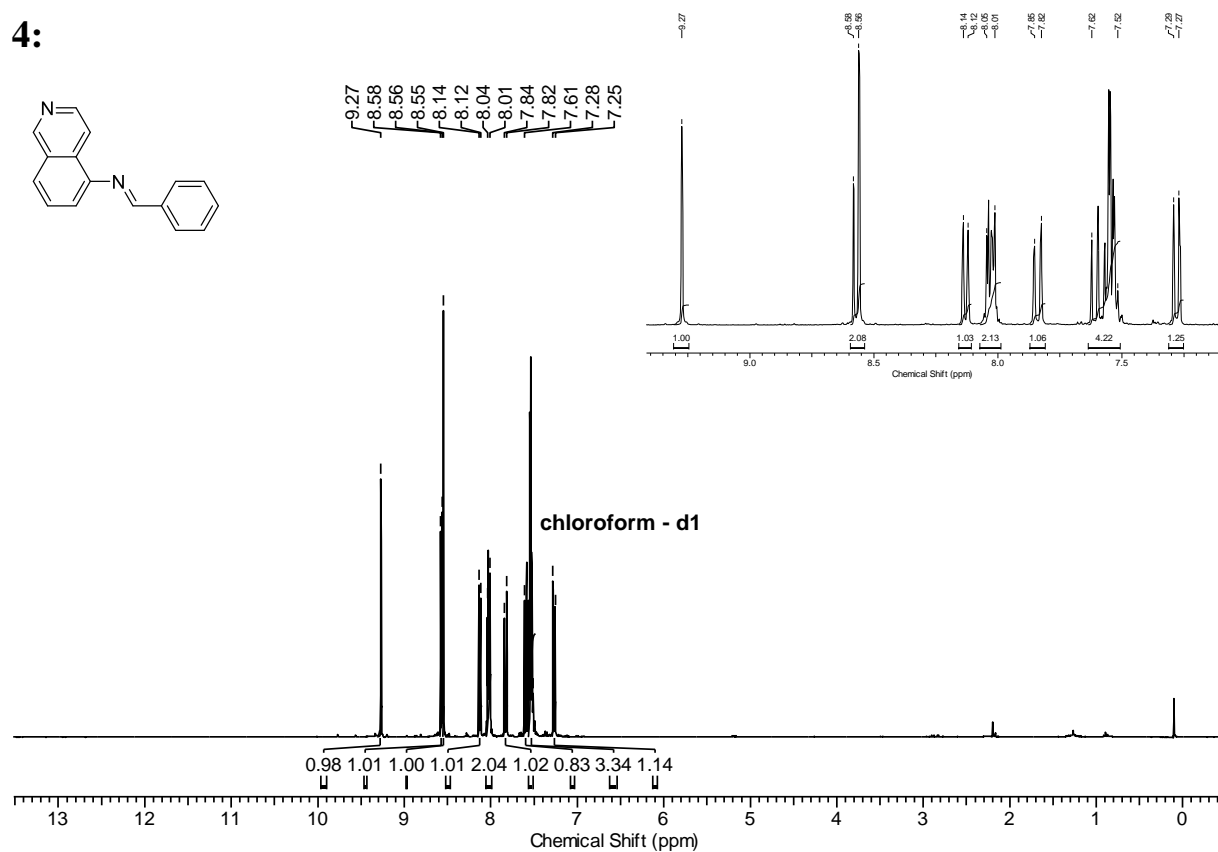
3d:



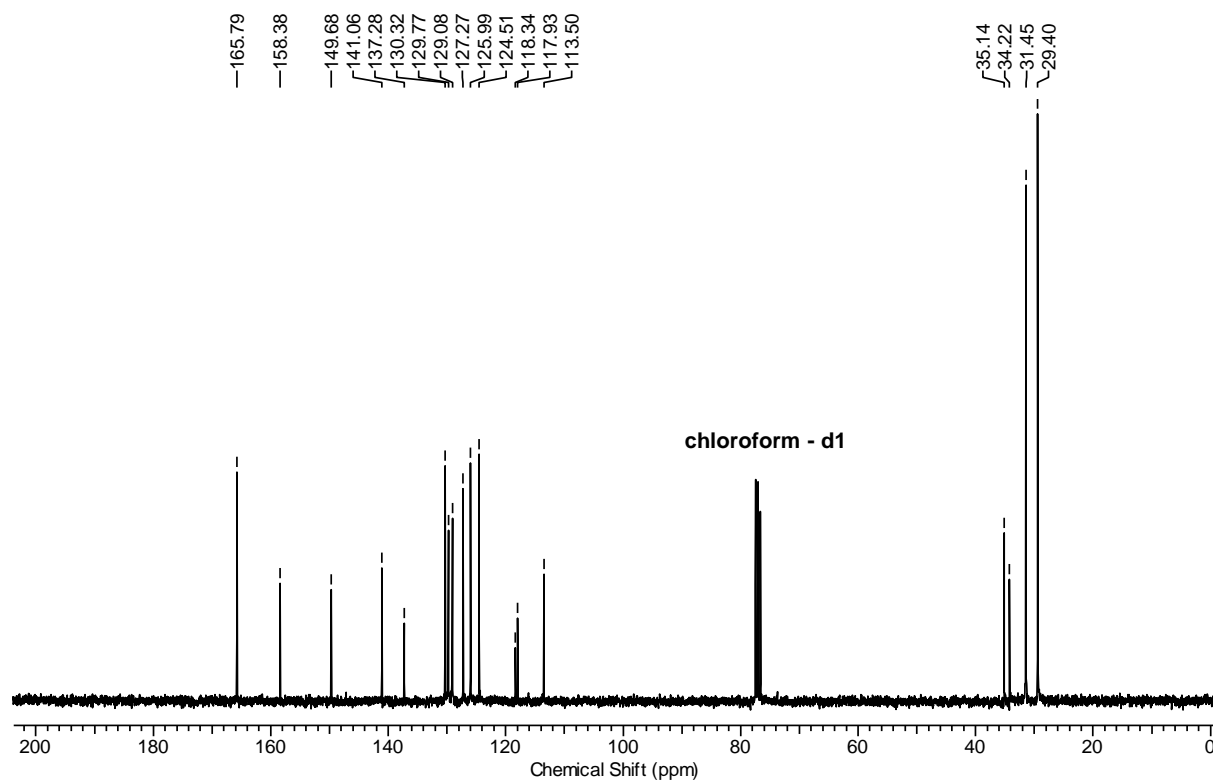
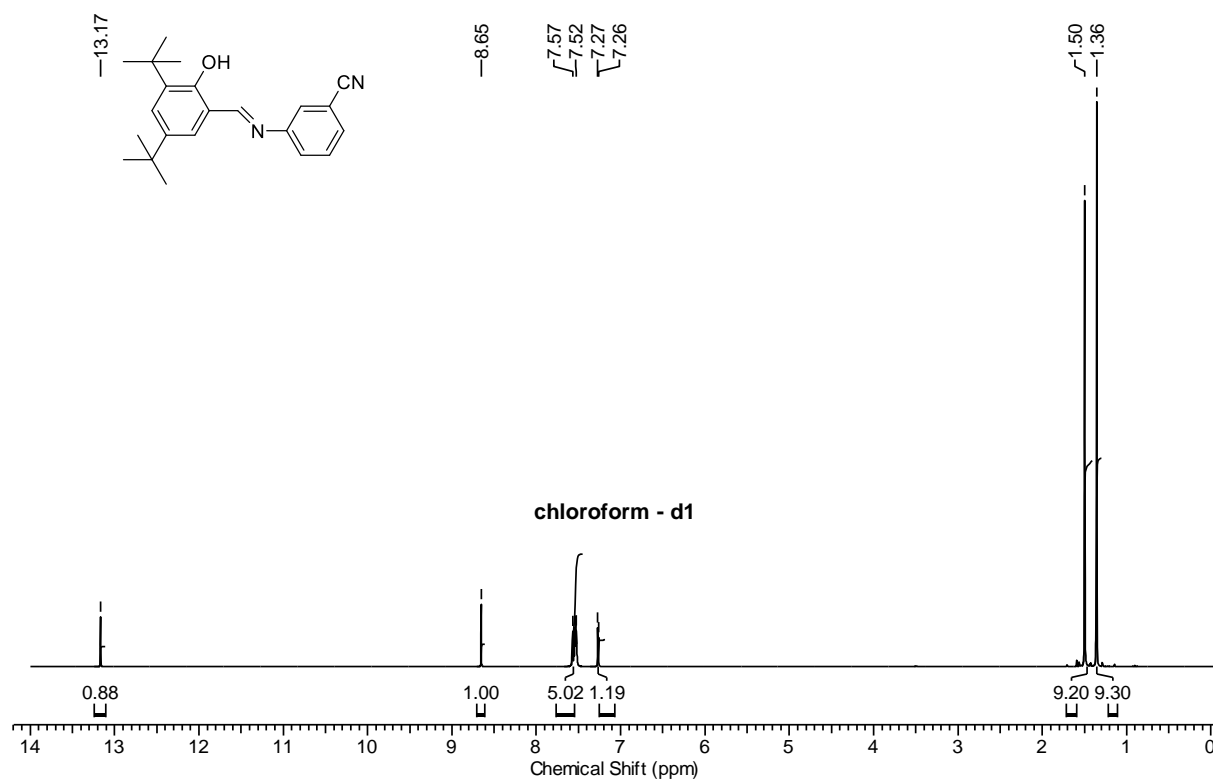
3e:



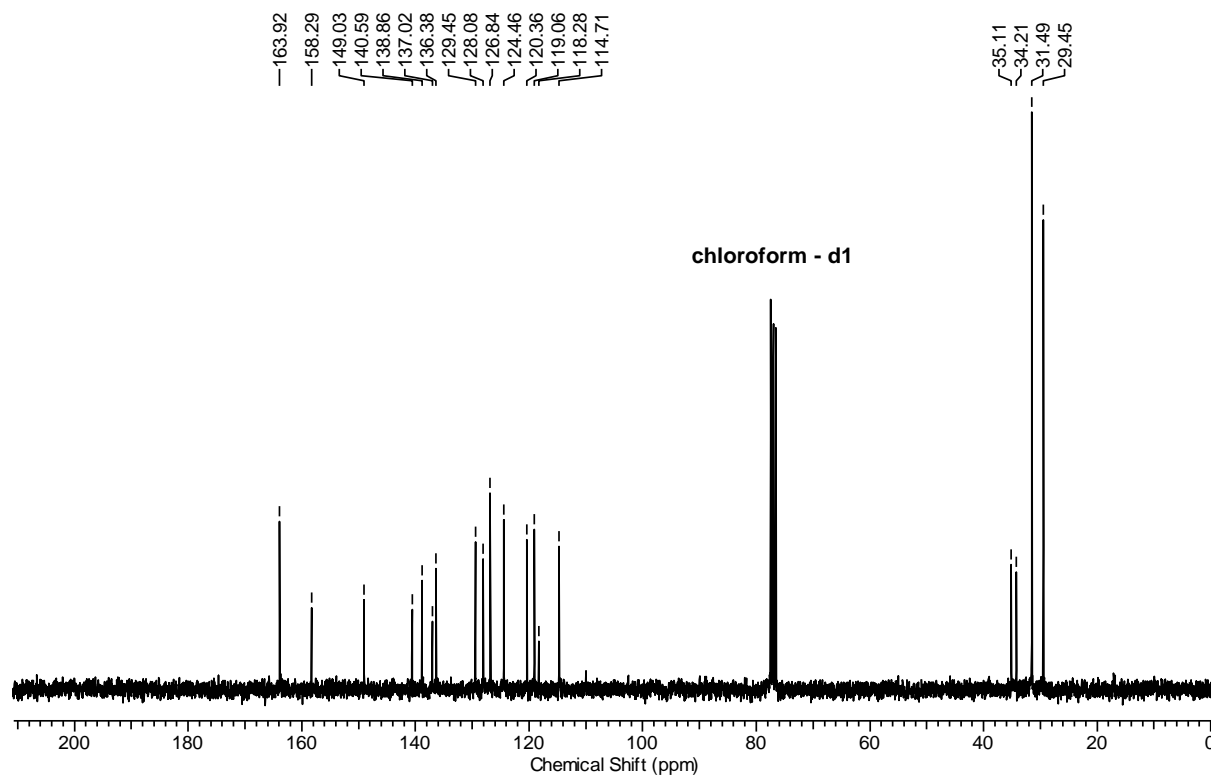
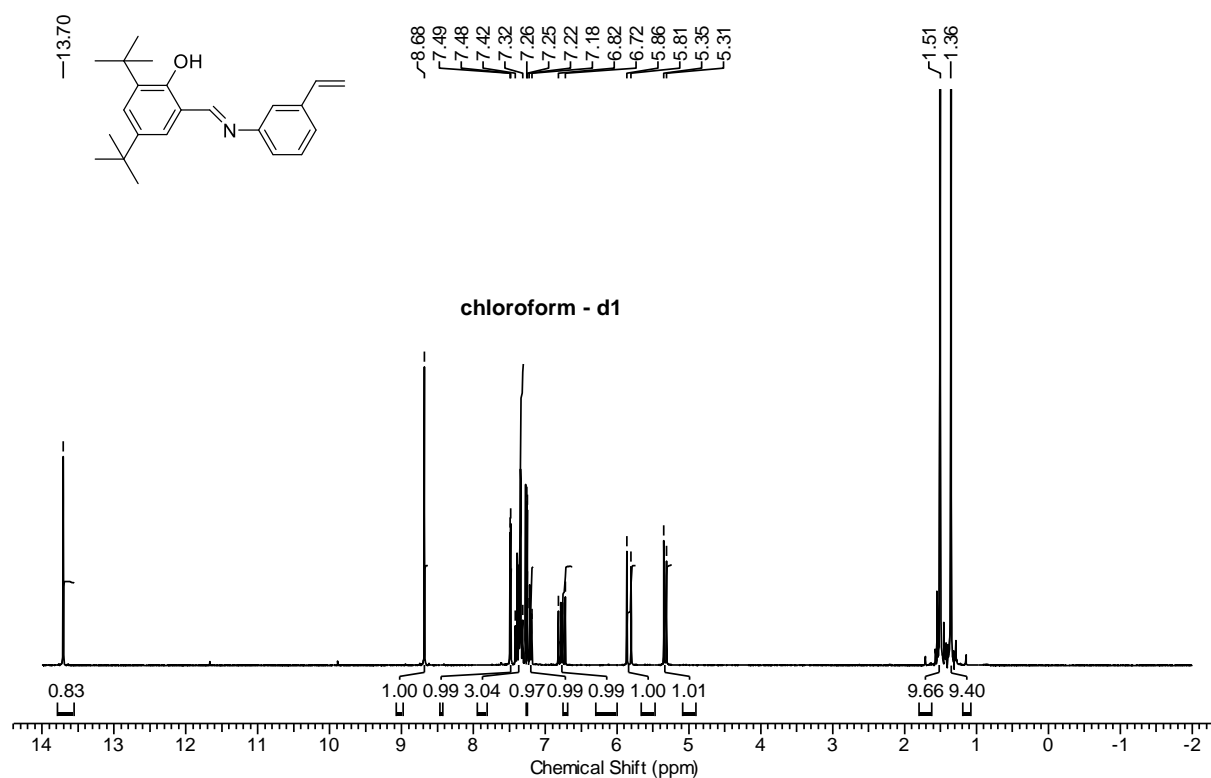
4:



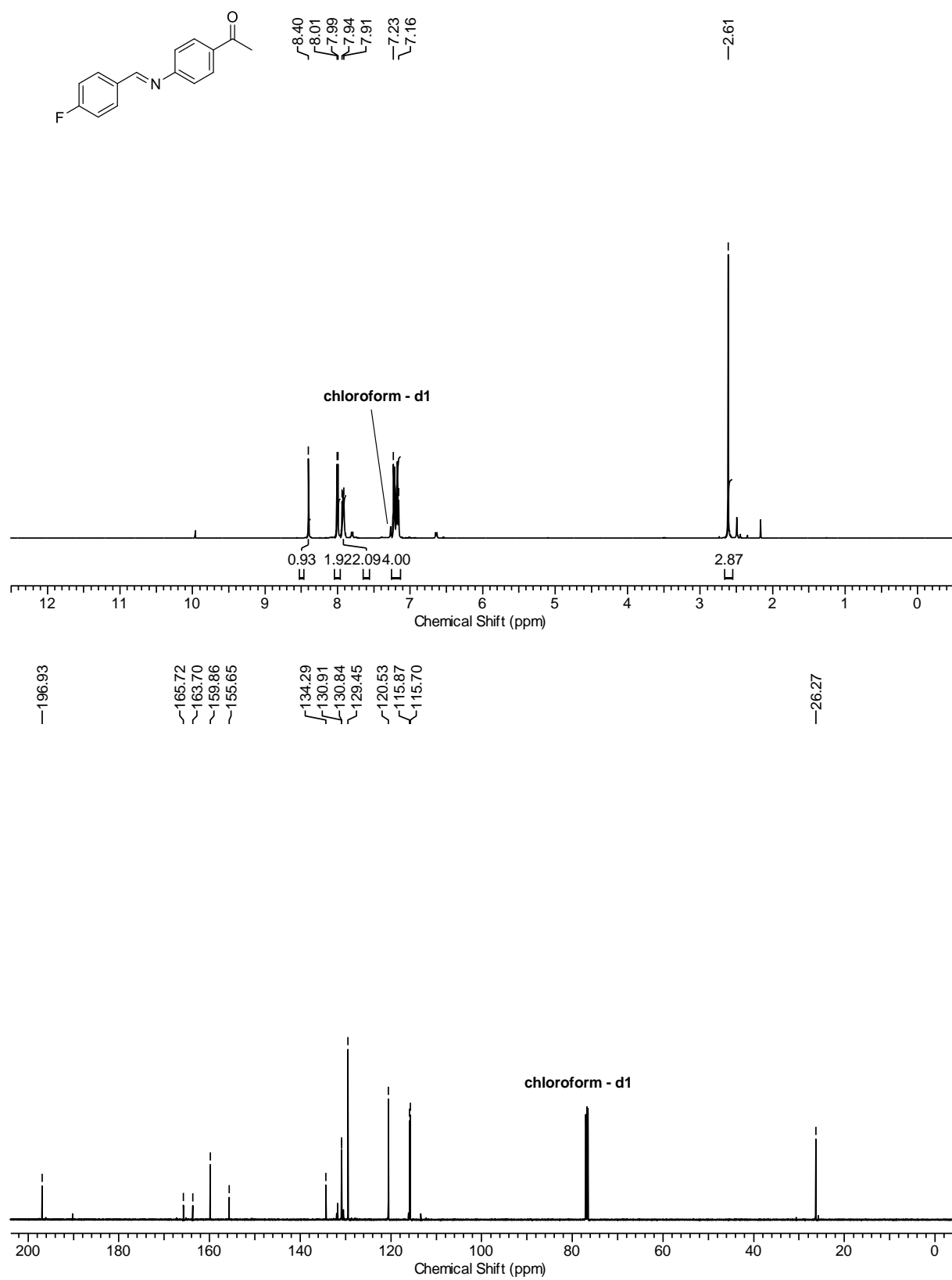
5a:



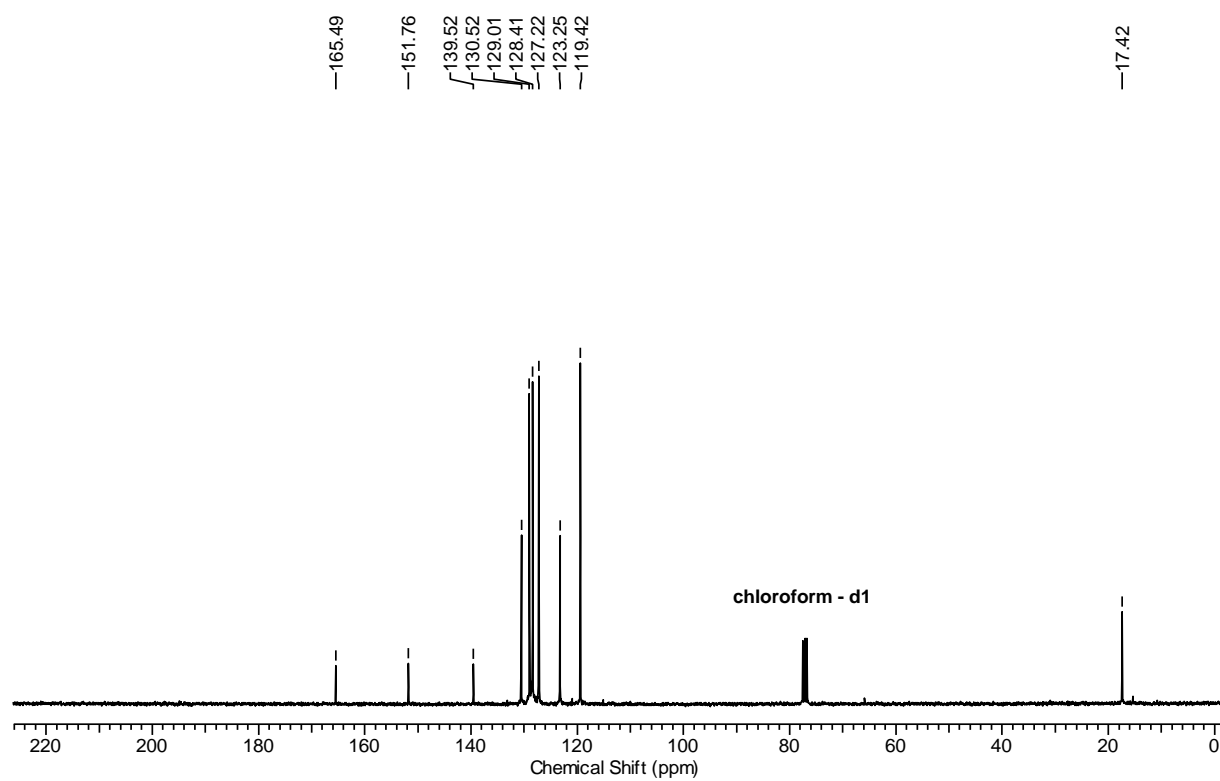
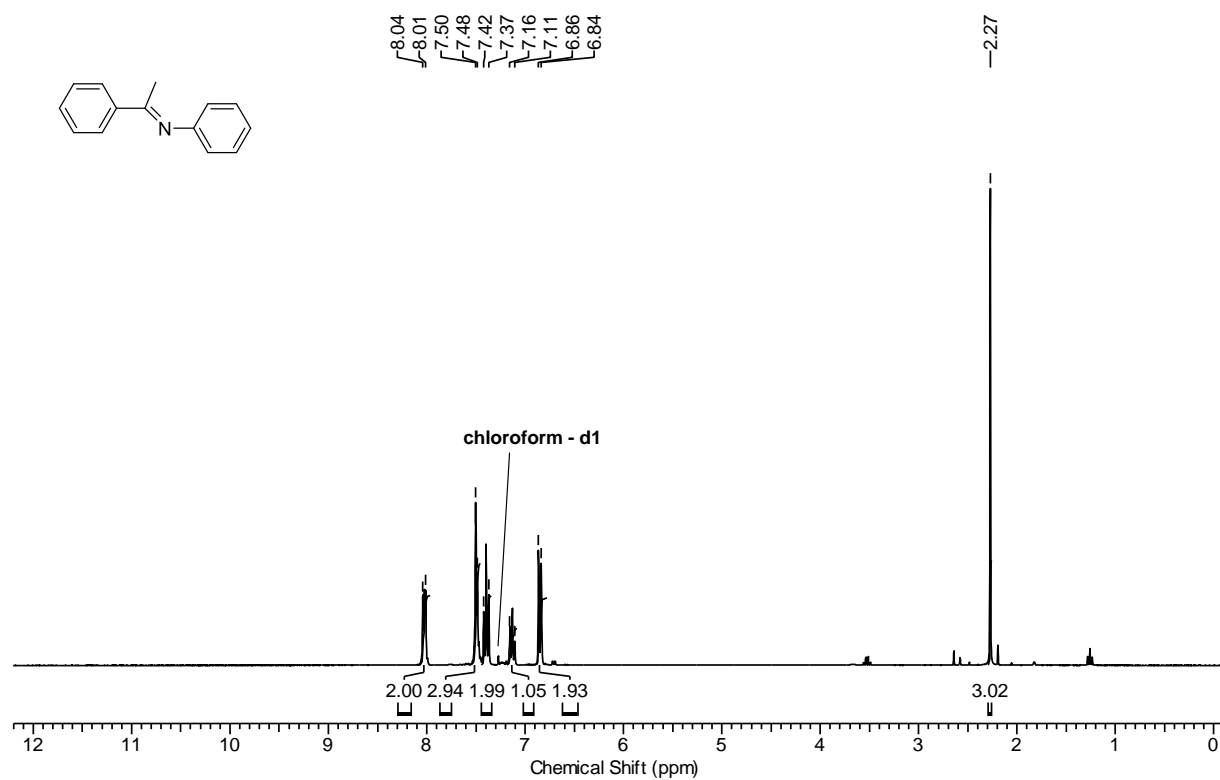
5b:



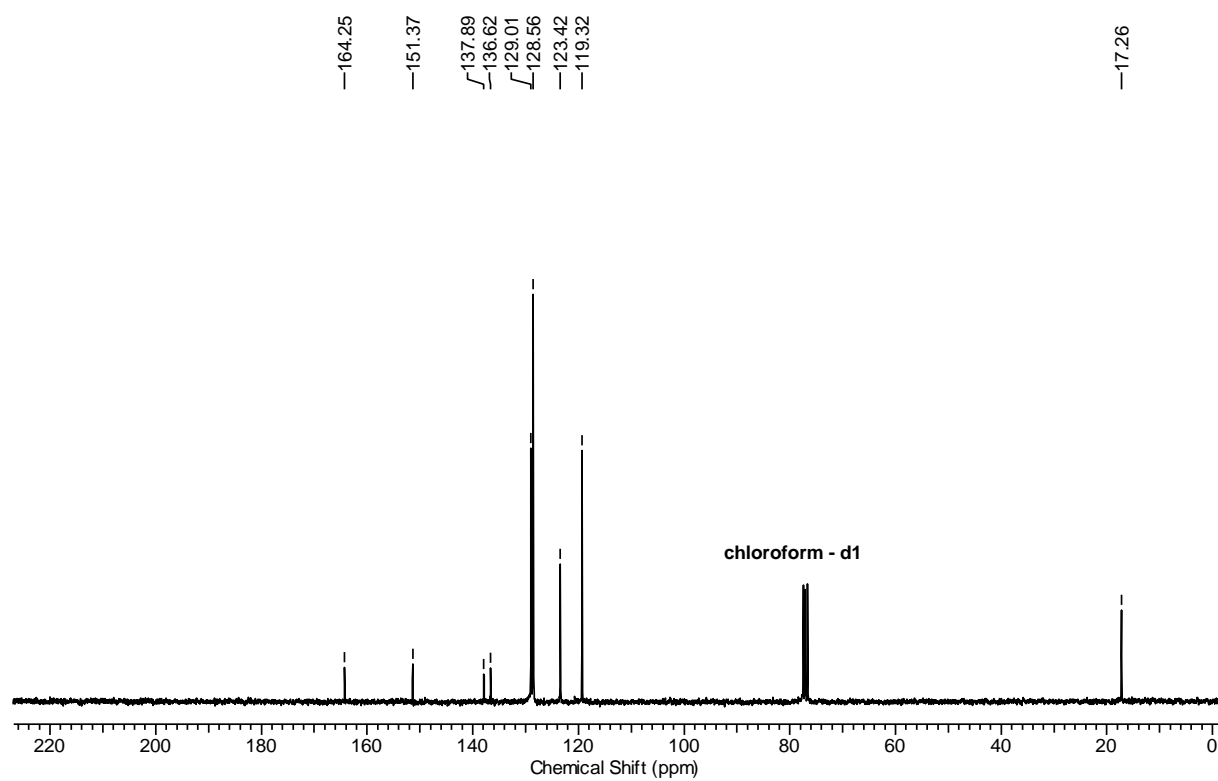
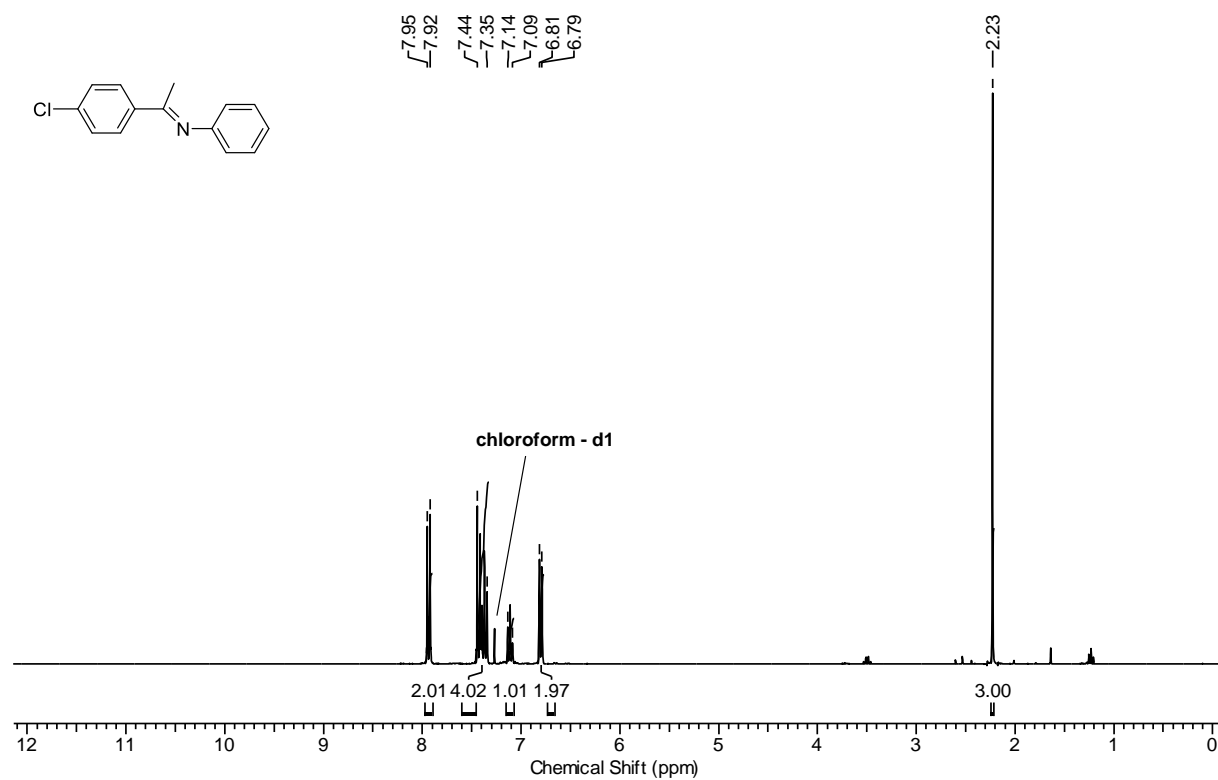
6:



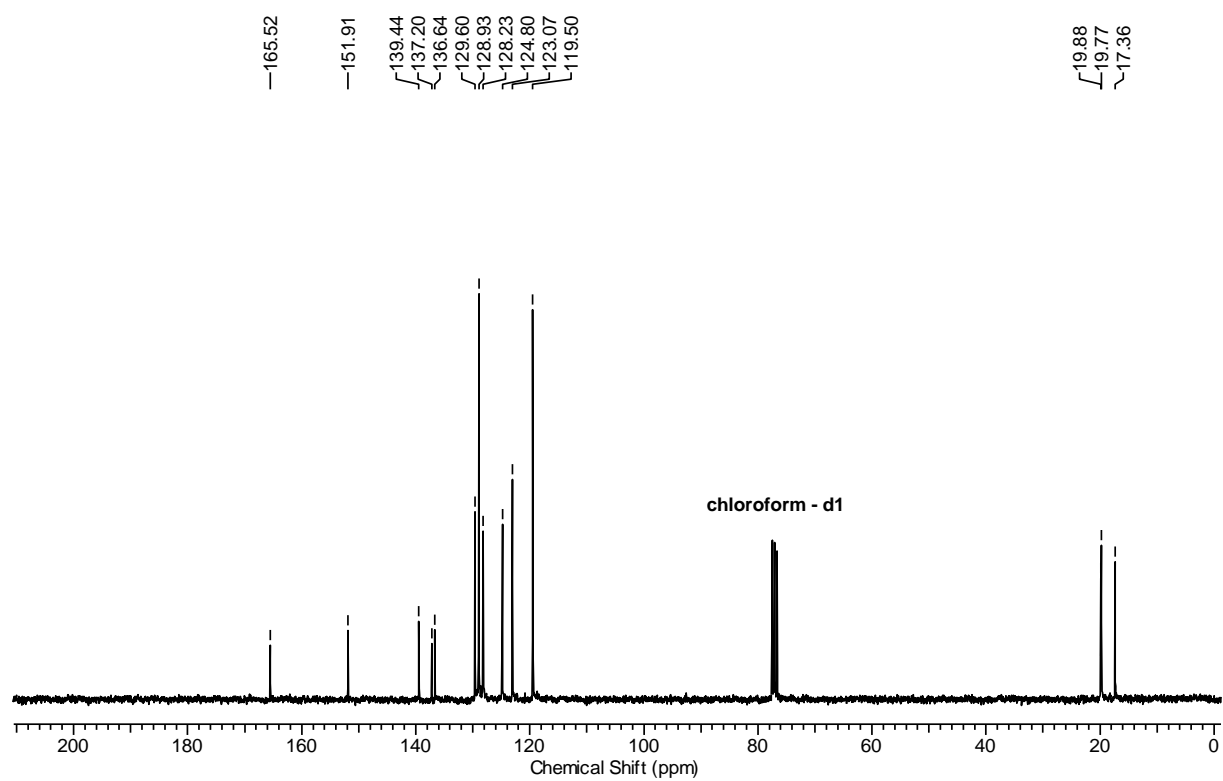
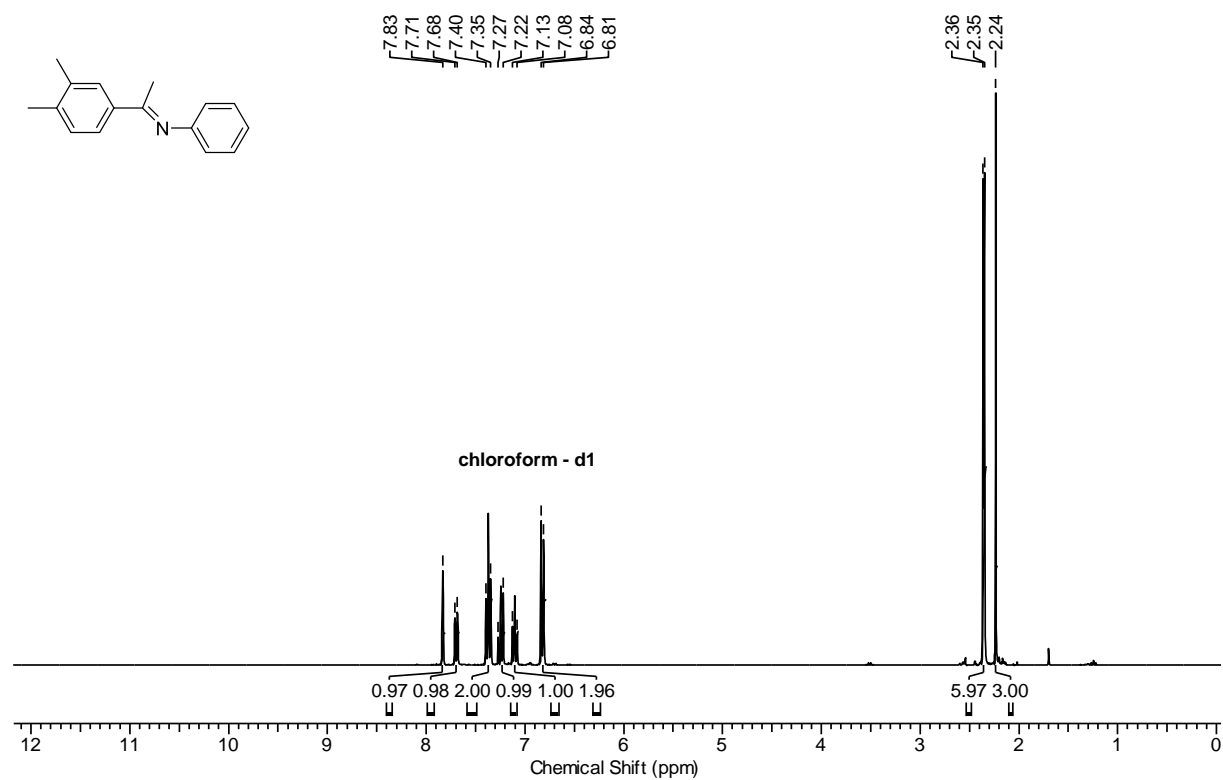
7a:



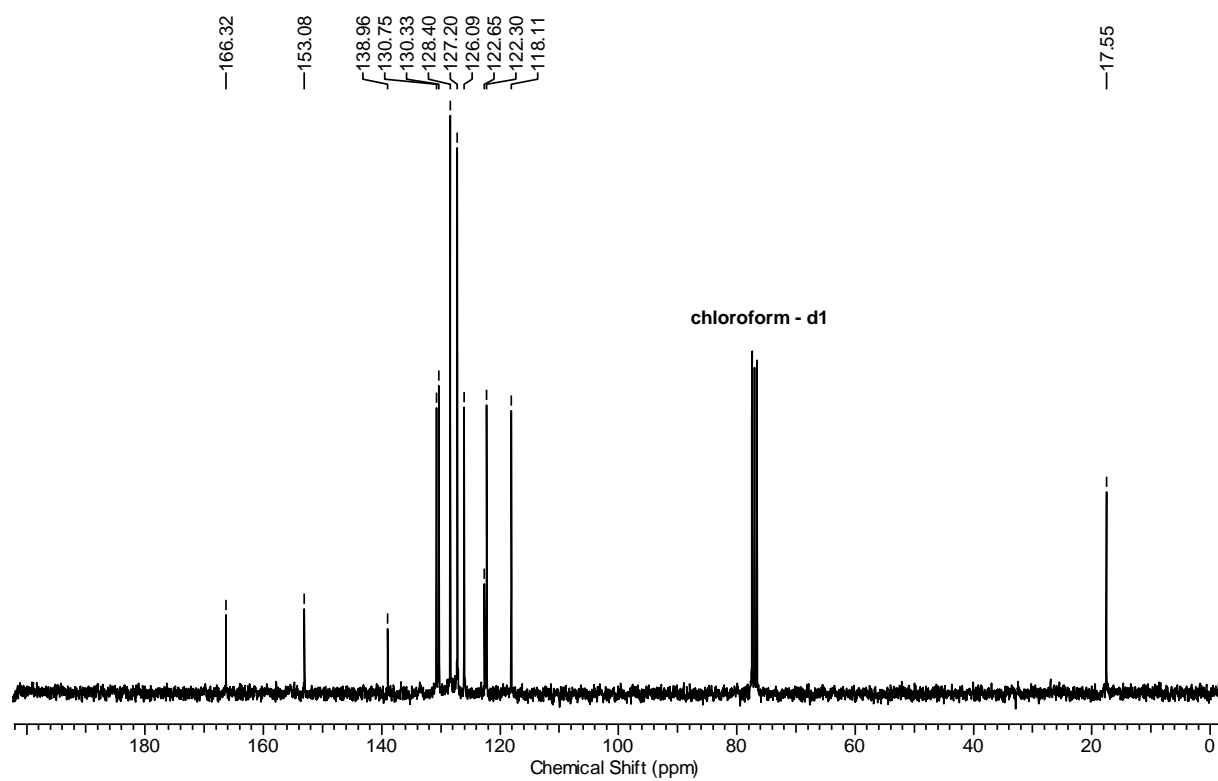
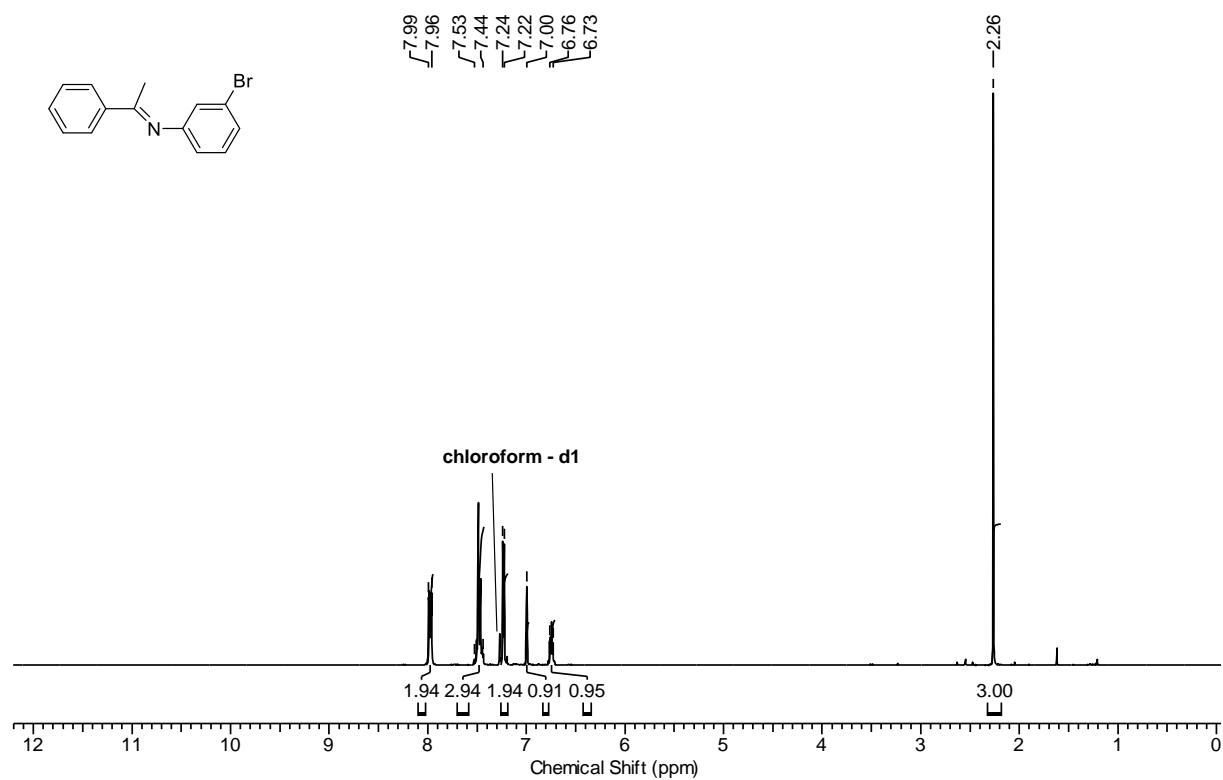
7b:



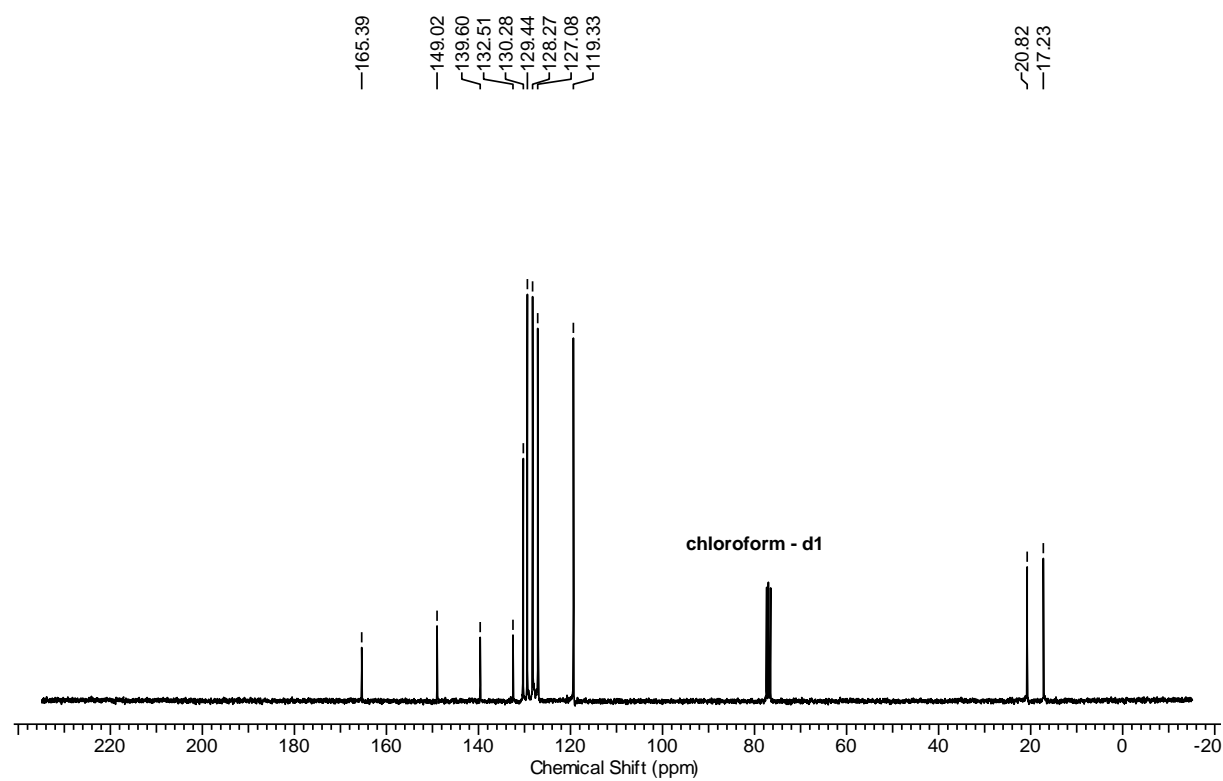
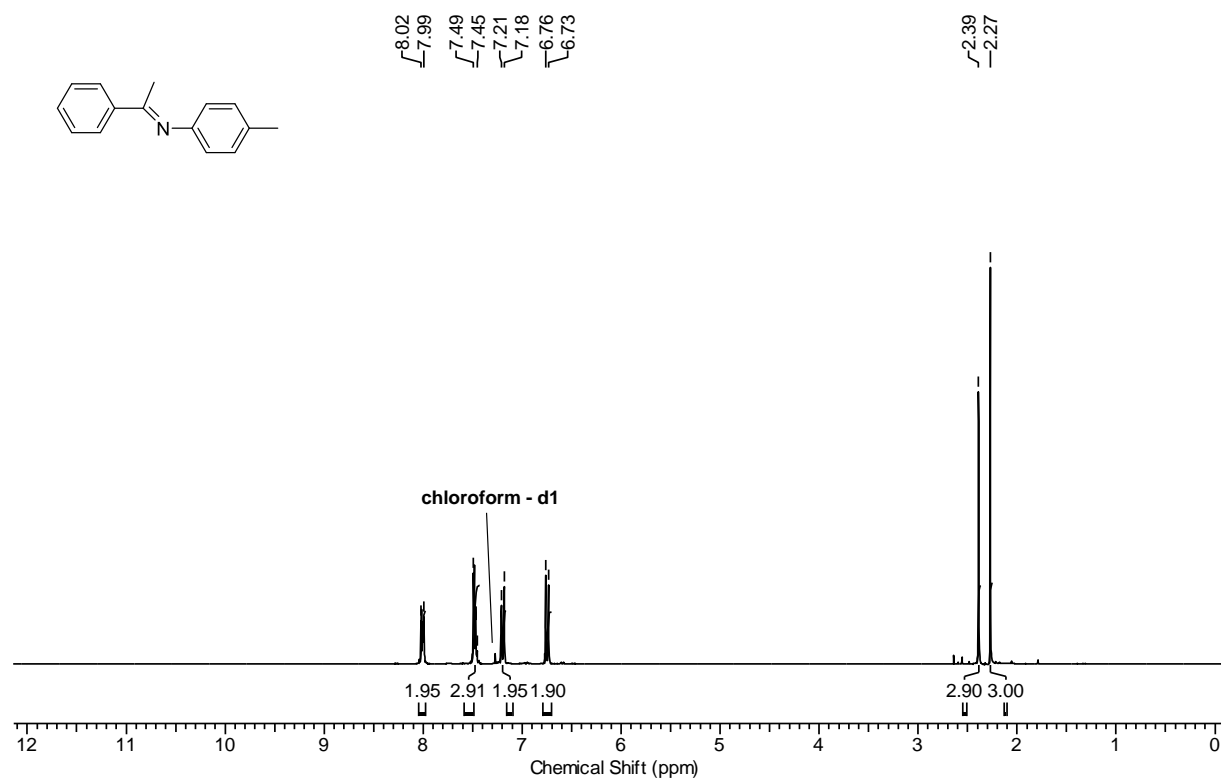
7c:



8a:

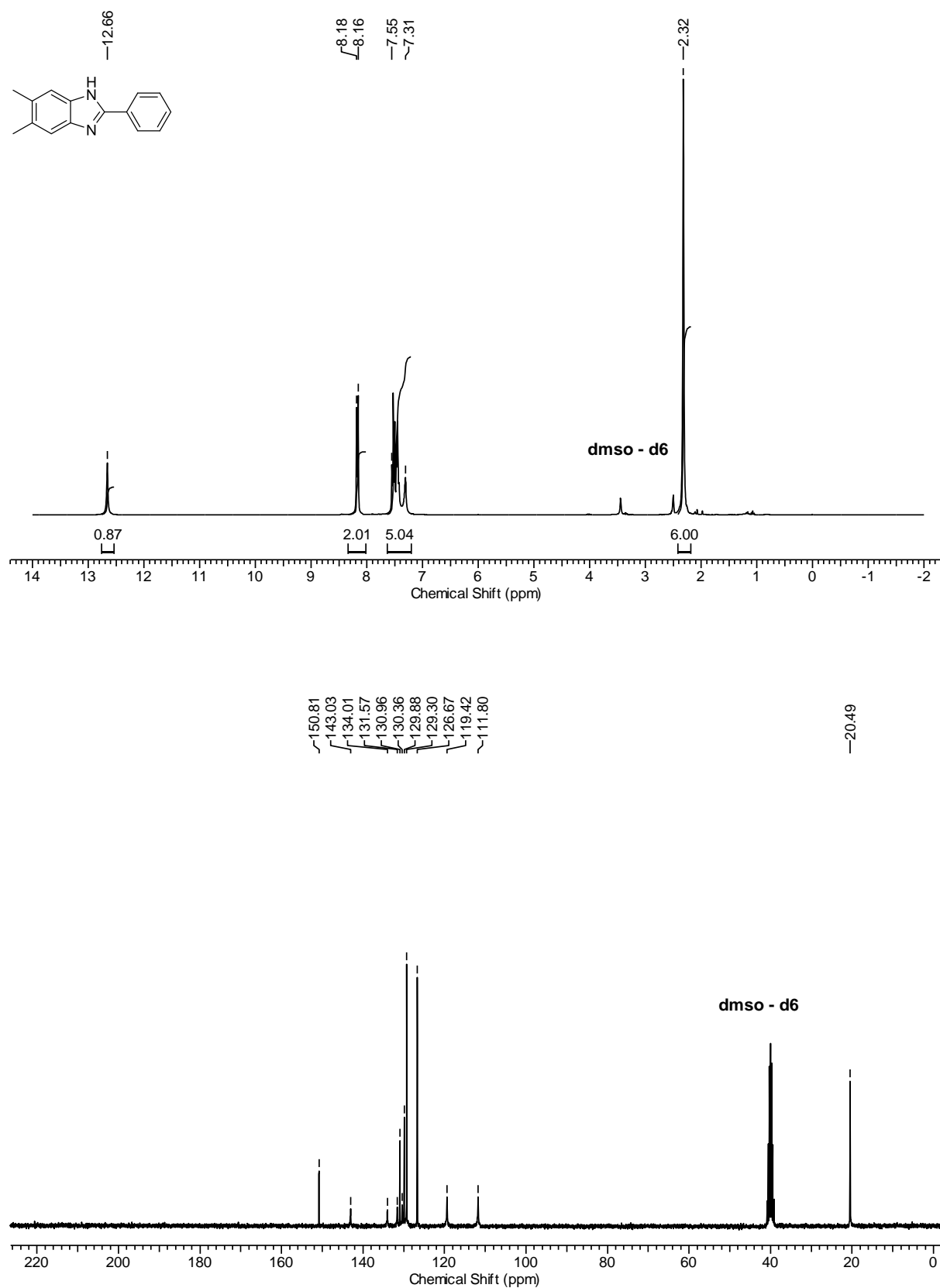


8b:

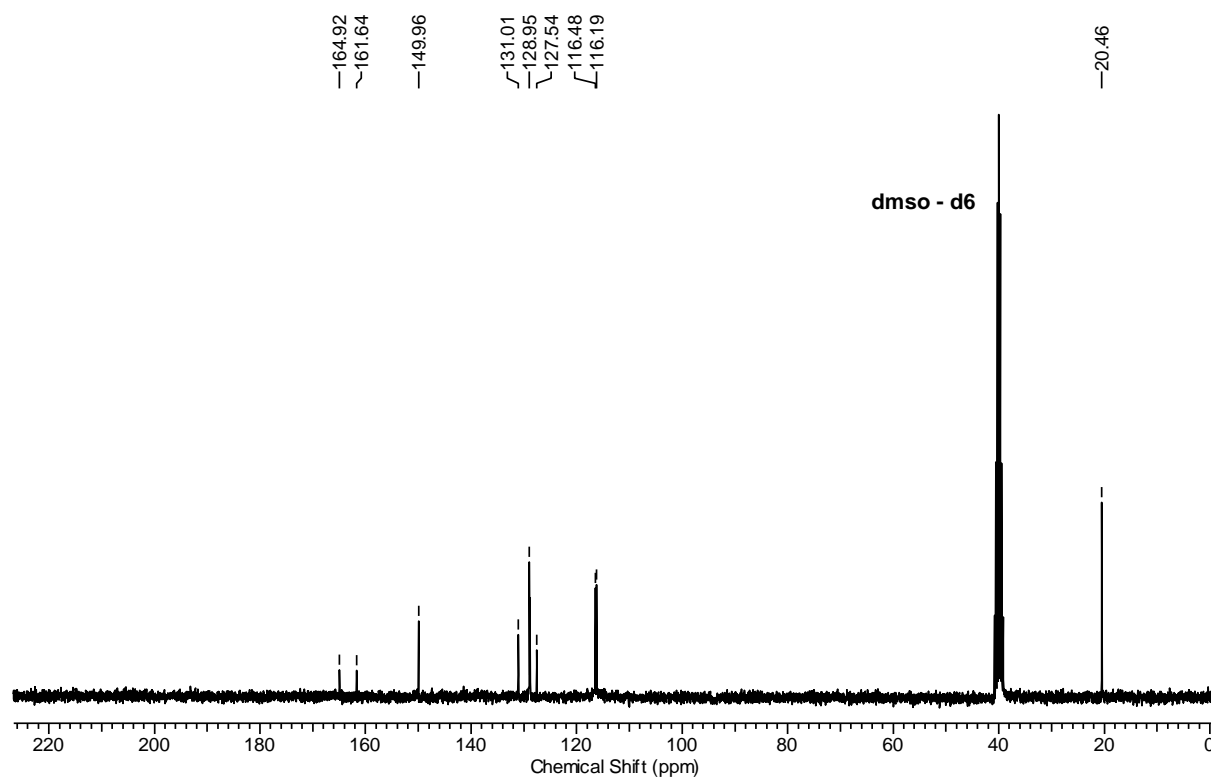
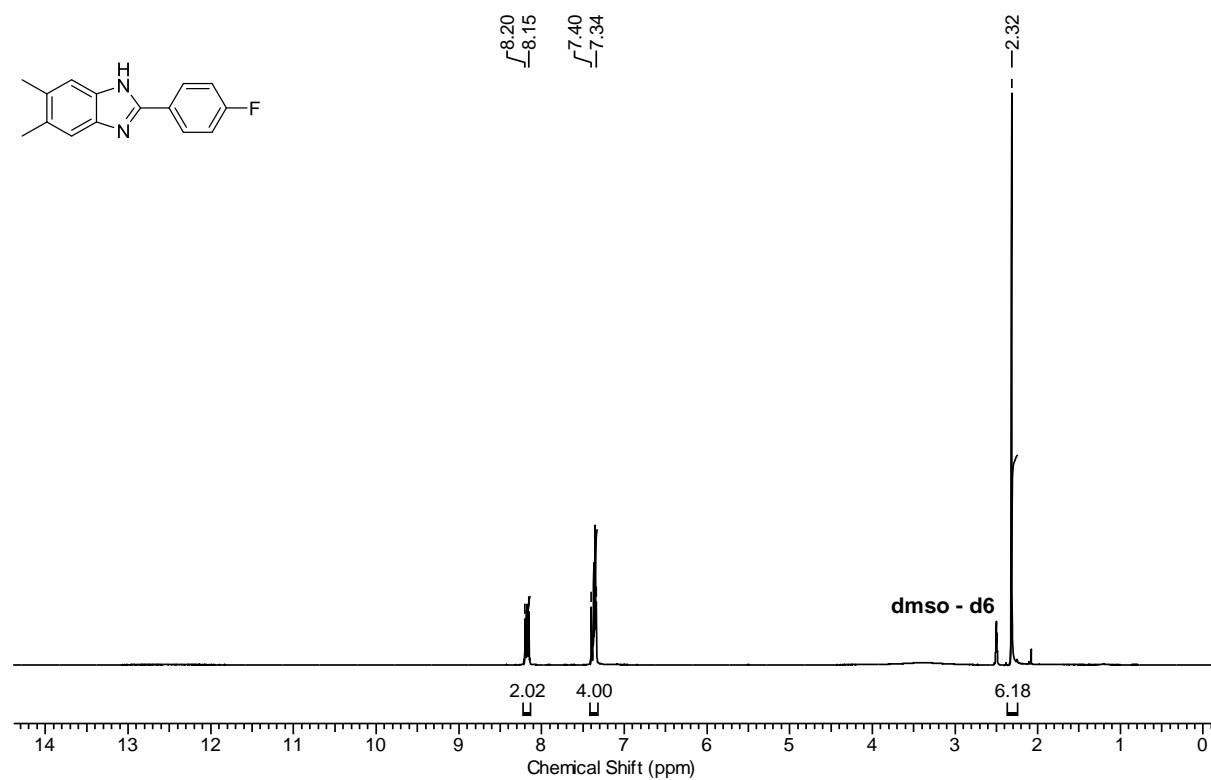


Benzimidazoles

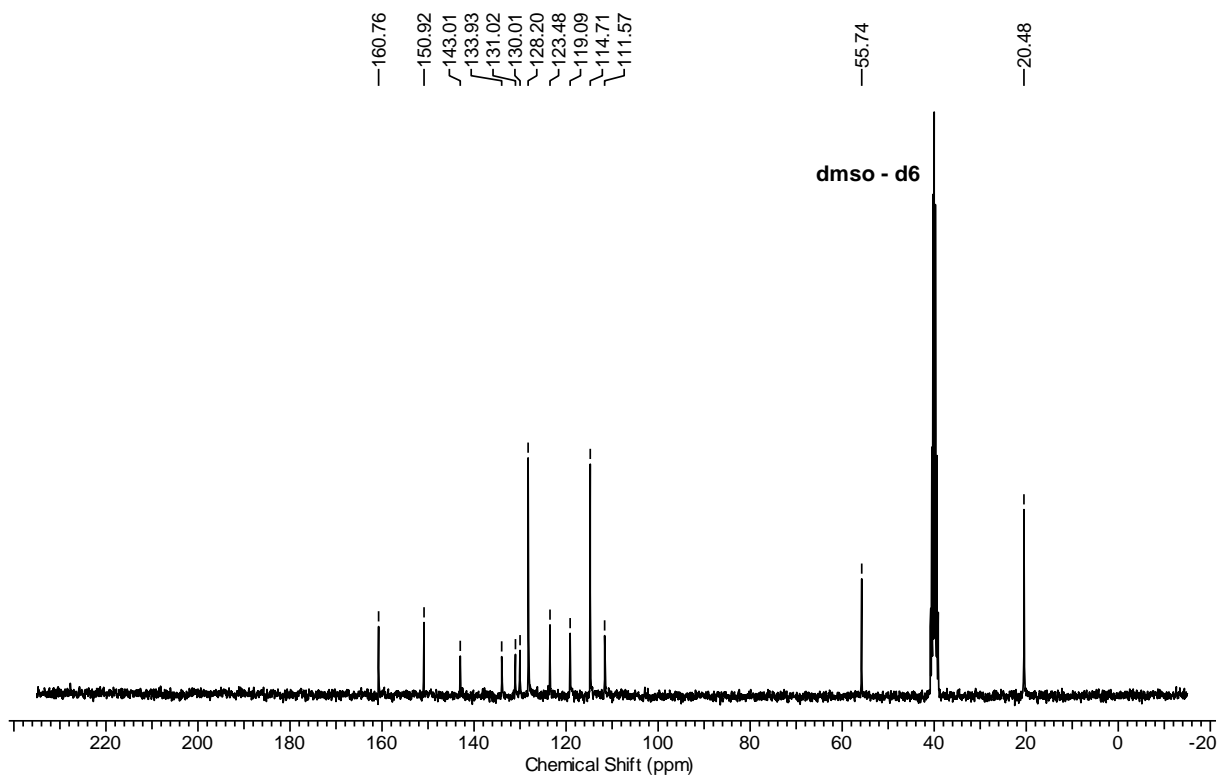
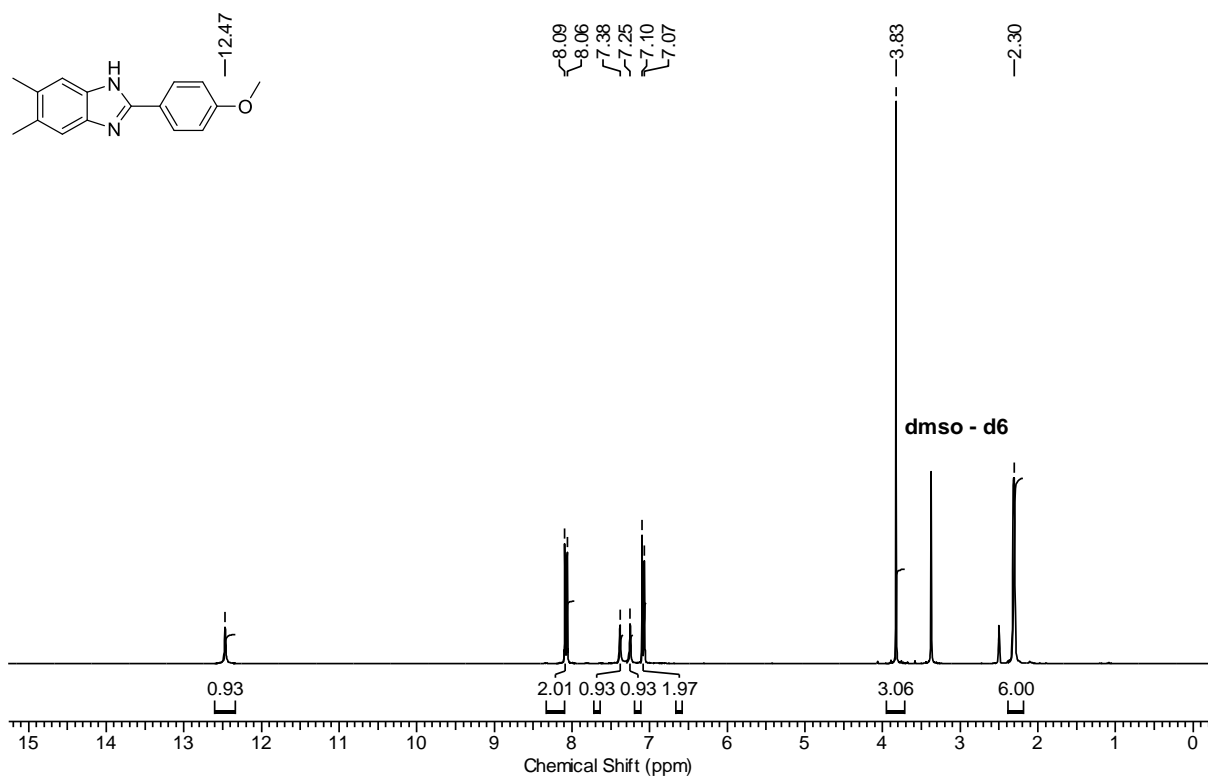
1a:



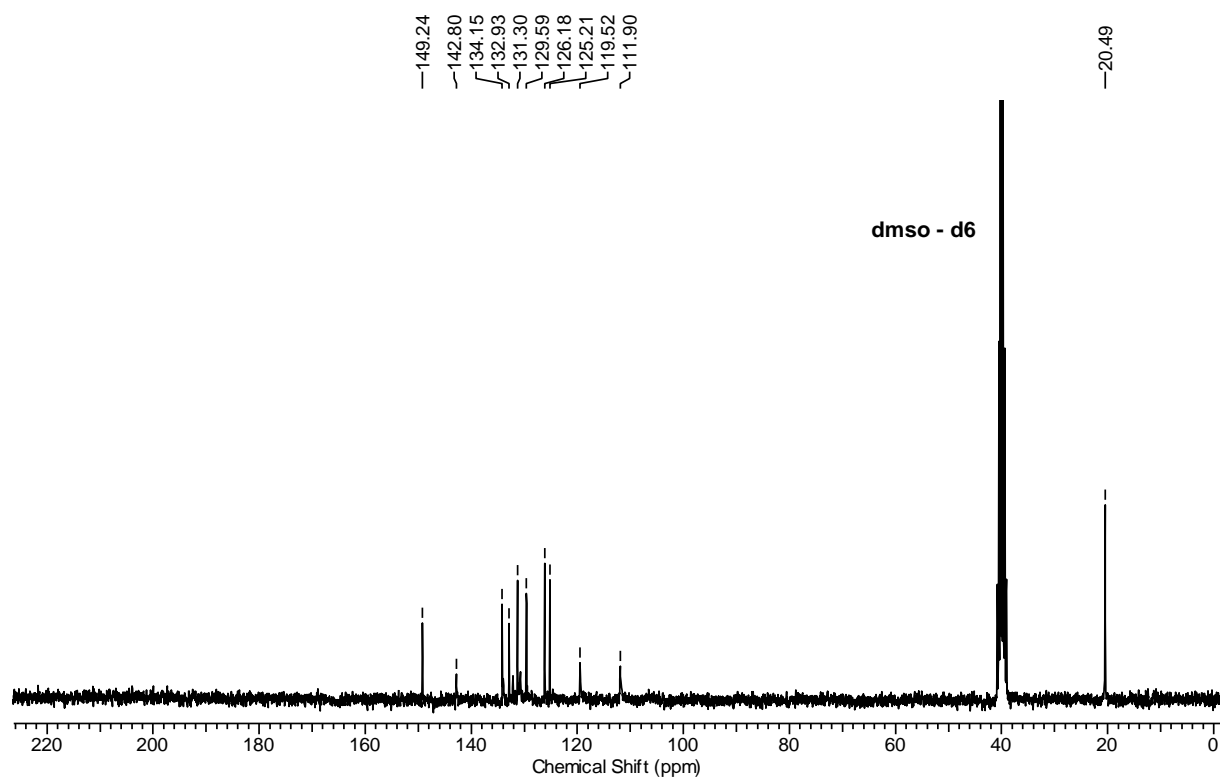
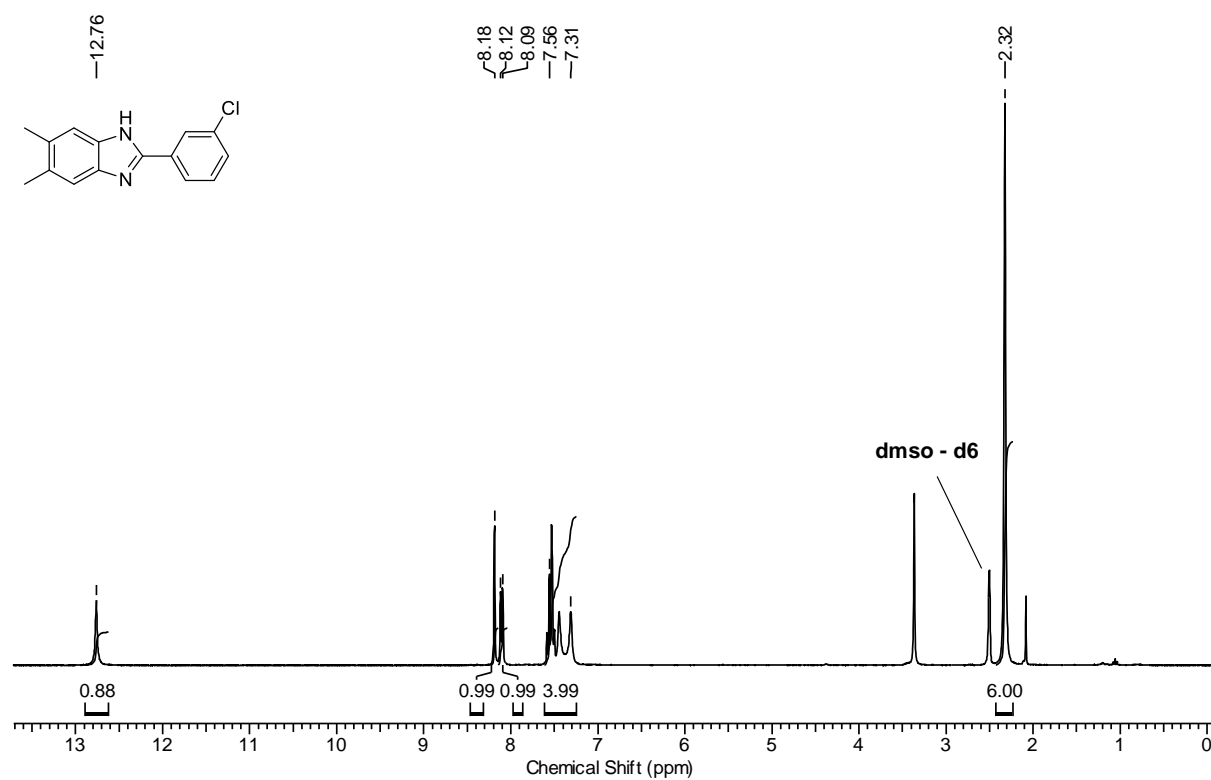
1b:



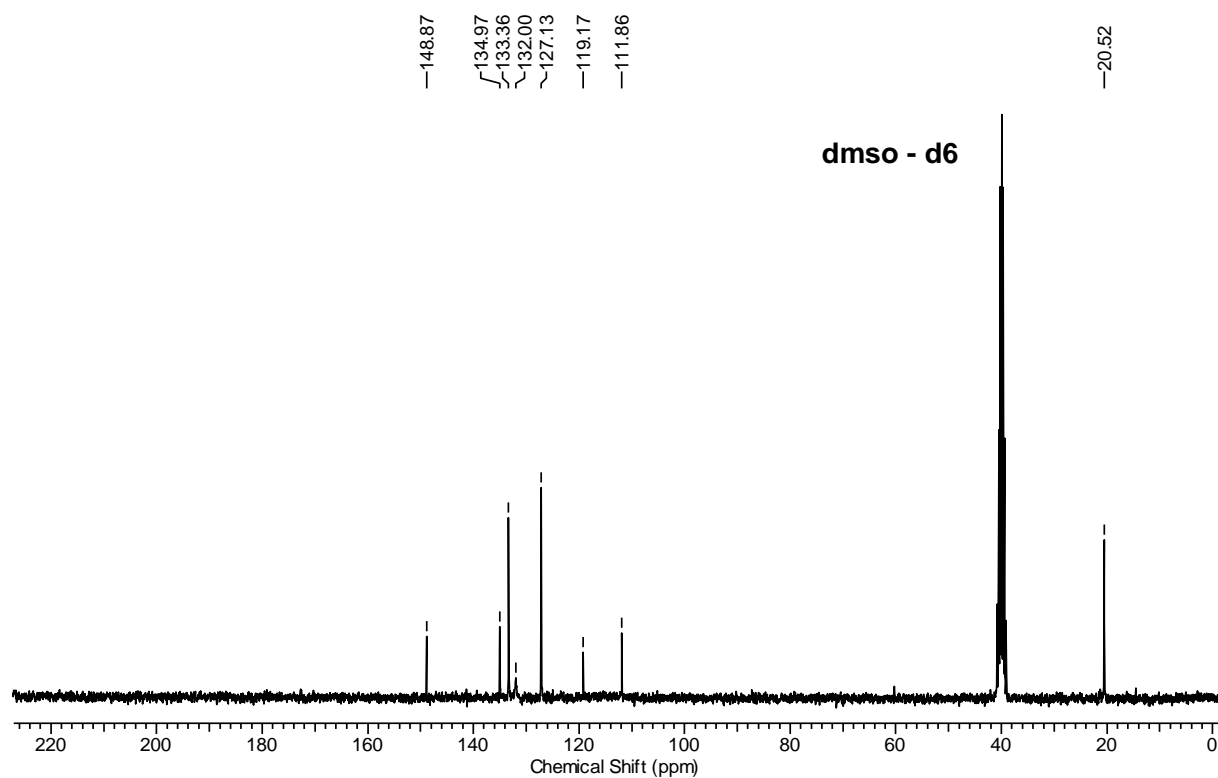
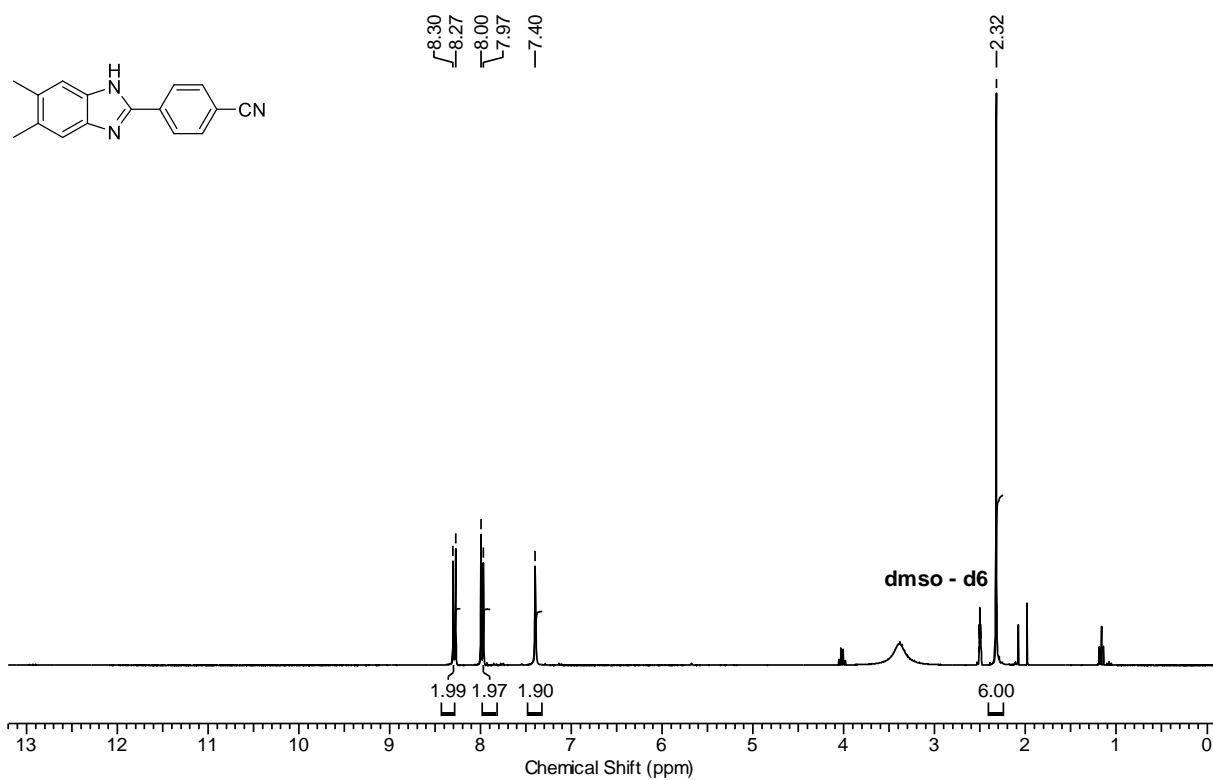
1c:



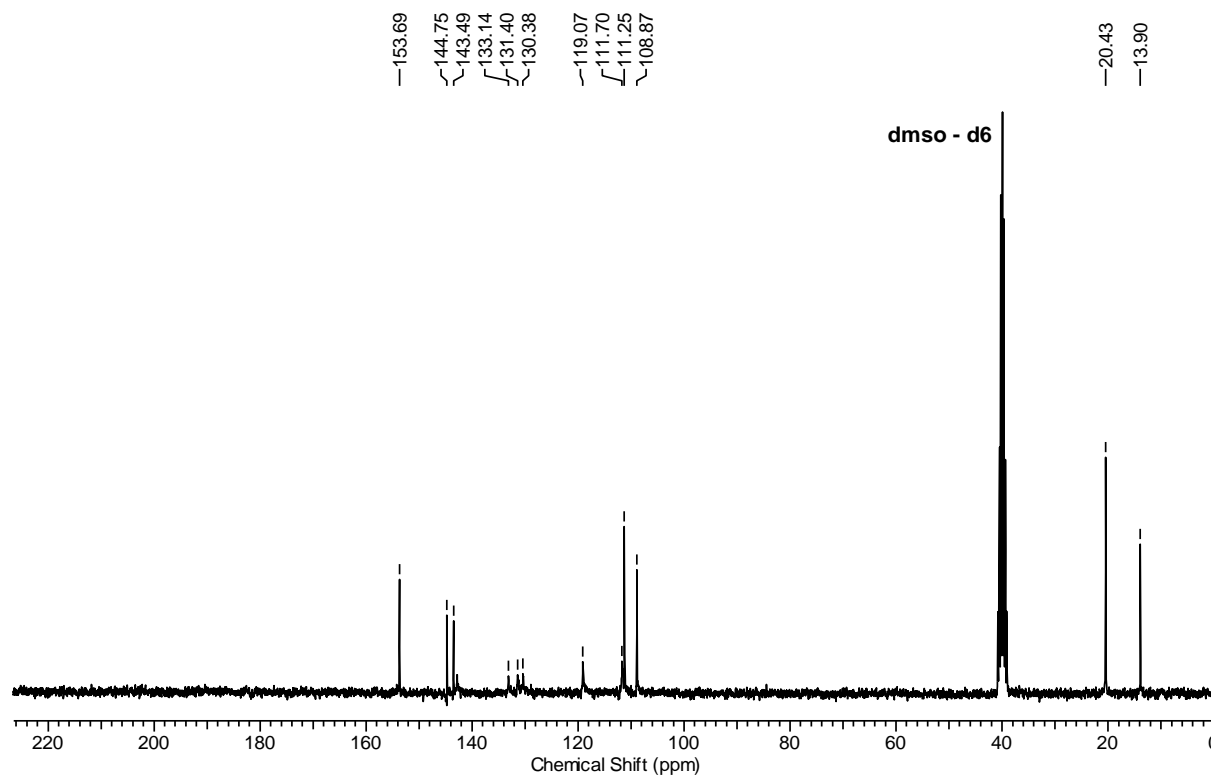
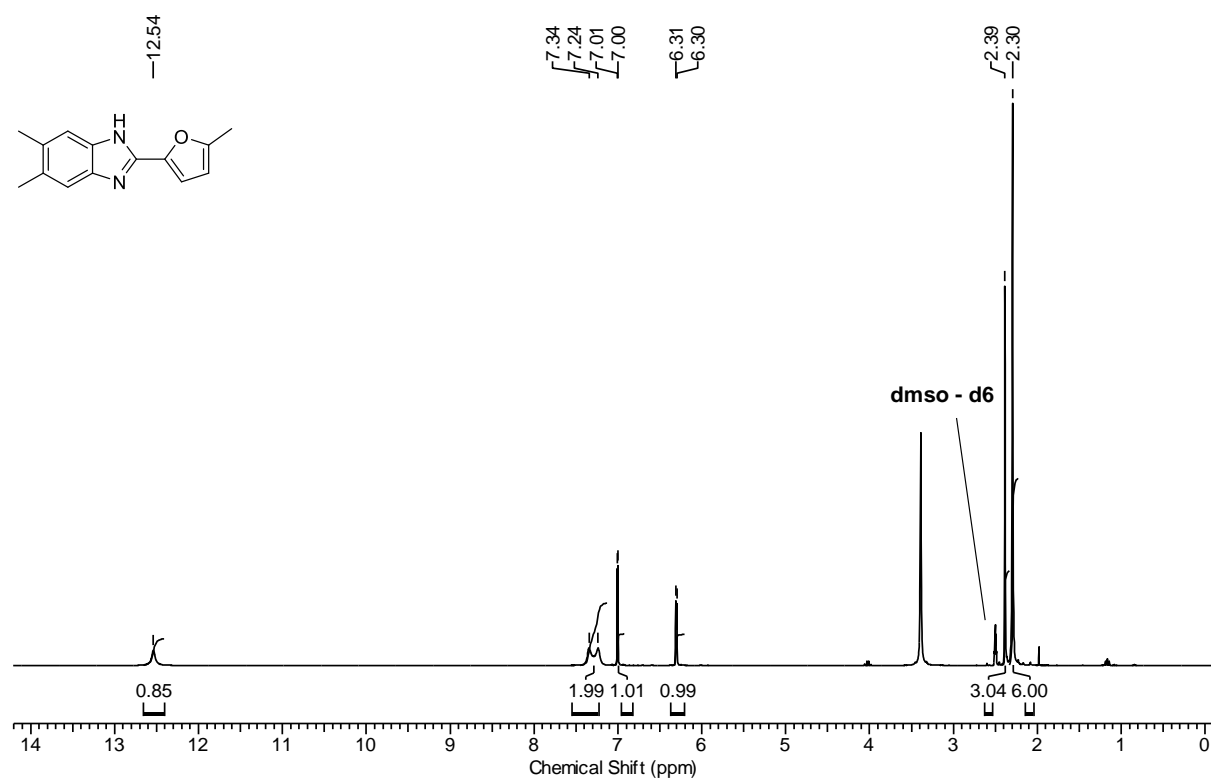
1d:



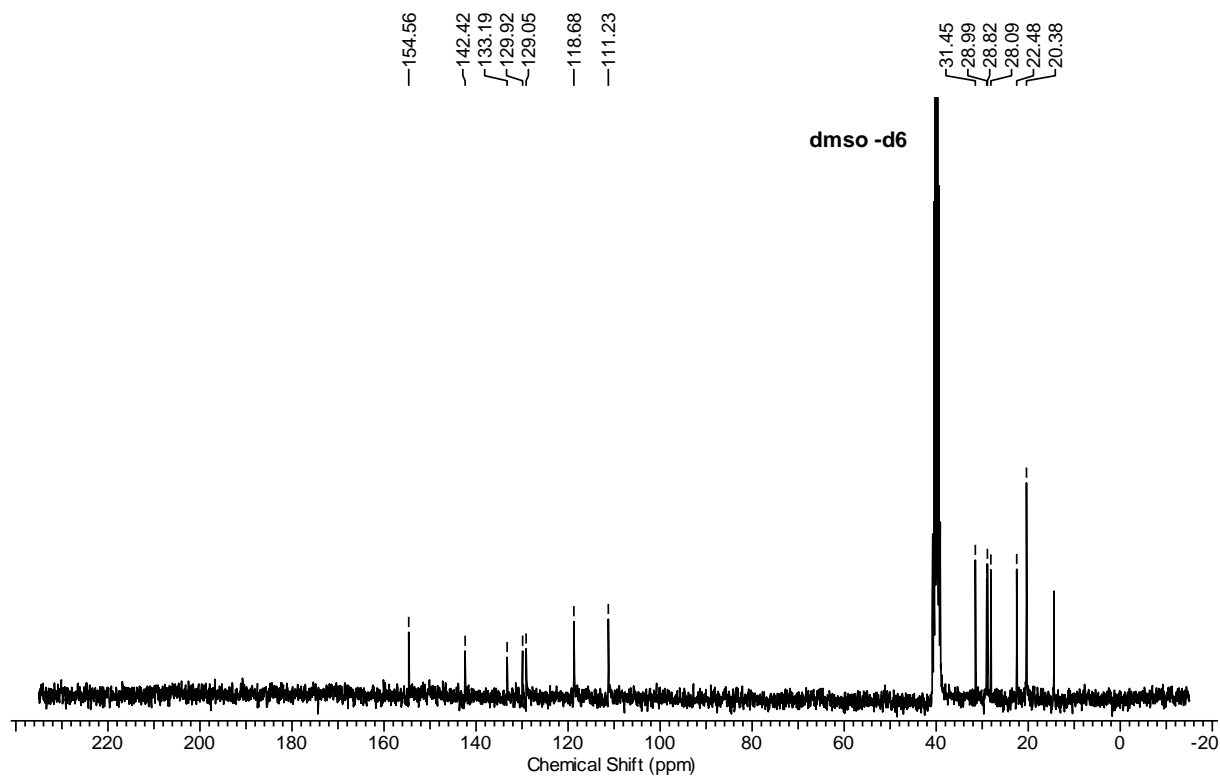
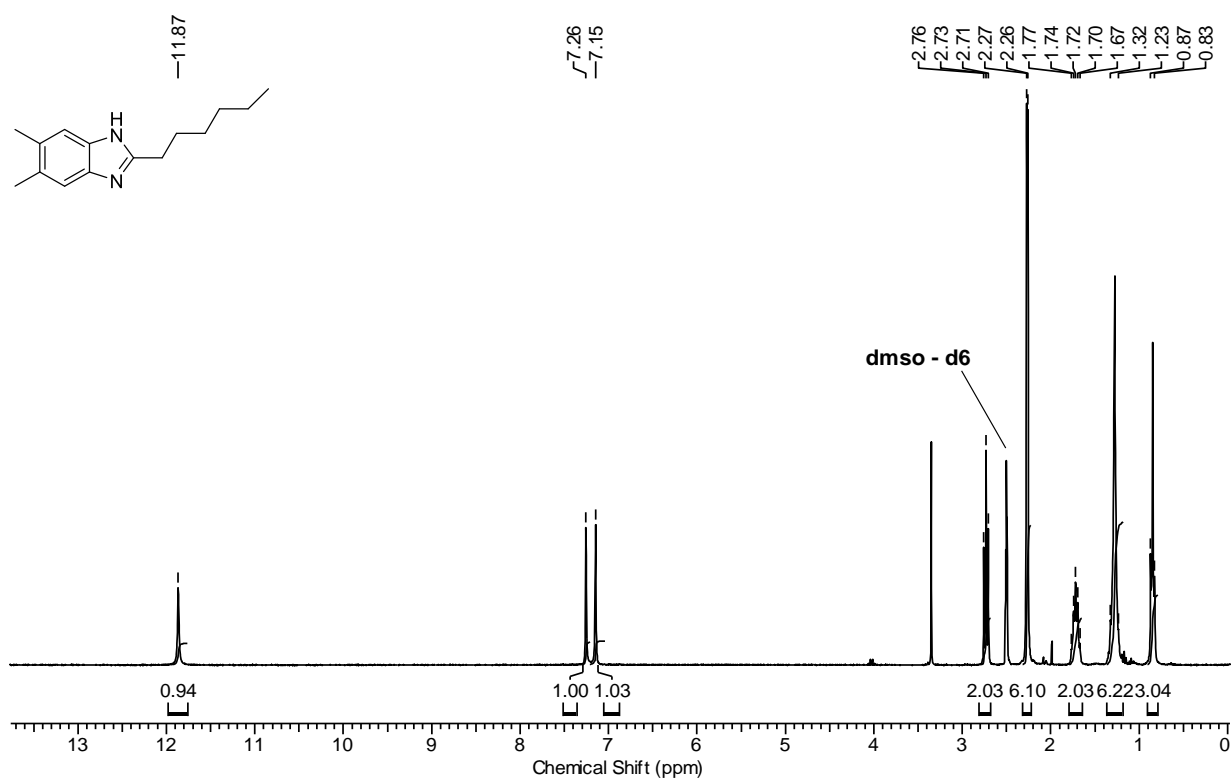
1e:



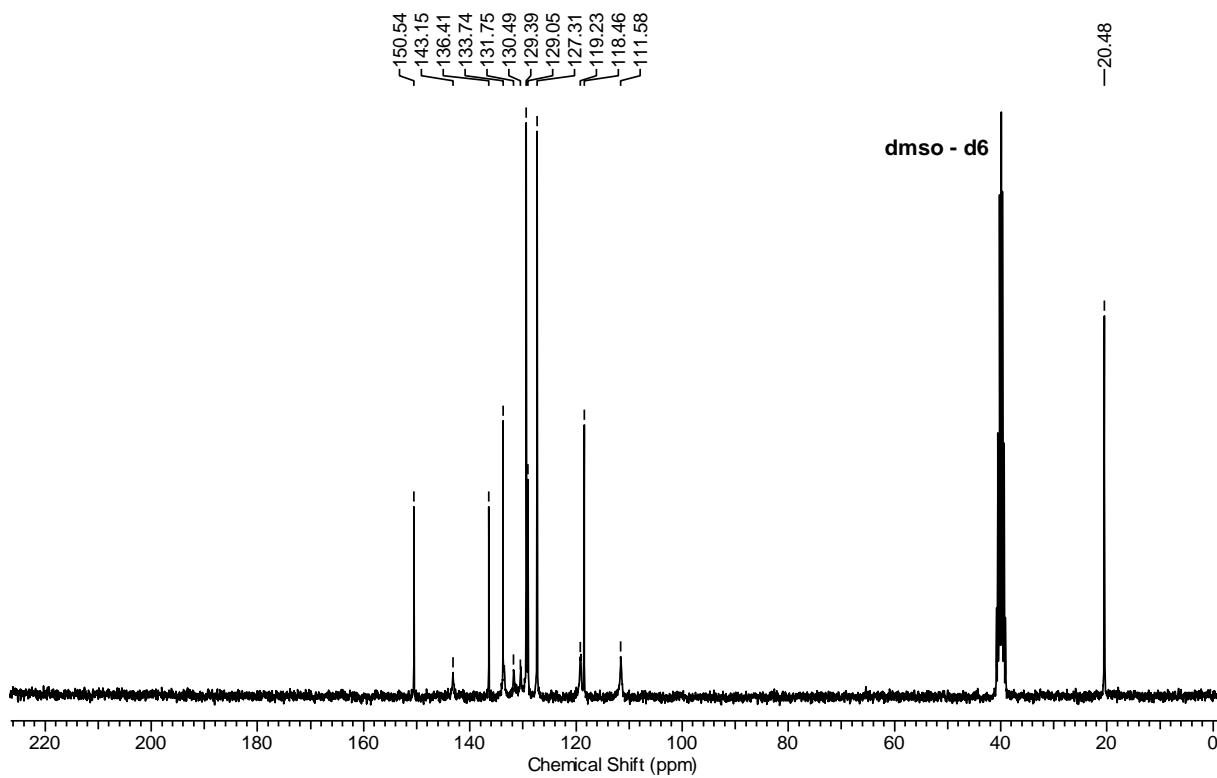
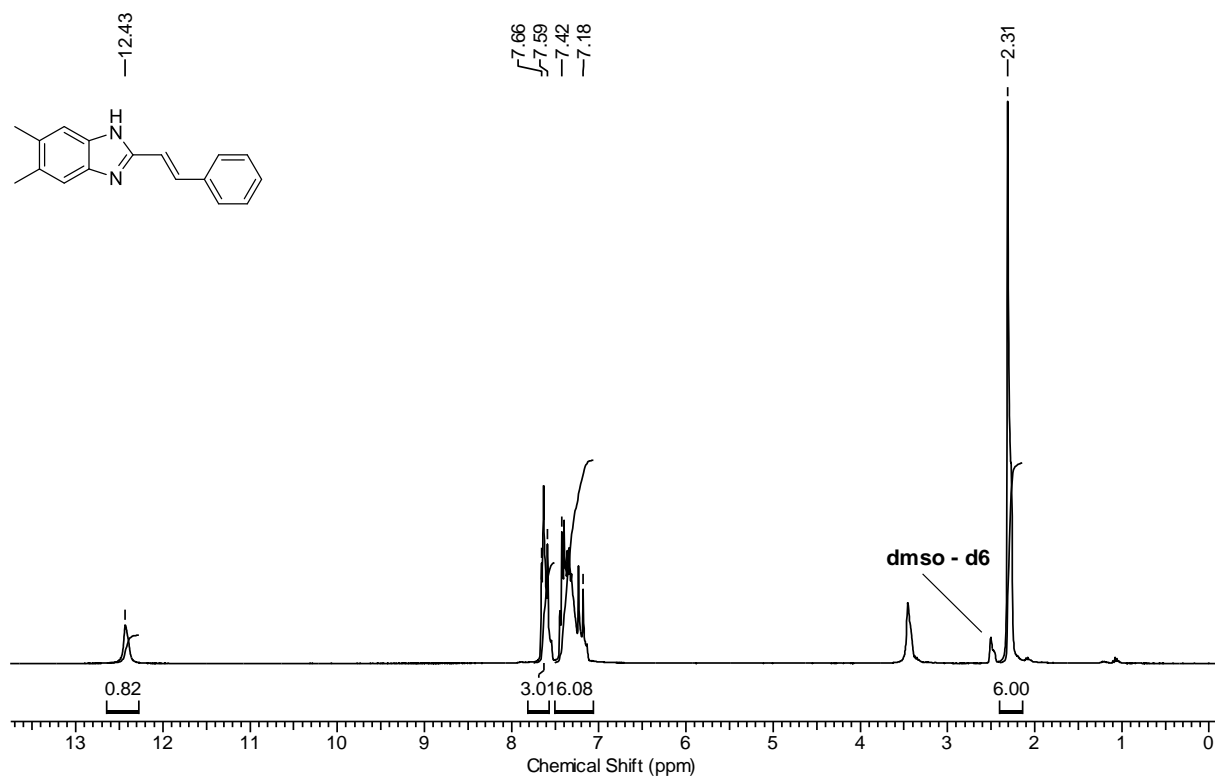
2:



3:



4:



References

- [1] B. S. Lim, A. Rahtu, J.-S. Park, R. G. Gordon, *Inorg. Chem.* **2003**, *24*, 7951–7958.

6 A Co catalyst permits the direct hydrogenative synthesis of 1H-perimidines from a dinitroarene and an aldehyde

Tobias Schwob,^[a] Mirco Ade,^[a] and Rhett Kempe*^[a]

[a] Anorganische Chemie II, Universität Bayreuth, 95440, Bayreuth.

Submitted to ChemSusChem and out for review.

Now published as:

T. Schwob, M. Ade, R. Kempe, *ChemSusChem* **2019**, *12*, 3013.

Abstract: We report here on a novel sustainable catalytic reaction: The synthesis of 1H-perimidines from a dinitroarene and an aldehyde in the presence of dihydrogen. We had to develop a novel earth-abundant metal catalyst permitting the efficient, highly chemoselective and consecutive hydrogenation of dinitroarenes. The catalyst is reusable and easy to handle. The use of a specific Co complex and its pyrolysis at a certain temperature is crucial to achieve high activity for the complex organic transformation. Benzylic and aliphatic aldehydes can undergo the hydrogenative condensation and many functional groups, including hydrogenation-sensitive examples such as an iodo aryl, nitrile, olefins and alkyne, can be tolerated.

6.1 Introduction

The development of catalysts based on earth-abundant metals is an important area of research, as their industrial application, here mostly reusable and nanostructured catalysts are employed, could contribute to a more sustainable chemistry - specifically regarding the conservation of rare noble metal resources. The substitution of precious metals is especially attractive if novel selectivity patterns are observed permitting novel syntheses. Impressive progress has been achieved in the field of selective nitroarene hydrogenation employing reusable earth-abundant metal catalysts in recent years. The hydrogenation of nitroarenes is an important reaction in chemical industry since it is the method of choice for the production of aniline and its derivatives.^[1] After Beller and coworkers showed^[1] that reusable catalysts based on abundantly available transition metals, such as iron^[2] and cobalt^[3] can mediate the chemoselective hydrogenation of nitroarenes^[4], many workgroups focused on the development of catalyst systems based on non-precious metals, such as Fe^[5], Co^[6], Ni^[7]. However, the direct use of

nitro derivatives in more complex hydrogenative catalytic syntheses has so far been rarely disclosed. Beller and coworkers introduced the reductive amination of carbonyl compounds with nitroarenes applying cobalt-based catalyst systems^[8], while the selective synthesis of benzimidazoles and quinoxalines from amino nitroarenes was introduced by our group^[5e,9]. We also reported recently on a nickel catalyst formed from a salene complex and a porous alumina support^[10] and wanted to extend this catalyst synthesis concept to other earth-abundant metals such as Co. Herein, we report on the direct synthesis of 1*H*-perimidines from a dinitroarene and an aldehyde in the presence of a catalyst and hydrogen. Benzylic and purely aliphatic aldehydes can be employed in this novel reaction. The hydrogenative synthesis tolerates many functional groups including hydrogenation-sensitive examples (aryl iodides, nitriles and C-C double and triple bonds). Our catalyst is based on the earth-abundant metal Co, is efficient, easy to handle and its synthesis is simple and straightforward. The key to a high catalytic activity is the combination of a specific Co coordination compound with commercially available charcoal. There is no direct synthesis of 1*H*-perimidines from nitroarenes and aldehydes described in the literature to the best of our knowledge and dinitro compounds could not be employed in any of the direct hydrogenative syntheses of aromatic *N*-heterocyclic compounds yet. Perimidines are a very important class of chemical compounds, due to their biological activity^[11] and their application as ligands^[12]. In addition, 1*H*-perimidines are common starting materials for the synthesis of azapyrenes, which are promising materials for the manufacturing of organic semiconductor devices.^[13]

6.2 Results and Discussion

Our novel catalyst (Co-Co_xO_y/C) was synthesized in a practical two-step procedure (Figure 1). At first, commercially available activated charcoal (Norit CA1, Cabot Corporation) was impregnated with Complex I, followed by pyrolysis under a nitrogen atmosphere at 700 °C and reduction (N₂/H₂ 90/10) at 550 °C (Figure 1A; for a detailed description, please see SI). The active catalyst obtains a specific surface area (Brunauer-Emmet-Teller) of 723 m²/g and the amount of mesopores is about 40 %. This is in good accordance with the results of the pure carbon support. The hierarchical pore structure remains intact after impregnation and pyrolysis (Figure S1). Energy-dispersive X-ray spectroscopy (EDX) verifies the homogeneous distribution of the metal species over the whole carbon support indicating a clean and smooth impregnation process (Figure S2). Transmission electron microscopy (TEM) in combination

with the corresponding particle size distribution provide evidence for the presence of small, homogeneously distributed Co nanoparticles with a mean diameter of 7 nm (Figure 1B,C).

X-ray photoelectron spectroscopy (XPS) verifies the presence of metallic cobalt and cobalt oxides/hydroxides (Figure 1D). Inductively coupled plasma optical emission spectrometry (ICP-OES) revealed 3.5 wt% Co in the as-synthesized catalyst, which is in good agreement with the Co loading expected theoretically.

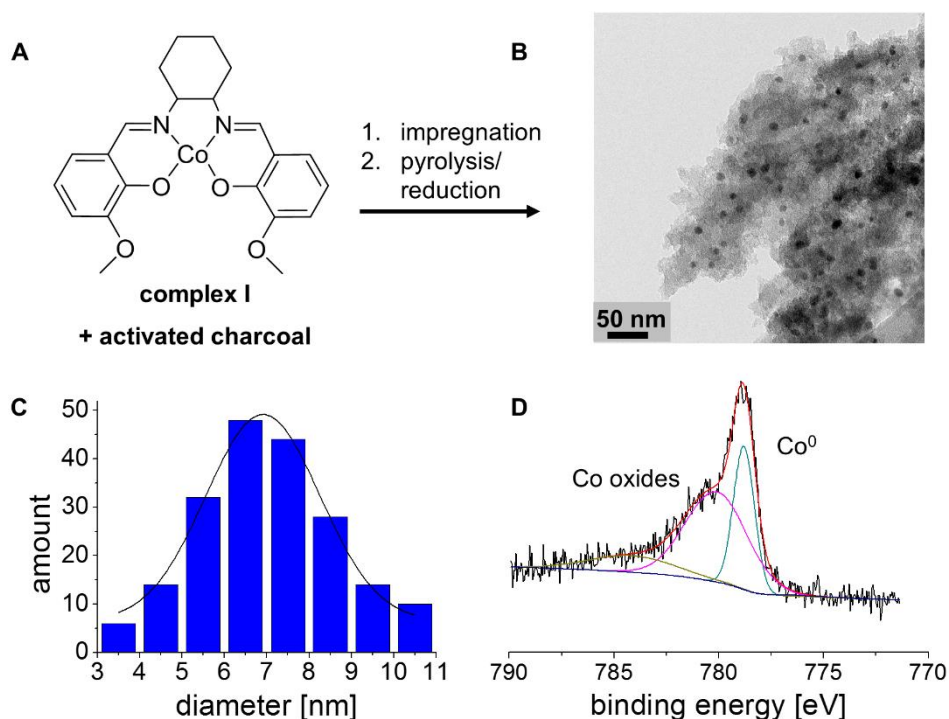
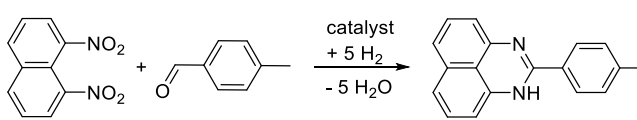


Figure 1: Catalyst synthesis and characterization. A) Synthesis of the novel catalyst by wet impregnation of commercially available charcoal with Complex I, followed by pyrolysis and reduction. B) TEM analysis of the catalyst indicates homogeneously distributed Co nanoparticles. (C) Size distribution of these nanoparticles with a mean diameter of 7 nm. D) XPS analysis confirms the presence of metallic cobalt and cobalt oxides or hydroxides.

The reductive coupling of 1,8-dinitronaphthalene and 4-methylbenzaldehyde was chosen for the optimization of the reaction conditions. We decided to use the nitro derivative in a technical grade, around 90 % purity, as determined by GC and GC-MS. This lowers the isolated yields of the products (Figure 2), however, the purification step of the dinitroarene can be avoided. Varying the solvent (Table S1), the reaction temperature and the pressure, led to 87 % product formation [2-(*p*-tolyl)-1*H*-perimidine] in toluene at 130 °C with a hydrogen pressure of 6.0 MPa. A pyrolysis temperature of 700 °C during catalyst synthesis was found to be optimal. Pyrolysis at 600 or 800 °C led to less active catalysts (Table 1, entries 1-3). Regarding to catalyst supports, we investigated TiO₂, Al₂O₃ and CeO₂. A decrease in the product yield (Table 1 entries 4-6) was observed in all cases. The use of metal oxides as support materials led

to a significant amount of aldehyde hydrogenation even at incomplete conversion of the dinitroarene derivative. This is in good agreement with the results of the Beller group, who demonstrated the hydrogenation of carbonyl compounds applying Al₂O₃- and CeO₂- based Co catalysts.^[14] In addition, Complex I was replaced by the common metal salt cobalt acetate, however, a significant decrease in product formation was observed (Table 1, entry 7), verifying the importance of our Co-salen complex which had already been observed in a previous work of our group.^[10] In summary, the synthesis proceeded well with a catalyst synthesized from Complex I in combination with commercially available activated charcoal at a reaction temperature of 130 °C (Table 1, entry 8), 6.0 MPa hydrogen pressure applying toluene as the solvent (Table S1, entry 4).

Table 1. Catalyst screening.^[a]



Entry	Metal source	Pyrolysis temperature [°C]	Support	Yield [%]
1	Complex I	600	Activated charcoal	41
2	Complex I	700	Activated charcoal	72
3	Complex I	800	Activated charcoal	61
4	Complex I	700	TiO ₂	31
5	Complex I	700	CeO ₂	18
6	Complex I	700	γ-Al ₂ O ₃	54
7	Co(OAc) ₂ * 4 H ₂ O	700	Activated charcoal	15
8 [§]	Complex I	700	Activated charcoal	87

[a] Reaction conditions: 0.5 mmol nitro derivative, 1.1 eq aldehyde, 35 mg catalyst (4 mol% Co), 120 °C, 6.0 MPa H₂, 3 mL toluene, 20 h; [§]130 °C reaction temperature; yields were determined by GC and GC-MS using *n*-dodecane as an internal standard. OAc = acetate.

With the optimized reaction conditions in hand, we were interested in the substrate scope and the functional group tolerance of our novel catalyst system. The reductive coupling of 1,8-dinitronaphthalene and benzylic aldehydes was investigated first. The introduction of methyl groups at other positions than para proceeded well, and the corresponding products were obtained in up to 84 % isolated yield (Figure 2, 2-4). To our delight, the use of halogenated substrates showed minor influence on the catalytic activity and the corresponding 1*H*-perimidines were obtained in 67-71 % yield (Figure 2, 5-9). Trace amounts of dehalogenated product were observed only in the case of 4-iodobenzaldehyde. Further aldehydes bearing functional groups, such as ethers, amides and hydroxy functionalities, were well tolerated (Figure 2, 10-13). The stability of boronic esters under reaction conditions is of special

importance, since they are common starting materials for cross-coupling reactions (Figure 2, 14). The reductive coupling of 1,8-dinitronaphthalene with a heterocyclic and an aliphatic aldehyde proceeded smoothly and product yields of 75 and 85 % were observed, respectively (Figure 2, compound 17, 19).

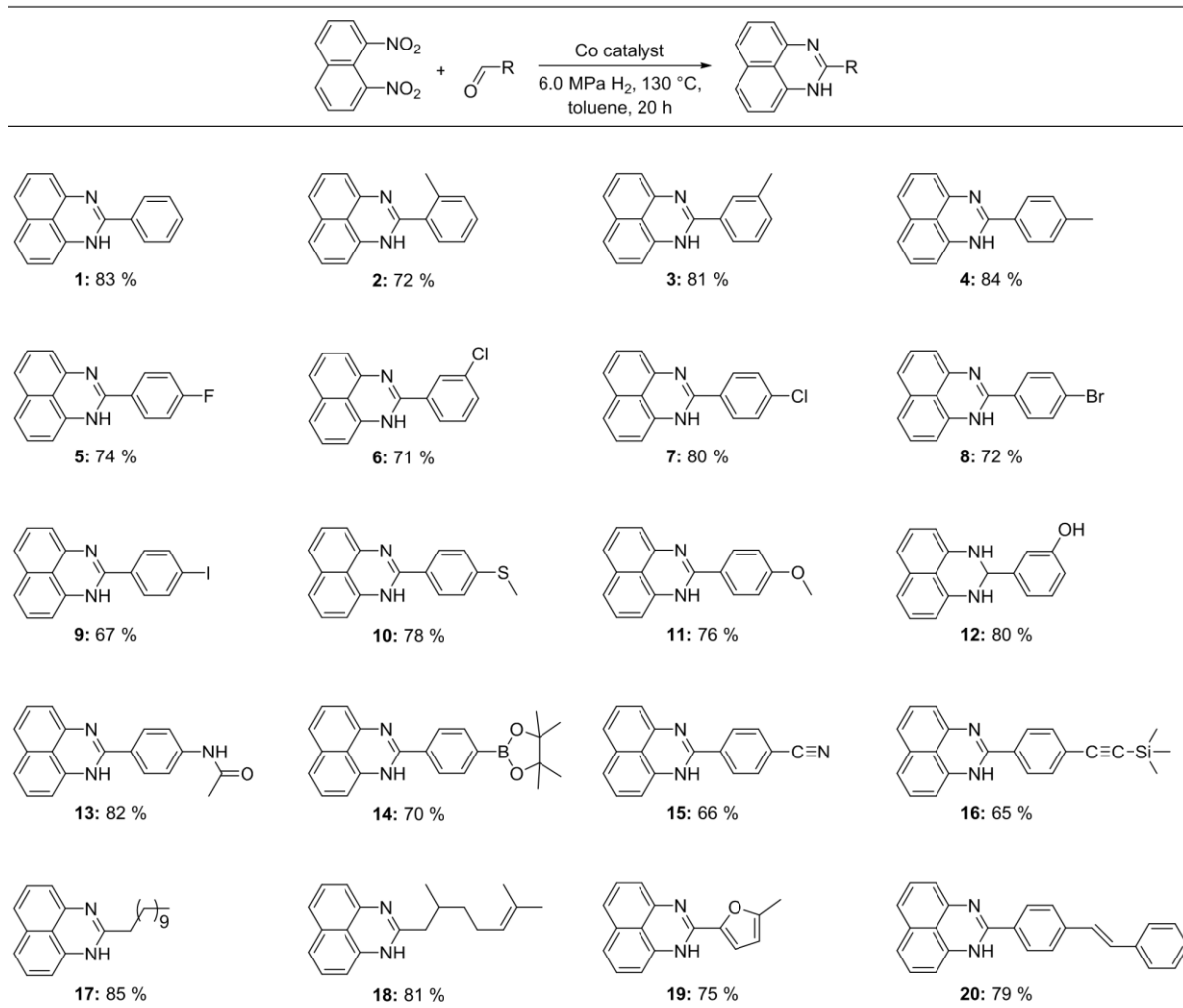


Figure 2: Highly selective synthesis of 1*H*-perimidines from 1,8-dinitronaphthalene and various aldehydes. Reaction conditions: 1.5 mmol nitro derivative, 1.1 eq. aldehyde, 120 mg catalyst (4.7 mol% Co), 130 °C, 6.0 MPa H₂, 3 mL toluene, 20 h; yields of isolated products. Note that technical grade, around 90 % purity, 1,8-dinitronaphthalene was used. Yields of isolated product were calculated assuming 100% purity, since the purity was not uniform.

Finally, we demonstrated the possibility of an introduction of further reducible functionalities, such as nitriles, as well as C-C double and triple bonds. The 1*H*-perimidines desired were obtained in good to excellent yields confirming the broad applicability (Figure 2, compound 15, 16, 18, 20). It is noteworthy to mention that we were able to synthesize six new products with our direct synthesis concept, starting from a technical grade 1,8-dinitronaphthalene and various benzylic and aliphatic aldehydes. The catalyst was reused in five consecutive runs to

confirm its stability under reaction conditions and no remarkable decrease in catalytic activity could be detected (Figure S3). An up-scaling of the reaction (10 mmol nitro derivative) proceeded well and the 1*H*-perimidine desired was obtained in 80 % isolated yield (For a detailed description please see SI).

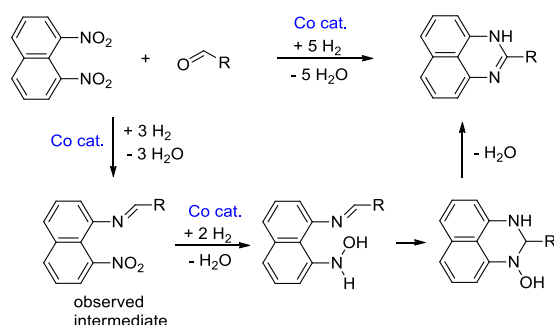


Figure 3: Proposed reaction pathway for the direct synthesis of 1*H*-perimidines via a nitro-imine intermediate (R = aryl or alkyl substituent).

Mechanistically, we propose a reductive cyclization pathway via *in situ* nitroarene reduction as shown in Figure 3. The role of the catalyst is the selective and consecutive hydrogenation of the two nitro groups of the naphthalene derivative. We observed the formation of the nitro-imine intermediate as shown in Figure 3. The reaction of the hydroxylamine nucleophile, a common intermediate in the hydrogenation of nitroarenes^[15], with the electrophilic carbon of the imine is highly likely, especially under the sterically constrained conditions. This is in good agreement with the results of *Yang et al.*, who described a similar pathway for the synthesis benzimidazoles from *o*-nitroanilines and aldehydes via reduction applying stoichiometric amounts of sodium dithionite.^[16] Our catalyst cannot dehydrogenate 2,3-dihydroperimidines in toluene at 130 °C, even in an Ar atmosphere open to air via a bubble counter, assuming that a dehydrogenative pathway in the presence of 6.0 MPa hydrogen pressure is extremely unlikely. 1,8-Diaminonaphthalene reacts smoothly under reaction conditions with aldehydes to form 2,3-dihydroperimidines supporting that diaminonaphthalene is not formed under reaction conditions. In conclusion, a novel earth-abundant catalyst permits the first direct synthesis of 1*H*-perimidines from 1,8-dinitronaphthalene and various benzylic and aliphatic aldehydes. The catalyst is easy to synthesize by wet impregnation of commercially available charcoal with a specific cobalt complex, which is crucial for a high catalytic activity. Our methodology permits tolerance towards a variety of functional groups, including hydrogenation-sensitive examples (aryl iodides, nitriles, as well as C-C double and triple bonds). We synthesized six new 1*H*-perimidine derivatives and could use a technical grade dinitro derivative without purification.

An up-scaling of the reaction proceeds smoothly and the catalyst shows stability over several consecutive runs without any remarkable decrease in catalytic activity.

A number of challenges are associated with our novel synthesis. The key seems to be that our catalyst can selectively and consecutively hydrogenate dinitroarenes. The aldehyde must remain unaffected, even at the higher temperatures, needed for the condensation step. In addition, formation of the diaminoarene, as well as the hydrogenation of the 1*H*-perimidine have to be avoided.

6.3 Acknowledgements

We thank Prof. Sven Hüttner for XPS analysis and the DFG KESFB 840, B1 and KE-756/29-1 for financial support.

Keywords: cobalt • hydrogenation • nitroarene • perimidines

6.4 References

- [1] K. Eller, E. Henkes, R. Rossbacher, H. Höke in Ullmann's Encyclopedia of Industrial Chemistry, Wiley-VCH, Weinheim, Germany, **2012**, p. 654.
- [2] R. V. Jagadeesh, A.-E. Surkus, H. Junge, M.-M. Pohl, J. Radnik, J. Rabeah, H. Huan, V. Schunemann, A. Brückner, M. Beller, *Science* **2013**, *342*, 1073–1076; b) R. V. Jagadeesh, T. Stemmler, A.-E. Surkus, H. Junge, K. Junge, M. Beller, *Nat. Protoc.* **2015**, *10*, 548–557.
- [3] F. A. Westerhaus, R. V. Jagadeesh, G. Wienhofer, M.-M. Pohl, J. Radnik, A.-E. Surkus, J. Rabeah, K. Junge, H. Junge, M. Nielsen, A. Brückner, M. Beller, *Nat. Chem.* **2013**, *5*, 537–543.
- [4] D. Formenti, F. Ferretti, F.-K. Scharnagl, M. Beller, *Chem. Rev.*, DOI: 10.1021/acs.chemrev.8b00547.
- [5] For selected key papers please see: a) J. Chen, Y. Yao, J. Zhao, Y. Zhao, Y. Zheng, M. Li, Q. Yang, *RSC Adv.* **2016**, *6*, 96203–96209; b) J. Shi, Y. Wang, W. Du, Z. Hou, *Carbon* **2016**, *99*, 330–337; c) S. Xu, D. Yu, S. Liao, T. Ye, H. Sheng, *RSC Adv.* **2016**,

- 6, 96431–96435; d) B. Ma, X. Tong, C. Guo, X. Guo, X. Guo, F. J. Keil, *RSC Adv.* **2016**, *6*, 55220–55224; e) C. Bäumlner, R. Kempe, *Chem. Eur. J.* **2018**, *24*, 8989–8993.
- [6] For selected key papers please see: a) Z. Wei, J. Wang, S. Mao, D. Su, H. Jin, Y. Wang, F. Xu, H. Li, Y. Wang, *ACS Catal.* **2015**, *5*, 4783–4789; b) D. Formenti, C. Topf, K. Junge, F. Ragaini, M. Beller, *Catal. Sci. Technol.* **2016**, *6*, 4473–4477; c) L. Liu, P. Concepción, A. Corma, *J. Catal.* **2016**, *340*, 1–9; d) B. Chen, F. Li, Z. Huang, G. Yuan, *ChemCatChem.* **2016**, *8*, 1132–1138; e) P. Ji, K. Manna, Z. Lin, X. Feng, A. Urban, Y. Song, W. Lin, *J. Am. Chem. Soc.* **2017**, *139*, 7004–7011; f) P. Zhou, Z. Zhang, *ChemSusChem* **2017**, *10*, 1892–1897; g) H. Alex, P. Loos, T. Baramov, J. Barry, T. Godiawala, J. Hassfeld, N. Steinfeldt, *ChemCatChem* **2017**, *9*, 3210–3217; h) I. Sorribes, L. Liu, A. Corma, *ACS Catalysis* **2017**, *7*, 2698–2708; i) F. Zhang, C. Zhao, S. Chen, H. Li, H. Yang, X.-M. Zhang, *J. Catal.* **2017**, *348*, 212–222; j) L. Jiang, P. Zhou, Z. Zhang, Q. Chi, S. Jin, *New J. Chem.* **2017**, *41*, 11991–11997; k) X. Cui, K. Liang, M. Tian, Y. Zhu, J. Ma, Z. Dong, *J. Colloid Interface Sci.* **2017**, *501*, 231–240; l) B. Sahoo, D. Formenti, C. Topf, S. Bachmann, M. Scalone, K. Junge, M. Beller, *ChemSusChem* **2017**, *10*, 3035–3039; m) Li. Liu, F. Gao, P. Concepción, A. Corma, *J. Catal.* **2017**, *350*, 218–225; n) Z. Wei, S. Mao, F. Sun, J. Wang, B. Mei, Y. Chen, H. Li, Y. Wang, *Green Chem.* **2018**, *20*, 671–679; o) X. Sun, A. I. Olivos-Suarez, D. Osadchii, M. J. V. Romero, F. Kapteijn, J. Gascon, *J. Catal.* **2018**, *357*, 20–28; p) M. Eckardt, M. Zaheer, R. Kempe, *Sci. Rep.* **2018**, *8*, 2567–2572; q) K. Murugesan, T. Senthamarai, M. Sohail, A. S. Alshammari, M.-M. Pohl, M. Beller, R. V. Jagadeesh, *Chem. Sci.* **2018**, *9*, 8553–8560; r) W. Li, J. Artz, C. Broicher, K. Junge, H. Hartmann, A. Besmehn, R. Palkovits, M. Beller, *Catal. Sci. Technol.* **2019**, *9*, 157–162; s) Y. Duan, T. Song, X. Dong, Y. Yang, *Green. Chem.* **2018**, *20*, 2821–2828; t) X. Wei, Z. Zhang, M. Zhou, A. Zhang, W. D. Wu Z. Wu, *Nanoscale* **2018**, *10*, 16839–16874.
- [7] For selected key papers please see: a) M. A. Harrad, B. Boualy, L. E. Firdoussi, A. Mehdi, C. Santi, S. Giovagnoli, M. Nocchetti, M. A. Ali, *Catal. Commun.* **2013**, *32*, 92–100; b) P. Zhang, C. Yu, X. Fan, X. Wang, Z. Ling, Z. Wang, J. Qiu, *Chem. Chem. Phys.* **2015**, *17*, 145–150; c) S. Pisiewicz, D. Formenti, A.-E. Surkus, M.-M. Pohl, J. Radnik, K. Junge, C. Topf, S. Bachmann, M. Scalone, M. Beller, *ChemCatChem* **2016**, *8*, 129–134; d) G. Hahn, J.-K. Ewert, C. Denner, D. Tilgner, R. Kempe, *ChemCatChem* **2016**, *8*, 2461–2465; e) Y. Ren, H. Wei, G. Yin, L. Zhang, A. Wang, T. Zhang, *Chem. Commun.* **2017**, *53*, 1969–1972.

- [8] a) T. Stemmler, A.-E. Surkus, M.-M. Pohl, K. Junge, M. Beller, *ChemSusChem* **2014**, *7*, 3012–3016; b) T. Stemmler, F. A. Westerhaus, A.-E. Surkus, M.-M. Pohl, K. Junge, M. Beller, *Green Chem.* **2014**, *16*, 4535–4540; c) R. V. Jagadeesh, K. Murugesan, A. S. Alshammari, H. Neumann, M.-M. Pohl, J. Radnik, M. Beller, *Science* **2017**, *358*, 326–332. For work of others see: a) L. Jiang, P. Zhou, Z. Zhang, Q. Chi, S. Jin, *New J. Chem.* **2017**, *41*, 11991–11997; b) X. Cui, K. Liang, M. Tian, Y. Zhu, Y. Ma, Z. Dong, *J. Colloid Interface Sci.* **2017**, *501*, 231–240.
- [9] a) T. Schwob, R. Kempe, *Angew. Chem. Int. Ed.* **2016**, *55*, 15175–15179; For work of others see: a) P. Zhou, L. Jiang, F. Wang, K. Deng, K. Lv, Z. Zhang, *Sci. Adv.* **2017**, *3*, No. e1601945; b) T. Song, P. Ren, Y. Duan, Z. Wang, X. Chen, Y. Yang, *Green Chem.* **2018**, *20*, 4629–4637.
- [10] G. Hahn, P. Kunnas, N. de Jonge, R. Kempe, *Nat. Catal.* **2019**, *2*, 71–77.
- [11] a) J. M. Herbert, P. D. Woodgate, W. A. Denny, *J. Med. Chem.* **1987**, *30*, 2081–2086; b) X. Bu, L. W. Deady, G. J. Finlay, B. C. Baguley, W. A. Denny, *J. Med. Chem.* **2001**, *44*, 11, 2004–2014; c) T. A. Farghaly, H. K. Mahmoud, *Arch. Pharm. Chem. Life Sci.* **2013**, *346*, 392–402.
- [12] a) L. Oehninger, L. N. Küster, C. Schmidt, A. Munoz-Castro, A. Prokop, I. Ott, *Chem. Eur. J.* **2013**, *19*, 17871–17880; b) I. N. Booyesen, I. Ebinumoliseh, S. Sithebe, M. P. Akerman, B. Xulu, *Polyhedron* **2016**, *117*, 755–760.
- [13] A. V. Aksenov, S. V. Shcherbakov, I. V. Lobach, L. G. Voskressensky, M. Rubin, *Eur. J. Org. Chem.* **2018**, *2018*, 4121–4127.
- [14] a) F. Cheng, C. Topf, J. Radnik, C. Kreyenschulte, H. Lund, M. Schneider, A.-E. Surkus, L. He, K. Junge, M. Beller, *J. Am. Chem. Soc.* **2016**, *138*, 8781–8788; b) T. Stemmler, F. Chen, S. Pisiewicz, A.-E. Surkus, M.-M. Pohl, C. Topf, M. Beller, *J. Mater. Chem. A* **2015**, *3*, 17728–17737.
- [15] H.-U. Blaser, H. Steiner, M. Studer, *ChemCatChem* **2009**, *1*, 210–221.
- [16] D. Yang, D. Fokas, J. Li, L. Yu C. M. Baldino, *Synthesis* **2005**, *1*, 47–56.

6.5 Supplementary Information

General considerations

Air- and moisture sensitive reactions were carried out under dry argon or nitrogen atmosphere using standard Schlenk or glove box techniques. Solvents were dried and distilled from sodium benzophenone, stored over molecular sieves (3 Å) before use, or were obtained from Acros. 1,8-Dinitronaphthalene was purchased from TCI with a purity >85 % and used without further purification. All other chemicals were purchased from commercial sources with purity over 95 %. Activated charcoal (Norit CA1) was purchased from Cabot Corporation and heated up to 700 °C (10 K/min, dwelling time 3 h) before use. NMR-Spectra were collected on Varian INOVA 300 (300 MHz for ¹H, 75 MHz for ¹³C) or Bruker Avance III HD 500 (500 MHz for ¹H, 125.7 MHz for ¹³C) instruments at 298 K. Chemical shifts are reported in ppm relative to the residual solvent signal (CDCl₃: 7.26 ppm (¹H), 77.16 ppm (¹³C); DMSO-D₆: 2.50 ppm (¹H), 39.51 ppm (¹³C); C₆D₆: 7.16 ppm (¹H), 128.39 ppm (¹³C)). Coupling constants (*J*) are reported in Hz (coupling patterns: s = singlet, d = doublet, t = triplet, q = quartet, quint = quintet, sxt = sextet, spt = septet, m = multiplet). GC analyses were carried out on an Agilent 6850 GC system equipped with an Optima 17 column (30 m x 0.32 mm x 0.25 μm) or an Agilent 6890N GC system equipped with a HP-5 column (30 m x 0.32 mm x 0.25 μm). GC-MS analyses were carried out on an Agilent 7890A GC system equipped with a HP-5MS column (30 m x 0.32 mm x 0.25 μm) and a 5975C inert MSD detector (EI, 70 eV). X-ray photoelectron spectroscopy (XPS) was performed using a PHI Versa Probe III instrument of Physical Electronics. As X-ray source a monochromatic Al K α with a spot size of 100 μm (24.5 W) was used. The kinetic pass energy of the photoelectrons was determined with a hemispheric analyzer (45°) set to pass energy of 26 eV for high-resolution spectra. The samples were prepared on a carbon tape. N₂ physisorption measurements were determined at -196 °C using a Nova2000e (Quantachrome) apparatus. The specific surface areas were calculated using p/p₀ values from 0.05-0.3 (BET). The pore width and average pore volume were calculated by DFT calculations [N₂ at -196.15 °C on carbon (slit/cylindrical pore model, NLDFE equilibrium model)]. Pyrolysis and reduction were carried out under nitrogen atmosphere and forming gas (90/10) in a high temperature furnace (EHA 12/450B200, Carbolite) or alternative using ChemBET *Pulsar* TPR/TPD. Macherey Nagel silica gel 60 (40–63 μm particle size) was used for column chromatography.

Catalyst synthesis and characterization

Ligand Synthesis

3.08 g (20 mmol, 2 eq) *o*-vanillin were dissolved in 100 mL ethanol and 1.32 mL (11 mmol, 1.1 eq) trans-1,2-diaminocyclohexane were added. The solution was heated under reflux for 1 h. After removal of the solvent under reduced pressure, recrystallization from diethyl ether yielded the product as a yellow crystalline powder (ligand I, 2.98 g, 78 %).

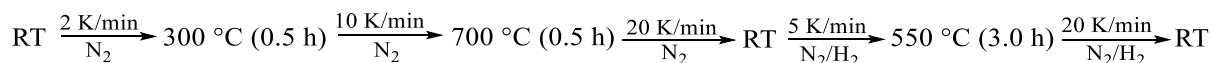
Complex synthesis

Complex I (Co-Salen) was synthesized according to a modified literature procedure.^[1] Ligand I (1.71 g, 4.5 mmol, 1 eq) was dissolved in ethanol and the solution was degassed by purging with argon for 15 min. Dry cobalt(II) acetate (0.797 g, 4.5 mmol, 1 eq) was added and the mixture was stirred at 50 °C for 2 h. Next, the solution was refluxed overnight. After removal of the solvent, the resulting solid was washed with cold ethanol and the collected product was dried in vacuo (1.33 g, 3.03 mmol, 67 %).

Elemental analysis: calcd for C₂₂H₂₄CoN₂O₄: C 60.14, H 5.51, N 6.38; found: C 59.60, H 5.32, N 6.14

Catalyst synthesis

To a solution of 89 mg (M = 439.38 g mol⁻¹, 0.203 mmol) complex I in 3 mL acetonitrile, 300 mg activated charcoal were added, and the suspension was stirred at 95 °C. After evaporation of the solvent, the sample was pyrolyzed under nitrogen atmosphere at 700 °C followed by reduction at 550 ° (N₂/H₂, 90/10). The catalysts used for the screening reactions were synthesized using equivalent amounts support material or metal salt.



Catalyst characterization

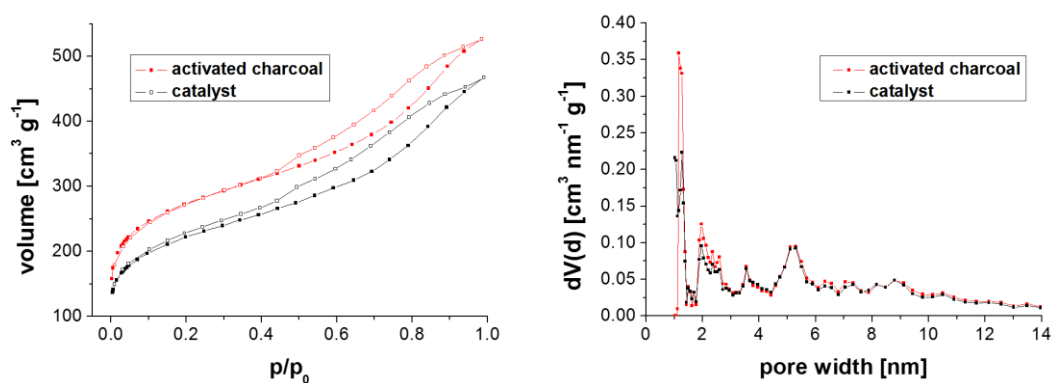


Figure S1: Nitrogen physisorption measurements of the catalyst in comparison to the pure carbon support. Both materials show the typical hysteresis of mesoporous materials. The catalyst features a specific surface area (Brunauer-Emmet-Teller) of 723 m²/g. The corresponding pore size distributions [N₂ at -196.15 °C on carbon (slit/cylindrical pore, NLDFT equilibrium model)] indicate a small decrease in the amount of micropores after wet impregnation and pyrolysis.

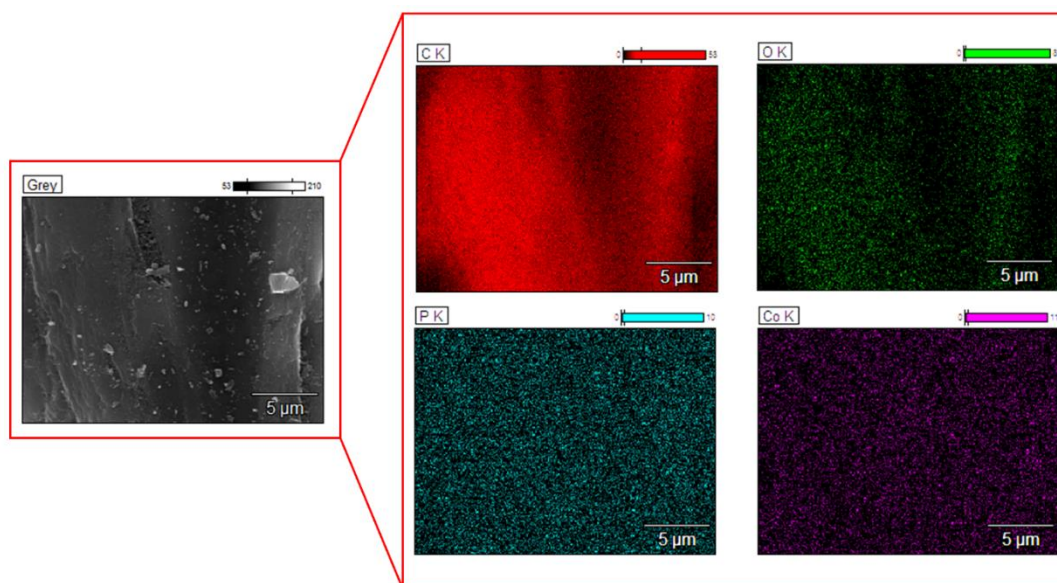
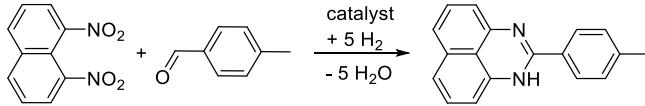


Figure S2: SEM- in combination with EDX element maps of the active catalyst system. A homogeneous distribution of the metal species is verified. No phase separation could be detected, indicating a clean and smooth impregnation process. The presence of phosphorus can be reduced to the use of a chemically activated carbon support.

Catalytic studies

Screening of reaction parameters

Table S1: Screening of reaction parameters – solvent.



Entry	Solvent	Yield [%]
1	Ethanol	18
2	Dioxane	42
3	Diglyme	64
4	Toluene	87
5	Methylcyclohexane	34

Reaction conditions: 0.5 mmol nitro derivative, 1.1 eq. aldehyde, 35 mg catalyst (4 mol% Co), 130 °C, 6.0 MPa H₂, 3 mL toluene, 20 h; yields were determined by GC and GC-MS using *n*-dodecane as an internal standard.

Synthesis of 1*H*-perimidines – general procedure

A 10 mL reaction vial was charged with a magnetic stirring bar, 1.5 mmol 1,8-dinitronaphthalene, 1.1 eq aldehyde, 3 ml toluene and 120 mg catalyst. The vial was placed in a 300 mL high-pressure autoclave (Parr Instruments) and the autoclave was flushed three times with 2.0 MPa hydrogen. Afterwards, the final pressure was applied and the reaction was stirred at the desired temperature for 20 h. After completion of the reaction time, the autoclave was cooled to room temperature and the hydrogen was released. Quantitative GC analysis was accomplished using *n*-dodecane as an internal standard. For an isolation of the products, the catalyst was removed using a magnet and washed several times with acetone. The organic phases were combined and the solvent was removed under reduced pressure. Purification was accomplished by column chromatography applying pentane/ether as the eluent. The products were analyzed by NMR spectroscopy. For new compounds, elemental analysis was carried out.

Up-scaling

10 mmol 1,8-dinitronaphthalene were chosen for the up-scaling reaction. A 25 ml high-pressure autoclave (Parr Instruments) equipped with a teflon inlet and a magnetic stirring bar was filled with 10 mmol nitro derivative, 1.1 eq 4-methylbenzaldehyde, 800 mg catalyst (4 mol% Co) and 15 ml toluene. The autoclave was flushed three times with 2.0 MPa of hydrogen and afterwards the final pressure of 6.0 MPa was applied. The reaction was stirred for 20 h at 130 °C. After

completion of the reaction time, the autoclave was cooled to room temperature and the hydrogen was released. The catalyst was removed using a magnet and washed several times with acetone. The organic phases were combined and the solvent was removed under reduced pressure. Purification was accomplished by column chromatography applying pentane/ether as the eluent and the product was obtained in 80 % isolated yield.

Recycling studies

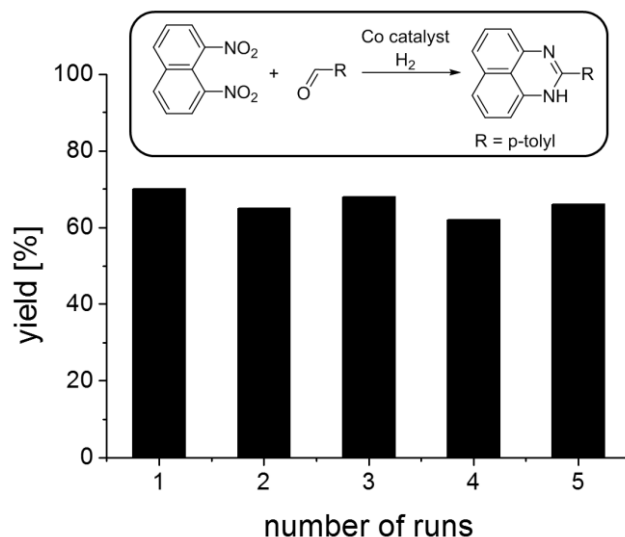
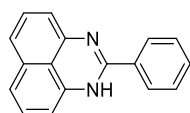


Figure S3: Recycling study. The catalyst was reused in five consecutive runs without any remarkable decrease in catalytic activity. Reaction conditions: 0.5 mmol 1,8-dinitronaphthalene, 1.1 eq. aldehyde, 30 mg catalyst (3.6 mol% Co), 3 ml toluene, 120 °C, 6.0 MPa H₂, 20 h; yields were determined by GC and GC-MS using *n*-dodecane as internal standard. The catalyst was separated using a magnet, washed and reused again.

Characterization of isolated products

2-phenyl-1*H*-perimidine (1)



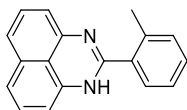
FW (C₁₇H₁₂N₂) = 244.30 g mol⁻¹

¹H NMR (300 MHz, dms_o-d₆): δ = 10.68 (s, 1 H), 8.04-8.01 (m, 2 H), 7.57-7.50 (m, 3 H), 7.21-7.01 (m, 4 H), 6.72-6.56 (m, 2 H) ppm.

¹³C NMR (75 MHz, dms_o-d₆): δ = 152.67, 145.02, 138.49, 135.06, 133.47, 130.98, 128.94, 128.37, 127.98, 126.80, 121.58, 119.25, 117.71, 113.92, 102.76 ppm.

Yield: 83 % (1.25 mmol, 305 mg), yellow solid.

2-(*o*-tolyl)-1*H*-perimidine (2)



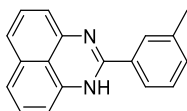
FW (C₁₈H₁₄N₂) = 258.32 g mol⁻¹

¹H NMR (300 MHz, dms_o-d₆): δ = 10.76 (s, 1 H), 7.49-7.48 (m, 1 H), 7.42-7.39 (m, 1 H), 7.33-7.30 (m, 2 H), 7.20-7.17 (m, 1 H), 7.12-7.02 (m, 3 H), 6.65-6.64 (m, 1 H), 6.41-6.39 (m, 1 H), 2.47 (s, 3 H) ppm.

¹³C NMR (75 MHz, dms_o-d₆): δ = 154.99, 145.32, 138.57, 135.77, 135.23, 130.56, 129.58, 128.97, 128.21, 128.00, 125.82, 121.58, 119.21, 117.68, 113.66, 102.76, 19.43 ppm.

Yield: 72 % (1.08 mmol, 279 mg), yellow solid.

2-(*m*-tolyl)-1*H*-perimidine (3)



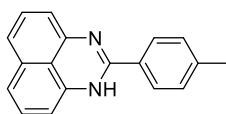
FW (C₁₈H₁₄N₂) = 258.32 g mol⁻¹

¹H NMR (300 MHz, dms_o-d₆): δ = 10.62 (s, 1 H), 7.83-7.79 (m, 2 H), 7.44-7.36 (m, 2 H), 7.20-7.00 (m, 4 H), 6.69-6.53 (m, 2 H), 2.41 (s, 3 H) ppm.

¹³C NMR (75 MHz, dms_o-d₆): δ = 152.74, 145.07, 138.51, 137.70, 135.06, 133.44, 131.62, 128.95, 128.30, 127.99, 127.25, 123.98, 121.57, 117.66, 113.86, 102.71, 21.03 ppm.

Yield: 81 % (1.22 mmol, 314 mg), yellow solid.

2-(*p*-tolyl)-1*H*-perimidine (4)



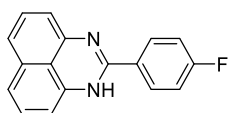
FW (C₁₈H₁₄N₂) = 258.32 g mol⁻¹

¹H NMR (300 MHz, dms_o-d₆): δ = 10.58 (s, 1 H), 7.94-7.91 (m, 2 H), 7.35-7.33 (m, 2 H), 7.14-7.02 (m, br, 4 H), 6.65-6.57 (m, br, 2 H), 2.39 (s, 3 H) ppm.

¹³C NMR (75 MHz, dms_o-d₆): δ = 152.95, 145.56, 141.40, 138.99, 135.54, 131.07, 129.42, 128.46, 127.21, 122.02, 119.02, 119.56, 118.13, 114.30, 103.16, 21.47 ppm.

Yield: 84 % (1.26 mmol, 325 mg), yellow solid.

2-(4-fluorophenyl)-1*H*-perimidine (5)



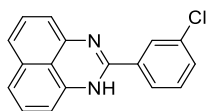
FW (C₁₇H₁₁FN₂) = 262.29 g mol⁻¹

¹H NMR (300 MHz, dms_o-d₆): δ = 10.67 (s, 1 H), 8.10-8.06 (m, 2 H), 7.40-7.34 (m, 2 H), 7.21-7.01 (m, 4 H), 6.69-6.53 (m, 2 H) ppm.

¹³C NMR (75 MHz, dms_o-d₆): δ = 165.41, 162.11, 151.72, 144.87, 135.03, 129.93, 129.41, 129.29, 128.95, 128.95, 128.01, 121.48, 119.33, 117.80, 115.51, 115.22, 113.94, 102.80 ppm.

Yield: 74 % (1.11 mmol, 291 mg), light yellow solid.

2-(3-chlorophenyl)-1*H*-perimidine (6)



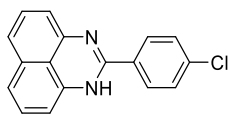
FW (C₁₇H₁₁ClN₂) = 278.74 g mol⁻¹

¹H NMR (300 MHz, dms_o-d₆): δ = 10.70 (s, 1 H), 8.06-7.98 (m, 2 H), 7.64-7.53 (m, 2 H), 7.21-7.01 (m, 4 H), 6.72-6.69 (m, 1 H), 6.55-6.53 (m, 1 H) ppm.

¹³C NMR (75 MHz, dms_o-d₆): δ = 151.34, 144.67, 138.29, 135.39, 135.01, 133.29, 130.77, 130.31, 128.92, 128.01, 126.47, 125.51, 121.65, 119.60, 117.89, 114.15, 102.89 ppm.

Yield: 71 % (1.07 mmol, 297 mg), yellow solid.

2-(4-chlorophenyl)-1*H*-perimidine (7)



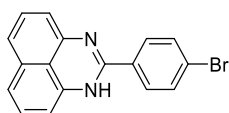
FW (C₁₇H₁₁ClN₂) = 278.74 g mol⁻¹

¹H NMR (300 MHz, dms_o-d₆): δ = 10.69 (s, 1 H), 8.05-8.02 (m, 2 H), 7.61-7.58 (m, 2 H), 7.20-7.01 (m, 4 H), 6.70-6.67 (m, 1 H), 6.55-6.53 (m, 1 H) ppm.

¹³C NMR (75 MHz, dms_o-d₆): δ = 151.66, 144.76, 138.34, 135.77, 135.04, 132.17, 128.95, 128.65, 128.48, 128.02, 121.57, 119.49, 117.88, 114.06, 102.88 ppm.

Yield: 80 % (1.07 mmol, 334 mg), yellow solid.

2-(4-bromophenyl)-1*H*-perimidine (8)



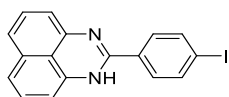
FW (C₁₇H₁₁BrN₂) = 323.19 g mol⁻¹

¹H NMR (300 MHz, dms_o-d₆): δ = 10.68 (s, 1 H), 7.98-7.96 (m, 2 H), 7.76-7.73 (m, 2 H), 7.21-7.01 (m, 4 H), 6.69-6.67 (m, 1 H), 6.55-6.52 (m, 1 H) ppm.

¹³C NMR (75 MHz, dms_o-d₆): δ = 151.73, 144.75, 138.32, 135.03, 132.51, 131.41, 128.94, 128.85, 128.02, 124.64, 121.55, 119.49, 117.86, 114.06, 102.86 ppm.

Yield: 72 % (1.07 mmol, 349 mg), orange solid.

2-(4-iodophenyl)-1*H*-perimidine (9), new compound



FW (C₁₇H₁₁IN₂) = 370.19 g mol⁻¹

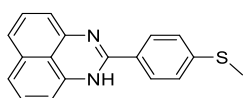
¹H NMR (300 MHz, dms_o-d₆): δ = 10.67 (s, 1 H), 7.92-7.80 (m, 4 H), 7.14-7.02 (m, br, 4 H), 6.67-6.56 (m, br, 2 H) ppm.

¹³C NMR (75 MHz, dms_o-d₆): δ = 151.92, 144.78, 138.34, 137.22, 135.01, 132.81, 128.92, 128.68, 127.99, 121.60, 119.48, 117.86, 114.06, 102.86, 99.38 ppm.

Elemental analysis: calcd.: C 55.16, H 3.00, N 7.57; found: C 54.79, H 3.18, N 7.19

Yield: 67 % (1.01 mmol, 372 mg), orange solid.

2-(4-(methylthio)phenyl)-1*H*-perimidine (10), new compound



FW (C₁₈H₁₄SN₂) = 290.38 g mol⁻¹

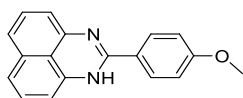
¹H NMR (300 MHz, dms_o-d₆): δ = 10.60 (s, 1 H), 7.99-7.97 (m, 2 H), 7.40-7.38 (m, 2 H), 7.20-7.00 (m, 4 H), 6.69-6.66 (m, 1 H), 6.56-6.54 (m, 1 H) ppm.

¹³C NMR (75 MHz, dms_o-d₆): δ = 152.02, 144.99, 142.29, 138.44, 135.03, 129.40, 128.94, 127.96, 127.17, 124.99, 121.49, 119.11, 117.66, 113.82, 102.69, 14.18 ppm.

Elemental analysis: calcd.: C 74.45, H 4.86, N 9.65; found: C 74.81, H 4.49, N 9.49

Yield: 78 % (1.17 mmol, 340 mg), yellow solid.

2-(4-methoxyphenyl)-1*H*-perimidine (11)



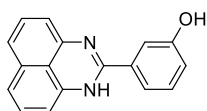
FW (C₁₈H₁₄ON₂) = 274.32 g mol⁻¹

¹H NMR (300 MHz, dmsd-d₆): δ = 10.56 (s, 1 H), 8.03-8.00 (m, 2 H), 7.20-6.97 (m, 6 H), 6.69-6.55 (m, 2 H), 3.83 (s, 3 H) ppm.

¹³C NMR (75 MHz, dmsd-d₆): δ = 161.50, 152.09, 145.16, 138.55, 135.04, 128.94, 128.50, 127.95, 125.58, 121.37, 118.87, 117.57, 133.68, 102.62, 55.38 ppm.

Yield: 76 % (1.14 mmol, 313 mg), orange solid.

3-(1*H*-perimidin-2-yl)phenol (12)



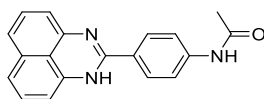
FW (C₁₇H₁₂N₂O) = 260.30 g mol⁻¹

¹H NMR (300 MHz, dmsd-d₆): δ = 10.59 (s, 1 H), 9.76 (s, 1 H), 7.46-7.42 (m, 2 H), 7.35-7.30 (m, 1 H), 7.20-6.96 (m, 5 H), 6.68-6.66 (m, 1 H), 6.56-6.54 (m, 1 H) ppm.

¹³C NMR (75 MHz, dmsd-d₆): δ = 157.44, 152.79, 145.10, 138.54, 135.09, 134.90, 129.49, 128.97, 128.02, 121.65, 119.20, 118.09, 117.69, 117.45, 113.83, 113.76, 102.77 ppm.

Yield: 80 % (1.20 mmol, 312 mg), orange solid.

N-(4-(1*H*-perimidin-2-yl)phenyl)acetamide (13)



FW (C₁₉H₁₅N₃O) = 301.35 g mol⁻¹

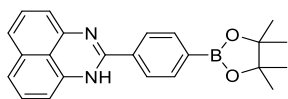
¹H NMR (300 MHz, dmsd-d₆): δ = 10.56 (s, 1 H), 10.22 (s, 1 H), 7.99-7.96 (m, 2 H), 7.75-7.73 (m, 2 H), 7.20-6.99 (m, 4 H), 6.68-6.53 (m, 2 H), 2.09 (s, 3 H) ppm.

¹³C NMR (75 MHz, dmsd-d₆): δ = 169.20, 152.61, 145.59, 142.30, 138.97, 135.52, 129.43, 128.44, 128.12, 128.03, 121.91, 119.47, 118.72, 118.10, 114.21, 103.13, 24.62 ppm.

Yield: 82 % (1.23 mmol, 371 mg), yellow solid.

2-(4-(4,4,5,5-tetramethyl-1,3,2-dioxaborolan-2-yl)phenyl)-1*H*-perimidine (14),

new compound



FW (C₂₃H₂₃BN₂O₂) = 370.26 g mol⁻¹

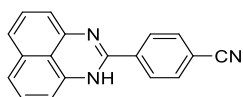
¹H NMR (300 MHz, dms_o-d₆): δ = 10.69 (s, 1 H), 8.08-8.05 (m, 2 H), 7.85-7.82 (m, 2 H), 7.21-6.99 (m, 4 H), 6.72-6.56 (m, 2 H), 1.32 (s, 12 H) ppm.

¹³C NMR (75 MHz, dms_o-d₆): δ = 152.25, 144.88, 138.41, 135.82, 135.04, 134.37, 128.92, 128.01, 126.09, 121.65, 119.43, 117.77, 115.02, 114.03, 102.83, 83.94, 24.69 ppm.

Elemental analysis: calcd.: C 74.61, H 6.26, N 7.57; found: C 74.23, H 6.54, N 7.24

Yield: 70 % (1.05 mmol, 389 mg), red solid.

4-(1*H*-perimidin-2-yl)benzonitrile (15)



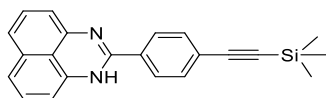
FW (C₁₈H₁₁N₃) = 269.31 g mol⁻¹

¹H NMR (300 MHz, dms_o-d₆): δ = 10.78 (s, 1 H), 8.19-8.16 (m, 2 H), 8.01-7.98 (m, 2 H), 7.21-7.00 (m, 4 H), 6.72-6.69 (m, 1 H), 6.54-6.52 (m, 1 H) ppm.

¹³C NMR (75 MHz, dms_o-d₆): δ = 151.37, 144.55, 138.23, 137.44, 135.03, 132.39, 128.94, 128.05, 127.58, 121.68, 119.92, 118.43, 118.03, 114.38, 113.22, 103.02 ppm.

Yield: 66 % (0.99 mmol, 267 mg), red solid.

2-(4-((trimethylsilyl)ethynyl)phenyl)-1*H*-perimidine (16), new compound



FW (C₂₂H₂₀N₂Si) = 340.50 g mol⁻¹

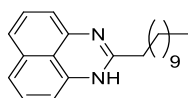
¹H NMR (300 MHz, dms_o-d₆): δ = 10.68 (s, 1 H), 8.06-8.03 (m, 2 H), 7.64-7.61 (m, 2 H), 7.21-7.00 (m, 4 H), 6.70-6.68 (m, 1 H), 6.56-6.54 (m, 1 H), 0.26 (s, 9 H) ppm.

¹³C NMR (75 MHz, dms_o-d₆): δ = 151.70, 144.79, 138.35, 135.01, 133.36, 131.58, 128.91, 127.99, 126.97, 124.54, 121.57, 119.48, 117.80, 114.08, 104.53, 102.83, 99.59, 0.19 ppm.

Elemental analysis: calcd.: C 77.60, H 5.92, N 8.28; found: C 77.98, H 5.61, N 8.71

Yield: 65 % (0.98 mmol, 332 mg), red solid.

2-undecyl-1*H*-perimidine (17)



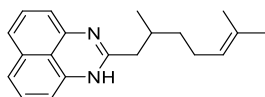
FW (C₂₂H₃₀N₂) = 322.50 g mol⁻¹

¹H NMR (500 MHz, chloroform-d₁): δ = 8.14 (s, 1 H), 7.14-7.08 (m, 4 H), 6.56-6.55 (m, 2 H), 2.36 (t, *J* = 7.62 Hz, 2 H), 1.72 (quint, *J* = 7.62 Hz, 2 H), 1.38-1.19 (m, 16 H), 0.88 (t, *J* = 7.02 Hz, 3 H) ppm.

¹³C NMR (125.76 MHz, chloroform-d₁): δ = 157.84, 140.41, 135.44, 128.30, 121.81, 119.61, 107.91, 35.81, 31.94, 29.64, 29.62, 29.52, 29.42, 29.41, 29.37, 27.65, 22.73, 14.17 ppm.

Yield: 85 % (1.28 mmol, 411 mg), white solid.

2-(2,6-dimethylhept-5-en-1-yl)-1*H*-perimidine (18), new compound



FW (C₂₀H₂₄N₂) = 292.43 g mol⁻¹

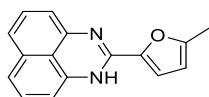
¹H NMR (300 MHz, dms_o-d₆): δ = 10.40 (s, 1 H), 7.10-7.06 (m, 2 H), 6.97-6.94 (m, 2 H), 6.50-6.30 (m, br, 2 H), 5.09 (t, *J* = 7.03 Hz, 1 H), 2.29-2.23 (m, 1 H), 2.08-1.92 (m, 4 H), 1.62 (s, 3 H), 1.55 (s, 3 H), 1.46-1.36 (m, 1 H), 1.26-1.14 (m, 1 H), 0.94 (d, *J* = 6.45 Hz, 3 H) ppm.

¹³C NMR (75 MHz, dms_o-d₆): δ = 156.69, 145.31, 138.40, 135.13, 130.60, 128.76, 128.05, 124.48, 121.42, 118.33, 117.34, 112.92, 101.50, 42.20, 36.40, 30.87, 25.49, 24.97, 19.14, 17.48 ppm.

Elemental analysis: calcd.: C 82.15, H 8.27, N 9.58; found: C 81.67, H 7.75, N 9.61

Yield: 81 % (1.22 mmol, 355 mg), light yellow oil.

2-(5-methylfuran-2-yl)-1*H*-perimidine (19)



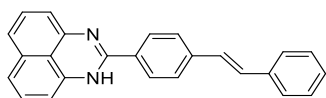
FW (C₁₆H₁₂N₂O) = 248.29 g mol⁻¹

¹H NMR (300 MHz, dms_o-d₆): δ = 10.55 (s, 1 H), 7.18-6.98 (m, 5 H), 6.64-6.61 (m, 1 H), 6.55-6.53 (m, 1 H), 6.334-6.327 (m, 1 H), 2.39 (s, 3 H) ppm.

¹³C NMR (75 MHz, dms_o-d₆): δ = 154.71, 145.40, 144.76, 144.73, 137.88, 135.07, 128.89, 127.93, 121.39, 119.07, 117.66, 113.79, 113.53, 108.71, 102.66, 13.60 ppm.

Yield: 75 % (1.13 mmol, 279 mg), red solid.

2-(4-styrylphenyl)-1*H*-perimidine (20), new compound



FW (C₂₅H₁₈N₂) = 346.43 g mol⁻¹

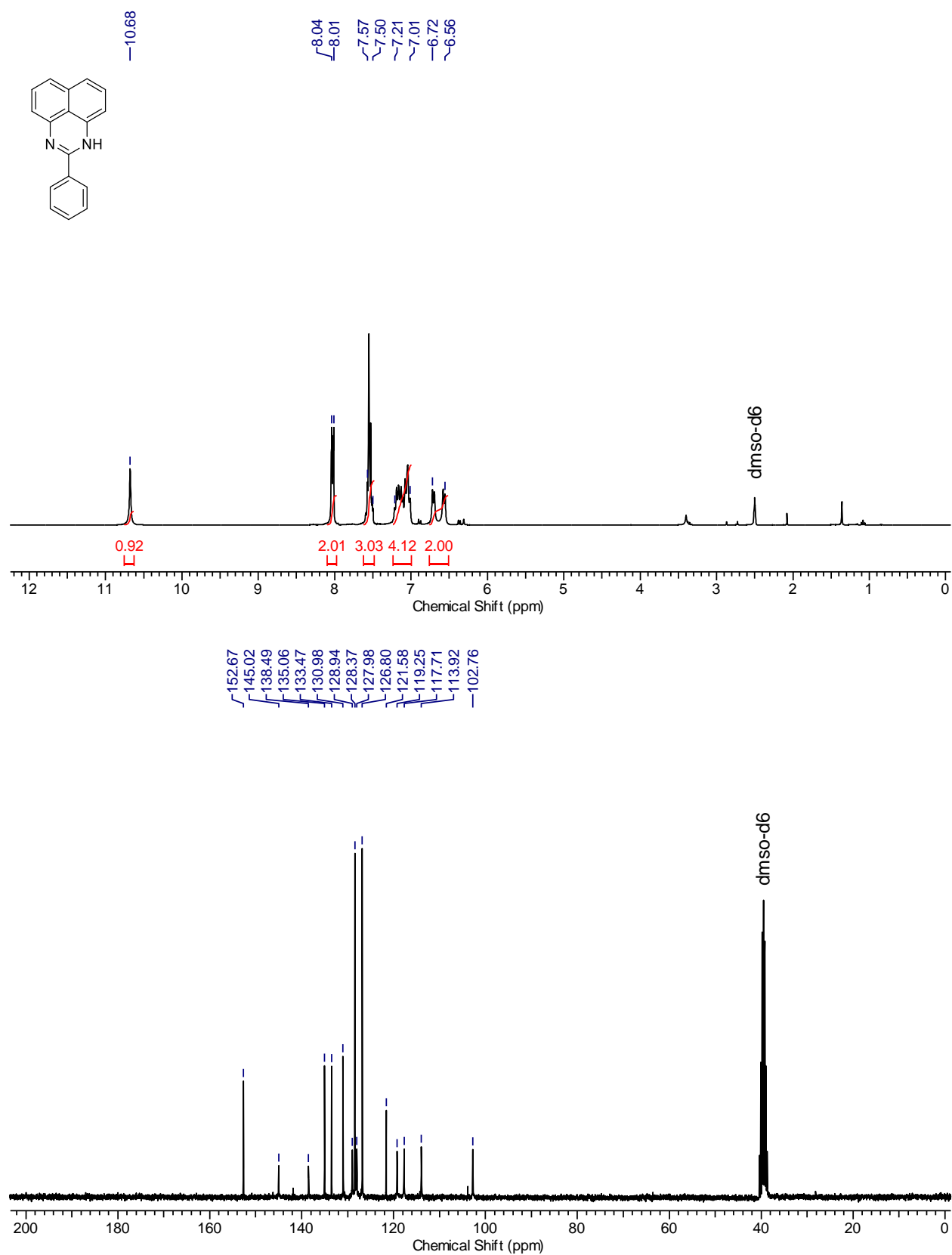
¹H NMR (300 MHz, dms_o-d₆): δ = 10.66 (s, 1 H), 8.09-8.06 (m, 2 H), 7.78-7.75 (m, 2 H), 7.65-7.63 (m, 2 H), 7.44-7.02 (m, 9 H), 6.75-6.72 (m, 1 H), 6.61-6.59 (m, 1 H) ppm.

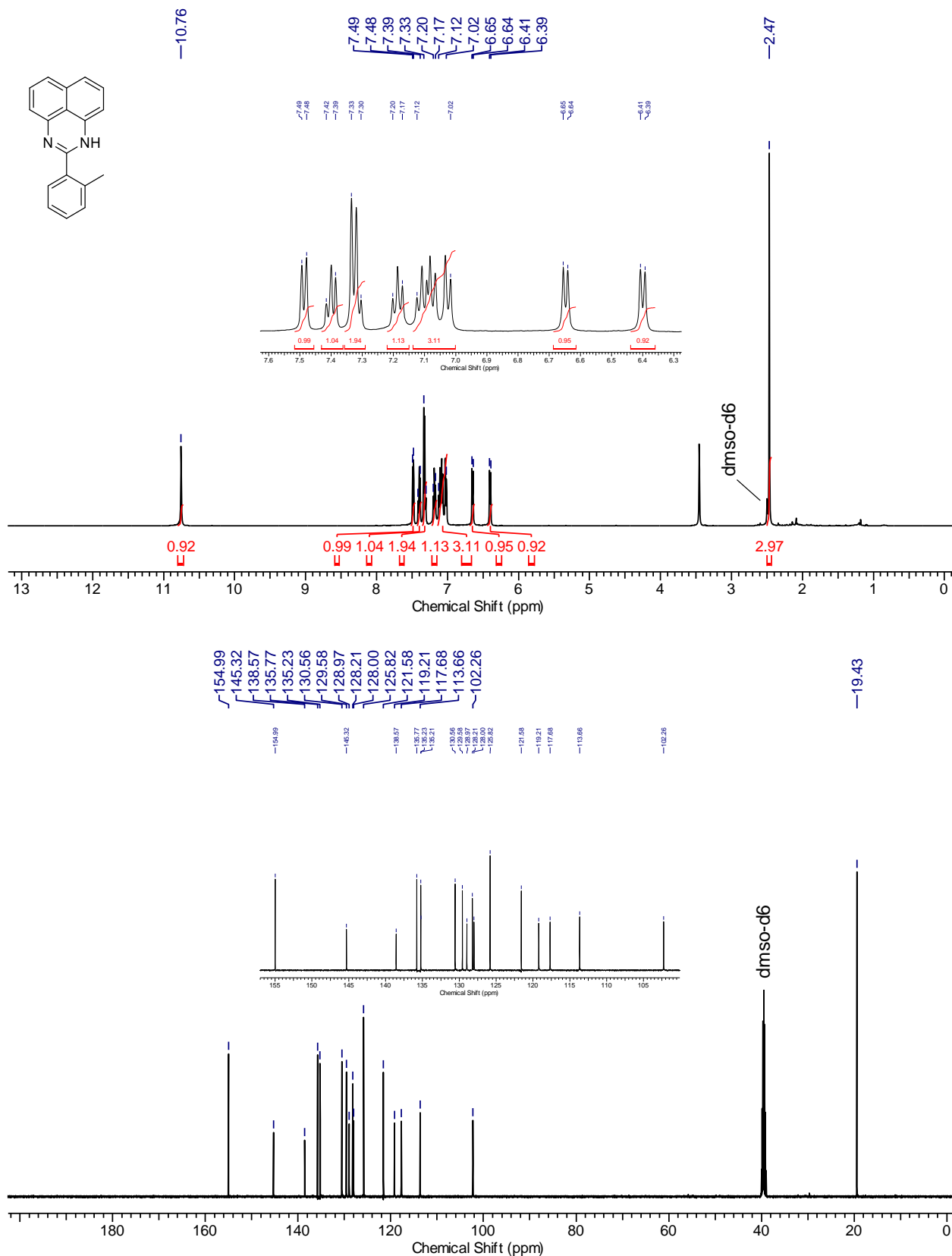
¹³C NMR (75 MHz, dms_o-d₆): δ = 152.69, 145.56, 140.16, 139.02, 137.25, 135.58, 132.64, 130.64, 129.46, 129.25, 129.16, 128.50, 128.02, 127.68, 127.21, 126.86, 122.08, 119.75, 118.20, 114.47, 103.27 ppm.

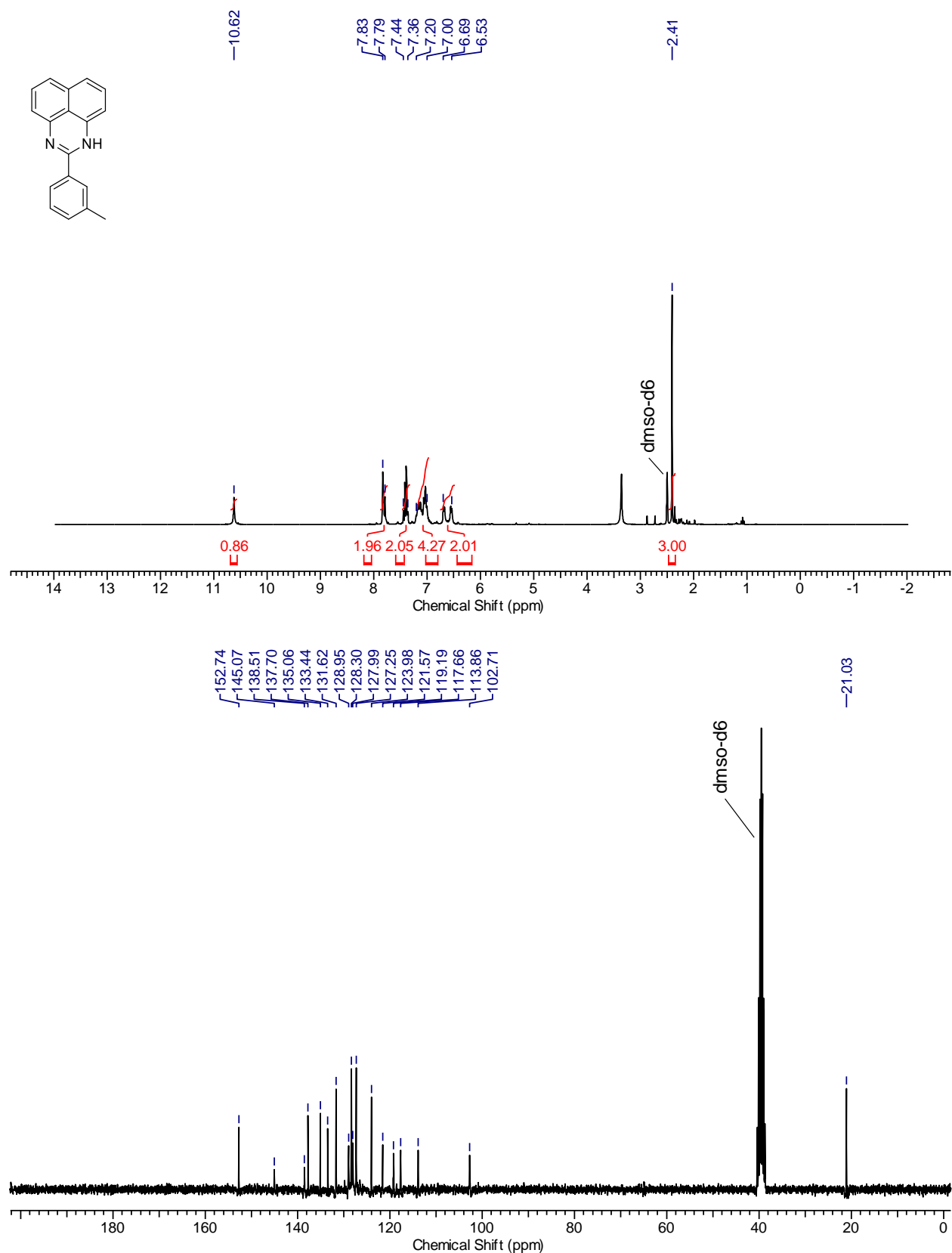
Elemental analysis: calcd.: C 86.68, H 5.24, N 8.09; found: C 87.12, H 5.18, N 8.13

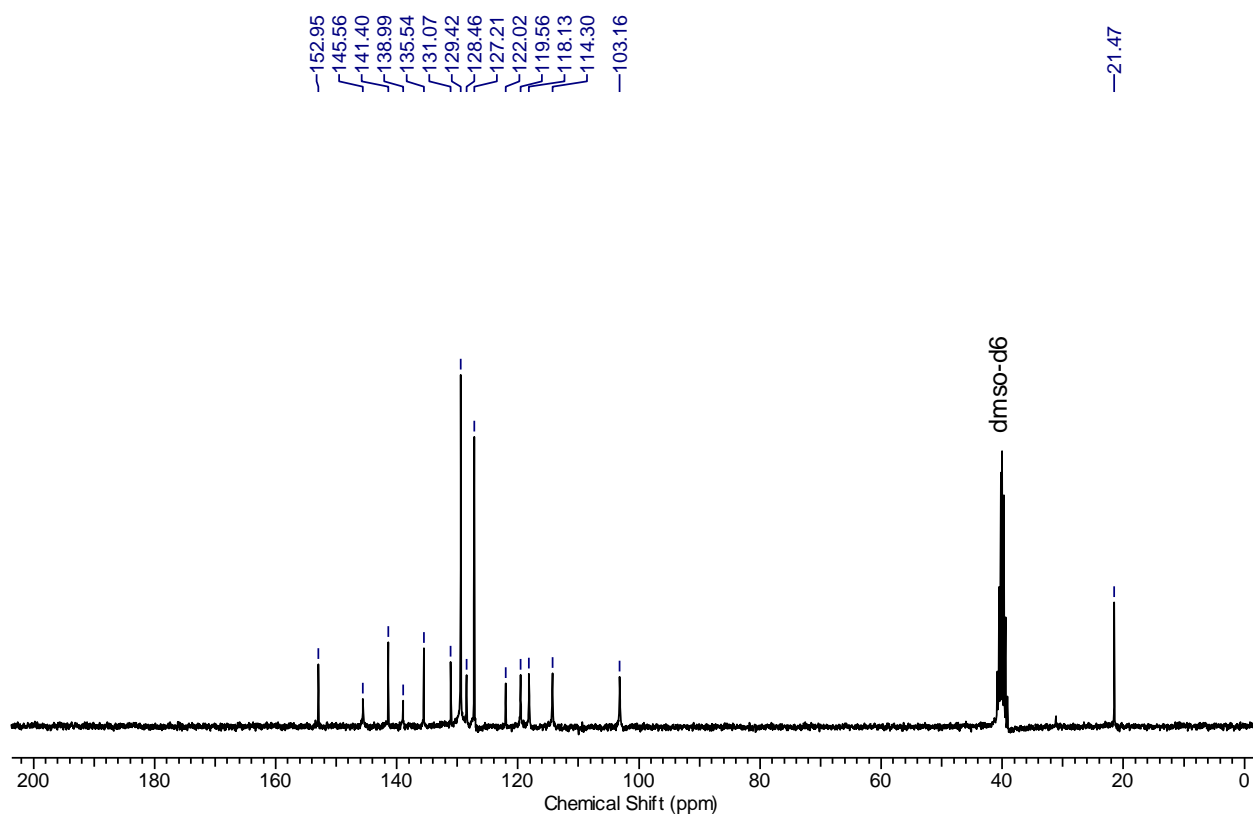
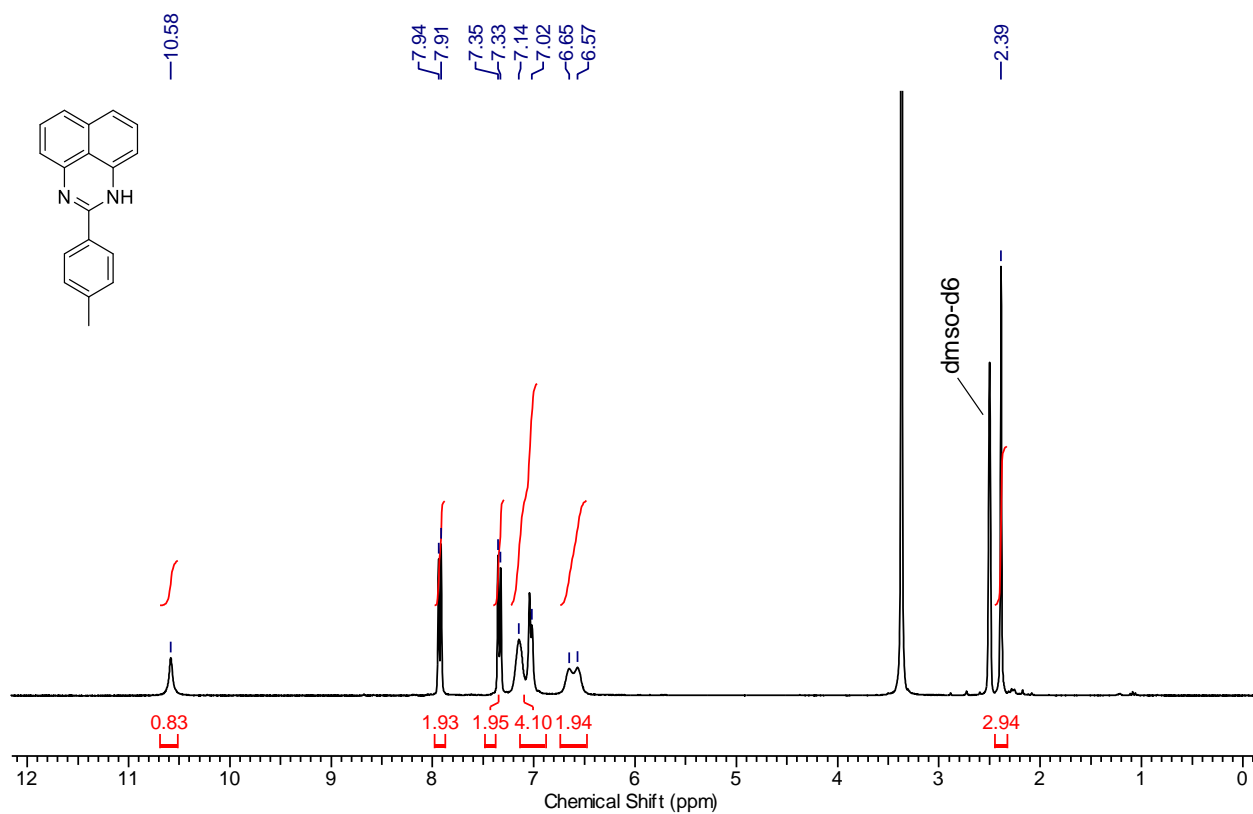
Yield: 79 % (1.19 mmol, 410 mg), red solid.

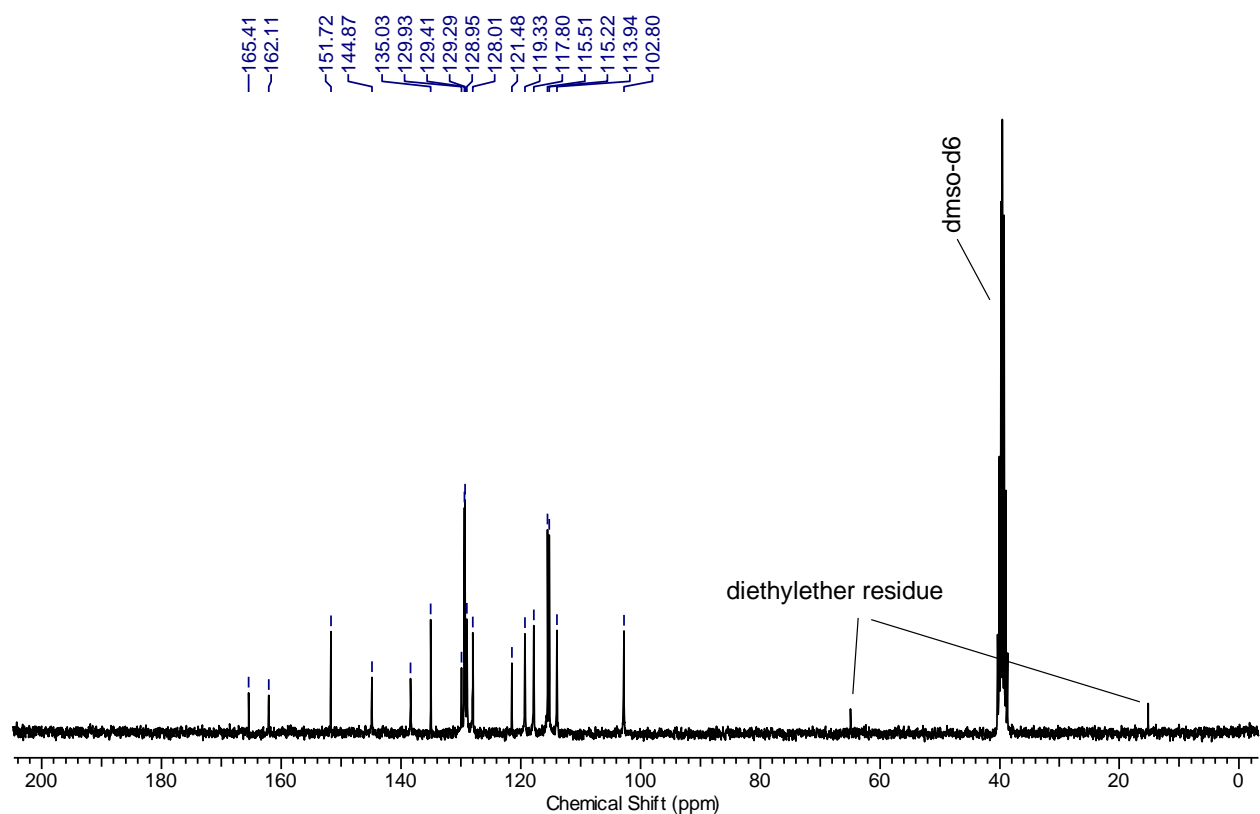
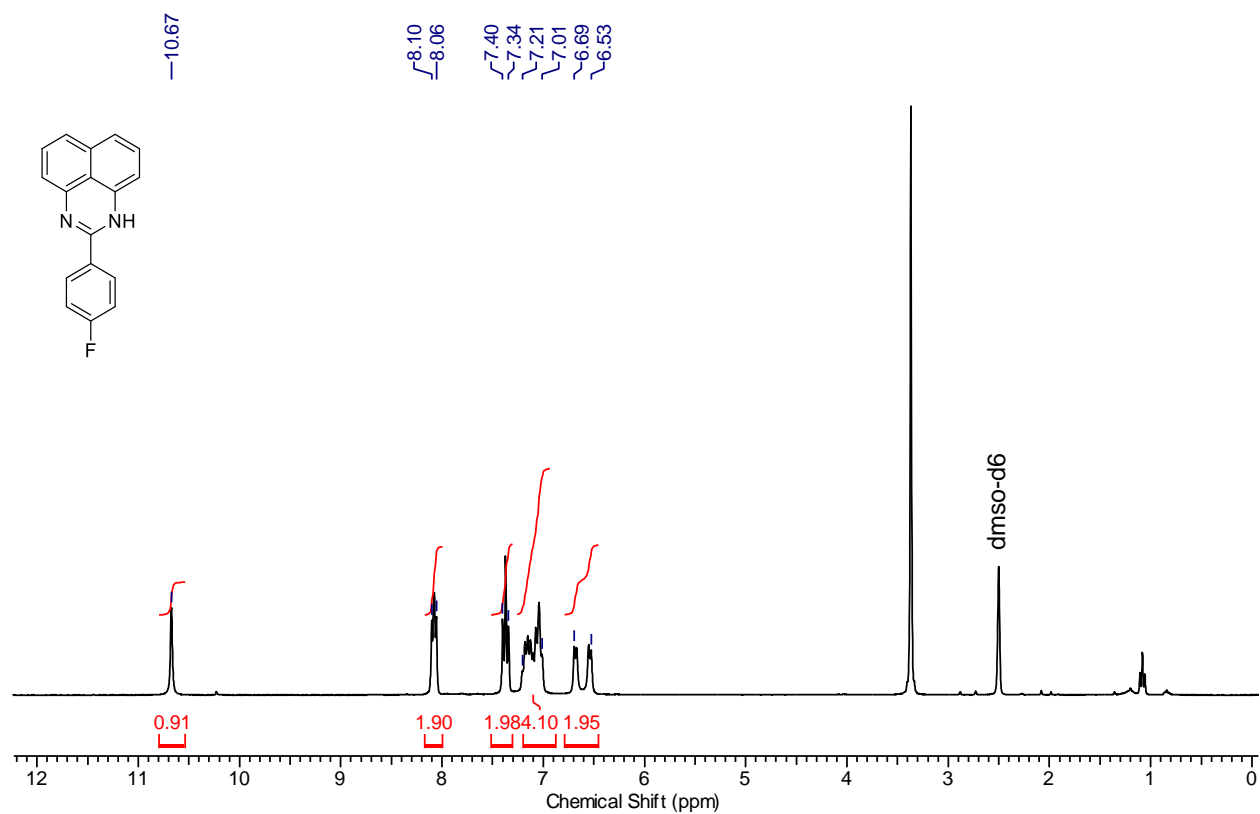
NMR spectra

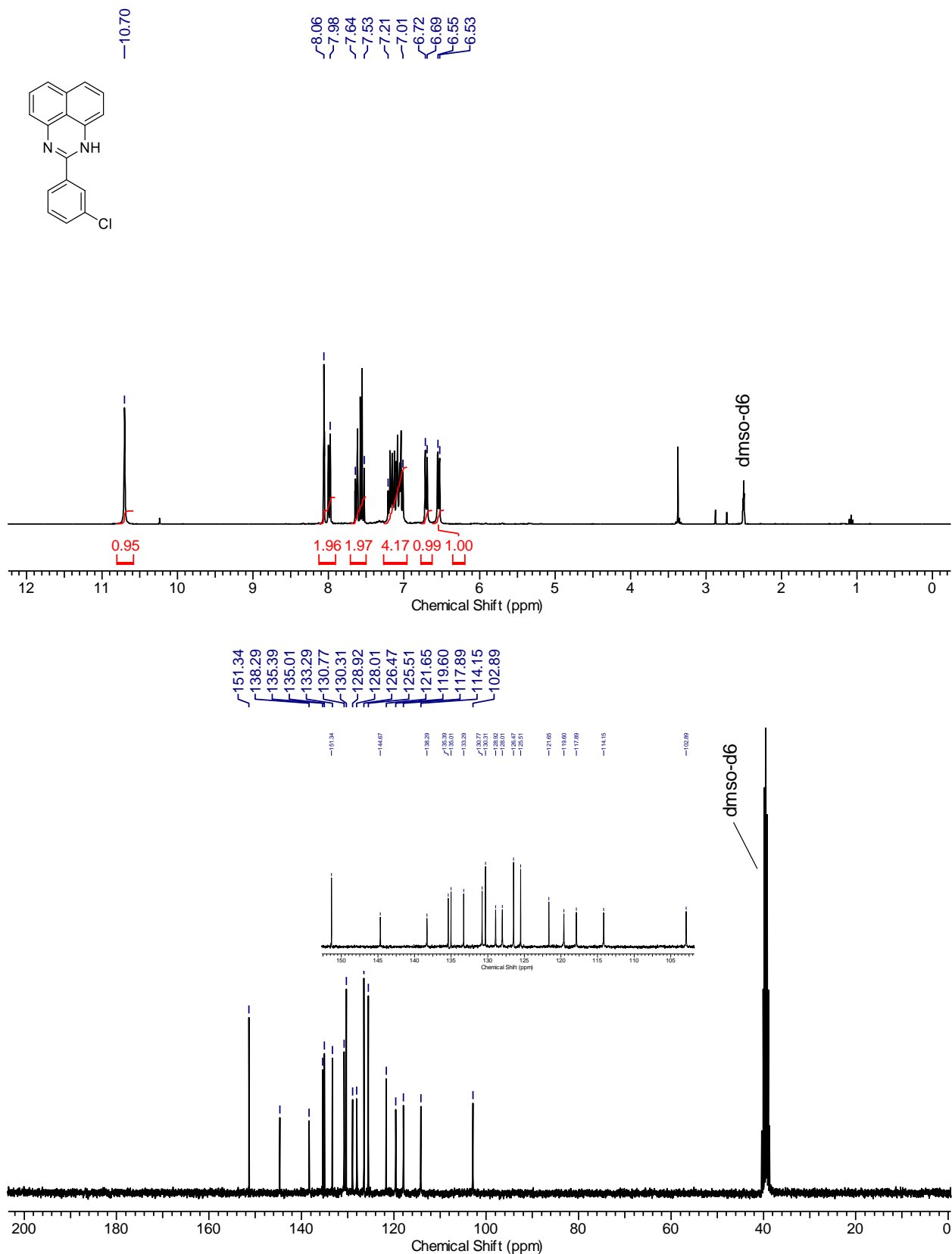


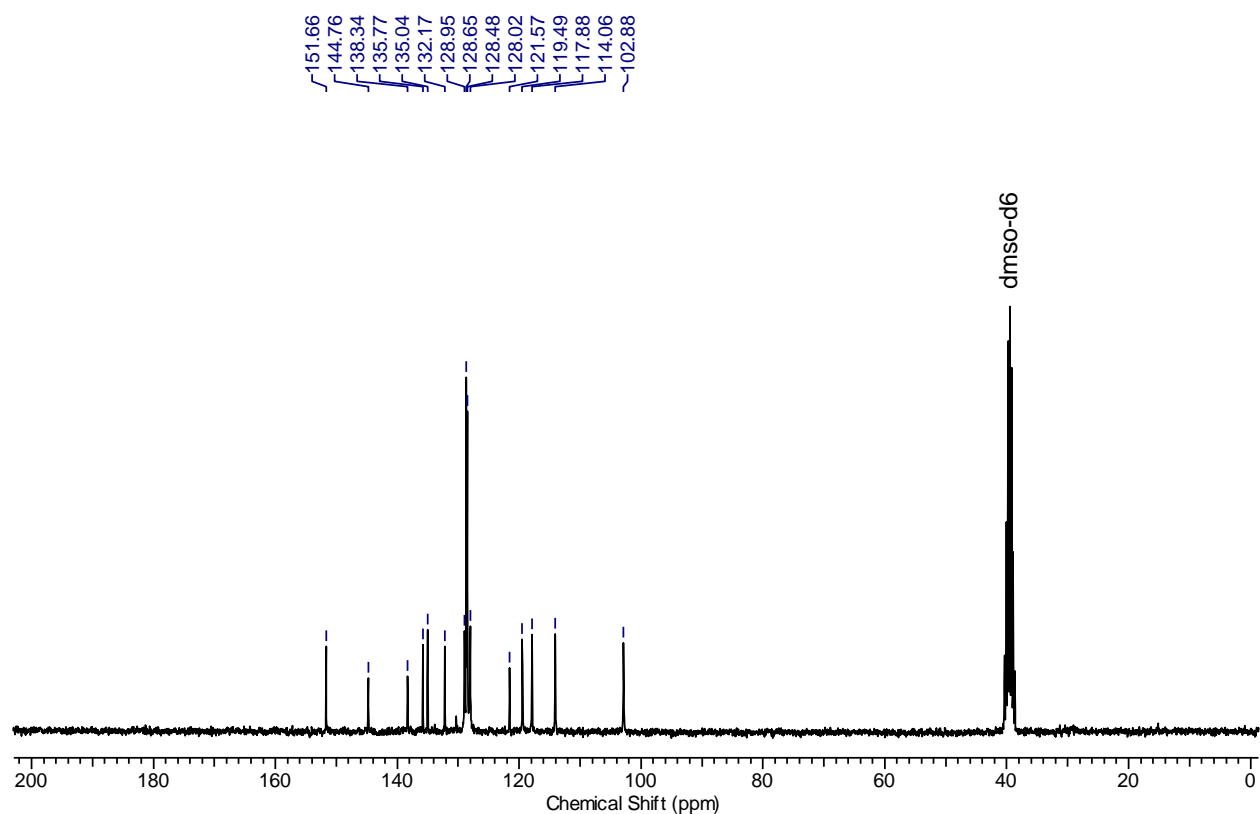
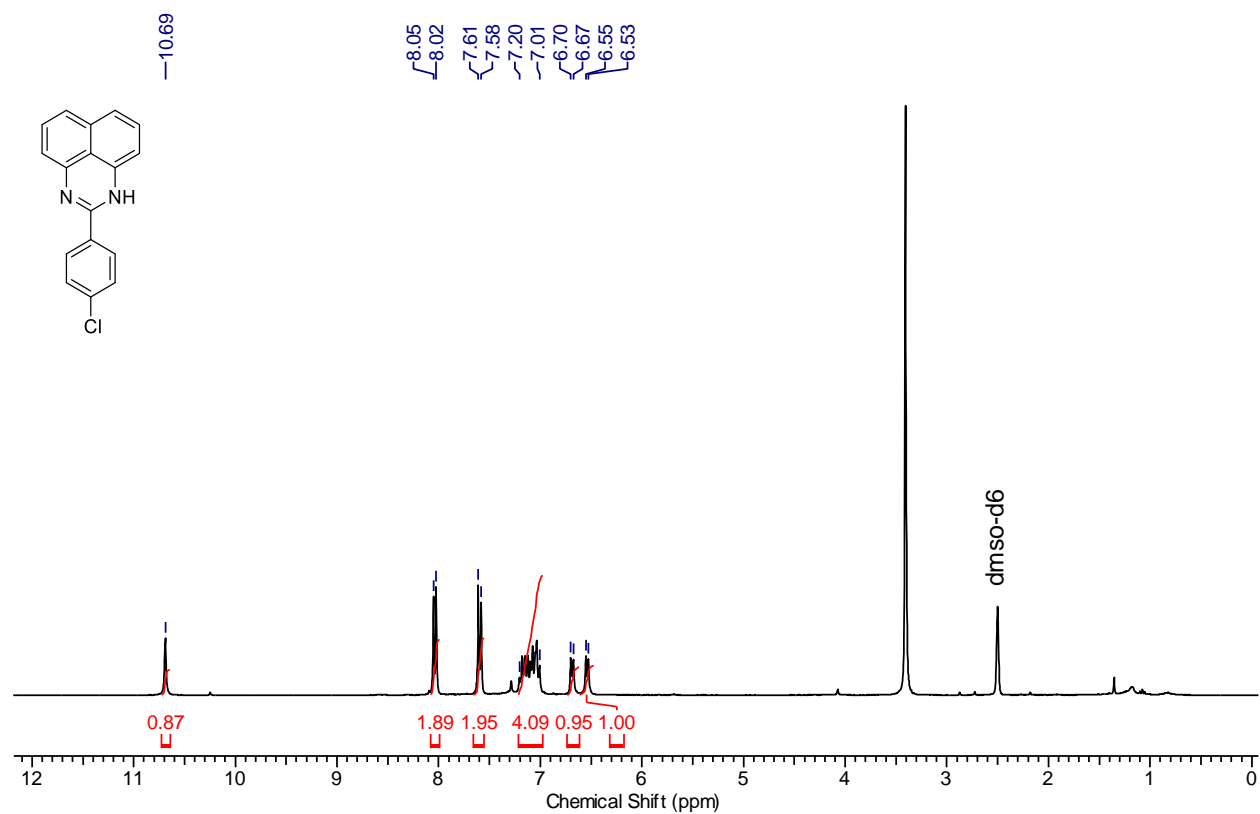


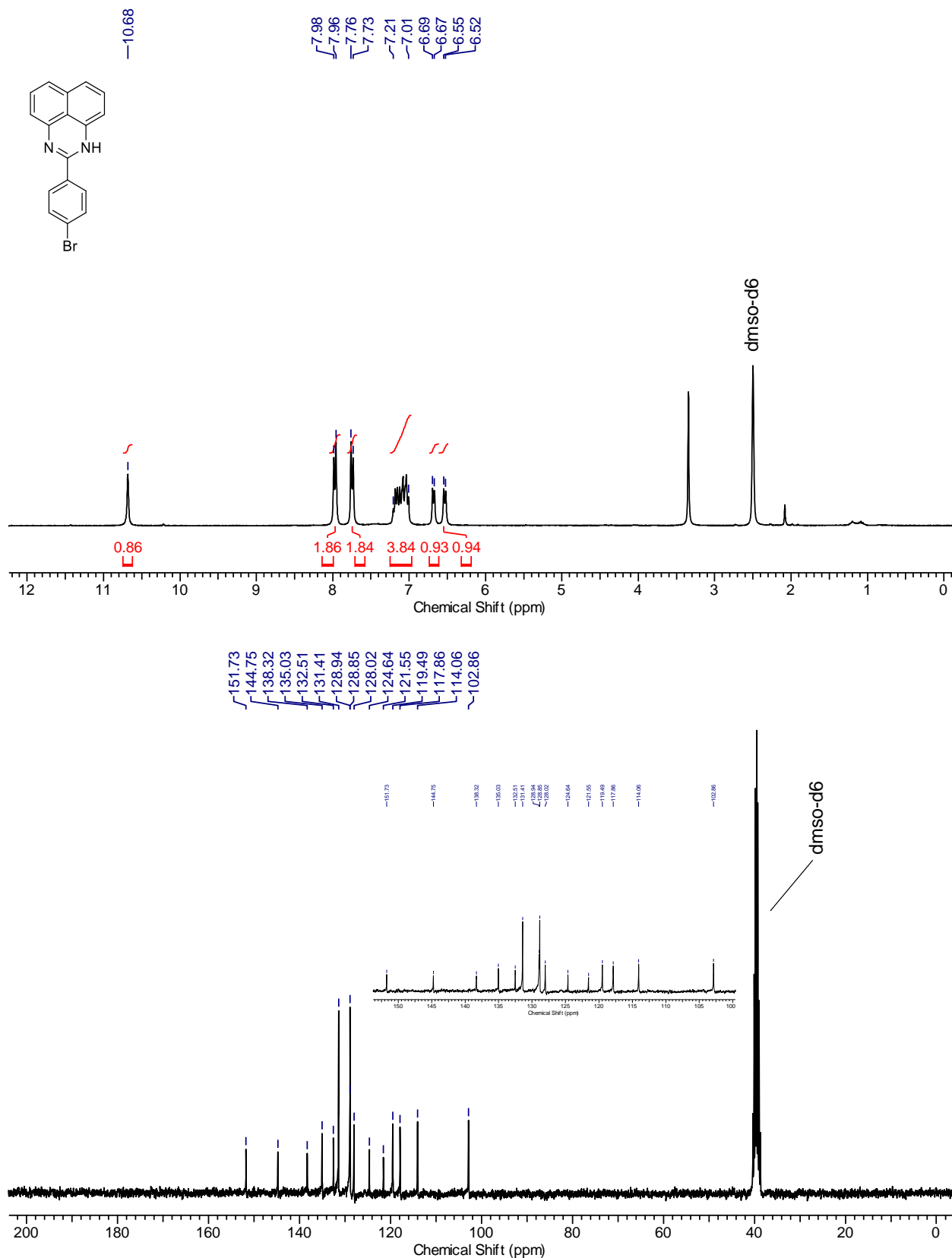


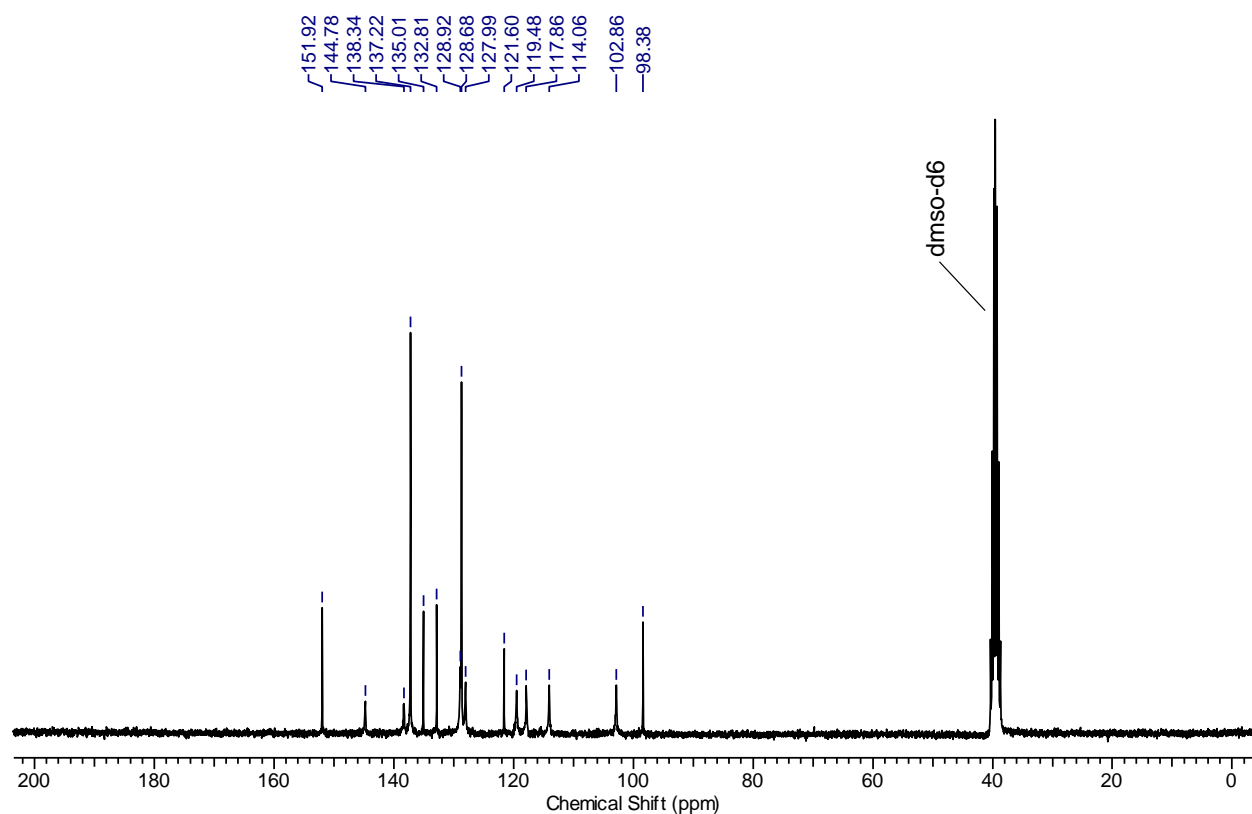
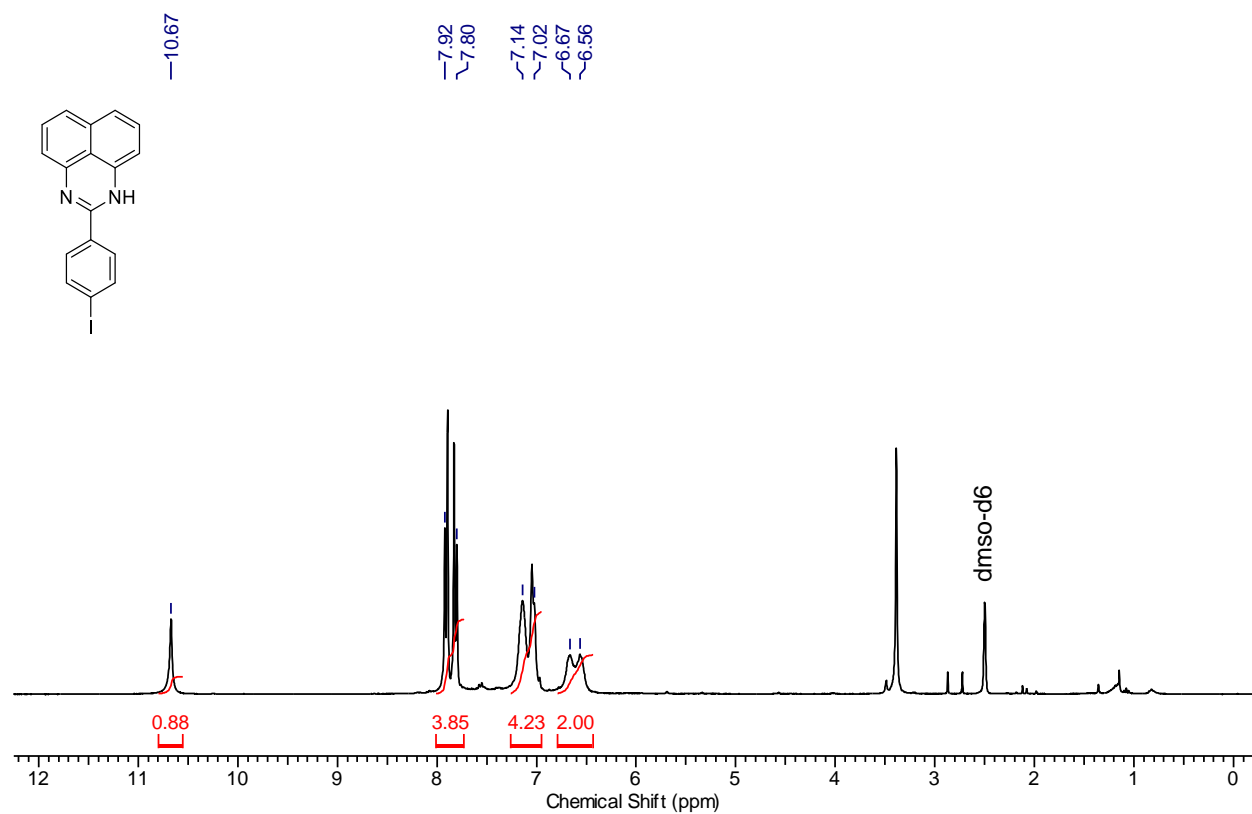


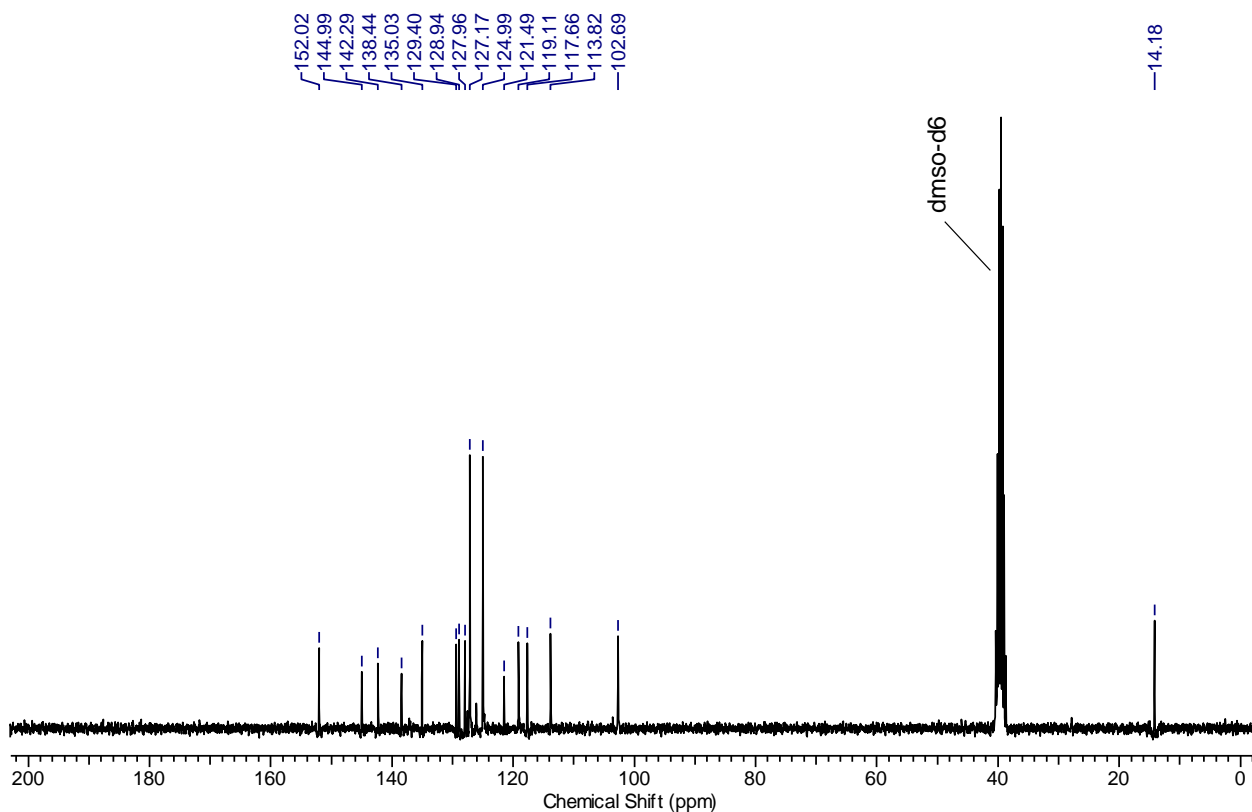
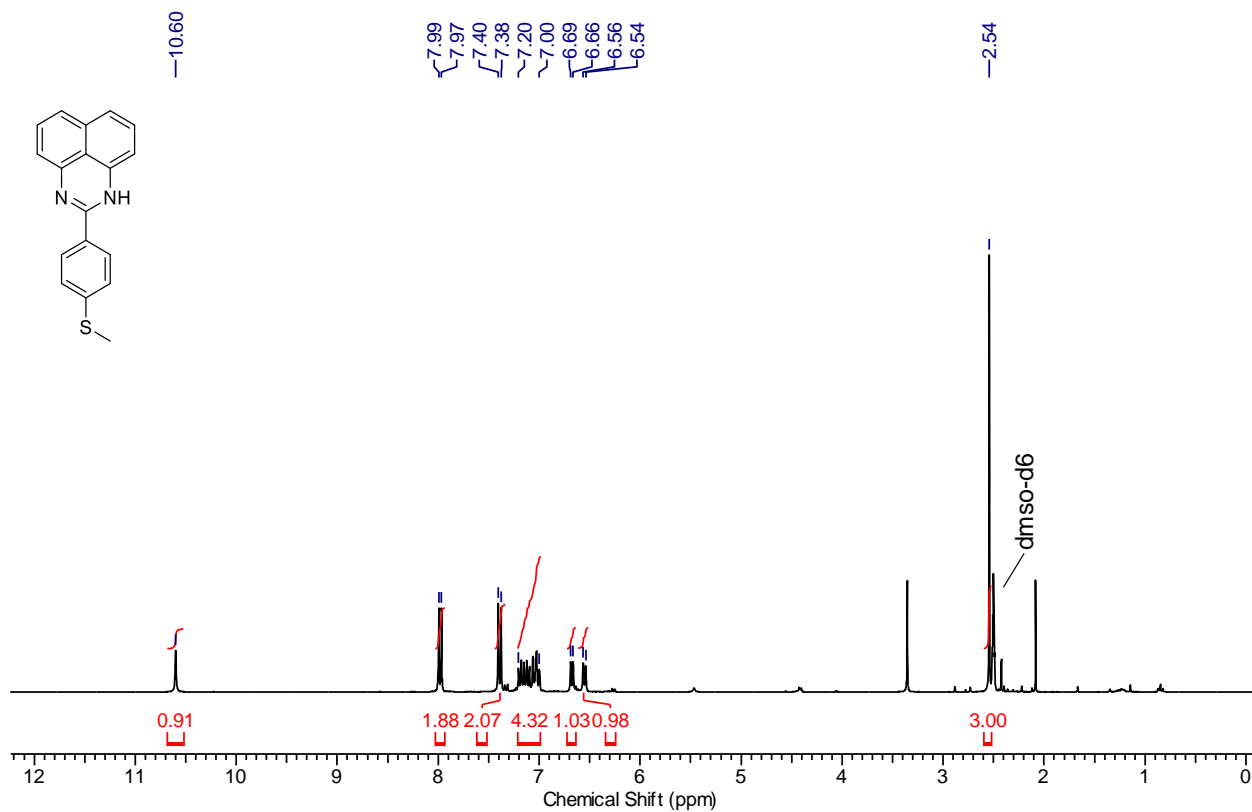


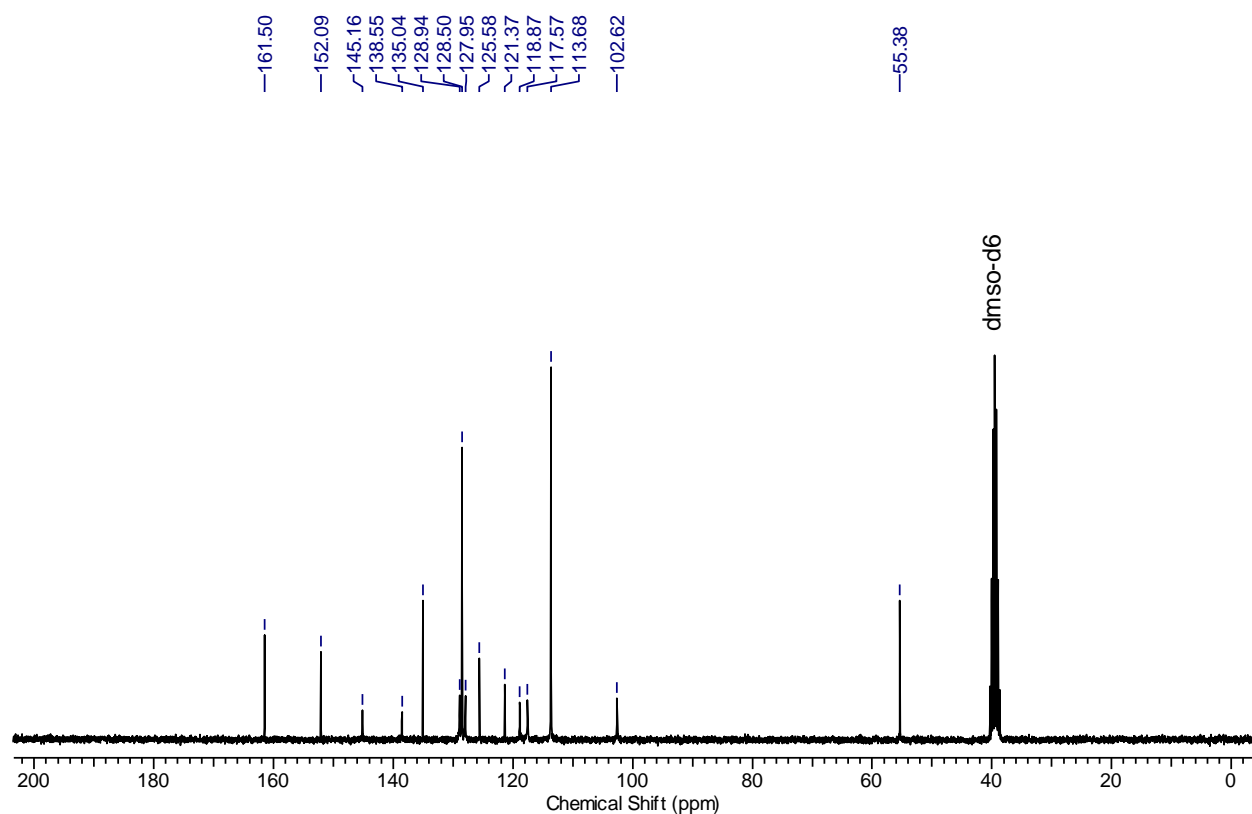
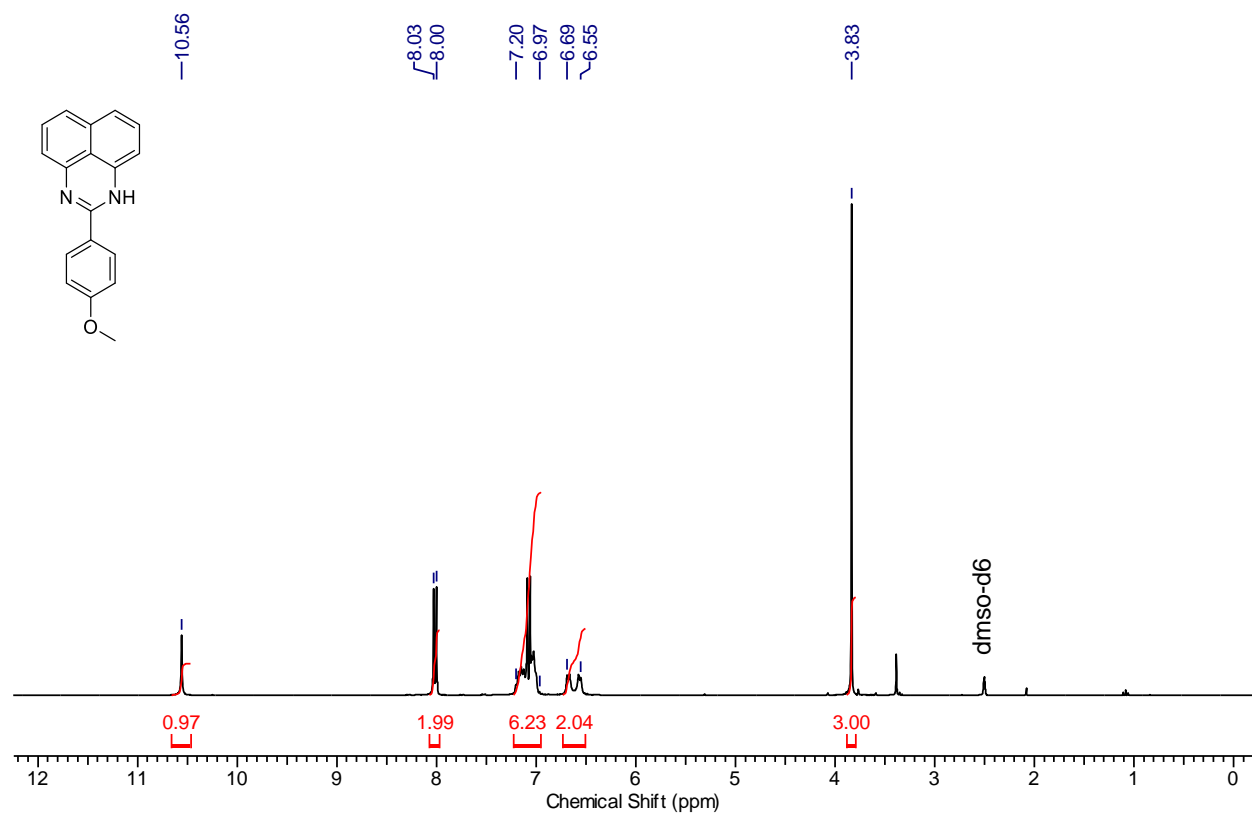


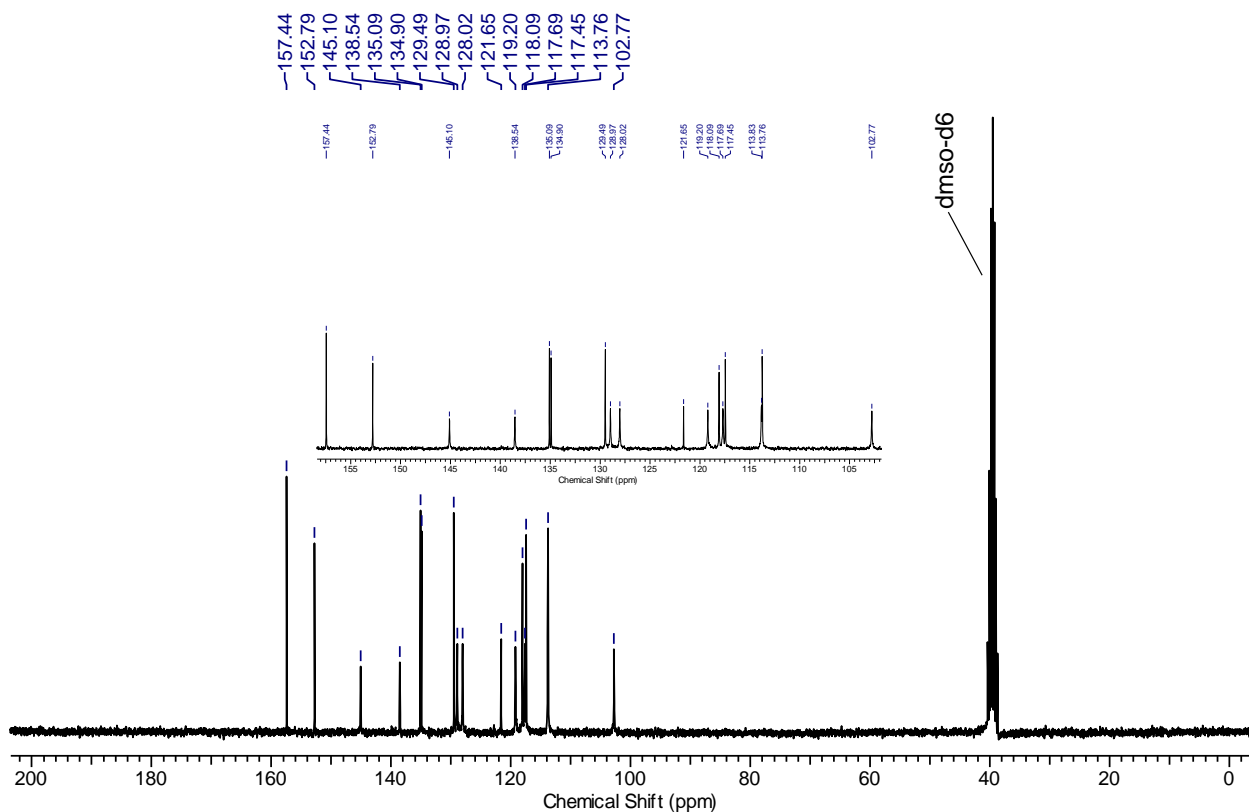
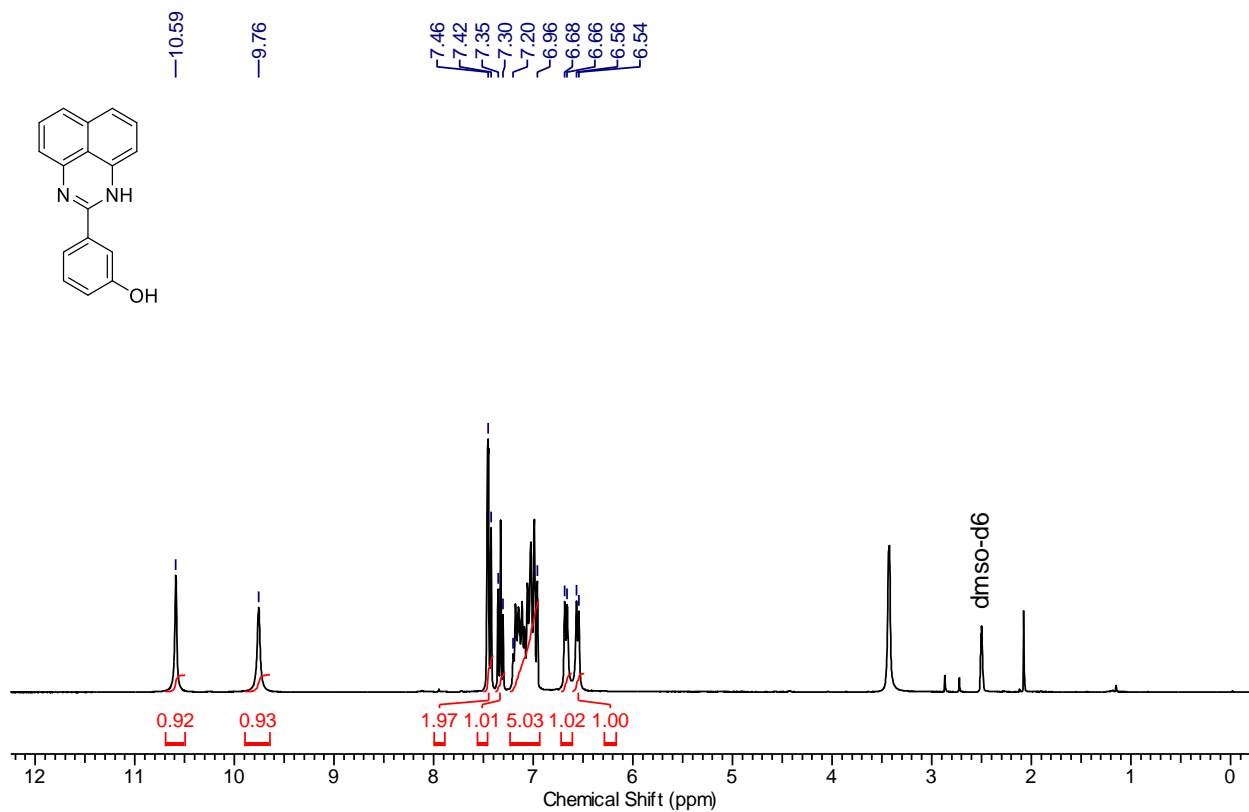


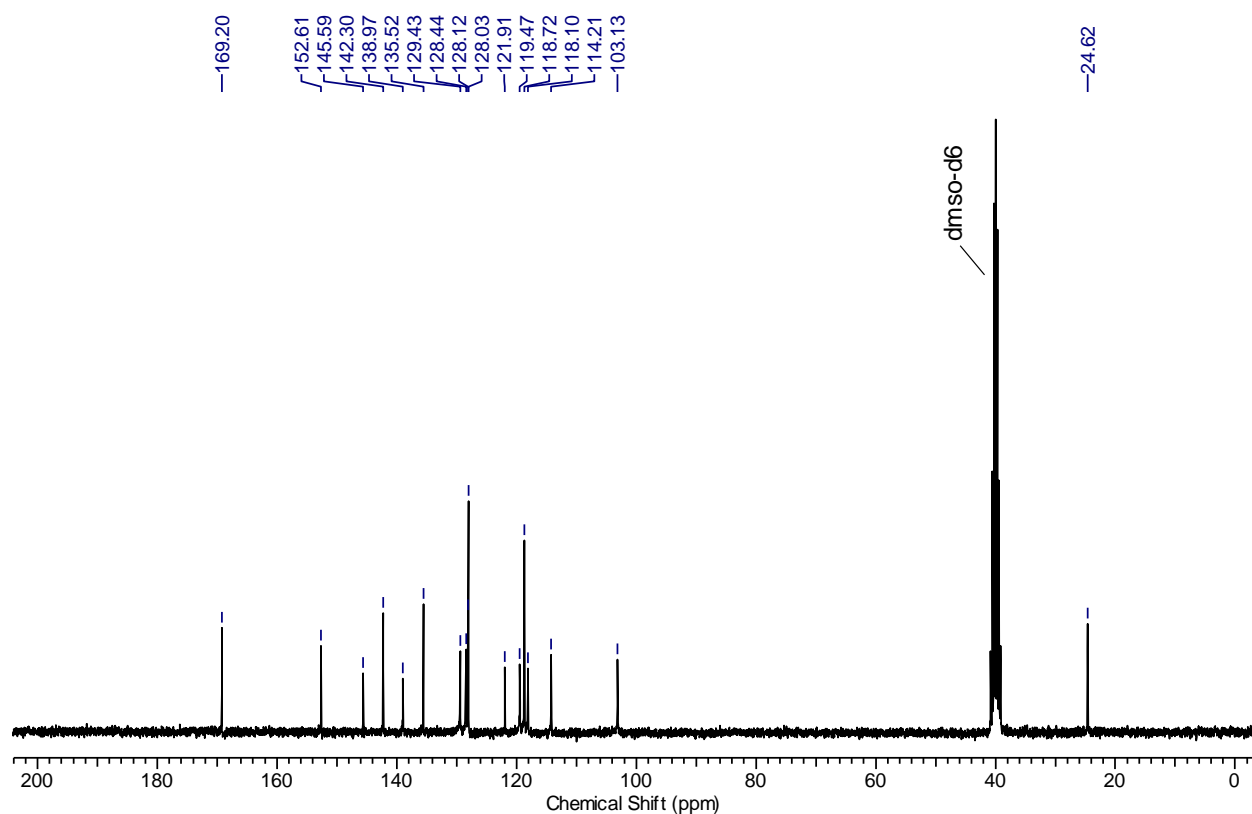
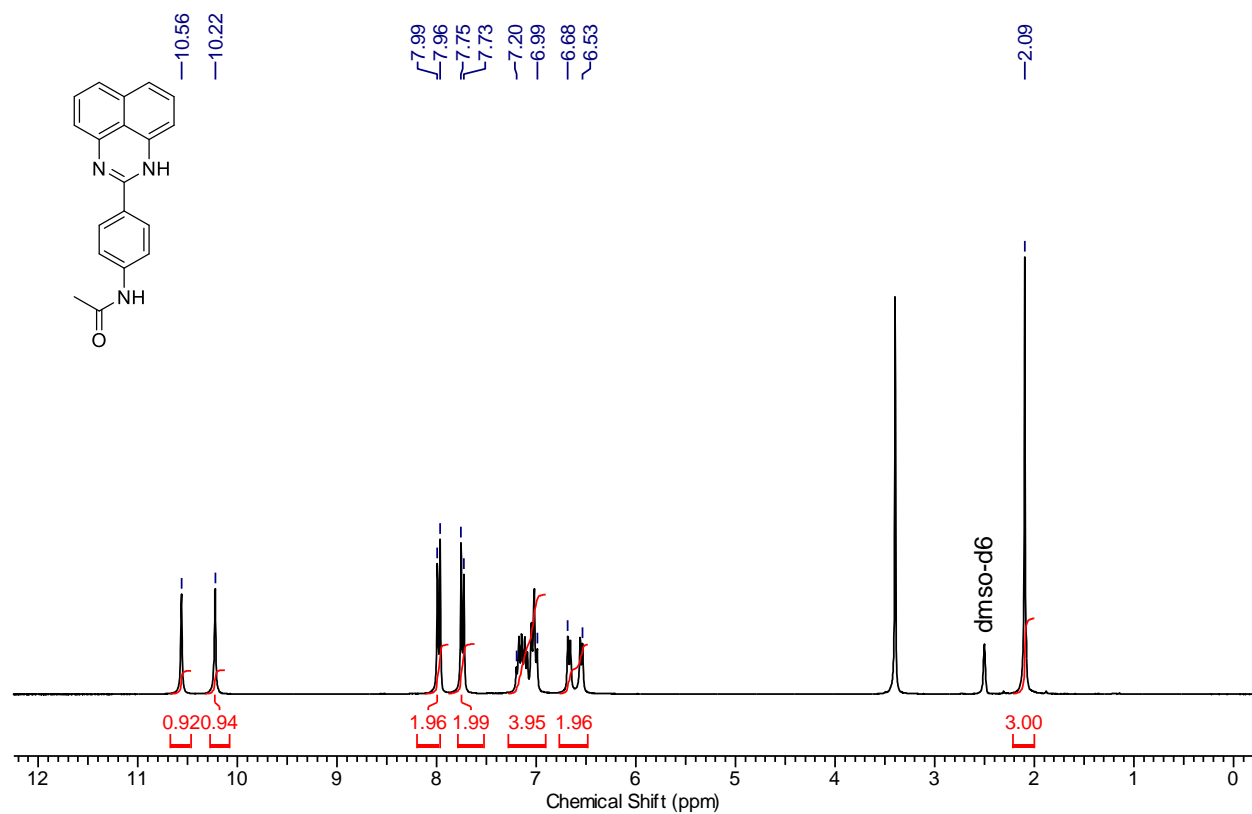


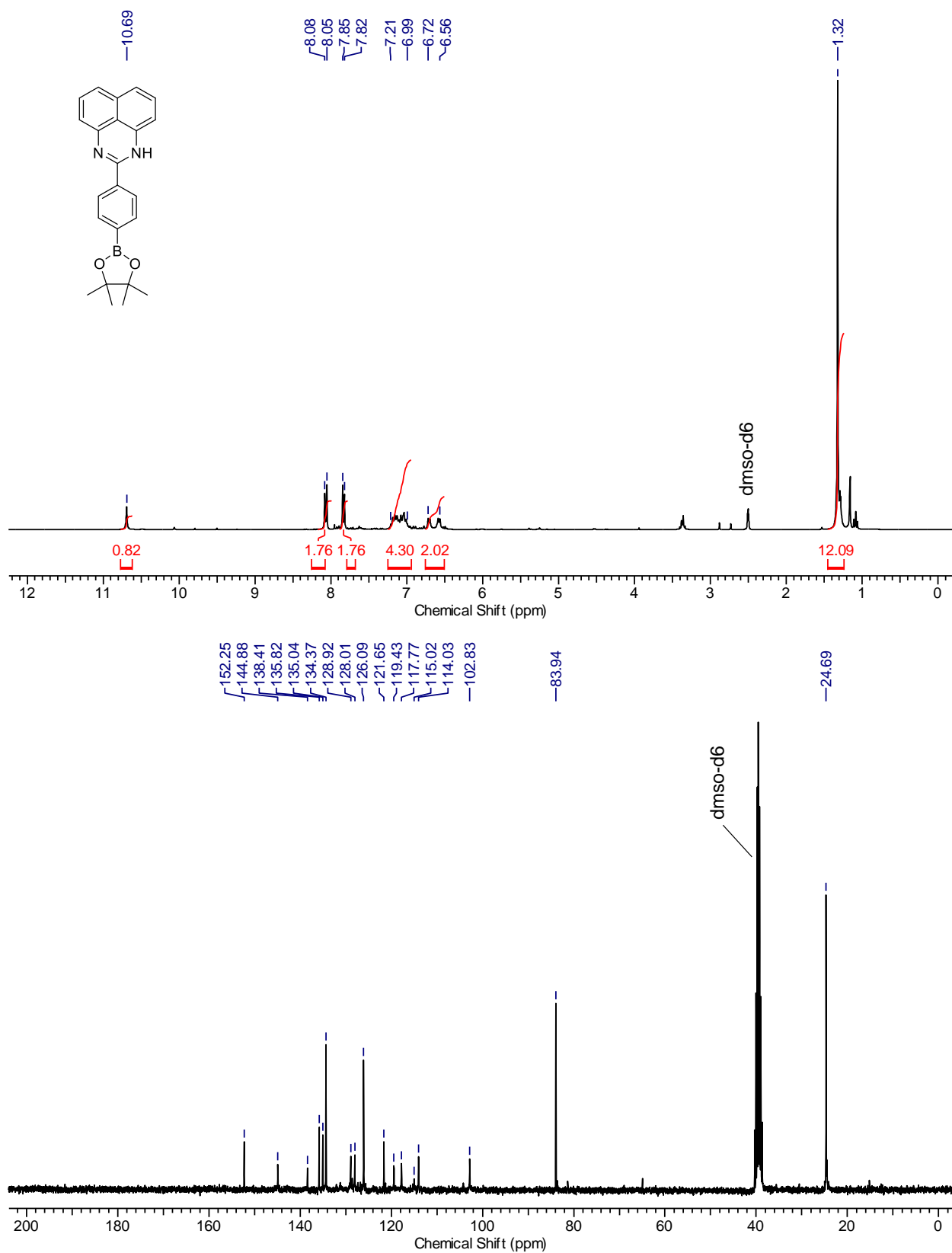


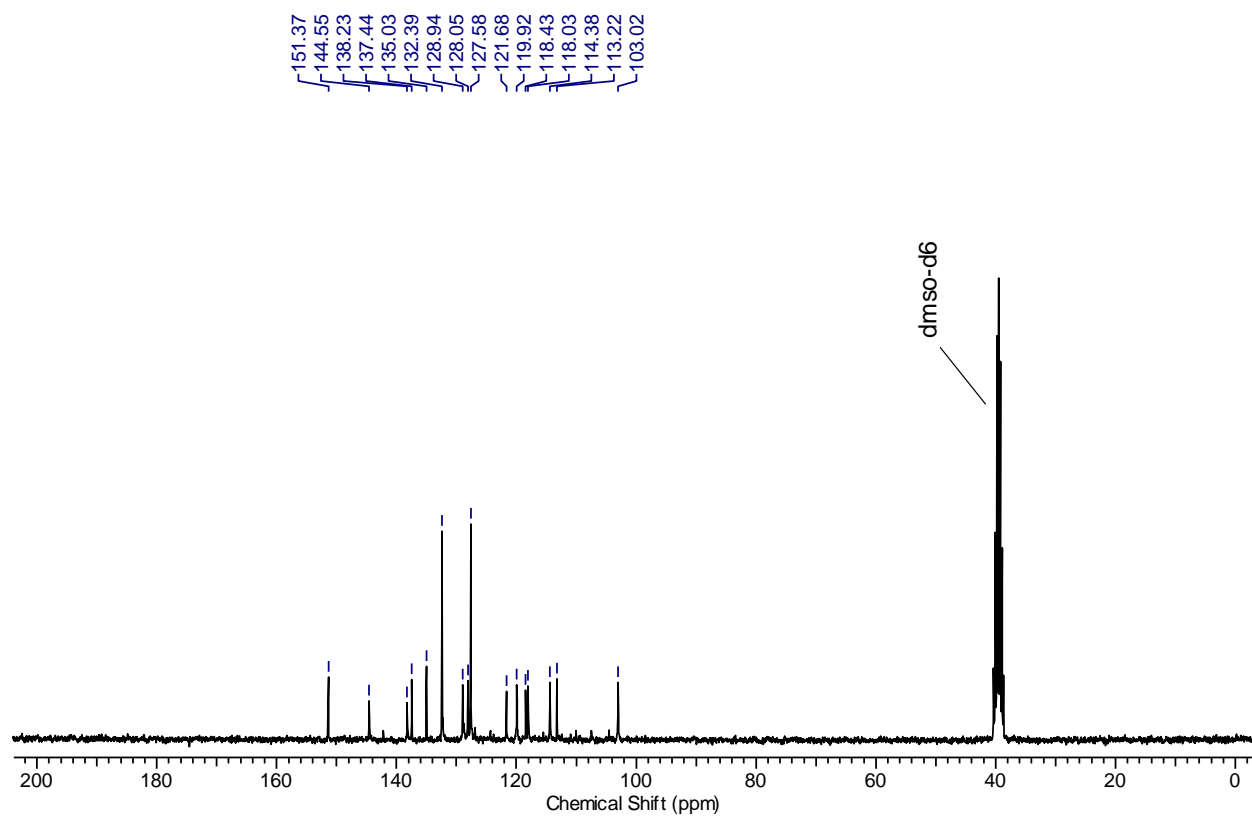
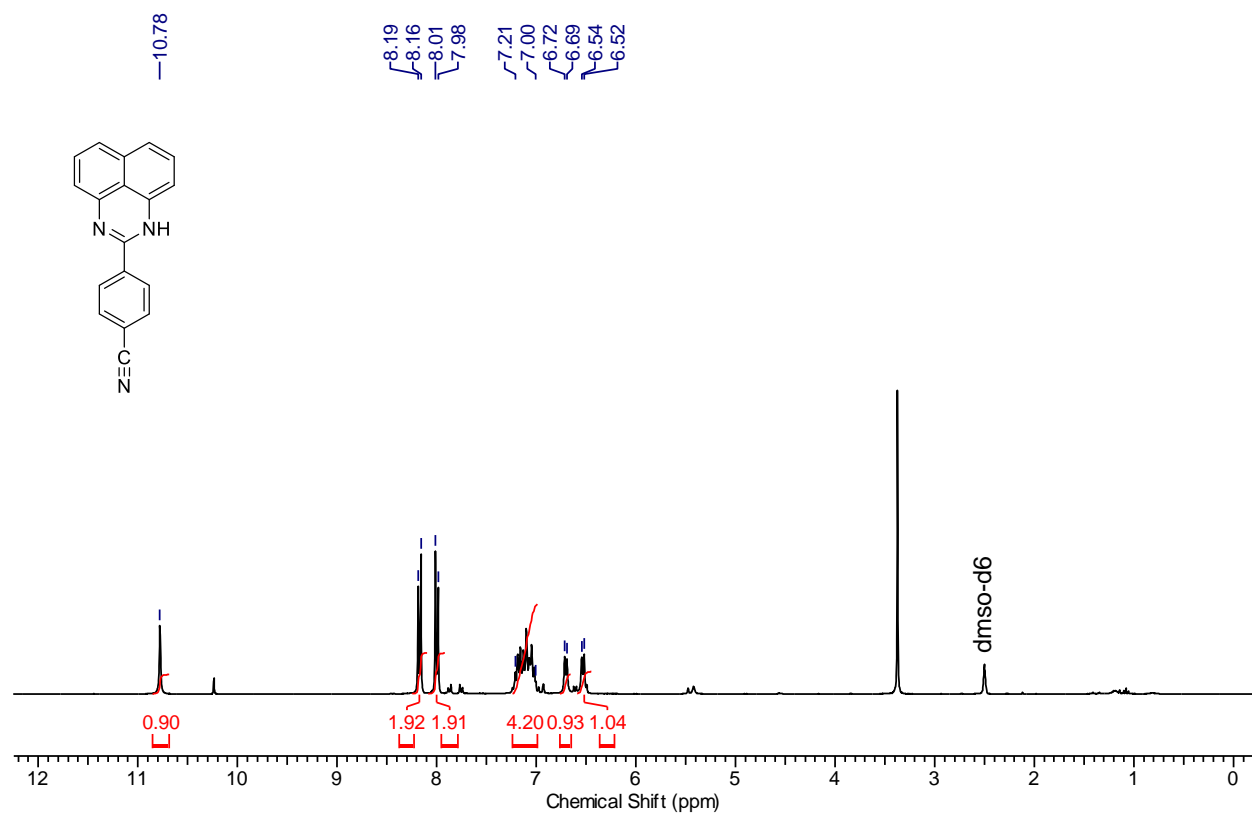


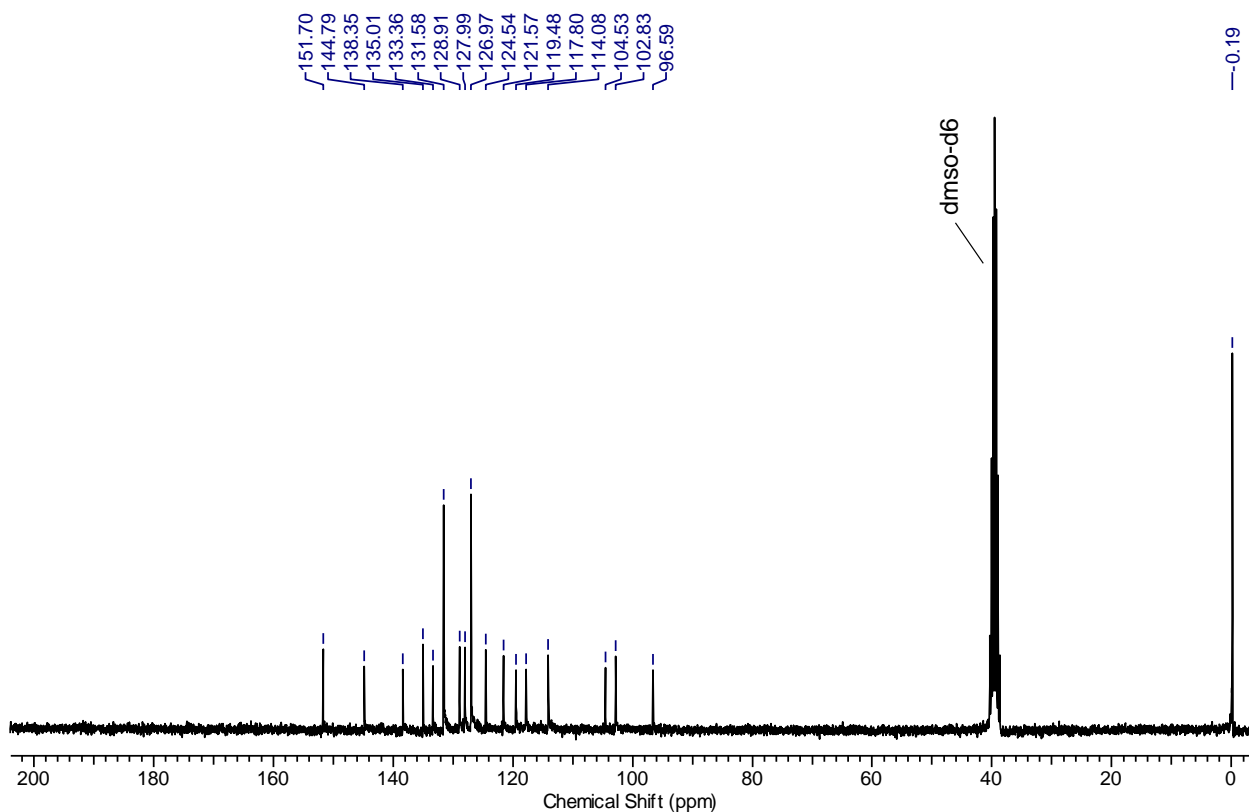
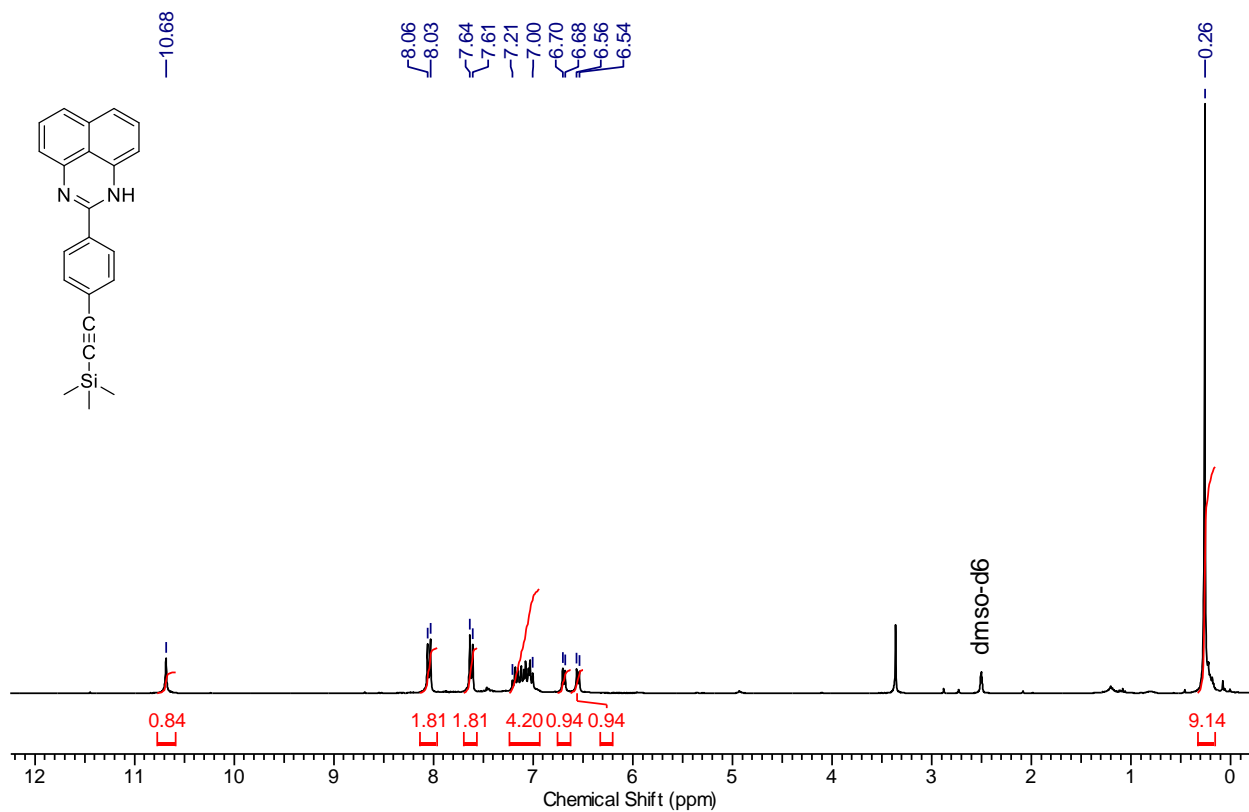


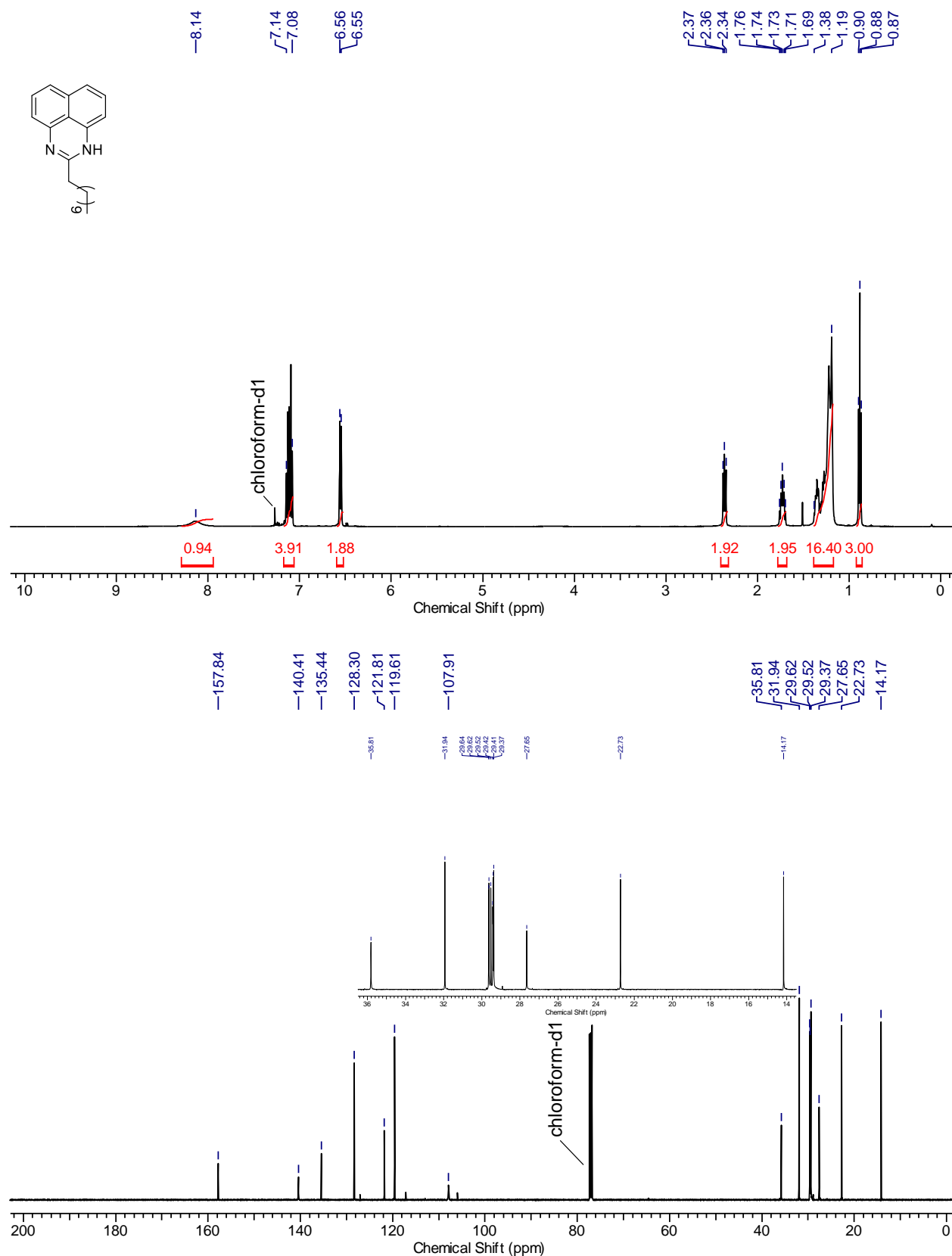


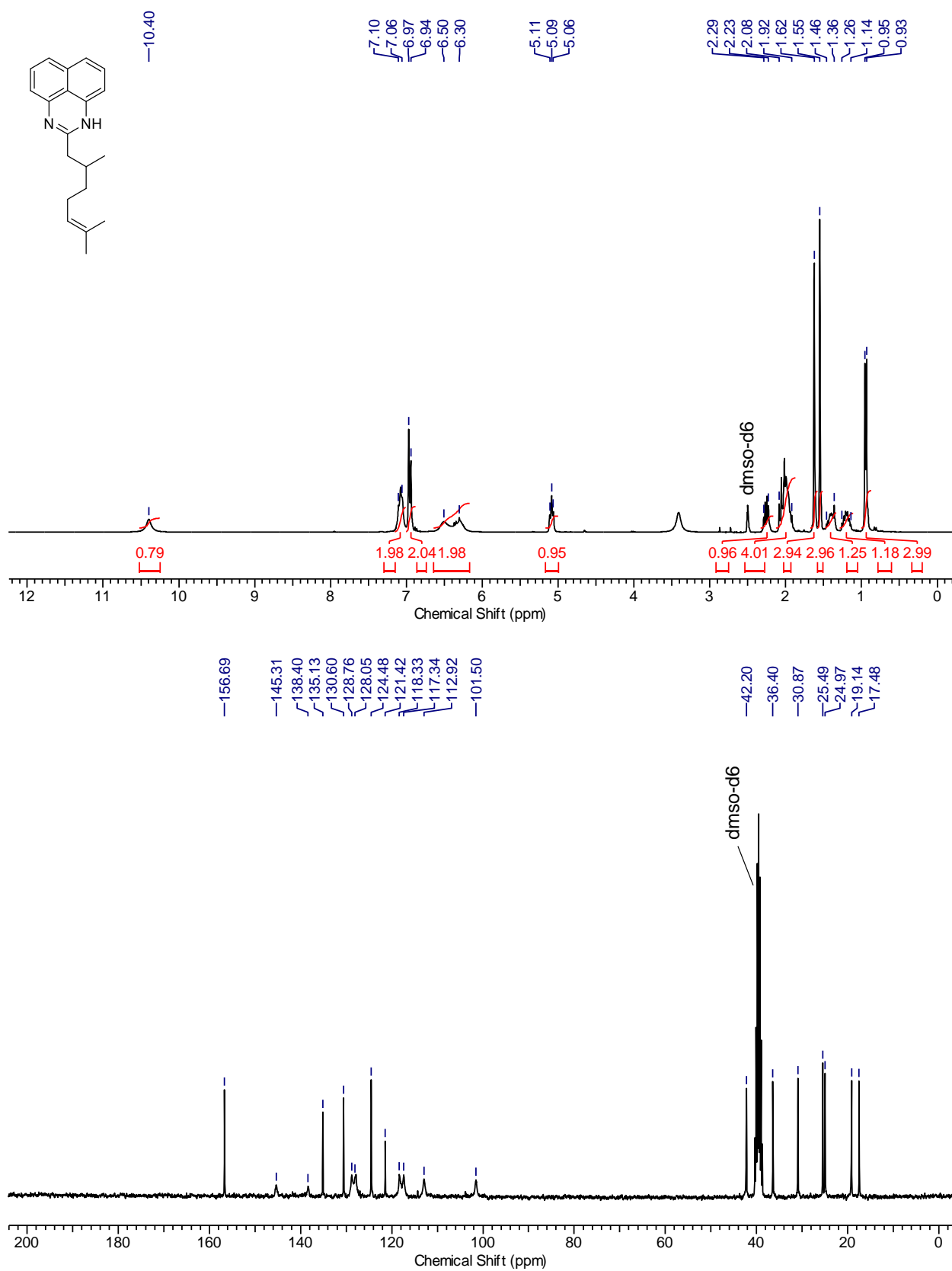


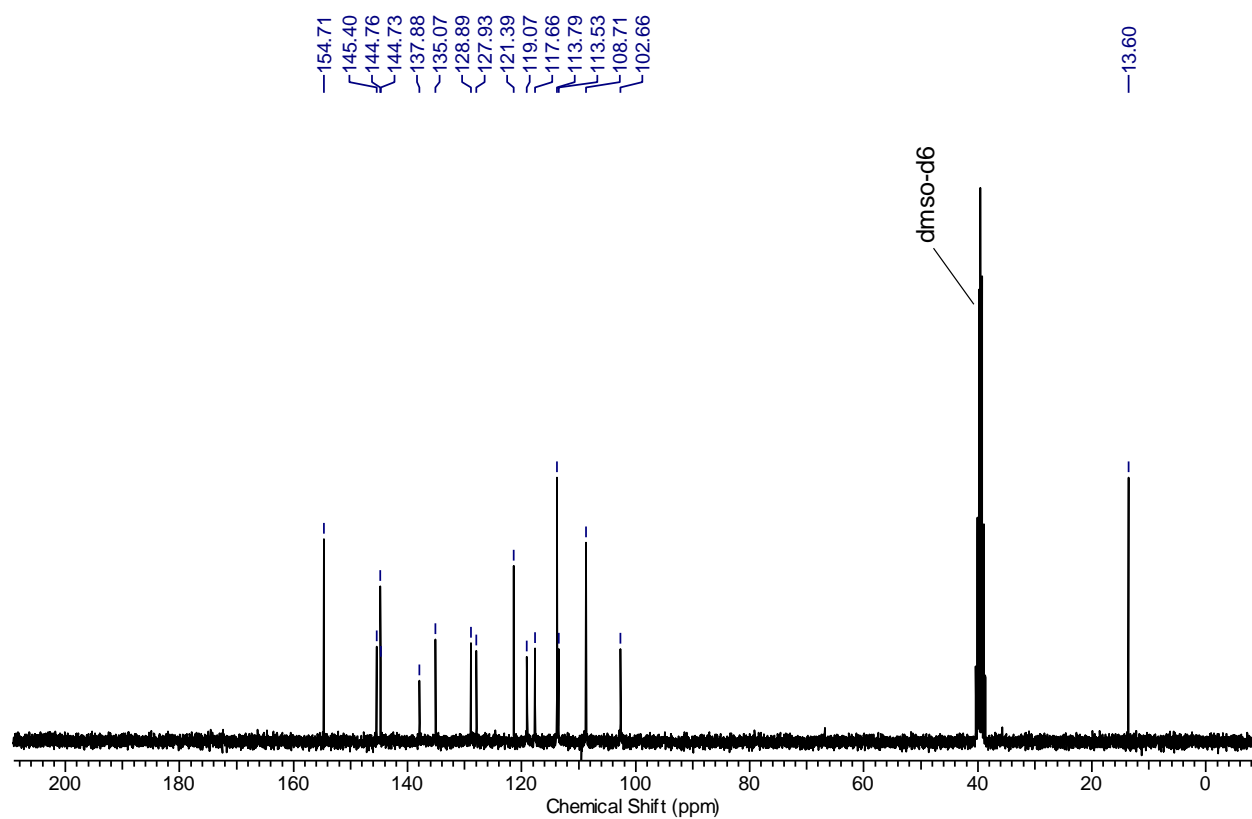
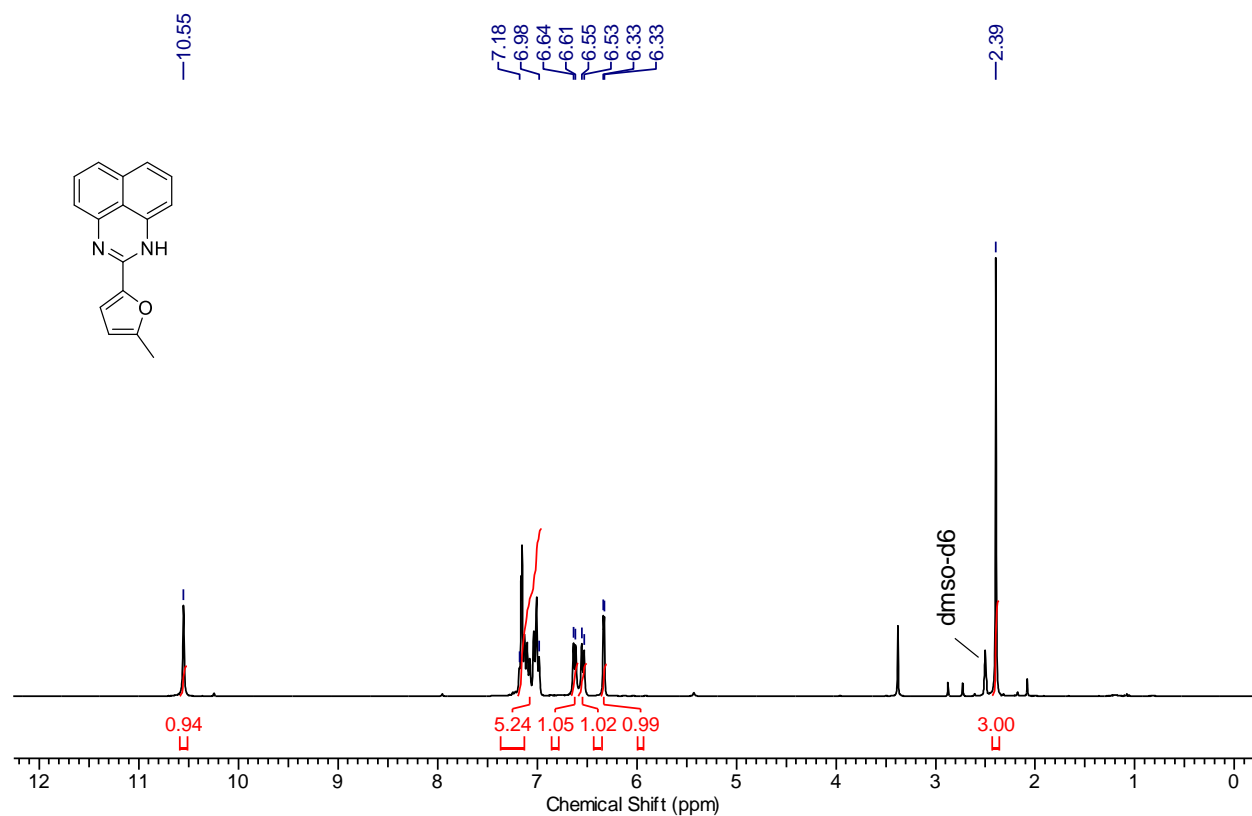


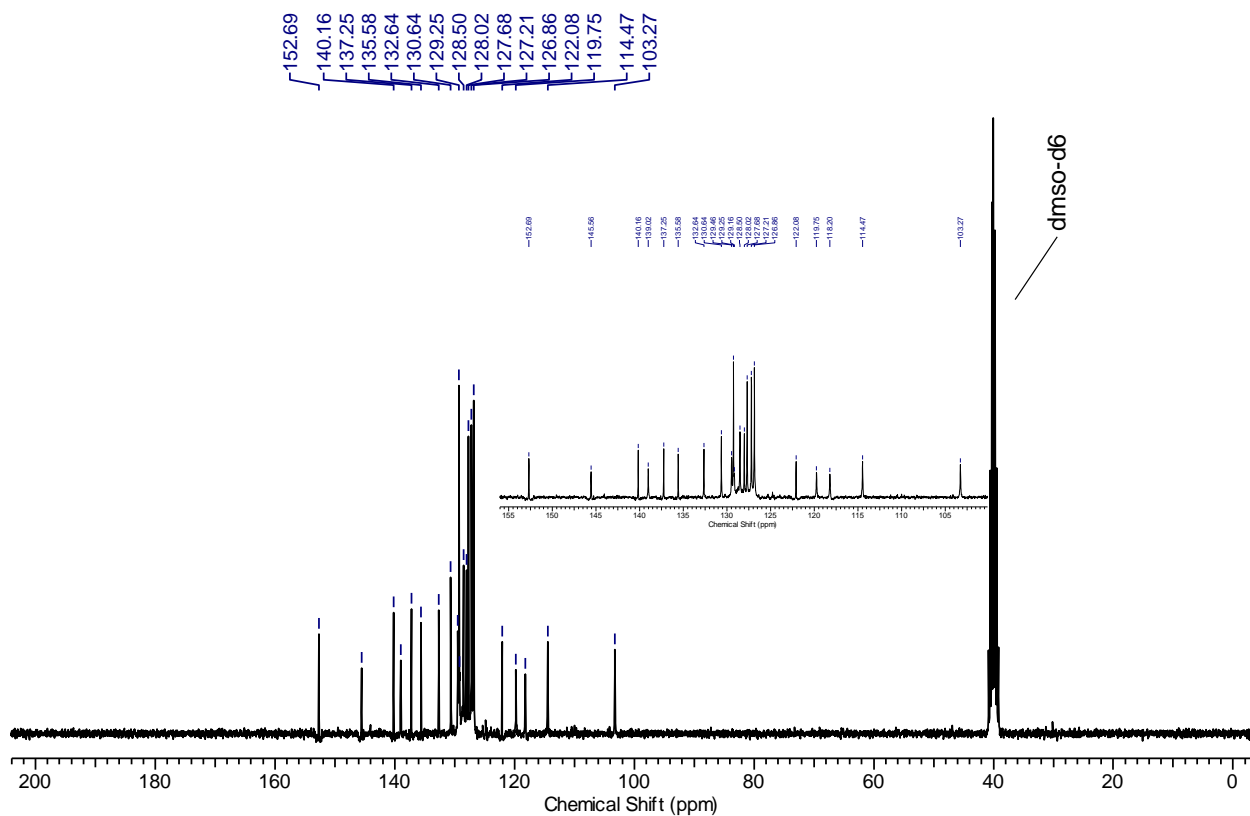
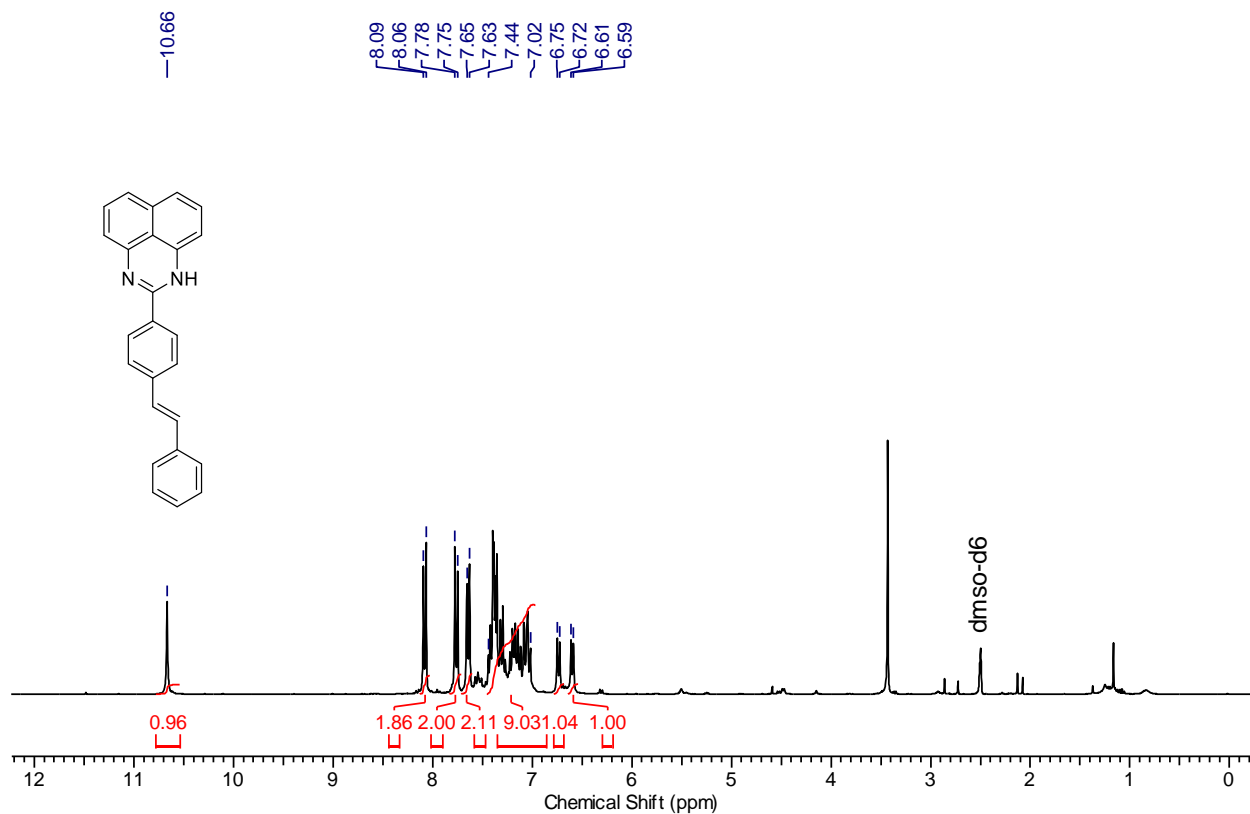












Supplementary references

- [1] B. Morandi, B. Mariampillai, E. M. Carreira, *Angew. Chem. Int. Ed.* **2011**, *50*, 1101–1104.

7 General and selective deoxygenation by hydrogen employing a reusable earth-abundant metal catalyst

T. Schwob^[1], P. Kunnas^[2], N. de Jonge^[2,3], C. Papp^[4], H.-P. Steinrück^[4], R. Kempe^[1,*]

- [1] Inorganic Chemistry II – Catalyst Design, University of Bayreuth, 95440 Bayreuth, Germany.
- [2] INM – Leibniz Institute for New Materials, Campus D2 2, 66123 Saarbrücken, Germany.
- [3] Department of Physics, Saarland University, Campus A5 1, 66123 Saarbrücken, Germany.
- [4] Physical Chemistry II, Department Chemistry and Pharmacy, 91058 Erlangen, Germany.

*Corresponding author. E-mail: kempe@uni-bayreuth.de

Submitted to Sciences Advances and out for review.

Now published as:

T. Schwob, P. Kunnas, N. de Jonge, C. Papp, H.-P. Steinrück, *Sci. Adv.* **2019**, *5*, eaav3680.

Abstract: Chemoselective deoxygenation by hydrogen is particularly challenging but crucial for an efficient late-stage modification of functionality-laden fine chemicals, natural products or pharmaceuticals and the economic upgrading of biomass-derived molecules into fuels and chemicals. We report here on a reusable earth-abundant metal catalyst that permits highly chemoselective deoxygenation employing inexpensive hydrogen gas. Primary, secondary and tertiary alcohols, as well as alkyl and aryl aldehydes and ketones can be selectively deoxygenated, even when part of complex natural products, pharmaceuticals or biomass-derived platform molecules. We can tolerate many functional groups including hydrogenation-sensitive examples. Our catalyst is efficient, easy to handle and conveniently synthesized from a specific bimetallic coordination compound and commercially available charcoal. Selective, sustainable and cost-efficient deoxygenation under industrially viable conditions seems feasible.

One Sentence Summary: A nanostructured Co-Ce catalyst permits the hydrodeoxygenation of alcohols, aldehydes and ketones tolerating numerous functional groups.

7.1 Introduction

The use of earth-abundant metals in key technologies classically associated with noble metals, such as catalysis, helps to conserve rare elements and becomes especially attractive if novel selectivity patterns are observed. Significant progress has been made recently concerning the use of homogeneous earth-abundant metal catalysts(1-10) for reactions customarily mediated by noble metals. However, the highly desirable employment of reusable nanostructured catalysts of such metals, broadly applicable in organic synthesis and essential for the production of fine and agrochemicals and pharmaceuticals, has been rarely shown.(11-14) One of the haunting problems of organic synthesis is the mild and selective defunctionalization of C-O bonds in the presence of other functional groups, such as in high-value fine chemicals, pharmaceuticals or natural products.(15) Such a selective and pinpoint deoxygenation method would allow the fine-tuning of highly functionalized molecules at a late stage of their synthesis. In addition, many biomass-derived platform molecules are highly oxidized and the removal of surplus oxygen is key to their usability as fuels and bulk chemicals.(16-17) C-O bond cleavage using inexpensive hydrogen gas (hydrodeoxygenation) is challenging, but highly attractive for economic reasons. The hydrodeoxygenations of alcohols and carbonyl compounds in the presence of functional groups have been realized by means of a homogeneous noble metal catalyst.(18) This impressive progress has been accomplished using a Ru complex and the tolerance of phenolic hydroxyl groups, aryl and alkylethers, olefins, fluorides, chlorides, a nitroarene and an amide was observed. In addition, selective hydrodeoxygenation of diols has been demonstrated. A homogeneous or heterogeneous earth-abundant metal catalyst for the highly chemoselective hydrodeoxygenation of alcohols and carbonyl compounds has not been disclosed yet. We report here on a novel nanostructured earth-abundant metal catalyst for the deoxygenation of various classes of chemical compounds using inexpensive hydrogen gas as the reducing agent (hydrodeoxygenation). The process is highly chemoselective and functional groups, easily reduced by hydrogen in the presence of conventional catalysts, remain unaffected. Halides (including reactive iodides), ethers (including thio- and benzylethers), an olefin, esters (including boronic esters), amides, carboxylic acids, phenols and N-heterocycles survive the catalytic hydrodeoxygenation process. Furthermore, the selective removal of an OH group of a secondary or a tertiary alcohol in the presence of a primary alcohol was demonstrated. The scope of possible substrates is large regarding their nature and oxidation state. Aldehydes, benzylic and purely aliphatic, dialkyl, aryl-alkyl and diaryl ketones, as well as primary, secondary and tertiary alcohols including purely aliphatic ones, complex natural

products, pharmaceuticals and biomass-derived platform molecules have been hydrodeoxygenated selectively. Our novel catalyst is efficient, easy to handle and its synthesis is simple and straightforward, starting from a specific Co-Ce bimetallic complex and commercially available charcoal. Cerium is the most abundant element of the lanthanoids. It is more abundant in the earth's crust than the 3d metal cobalt.⁽¹⁹⁾ The catalyst proved stable over at least five consecutive runs without any remarkable decrease in product formation. Up-scaling proceeds smoothly and in high yields, for example, small scale: 86 %, large scale: 92 %. We have recently introduced a variety of homogeneous earth-abundant catalysts⁽²⁰⁻²⁶⁾ and reusable nanostructured catalysts for hydrogen storage⁽²⁷⁾ and novel organic reactions⁽²⁸⁾, including an earth-abundant metal catalyst.⁽²⁹⁾

7.2 Results and Discussion

Our catalyst (Co-Ce/C) was synthesized in a convenient and practical two-step procedure. At first, commercially available activated charcoal (Norit CA1, Cabot Corporation) was impregnated with the bimetallic complex **I**, followed by pyrolysis under nitrogen atmosphere at 700 °C and reduction (N₂/H₂ 90/10) at 550 °C (Fig. 1A; Supplementary Material (SM) for detailed information). Scanning electron microscopy (SEM) and energy-dispersive X-ray spectroscopy (EDX) indicates a homogeneous distribution of both metal species over the entire catalyst sample analyzed (Fig. S1). High-angle annular dark-field scanning transmission electron microscopy (HAADF-STEM) provides evidence for the presence of two types of nanosized species more or less homogeneously embedded in the matrix: nanoparticles with mean diameter of 6.8 nm and smaller (~1 nm) structures (Fig. 1B). HAADF-STEM in combination with EDX-mapping reveals that the 6.8 nm-diameter nanoparticles consist of Co, while the element Ce is distributed in the matrix (Fig. 1 C, D; Fig. S2). HAADF-STEM combined with electron energy loss spectroscopy (EELS) mapping indicates the presence of ~1 nm-sized cerium-rich structures in the vicinity of a Co nanoparticle (Fig. S3). X-ray photoelectron spectroscopy (XPS) analysis of the Co 2p_{3/2} region confirms the presence of metallic cobalt species (~20 %) and oxides/hydroxides (~80 %). Cerium is present as an oxide of predominantly Ce³⁺ (~90 %) and small amounts of Ce⁴⁺ (~10 %) (Fig. 1E, Fig. S4), concluded from an analysis of the Ce 3d_{5/2} region. The catalyst features a specific surface area (Brunauer-Emmet-Teller) of 740 m²/g and a 40 % fraction of mesopores, which is in good accordance with the key figures of the pure carbon support (Fig. S5).

Inductively coupled plasma optical emission spectrometry (ICP-OES) revealed 3.6 wt% Co and 7.3 wt% Ce in the as-synthesized catalyst sample.

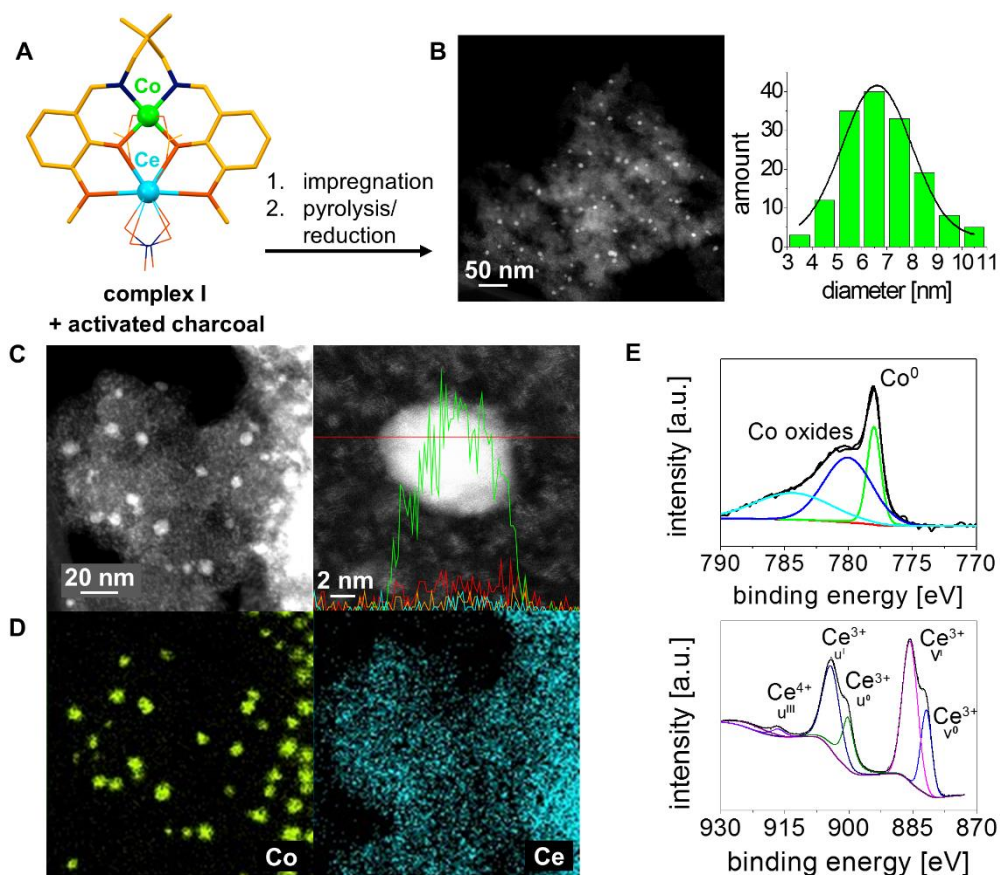


Fig. 1. Catalyst synthesis and characterization. A) Synthesis of the novel catalyst by wet impregnation of commercially available charcoal with the bimetallic precursor complex I, followed by pyrolysis and reduction. B) HAADF-STEM of the as-synthesized catalyst verifies the presence of homogeneously distributed metal nanoparticles with a mean diameter of 6.8 nm. C) Detailed HAADF-STEM image in combination with EDX mapping. D) EDX-based element mapping (Co: green; Ce: blue; O: red; P: orange) indicates that Co forms the nanoparticles and Ce is distributed over the whole carbon support. E) XPS analysis confirms the presence of metallic cobalt (~20 %) and cobalt oxide/hydroxide species (~80 %). Ce is mainly present as Ce^{3+} (~90 %) besides minor amounts of Ce^{4+} (~10 %).

The hydrodeoxygenation of acetophenone was chosen for optimization of the new catalyst system. A pyrolysis temperature of 700 °C during catalyst synthesis was found to be optimal. The desired product ethylbenzene was obtained in 81 % yield with a catalyst made by pyrolysis at this temperature. The use of catalysts produced by pyrolysis at 600 or 800 °C led to a distinct drop of product yields under the same reaction conditions (Table S1). Methylcyclohexane emerged as the most suitable reaction solvent from a comparison of eight different solvents (Table S2). We compared different supports and metal sources under identical reaction conditions to demonstrate the superiority of the new bimetallic Co-Ce/C catalyst. Only the

combination of TiO₂ with the bimetallic complex **I** gave moderate yields of the desired product, while poor yields were achieved using CeO₂ and Al₂O₃ as a support (Table 1, entries 1-4). When complex **I** was replaced by the common metal salts Co(NO₃)₂ and Ce(NO₃)₃, no ethylbenzene formation could be detected (Table 1, entry 6). To ensure the necessity of the bimetallic complex **I**, the monometallic Co complex **II** (essentially complex **I** without Ce) and the monometallic Ce complex **III** (essentially complex **I** without Co) were used for the catalyst synthesis (Fig. S6). Neither the use of complex **II** or **III** nor a combination of both led to comparable hydrodeoxygenation activities (Table 1, entries 7-9). In summary, the hydrodeoxygenation of acetophenone proceeded smoothly applying a catalyst system prepared from the bimetallic complex **I** and activated charcoal by pyrolysis at 700 °C (3.6 wt% Co, 7.3 wt% Ce). A further optimization of the reaction conditions led to the following parameters: 0.5 mmol substrate, 15 mg catalyst (1.8 mol% Co, 1.6 mol% Ce), 3 mL methylcyclohexane, 4.0 MPa H₂, 20 h. The reaction temperature was slightly increased to 110 °C in comparison to the temperature at which the optimization of the reaction conditions was accomplished (100 °C) to finally ensure maximum yields of the desired product (Table 1, entry 5).

Table 1. Catalyst screening.

Reaction scheme: Acetophenone reacts with a catalyst and 2 or 1 H₂ (losing H₂O) to produce ethylbenzene (a) and 1-phenylethanol (b).

Entry	Metal source	Support	Yield [%]	
			a	b
1	Bimetallic complex I	TiO ₂	62	27
2	Bimetallic complex I	CeO ₂	15	69
3	Bimetallic complex I	γ-Al ₂ O ₃	6	21
4	Bimetallic complex I	Activated charcoal	81	16
5 [§]	Bimetallic complex I	Activated charcoal	98	-
6	Co(NO ₃) ₂ + Ce(NO ₃) ₃	Activated charcoal	-	18
7 [‡]	Monometallic complex II	Activated charcoal	-	10
8 [§]	Monometallic complex III	Activated charcoal	-	-
9	Monometallic complex II + III	Activated charcoal	32	51

Reaction conditions: 0.5 mmol substrate, 15 mg catalyst (1.8 mol% Co, 1.6 mol% Ce), 100 °C, 4.0 MPa H₂, 3 mL methylcyclohexane, 20 h; [§]110 °C reaction temperature; [‡]1.8 mol% Co without Ce; [§]1.6 mol% Ce without Co; Yields were determined by GC and GC-MS using *n*-dodecane as an internal standard.

Having optimized the reaction conditions of our novel catalytic hydrodeoxygenation, we fathomed its substrate scope. The product yields of test reactions were determined via GC and GC-MS, and products were isolated for selected examples. The isolated yields are given additionally in parentheses in Figures 2 and 3.

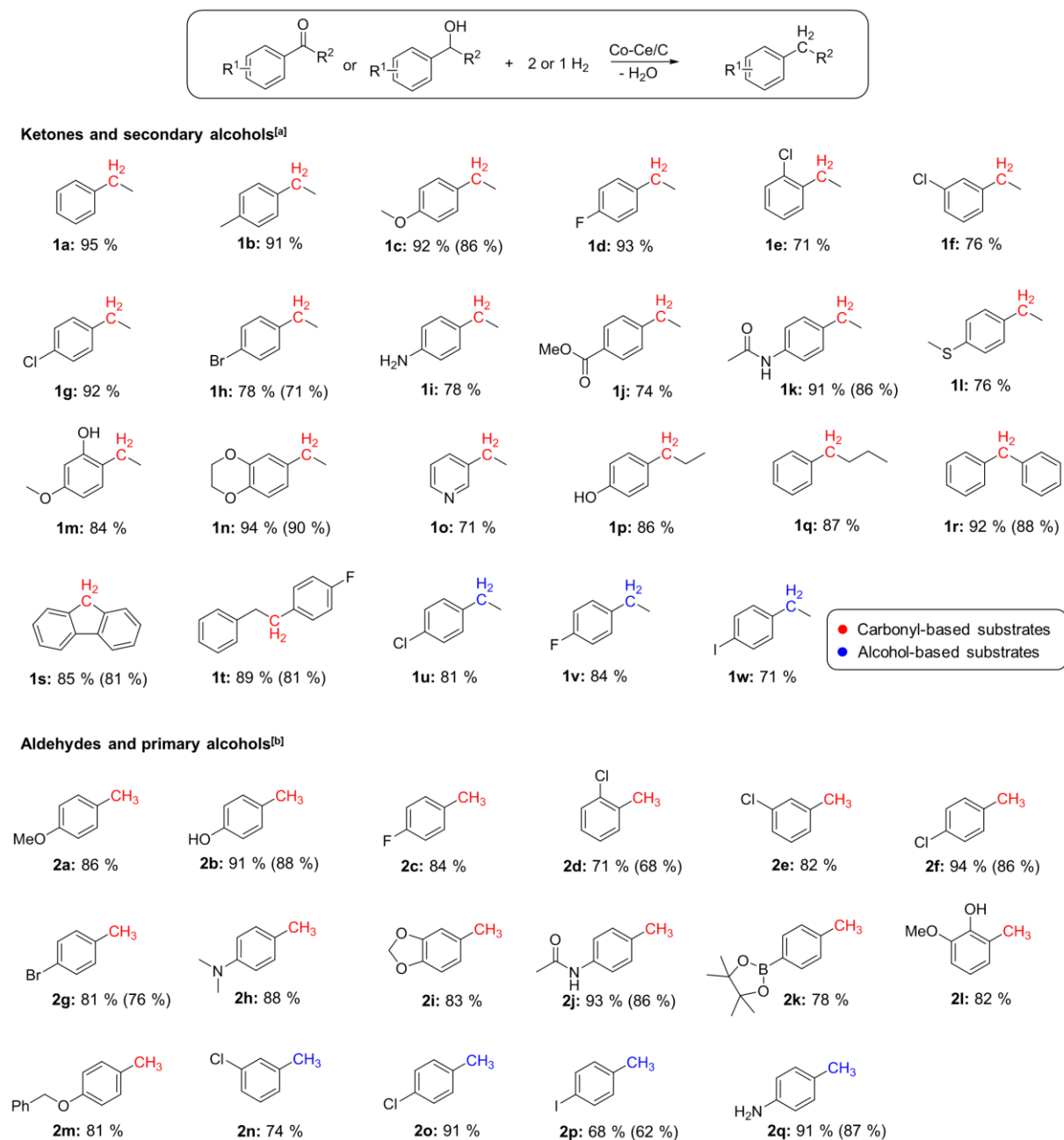


Fig. 2. Selective hydrodeoxygenation of alcohols and carbonyl compounds I. [a] Reaction conditions: 0.5 mmol substrate, 15 or 35 mg catalyst (1.8 mol% Co and 1.6 mol% Ce or 4.2 mol% Co and 3.7 mol% Ce, respectively), 110-130 °C, 5.0 MPa H₂, 3 mL methylcyclohexane, 20 h, (10 mg Amberlyst® 15 for halogenated substrates). [b] Reaction conditions: 0.5 mmol substrate, 50 mg catalyst (6.1 mol% Co, 5.2 mol% Ce), 130 °C, 6.0 MPa H₂, 3 mL methylcyclohexane, 20 h, (5 mol% Zn(OTf)₂ for halogenated substrates). Yields were determined by GC and GC-MS using *n*-dodecane as an internal standard. Isolated yields in parentheses.

Firstly, we investigated the hydrodeoxygenation of aryl-alkyl ketones and related secondary alcohols (Fig. 2, top). The introduction of methyl and electron-rich methoxy substituents had no significant influence on the conversion and the corresponding products were obtained in yields of around 90 % (Fig. 2, products **1b**, **c**). To our delight, the hydrodeoxygenation of halogenated substrates, which is challenging since dehalogenation can take place, proceeded well when 10 mg Amberlyst[®] 15 were applied as an additive (Table S3). 4-Fluoro- or 4-chloroacetophenone were smoothly converted, no dehalogenation was observed and nearly quantitative yields were obtained (Fig. 2, products **1d**, **g**). Product yields of around 70 % were observed for the sterically more demanding 2-chloroacetophenone and the corresponding 3-chloro-substituted derivative (Fig. 2, products **1e**, **f**). Aryl bromide withstood the deoxygenation well as can be seen from the formation of **1h** in nearly 80 % yield. Functional groups such as amines, esters, amides, thioethers and ethers, N-heterocycles or phenols, all tolerated the reaction conditions (Fig. 2, products **1i-p**). The performance of the new catalyst was further evaluated on diaryl ketones. Benzophenone, for instance, was deoxygenated to afford diphenylmethane in 92 % yield (Fig. 2, product **1r**). Fluorinated and chlorinated 1-phenylethanol derivatives could be deoxygenated as smoothly as the corresponding ketones. The desired products were obtained in yields higher than 80 % (Fig. 2, products **1u**, **v**). It is noteworthy that even the delicate iodo substituent of 1-(4-iodophenyl)ethanol resisted the deoxygenation conditions (Fig. 2, product **1w**). The transformation of benzylic aldehydes and related alcohols required slightly harsher reaction conditions and catalyst loadings for high conversions (130 °C, 6.0 MPa, 6.1 mol% Co, 5.2 mol% Ce). But even then, the hydrodeoxygenation of halogenated substrates proceeded well when 5 mol% Zn(OTf)₂ was added (Table S3). Substrates bearing electron-withdrawing or -donating moieties, such as halides, amides, heterocycles and amino, hydroxy- and methoxy functionalities were well tolerated (Fig. 2, products **2a-j**, **l**, **n-q**). 4-Benzyloxybenzaldehyde was deoxygenated selectively to give benzyl-*p*-tolyl ether **2m** in excellent yield without a significant amount of hydrogenolytic ether cleavage (Fig. 2). The stability of boronic esters, which are common starting materials for cross coupling reactions, is of special importance (Fig. 2, product **2k**). Next, we examined the transformation of aliphatic alcohols and carbonyl compounds, tertiary alcohols, diols, biomass-derived substrates and more complex organic molecules to further evaluate the scope of possible substrates (Fig. 3). Triphenylmethanol was easily reduced to triphenylmethane applying only 110 °C, 4.0 MPa hydrogen pressure and a catalyst loading of 1.8 mol% Co and 1.6 mol% Ce (Fig. 3, product **3f**). Hydrogenolysis of purely aliphatic compounds required typically harsher reaction conditions and higher catalyst loadings.

Gratifyingly, a variety of cyclic and linear substrates were deoxygenated in up to 91% yield (Fig. 3, products **3a-e**).

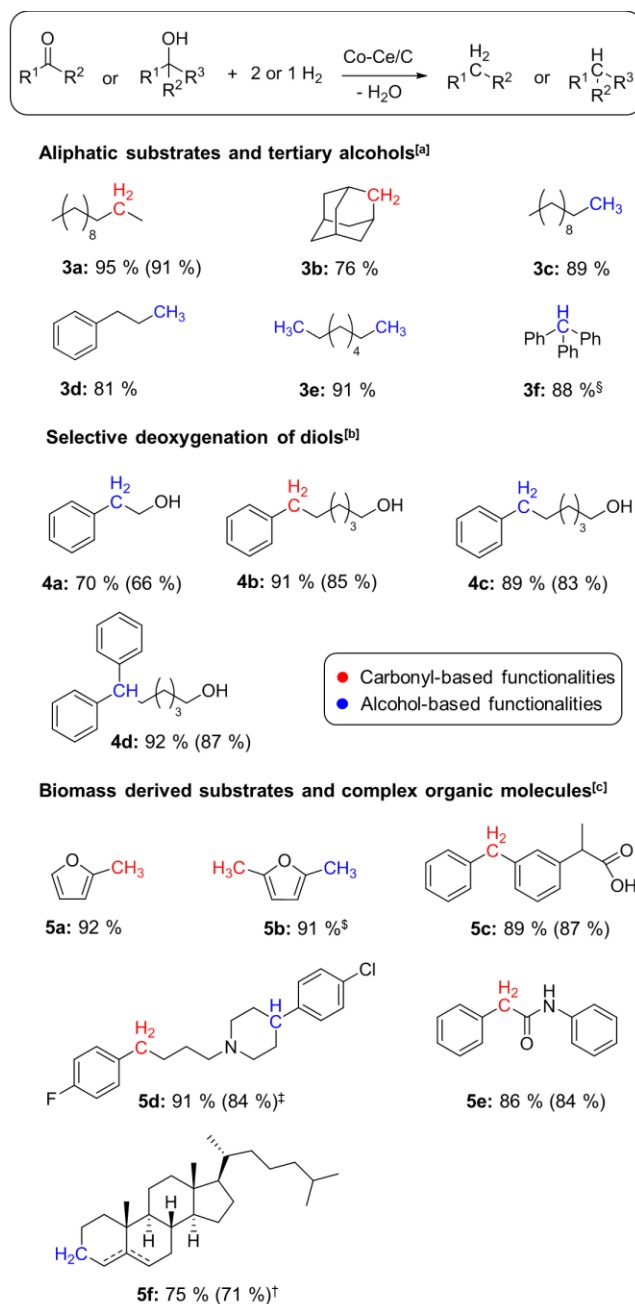


Fig. 3. Selective hydrodeoxygenation of alcohols and carbonyl compounds II. [a] Reaction conditions: 1.0 mmol substrate, 100 mg catalyst (6.1 mol% Co, 5.2 mol% Ce), 160 °C, 6.0 MPa H₂, 6 mL methylcyclohexane, 20 mg Amberlyst® 15, 20 h; §1 mmol substrate, 30 mg catalyst (1.8 mol% Co, 1.6 mol% Ce), 110 °C, 4.0 MPa H₂, 6 mL methylcyclohexane, 20 h, no additive. [b] Reaction conditions: 1.0 mmol substrate, 70 mg catalyst (4.2 mol% Co, 3.7 mol% Ce), 130 °C, 5.0 MPa H₂, 6 mL ethanol, 20 h. [c] Reaction conditions: 1.0 mmol substrate, 100 mg catalyst (6.1 mol% Co, 5.2 mol% Ce), 160 °C, 6.0 MPa H₂, 6 mL methylcyclohexane, 20 h; §diglyme was used as the solvent; ‡20 mg Amberlyst® 15 as additive; †5 mol% Zn(OTf)₂ as additive. Yields were determined by GC and GC-MS using *n*-dodecane as an internal standard. Isolated yields are given in parentheses.

We expected the selective removal of only one OH group in diols due to the different reaction conditions needed to deoxygenate primary, secondary and tertiary alcohols. A few diols were selectively deoxygenated in up to 92 % isolated yield (Fig. 3, products **4a,c,d**). The preferred removal of a secondary or tertiary alcohol in the presence of a primary alcohol was observed. This selectivity is inverse to that observed in a *Wolff-Kishner*-based catalytic deoxygenation approach.⁽³⁰⁾ Interestingly, even a ketone could be deoxygenated in the presence of a primary alcohol (Fig. 3, product **4b**). The transformation of biomass-derived furfural and hydroxymethylfurfural also proceeded well (Fig. 3, products **5a, b**).^(31,32) The new hydrodeoxygenation protocol may also be applied to more complex organic molecules (Fig. 3, bottom). Ketoprofen and haloperidol were deoxygenated to the respective products in up to 87 % isolated yield (Fig. 3, products **5c, d**). The reduction of a sterically demanding alpha-ketoamide was accomplished without any side product formation (Fig. 3, **5e**). In the case of cholesterol, surprisingly, we observed a chemoselectivity for carbonyl reduction over double bond hydrogenation and a mixture of olefin isomerization products was obtained in 71% isolated yield (Fig. 3, **5f**). The hydrodeoxygenation of acetophenone was chosen to demonstrate the recyclability of the catalyst, which could be reused in five consecutive runs without any noticeable reduction of catalytic activity (Fig. S7). An up-scaling of the reaction had no significant influence on the catalytic results. An amount of 10 mmol 4-acetamidoacetophenone were deoxygenated smoothly to afford the desired product in virtually quantitative yield (Table S4). Cost-efficient and selective late-stage deoxygenation of fine chemicals, natural products and pharmaceuticals under industrially viable and scalable conditions seems feasible now. The protocol is especially sustainable since a reusable earth-abundant metal catalyst is employed. Our work may inspire others to develop reusable and nano-structured earth-abundant metal catalysts for complex organic transformations in which tolerance of functional groups has so far been a key challenge.⁽³³⁾

Acknowledgments: We thank E. Arzt for his support through INM. In addition, we thank A. Gollwitzer and T. Dietel for the X-ray characterization of complex I. **Funding:** We acknowledge financial support from the Deutsche Forschungsgemeinschaft, KE 756/21-2. **Authors contributions:** T. S. carried out the synthesis of the catalyst, the catalyst characterization and the catalytic reactions. P. K. and N. d. J. performed the HAADF-STEM, EDX and EELS analysis. C. P. and H.-P. S. accomplished the XPS analysis. T. S. and R. K. designed the experiments and co-wrote the manuscript. **Competing interests:** Authors declare

no competing interests. **Data and materials availability:** Crystallographic data CCDC 1865045 contains the supplementary crystallographic data for this paper and can be obtained free of charge from *The Cambridge Crystallographic Data Centre*. All other data is included in the manuscript and supporting information or available from the authors upon reasonable request.

7.3 Supplementary Materials

Materials and Methods

Figures S1-S7

Tables S1-S4

NMR Spectra

Supplementary references

7.4 References

- 1 A. Boddien et al., Efficient dehydrogenation of formic acid using an iron catalyst. *Science* **333**, 1733–1736 (2011).
- 2 A. M. Tondreau et al., Iron catalysts for selective anti-Markovnikov alkene hydrosilylation using tertiary silanes. *Science* **335**, 567–570 (2012).
- 3 W. Zuo, A. J. Lough, Y. F. Li, R. H. Morris, Amine(imine)diphosphine iron catalysts for asymmetric transfer hydrogenation of ketones and imines. *Science* **342**, 1080–1083 (2013).
- 4 M. R. Friedfeld et al., Cobalt precursors for high-throughput discovery of base metal asymmetric alkene hydrogenation catalysts. *Science* **342**, 1076–1080 (2013).
- 5 J. M. Hoyt, V. A. Schmidt, A. M. Tondreau, P. J. Chirik, Iron-catalyzed intermolecular [2+2] cycloadditions of unactivated alkenes. *Science* **349**, 960–963 (2015).
- 6 T. J. Korstanje, J. I. van der Vlugt, C. J. Elsevier, B. de Bruin, Hydrogenation of carboxylic acids with homogeneous cobalt catalyst. *Science* **350**, 298–302 (2015).
- 7 R. P. Yu, D. Hesk, N. Rivera, I. Pelczer, P. J. Chirik, Iron-catalysed tritiation of pharmaceuticals. *Nature* **529**, 195–199 (2016).

- 8 M. R. Friedfeld, H. Zhong, R. T. Ruck, M. Shevlin, P. J. Chirik, Cobalt-catalyzed hydrogenation of enamides enabled by single-electron reduction. *Science* **360**, 888-893 (2018)
- 9 G. A. Filonenko, R. van Putten, E. J. M. Hensen, E. A. Pidko, Catalytic (de)hydrogenation promoted by non-precious metals – Co, Fe and Mn: recent advances in an emerging field. *Chem. Soc. Rev.* **47**, 1459–1483 (2018).
- 10 F. Kallmeier, R. Kempe, Manganese complexes for (de)hydrogenation catalysis: a comparison to cobalt and iron catalysts. *Angew. Chem. Int. Ed.* **57**, 46–60 (2018).
- 11 R. V. Jagadeesh et al., Nanoscale Fe₂O₃-based catalysts for selective hydrogenation of nitroarenes to anilines. *Science* **342**, 1073–1076 (2013).
- 12 F.A. Westerhaus et al., Heterogenized cobalt oxide catalysts for nitroarene reduction by pyrolysis of molecularly defined complexes. *Nat. Chem.* **5**, 537–543 (2013).
- 13 R. V. Jagadeesh et al., MOF-derived cobalt nanoparticles catalyze a general synthesis of amines. *Science* **358**, 326–332 (2017).
- 14 T. Zhang, K. Manna, W. Lin, Metal-organic frameworks stabilize solution-inaccessible cobalt catalysts for highly efficient broad-scope organic transformations. *J. Am. Chem. Soc.* **138**, 3241–3249 (2016).
- 15 J. M. Herrmann, B. König, Reductive deoxygenation of alcohols: catalytic methods beyond Barton McCombie deoxygenation. *Eur. J. Org. Chem.* **2013**, 7017-7027 (2013)
- 16 J. N. Chheda, G. W. Huber, J. A. Dumesic, Liquid-phase catalytic processing of biomass-derived oxygenated hydrocarbons to fuels and chemicals. *Angew. Chem. Int. Ed.* **46**, 7164–7183 (2007).
- 17 R. A. Sheldon, Green and sustainable manufacture of chemicals from biomass: state of the art. *Green Chem.* **16**, 950–963 (2014).
- 18 N. Kalutharage, C. S. Yi, Scope and mechanistic analysis for chemoselective hydrogenolysis of carbonyl compounds catalyzed by a cationic ruthenium hydride complex with a tunable phenol ligand. *J. Am. Chem. Soc.* **137**, 11105–11114 (2015).
- 19 U.S. Geological Fact Sheet 087-02.

- 20 S. Rösler, J. Obenauf, R. Kempe, A highly active and easily accessible cobalt catalyst for selective hydrogenation of C=O bonds. *J. Am. Chem. Soc.* **137**, 7998–8001 (2015).
- 21 S. Rösler M. Ertl, T. Irrgang, R. Kempe, Cobalt-catalyzed alkylation of aromatic amines by alcohols. *Angew. Chem. Int. Ed.* **54**, 15046–15050 (2015).
- 22 N. Deibl, R. Kempe, General and mild cobalt-catalyzed C-alkylation of unactivated amides and esters with alcohols. *J. Am. Chem. Soc.* **138**, 10786–10789 (2016).
- 23 F. Kallmeier, T. Irrgang, T. Dietel, R. Kempe, Highly active and selective manganese C=O bond hydrogenation catalysts: the importance of the multidentate ligand, the ancillary ligands, and the oxidation state. *Angew. Chem. Int. Ed.* **55**, 11806–11809 (2016).
- 24 N. Deibl, R. Kempe, Manganese-catalyzed multicomponent synthesis of pyrimidines from alcohols and amidines. *Angew. Chem. Int. Ed.* **56**, 1663–1666 (2017).
- 25 F. Kallmeier, B. Dudziec, T. Irrgang, R. Kempe, Manganese-catalyzed sustainable synthesis of pyrroles from alcohols and amino alcohols. *Angew. Chem. Int. Ed.* **56**, 7261–7265 (2017).
- 26 G. Zhang, T. Irrgang, T. Dietel, F. Kallmeier, R. Kempe, Manganese-catalyzed dehydrogenative alkylation or α -Olefination of alkyl-substituted N-heteroarenes with alcohols. *Angew. Chem. Int. Ed.* **56**, 9131–9135 (2018).
- 27 D. Forberg et al., Single-catalyst high-weight% hydrogen storage in an N-heterocycle synthesized from lignin hydrogenolysis products and ammonia. *Nat. Commun.* **7**, 13201 (2016).
- 28 D. Forberg, T. Schwob, R. Kempe, Catalytic condensation for the formation of polycyclic heteroaromatic compounds. *Nat. Commun.* **9**, 1751 (2018).
- 29 T. Schwob, R. Kempe, A reusable Co catalyst for the selective hydrogenation of functionalized nitroarenes and the direct synthesis of imines and benzimidazoles from nitroarenes and aldehydes. *Angew. Chem. Int. Ed.* **55**, 15175–15179 (2016).
- 30 X.-J. Dai, C.-J. Li, En route to a practical primary alcohol deoxygenation. *J. Am. Chem. Soc.* **138**, 5433–5440 (2016).

- 31 G. H. Wang et al., Platinum-cobalt bimetallic nanoparticles in hollow carbon nanospheres for hydrogenolysis of 5-hydroxymethylfurfural. *Nat. Mater.* **13**, 293–300 (2014).
- 32 M. J. Climent, A. Corma, S. Iborra, Conversion of biomass platform molecules into fuel additives and liquid hydrocarbon fuels. *Green. Chem.* **16**, 516–547 (2014).
- 33 D. C. Blakemore et al., Organic synthesis provides opportunities to transform drug discovery. *Nat. Chem.* **10**, 383–394 (2018).

7.5 Supplementary Materials

Materials and Methods

General considerations

Air- and moisture sensitive reactions were carried out under dry argon or nitrogen atmosphere using standard Schlenk or glove box techniques. Solvents were dried and distilled from sodium benzophenone, stored over molecular sieves (3 Å) before use or were obtained from Acros. All chemicals were purchased from commercial sources with purity over 95 % and used without further purification. Activated charcoal (Norit CA1) was purchased from Cabot Corporation and heated up to 700 °C (10 K/min, dwelling time 3 h) before use.

NMR-Spectra were collected on Varian INOVA 300 (300 MHz for ^1H , 75 MHz for ^{13}C) or Bruker Avance III HD 500 (500 MHz for ^1H , 125.7 MHz for ^{13}C) instruments at 298 K. Chemical shifts are reported in ppm relative to the residual solvent signal (CDCl_3 : 7.26 ppm (^1H), 77.16 ppm (^{13}C); $\text{DMSO-}d_6$: 2.50 ppm (^1H), 39.51 ppm (^{13}C); C_6D_6 : 7.16 ppm (^1H), 128.39 ppm (^{13}C)). Coupling constants (J) are reported in Hz (coupling patterns: s = singlet, d = doublet, t = triplet, q = quartet, quint = quintet, sxt = sextet, spt = septet, m = multiplet).

GC analyses were carried out on an Agilent 6850 GC system equipped with an Optima 17 column (30 m x 0.32 mm x 0.25 μm) or an Agilent 6890N GC system equipped with a HP-5 column (30 m x 0.32 mm x 0.25 μm). GC-MS analyses were carried out on an Agilent 7890A GC system equipped with a HP-5MS column (30 m x 0.32 mm x 0.25 μm) and a 5975C inert MSD detector (EI, 70 eV).

JEOL ARM200F equipped with EDX detector (JEOL) and an energy filter (GATAN) was used for the high-angle annular dark-field scanning transmission electron (HAADF-STEM) imaging and elemental mapping of the specimen. Data acquisition was accomplished with following parameters: HAADF-STEM collection angle 68–280 mrad, image size 1024x1024 pixels, pixel size 0.63 nm, dwell time 20 μs , probe current 80 pA. EDX-mapping image size 128x128 pixels, pixel size 1.1 nm, pixel dwell time 1 ms, 10 sweeps integrated, probe current 1000 pA. For high-resolution EDX-line scan analysis, single scan was done to avoid damaging of the carbon support. EELS spectrum image collection angle 111 mrad, electron probe convergence semi-angle 20–30 mrad, image size 42x46 pixels, pixel size 0.43 nm, pixel dwell time 100 ms, sample. In short, energy dispersion of the spectrometer was set to 0.25 eV/channel and the elemental maps were collected in the energy-loss range of 729–1240 eV. The data processing and analysis for EDX mapping was conducted with JEOL Analysis Station

v.3.8.0.34. Elemental peaks were identified, and their areas integrated in an automatic manner to produce the elemental maps presented here.

For the EELS-mapping, Gatan Digital Micrograph v2.1.1- software equipped with EELS Analysis-plugin v2.1.1 was used for the background subtraction and the production of elemental maps. In short, appropriate pre-edge area was manually chosen so that the real-time fit of the Power-law background model was fitting well the pre-edge background based on the visual inspection.

Elemental analysis was performed by standard protocols employing microwave assisted digestion (7 min at 170 °C (80 % power), 7 min at 180 °C (85 % power) and 20 min at 195 °C (90 % power)) in HCl (32 %, 4.5 ml), HNO₃ (65 %, 1.5 ml) and HF (40 %, 1 ml). The resulting solution was analyzed using a Vista-pro radical model from Varian.

The XPS (X-ray photoelectron spectroscopy) measurements were conducted in a PHI Quantera II apparatus. A monochromatic Al K α X-ray source (1486.6 eV) was used for excitation. The samples were prepared on a copper tape. The analysis was conducted along the lines of Refs. E. Beche et al., Ce 3d XPS investigation of cerium oxides and mixed cerium oxide (Ce_xTi_yO_z). *Surf. Interface Anal.* **40**, 264–267 (2008); Y. Lykhach et al., Counting electrons on supported nanoparticles. *Nat. Mater.* **15**, 284–288 (2016).

N₂ physisorption measurements were determined at -196 °C using a Nova2000e (Quantachrome) apparatus. The specific surface areas were calculated using p/p₀ values from 0.05-0.3 (BET). The pore width and average pore volume were calculated by DFT calculations [N₂ at -196.15 °C on carbon (slit/cylindrical pore model, NLDFE equilibrium model)].

Pyrolysis and reduction were carried out under nitrogen atmosphere and forming gas (90/10) in a high temperature furnace (EHA 12/450B200, Carbolite) or alternative using ChemBET *Pulsar* TPR/TPD.

Macherey Nagel silica gel 60 (40–63 μ m particle size) was used for column chromatography.

Ligand synthesis

3.08 g (20 mmol, 2 eq) *o*-vanillin were dissolved in 100 mL ethanol and 1.12 g (11 mmol, 1.1 eq) 2,2-dimethyl-1,3-propanediamine were added. The solution was heated under reflux for 1 h. After removal of the solvent under reduced pressure, recrystallization from diethylether yielded the product as a yellow crystalline powder (ligand I, 3.07 g, 83 %).

Complex synthesis

The bimetallic complex I was synthesized according to a modified literature procedure.⁽¹⁾ 1.71 g (4.62 mmol, 1 eq) ligand I were dissolved in 100 ml methanol at 50 °C and 1.15 g (4.62 mmol, 1 eq) cobalt(II) acetate tetrahydrate were added. The dark green solution was stirred for 2 h at 50 °C. Afterwards, the solvent was removed and the resulting solid was dissolved in 100 ml acetonitrile followed by the addition of 2.01 g (4.62 mmol, 1 eq) cerium(III) nitrate hexahydrate. The solution was stirred for 20 h at room temperature and thereafter for 2 h at 100 °C. After completion of the reaction time, the solvent was removed and the resulting solid was washed with cold ethanol. Complex I was obtained in 81 % isolated yield (3.72 mmol, 3.01 g). Crystallization from acetonitrile yielded the complex in form of dark green needles, suitable for X-ray crystallography.

The monometallic complex II (Co-Salen) was synthesized according to a modified literature procedure.⁽²⁾ Ligand I (1.71 g, 4.62 mmol, 1 eq) was dissolved in ethanol and the solution was degassed by purging with Argon for 15 min. Dry cobalt(II) acetate (0.818 g, 4.62 mmol, 1 eq) was added and the mixture was stirred at 50 °C for 2 h. Next, the solution was refluxed overnight. After removal of the solvent, the resulting solid was washed with cold ethanol and the collected product was dried in vacuo (1.39 g, 3.15 mmol, 68 %).

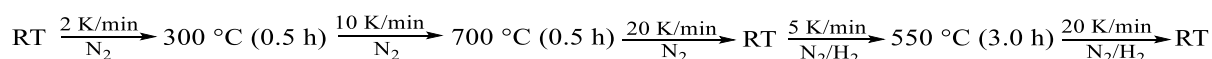
Elemental analysis: calcd for C₂₁H₂₄CoN₂O₄: C 59.02, H 5.66, N 6.56; found: C 59.58, H 5.42, N 6.31

The monometallic complex III (Ce-Salen) was synthesized according to a modified literature procedure.⁽¹⁾ Ligand I (1.71 g, 4.62 mmol, 1 eq) was dissolved in 100 ml ethanol at 50 °C and 2.01 g (4.62 mmol, 1eq) cerium(III) nitrate hexahydrate were added in portions whereupon a yellow precipitate appeared immediately. The suspension was refluxed overnight. The crude product was filtered over a frit, washed with cold ethanol and dried in vacuo (2.93 g, 4.21 mmol, 91 %).

Elemental analysis: calcd for C₂₁H₂₆CeN₅O₁₃: C 36.21, H 3.76, N 10.05; found: C 36.68, H 3.43, N 9.81

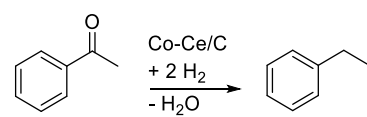
Catalyst synthesis

To a solution of 164 mg ($M = 809.58 \text{ g mol}^{-1}$, 0.2026 mmol) complex I in 3 mL acetonitrile, 300 mg activated charcoal were added and the suspension was stirred at 95 °C. After evaporation of the solvent, the sample was pyrolyzed under nitrogen atmosphere at 700 °C followed by reduction at 550 ° (N₂/H₂, 90/10). The catalysts used for the screening reactions were synthesized using equivalent amounts of monometallic complexes or metal salts.



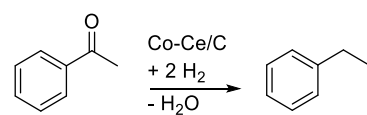
Synthesis of 6-hydroxy-1-phenylhexan-1-one

6-hydroxy-1-phenylhexan-1-one was synthesized according to a known literature procedure.⁽³⁾ A slurry of lactone (10 mmol), HN(OMe)Me-HCl (12 mmol) and NaOCH₃ (2.5 mmol) in THF (100 ml) was cooled to -20 °C under argon atmosphere. A solution of phenylmagnesium bromide in THF (30 mmol, 0.7 M, 42.9 ml) was added dropwise. After 2 h the mixture was allowed to warm to room temperature and stirred overnight. The reaction was quenched with 1 N HCl and stirred for another 2 h. THF was evaporated, the residue was treated with 50 ml of water and then extracted with CH₂Cl₂. The organic phases were combined, dried with Na₂SO₄, and concentrated under reduced pressure. The residue was purified by column chromatography on silica gel (ether/pentane) to give the desired hydroxyketone (substrate for product **4b**). 1,1-diphenylhexane-1,6-diol (substrate for product **4d**) was obtained as a side product. 1-phenylhexane-1,6-diol (substrate for product **4c**) was synthesized by hydrogenation of 6-hydroxy-1-phenylhexan-1-one (2 mmol substrate, 100 mg Co-Ce/C, 3 ml ethanol, 90 °C, 2.0 MPa H₂, 20 h).

Screening of reaction parameters**Table S1:** Screening of reaction parameters – pyrolysis temperature.


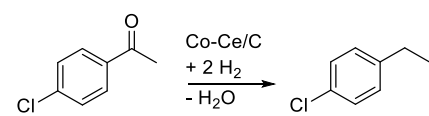
Entry	Pyrolysis temperature	Yield [%]
1	600	51
2	700	81
3	800	70

Reaction conditions: 0.5 mmol substrate, 15 mg catalyst (1.8 mol% Co, 1.6 mol% Ce), 100 °C, 4.0 MPa H₂, 3 ml methylcyclohexane, 20 h; Yields were determined by GC and GC-MS using *n*-dodecane as an internal standard.

Table S2: Screening of reaction parameters – solvent.


Entry	Solvent	Yield [%]
1	Toluene	12
2	1,4-Dioxane	5
3	Diglyme	72
4	tert-Butanol	49
5	Isopropanol	54
6	Ethanol	74
7	H ₂ O	18
8	Methylcyclohexane	81

Reaction conditions: 0.5 mmol substrate, 15 mg catalyst (1.8 mol% Co, 1.6 mol% Ce), 100 °C, 4.0 MPa H₂, 3 ml solvent, 20 h; Yields were determined by GC and GC-MS using *n*-dodecane as an internal standard.

Table S3: Screening of reaction parameters – additive.


Entry	Additive	Yield [%]
1	None	30
2	KOH	28
3	NaOH	8
4	KO ^t Bu	10
5	Amberlyst [®] 15	94
6	Zn(OTf) ₂	93

Reaction conditions: 0.5 mmol substrate, 35 mg catalyst (5.4 mol% Co, 4.8 mol% Ce), 130 °C, 6.0 MPa H₂, 3 ml methylcyclohexane, 5 mol% additive (10 mg Amberlyst[®] 15), 20 h; Yields were determined by GC and GC-MS using *n*-dodecane as an internal standard.

Hydrodeoxygenation of alcohols and carbonyl compounds I – general procedure

A 5 mL teflon reaction vial was charged with a magnetic stirring bar, 0.5 mmol substrate, 3 ml methylcyclohexane and 15 or 35 mg catalyst (1.8 mol% Co, 1.6 mol% Ce or respectively 4.2 mol% Co, 3.7 mol% Ce). For halogenated ketones and secondary alcohols 10 mg Amberlyst® 15 and for halogenated aldehydes and primary alcohols 5 mol% Zn(OTf)₂ were used as an additive. The vial was placed in a 300 mL high-pressure autoclave (Parr Instruments) and the autoclave was flushed three times with 2 MPa hydrogen. Afterwards, the final pressure was applied and the reaction was stirred at the desired temperature for 20 h (reaction conditions vary dependent on the substrate). After completion of the reaction time, the autoclave was cooled to room temperature and the hydrogen was released. Quantitative GC analysis was accomplished using *n*-dodecane as an internal standard.

Product 1a-c, 1p-s: 0.5 mmol substrate, 15 mg catalyst (1.8 mol% Co, 1.6 mol% Ce), 3 ml methylcyclohexane, 110 °C, 5.0 MPa H₂, 20 h.

Product 1d-h, 1t-w: 0.5 mmol substrate, 35 mg catalyst (4.2 mol% Co, 3.7 mol% Ce), 3 ml methylcyclohexane, 10 mg Amberlyst® 15, 130 °C, 6.0 MPa H₂, 20 h.

Product: 1i-o: 0.5 mmol substrate, 35 mg catalyst (4.2 mol% Co, 3.7 mol% Ce), 3 ml methylcyclohexane, 130 °C, 6.0 MPa H₂, 20 h.

Product: 2a-b, 2h-m: 0.5 mmol substrate, 50 mg catalyst (6.1 mol% Co, 5.2 mol% Ce), 3 ml methylcyclohexane, 130 °C, 6.0 MPa H₂, 20 h.

Product: 2c-g, 2n-q: 0.5 mmol substrate, 50 mg catalyst (6.1 mol% Co, 5.2 mol% Ce), 3 ml methylcyclohexane, 5 mol% Zn(OTf)₂, 130 °C, 6.0 MPa H₂, 20 h.

Hydrodeoxygenation of alcohols and carbonyl compounds II – general procedure

A 25 mL high-pressure autoclave (Parr Instruments) equipped with a teflon inlet was charged with a magnetic stirring bar, 1.0 mmol substrate, 6 ml solvent and the desired amount of catalyst and additive. The autoclave was flushed three times with 2 MPa of hydrogen. Afterwards, the final pressure was applied, and the reaction was stirred at the desired temperature for 20 h (reaction conditions vary dependent on the substrate). After completion of the reaction time, the autoclave was cooled to room temperature and the hydrogen was released. Quantitative GC analysis was accomplished using *n*-dodecane as internal standard.

Products: 3a-e: 1.0 mmol substrate, 100 mg catalyst (6.1 mol% Co, 5.2 mol% Ce), 6 ml methylcyclohexane, 20 mg Amberlyst® 15, 160 °C, 6.0 MPa H₂, 20 h.

Product: 3f: 1.0 mmol substrate, 30 mg catalyst (1.8 mol% Co, 1.6 mol% Ce), 6 ml methylcyclohexane, 110 °C, 4.0 MPa H₂, 20 h.

Products 4a-d: 1.0 mmol substrate, 70 mg catalyst (4.2 mol% Co, 3.7 mol% Ce), 6 ml ethanol, 130 °C, 5.0 MPa H₂, 20 h.

Products: 5a, c, e: 1.0 mmol substrate, 100 mg catalyst (6.1 mol% Co, 5.2 mol% Ce), 6 ml methylcyclohexane, 160 °C, 6.0 MPa H₂, 20 h.

Product: 5b: 1.0 mmol substrate, 100 mg catalyst (6.1 mol% Co, 5.2 mol% Ce), 6 ml diglyme, 160 °C, 6.0 MPa H₂, 20 h.

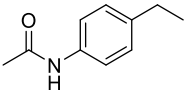
Product: 5d: 1.0 mmol substrate, 100 mg catalyst (6.1 mol% Co, 5.2 mol% Ce), 6 ml methylcyclohexane, 20 mg Amberlyst[®] 15, 160 °C, 6.0 MPa H₂, 20 h.

Product: 5f: 1.0 mmol substrate, 100 mg catalyst (6.1 mol% Co, 5.2 mol% Ce), 6 ml methylcyclohexane, 5 mol% Zn(OTf)₂, 160 °C, 6.0 MPa H₂, 20 h.

Up-scaling

10 mmol 4-acetamidoacetophenone were chosen for the up-scaling reaction. A 25 ml high-pressure autoclave (Parr Instruments) equipped with a teflon inlet and a magnetic stirring bar was filled with 10 mmol substrate, 700 mg catalyst (4.2 mol% Co, 3.7 mol% Ce) and 12 ml methylcyclohexane. The autoclave was flushed three times with 2 MPa of hydrogen and afterwards the final pressure of 6 MPa was applied. The reaction was stirred for 20 h at 130 °C. After completion of the reaction time, the autoclave was cooled to room temperature and the hydrogen was released. The catalyst was removed by centrifugation and the organic phases were combined. After removal of the solvent, the desired product was obtained without further purification.

Table S4: Up-scaling of the reaction.

Entry	Product	Isolated Yield [g]	Yield [%]
1		1.50	92

Reaction conditions: 10 mmol substrate, 700 mg catalyst (4.2 mol% Co, 3.7 mol% Ce), 130 °C, 6.0 MPa H₂, 12 ml methylcyclohexane, 20 h.

Catalyst characterization

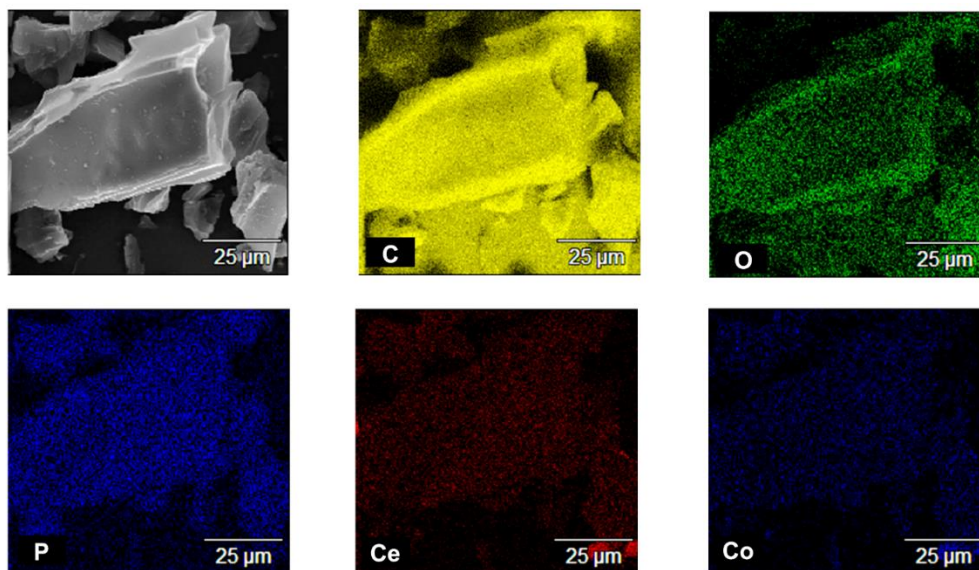


Fig. 1. SEM- in combination with EDX element maps of the active catalyst system. A homogeneous distribution of both metal species is verified. No phase separation could be detected, indicating a clean and smooth impregnation process. The presence of phosphorus can be reduced to the chemically activated carbon support.

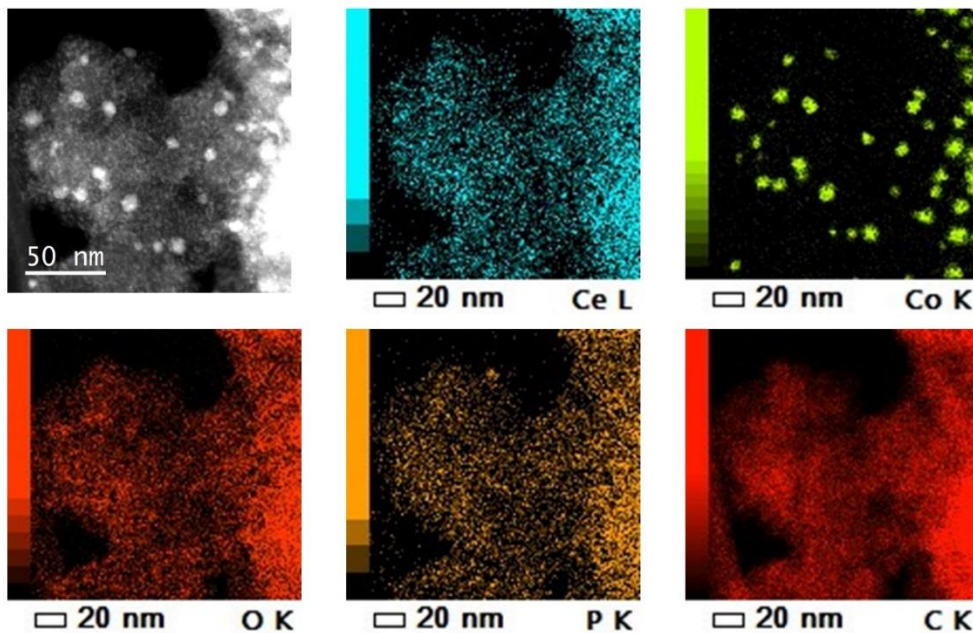


Fig. S2. Characterization of the active catalyst by high-angle annular dark-field scanning TEM (HAADF-STEM) analysis combined with energy-dispersed X-ray (EDX) element maps. Co nanoparticles with a mean diameter of 6.8 nm are clearly visible, Ce seems to be homogeneously distributed over the whole carbon support.

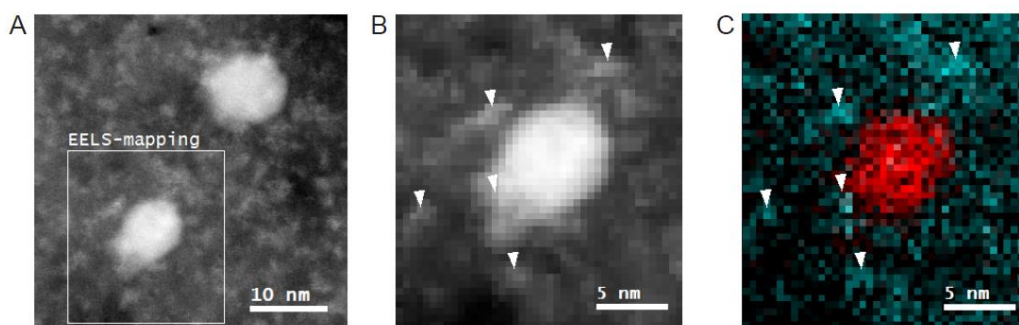


Fig. S3. High-angle annular dark-field scanning TEM (HAADF-STEM) imaging (A and B) combined with electron energy loss spectroscopy (EELS) elemental mapping for Cobalt (Red) and Cerium (Cyan) (C). Direct comparison of the HAADF-STEM data with the EELS mapping of Cerium suggests that nanometer sized bright features marked with arrows surrounding Co-particles are rich in Cerium.

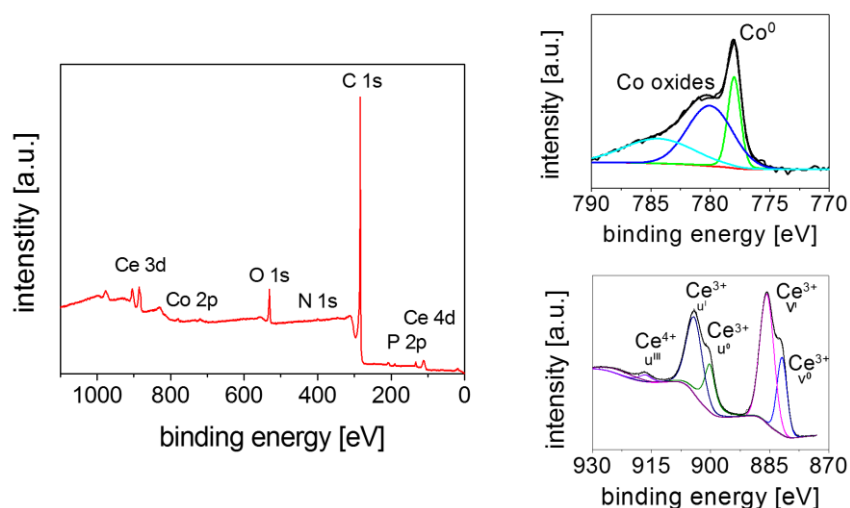
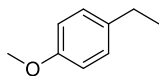


Fig. S4. XPS analysis of the Co-Ce catalyst.

Besides the elements C and O, the sample contained Ce, Co, N and P. The presence of phosphorus can be assigned to impurities of the chemically activated carbon support. An analysis of the Co $2p_{3/2}$ region verifies the presence of metallic cobalt, which can be identified due to its sharp line and its binding energy of 778 eV (20 % of the signal). At higher binding energies, different oxides and maybe also hydroxides are found that cannot be distinguished (80% of the signal). For Ce $3d_{5/2}$ the fits were carried out by comparing the results to the literature.⁽⁴⁾ The spectrum is dominated by signals of Ce^{3+} (85%). The contribution at 916 eV is due to the presence of ~15% of Ce^{4+} . The Ce^{4+} amount was calculated by taking into account the relative intensities of all Ce^{3+} and Ce^{4+} signals as described in Ref. (5).

Characterization of isolated products

1-ethyl-4-methoxybenzene (1c)



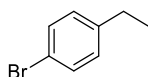
FW (C₉H₁₂O) = 136.19 g mol⁻¹

¹H NMR (300 MHz, C₆D₆): δ = 7.01-6.97 (m, 2 H), 6.82-6.78 (m, 2 H), 3.35 (s, 1 H), 2.46 (q, J = 7.62 Hz, 2 H), 1.11 (t, J = 7.62 Hz, 2 H) ppm.

¹³C NMR (75 MHz, C₆D₆): δ = 158.77, 136.66, 129.34, 114.54, 55.12, 28.72, 16.58 ppm.

Yield: 86 % (0.43 mmol, 58 mg), colorless liquid.

1-bromo-4-ethylbenzene (1h)



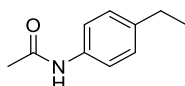
FW (C₈H₉Br) = 185.06 g mol⁻¹

¹H NMR (300 MHz, C₆D₆): δ = 7.27-7.22 (m, 2 H), 6.66-6.61 (m, 2 H), 2.21 (q, J = 7.62 Hz, 2 H), 0.93 (t, J = 7.62 Hz, 2 H) ppm.

¹³C NMR (75 MHz, C₆D₆): δ = 142.75, 131.30, 129.54, 119.36, 28.07, 14.98 ppm.

Yield: 71 % (0.36 mmol, 66 mg), colorless liquid.

N-(4-ethylphenyl)acetamide (1k)



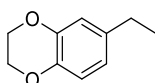
FW (C₁₀H₁₃NO) = 163.22 g mol⁻¹

¹H NMR (300 MHz, CDCl₃): δ = 8.11 (s, 1 H), 7.42 (d, J = 7.03 Hz, 2 H), 7.12 (d, J = 7.03 Hz, 2 H), 2.61 (q, J = 7.62 Hz, 2 H), 2.14 (s, 3 H), 1.22 (t, J = 7.62 Hz, 3 H) ppm

¹³C NMR (75 MHz, CDCl₃): δ = 168.79, 140.20, 135.58, 128.08, 120.27, 28.19, 24.21, 15.56 ppm.

Yield: 86 % (0.43 mmol, 70 mg), white solid.

6-ethyl-2,3-dihydrobenzo[b][1,4]dioxine (1n)



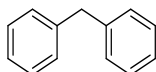
FW (C₁₀H₁₂O₂) = 164.20 g mol⁻¹

^1H NMR (300 MHz, CDCl_3): δ = 6.81-6.78 (m, 1 H), 6.73-6.67 (m, 2 H), 4.27-4.23 (m, 4 H), 2.60-2.53 (m, 2 H), 1.23-1.19 (m, 3 H) ppm

^{13}C NMR (75 MHz, CDCl_3): δ = 143.27, 141.47, 137.69, 120.77, 116.98, 116.43, 64.46, 28.15, 15.74 ppm.

Yield: 90 % (0.45 mmol, 74 mg), colorless liquid.

diphenylmethane (1r)



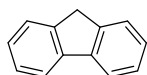
FW ($\text{C}_{13}\text{H}_{12}$) = 168.24 g mol^{-1}

^1H NMR (300 MHz, DMSO-d_6): δ = 7.31-7.16 (m, 10 H), 3.94 (s, 2 H) ppm

^{13}C NMR (75 MHz, DMSO-d_6): δ = 141.51, 128.92, 128.65, 126.19, 41.37 ppm.

Yield: 88 % (0.44 mmol, 74 mg), colorless liquid.

9H-fluorene (1s)



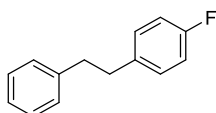
FW ($\text{C}_{13}\text{H}_{10}$) = 166.22 g mol^{-1}

^1H NMR (300 MHz, DMSO-d_6): δ = 7.91-7.89 (m, 2 H), 7.60-7.58 (m, 2 H), 7.41-7.29 (m, 4 H), 3.92 (s, 2 H) ppm

^{13}C NMR (75 MHz, DMSO-d_6): δ = 142.92, 141.04, 126.76, 126.70, 125.11, 119.95, 36.35 ppm.

Yield: 81 % (0.41 mmol, 67 mg), white solid.

1-fluoro-4-phenethylbenzene (1t)



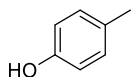
FW ($\text{C}_{14}\text{H}_{13}\text{F}$) = 200.26 g mol^{-1}

^1H NMR (300 MHz, CDCl_3): δ = 7.34-7.14 (m, 7 H), 7.04-6.99 (m, 2 H), 2.96 (s, 4 H) ppm

^{13}C NMR (75 MHz, CDCl_3): δ = 162.99, 159.75, 141.49, 137.37, 129.91, 129.82, 128.53, 128.41, 126.05, 115.21, 114.94, 38.07, 37.12 ppm.

Yield: 81 % (0.41 mmol, 81 mg), white solid.

p-cresol (2b)



FW (C₇H₈O) = 108.14 g mol⁻¹

¹H NMR (300 MHz, DMSO-d₆): δ = 9.08 (s, 1 H), 6.96-6.93 (m, 2 H), 6.66-6.63 (m, 2 H), 2.17 (s, 3 H) ppm

¹³C NMR (75 MHz, DMSO-d₆): δ = 155.02, 129.70, 127.12, 115.01, 20.09 ppm.

Yield: 88 % (0.44 mmol, 48 mg), colorless solid.

1-chloro-2-methylbenzene (2d)



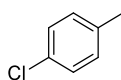
FW (C₇H₇Cl) = 126.58 g mol⁻¹

¹H NMR (300 MHz, DMSO-d₆): δ = 7.41-7.20 (m, 4 H), 2.32 (s, 3 H) ppm

¹³C NMR (75 MHz, DMSO-d₆): δ = 135.35, 133.24, 131.20, 128.77, 127.57, 127.03, 19.49 ppm.

Yield: 68 % (0.34 mmol, 43 mg), colorless liquid.

1-chloro-4-methylbenzene (2f)



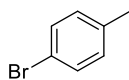
FW (C₇H₇Cl) = 126.58 g mol⁻¹

¹H NMR (300 MHz, C₆D₆): δ = 7.08-7.03 (m, 2 H), 6.67-6.64 (m, 2 H), 1.90 (s, 3 H) ppm.

¹³C NMR (75 MHz, C₆D₆): δ = 136.58, 131.85, 130.97, 128.92, 20.94 ppm.

Yield: 86 % (0.43 mmol, 54 mg), colorless liquid.

1-bromo-4-methylbenzene (2g)



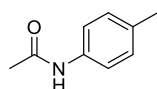
FW (C₇H₇Br) = 171.04 g mol⁻¹

¹H NMR (300 MHz, DMSO-d₆): δ = 7.44-7.41 (m, 2 H), 7.15-7.13 (m, 2 H), 2.26 (s, 3 H) ppm

¹³C NMR (75 MHz, DMSO-d₆): δ = 136.84, 131.17, 130.97, 118.30, 20.39 ppm.

Yield: 76 % (0.38 mmol, 65 mg), colorless liquid.

N-(p-tolyl)acetamide (2j)



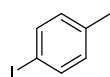
FW (C₇H₇Br) = 149.19 g mol⁻¹

¹H NMR (300 MHz, DMSO-d₆): δ = 9.85 (s, 1H), 7.50-7.47 (m, 2 H), 7.11-7.08 (m, 2 H), 2.25 (s, 3 H), 2.04 (s, 3 H) ppm

¹³C NMR (75 MHz, DMSO-d₆): δ = 168.46, 137.32, 132.26, 129.48, 119.46, 24.40, 20.87 ppm.

Yield: 86 % (0.43 mmol, 64 mg), white solid.

1-iodo-4-methylbenzene (2p)



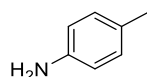
FW (C₇H₇I) = 218.96 g mol⁻¹

¹H NMR (300 MHz, C₆D₆): δ = 7.4 (d, *J* = 8.2 Hz, 2 H), 6.47 (d, *J* = 8.2 Hz, 2 H), 1.85 (s, 3 H) ppm.

¹³C NMR (75 MHz, C₆D₆): δ = 137.88, 137.70, 131.72, 90.96, 21.12 ppm.

Yield: 62 % (0.31 mmol, 68 mg), colorless liquid.

p-toluidine (2q)



FW (C₇H₉N) = 107.16 g mol⁻¹

¹H NMR (300 MHz, DMSO-d₆): δ = 6.82 (d, *J* = 8.2 Hz, 2 H), 6.47 (d, *J* = 8.2 Hz, 2 H), 4.77 (s, 2 H), 2.12 (s, 3 H) ppm

¹³C NMR (75 MHz, DMSO-d₆): δ = 146.06, 129.23, 123.92, 114.03, 20.12 ppm.

Yield: 87 % (0.43 mmol, 47 mg), colorless solid.

n-dodecane (3a)



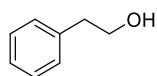
FW (C₁₂H₂₆) = 170.34 g mol⁻¹

¹H NMR (300 MHz, C₆D₆): δ = 1.3 (br, 20 H) 0.94-0.90 (m, 6H) ppm

¹³C NMR (75 MHz, C₆D₆): δ = 32.01, 29.83, 29.49, 22.78, 14.00 ppm.

Yield: 91 % (0.91 mmol, 155 mg), colorless liquid.

2-phenylethan-1-ol (4a)



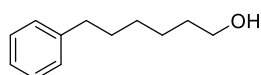
FW (C₈H₁₀O) = 122.17 g mol⁻¹

¹H NMR (300 MHz, C₆D₆): δ = 7.16-7.01 (m, 5 H), 3.50 (t, *J* = 7.03 Hz, 2 H), 2.57 (t, *J* = 7.03 Hz, 2 H), 1.24 (s, 1 H) ppm.

¹³C NMR (75 MHz, C₆D₆): δ = 139.65, 129.67, 129.02, 126.83, 64.01, 39.98 ppm.

Yield: 66 % (0.66 mmol, 81 mg), colorless liquid.

6-phenylhexan-1-ol (4b)



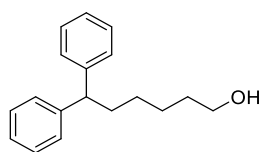
FW (C₁₂H₁₈O) = 178.28 g mol⁻¹

¹H NMR (300 MHz, C₆D₆): δ = 7.21-7.06 (m, 5 H), 3.43-3.38 (m, 2 H), 2.47 (t, *J* = 7.61 Hz, 2 H), 1.83 (s, 1 H), 1.56-1.46 (m, 2 H), 1.43-1.34 (m, 2 H), 1.28-1.17 (m, 4 H) ppm.

¹³C NMR (75 MHz, C₆D₆): δ = 143.30, 129.08, 128.94, 126.35, 62.96, 36.58, 33.41, 32.19, 29.73, 26.36 ppm.

Yield: 85 % (0.85 mmol, 152 mg), colorless liquid.

6,6-diphenylhexan-1-ol (4d)



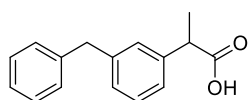
FW (C₁₈H₂₂O) = 254.37 g mol⁻¹

¹H NMR (500 MHz, CDCl₃): δ = 7.36-7.30 (m, 8 H), 7.25-7.22 (m, 2H), 3.96 (t, *J* = 7.94 Hz, 1 H), 3.62 (t, *J* = 6.41 Hz, 2 H), 2.14 (q; *J* = 7.94, 2 H), 1.99 (s, 1 H), 1.60-1.55 (m, 2 H), 1.48-1.42 (m, 2 H), 1.39-1.33 (m, 2 H) ppm.

¹³C NMR (125.7 MHz, CDCl₃): δ = 145.30, 128.50, 127.93, 126.15, 62.86, 51.39, 35.76, 32.62, 27.91, 25.83 ppm.

Yield: 87 % (0.87 mmol, 221 mg), colorless liquid.

2-(3-benzylphenyl)propanoic acid (5c)



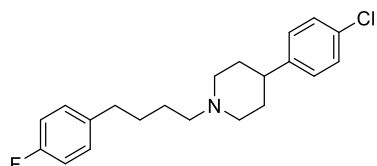
FW (C₁₆H₁₆O₂) = 240.30 g mol⁻¹

¹H NMR (300 MHz, DMSO-d₆): δ = 12.31 (s, 1 H), 7.36-7.08 (m, 9 H), 3.92 (s, 2 H), 3.66-3.59 (m, 1 H), 1.34-1.32 (m, 3 H) ppm

¹³C NMR (75 MHz, DMSO-d₆): δ = 175.79, 141.87, 141.63, 129.14, 128.99, 128.90, 128.27, 127.65, 126.44, 125.47, 45.12, 41.56, 19.04 ppm.

Yield: 87 % (0.87 mmol, 209 mg), white solid.

4-(4-chlorophenyl)-1-(4-(4-fluorophenyl)butyl)piperidine (5d)



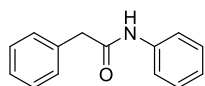
FW (C₂₁H₂₅ClFN) = 345.89 g mol⁻¹

¹H NMR (300 MHz, DMSO-d₆): δ = 7.34-7.19 (m, 6 H), 7.12-7.04 (m, 2 H), 2.93-2.89 (m, 2 H), 2.59-2.54 (m, 2H), 2.47-2.40 (m, 1 H), 2.31-2.26 (m, 2 H), 1.97-1.88 (m, 2 H), 1.72-1.38 (m, 8 H) ppm

¹³C NMR (75 MHz, DMSO-d₆): δ = 162.61, 159.42, 145.76, 138.83, 130.93, 130.47, 130.37, 129.07, 128.69, 115.46, 115.18, 58.39, 54.17, 41.78, 34.62, 33.44, 29.48, 26.46 ppm.

Yield: 84 % (0.84 mmol, 290 mg), white solid.

N,2-diphenylacetamide (5e)

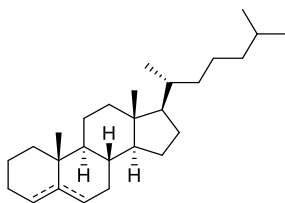


FW (C₁₄H₁₃NO) = 211.26 g mol⁻¹

¹H NMR (300 MHz, DMSO-d₆): δ = 10.17 (s, 1 H), 7.61-7.59 (m, 2H), 7.36-7.23 (m, 7 H), 7.05-7.00 (m, 1H), 3.64 (s, 2 H) ppm

¹³C NMR (75 MHz, DMSO-d₆): δ = 169.05, 139.21, 135.99, 129.08, 128.69, 128.28, 126.50, 123.17, 119.07, 43.32 ppm.

Yield: 84 % (0.84 mmol, 177 mg), light yellow solid.

cholesten (5f)

FW (C₂₇H₄₅) = 369.66 g mol⁻¹

¹H NMR (500 MHz, CDCl₃): δ = 5.30-5.28 (m, 1H), 2.28-2.16 (m, 1 H), 2.04-0.73 (m, 41 H), 0.69-0.67 (m, 3 H) ppm

¹³C NMR (125.7 MHz, CDCl₃): δ = 145.16, 143.71, 118.98, 118.90, 56.86, 56.26, 56.21, 54.45, 42.51, 39.51, 35.80, 32.63, 28.24, 28.01, 24.27, 23.84, 22.83, 22.56, 21.42, 19.45, 19.29, 18.65, 11.98 ppm.

A mixture of isomers was obtained.

Yield: 75 % (0.75 mmol, 277 mg), white solid.

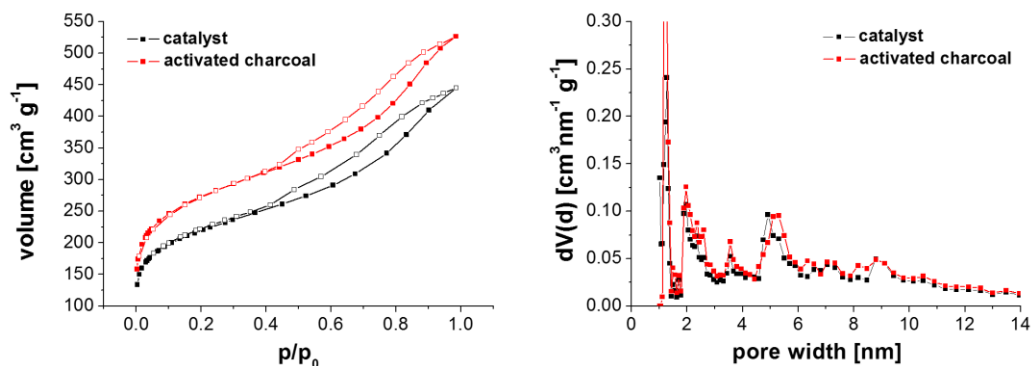
Additional supplementary figures

Fig. S5. Nitrogen physisorption measurements of the catalyst in comparison to the pure carbon support.

Both materials show the typical hysteresis of mesoporous materials. The catalyst features a specific surface area (Brunauer-Emmet-Teller) of 740 m²/g. The corresponding pore size distributions [N₂ at -196.15 °C on carbon (slit/cylindrical pore, NLDFT equilibrium model)] indicate a small decrease in the amount of micropores after wet impregnation and pyrolysis.

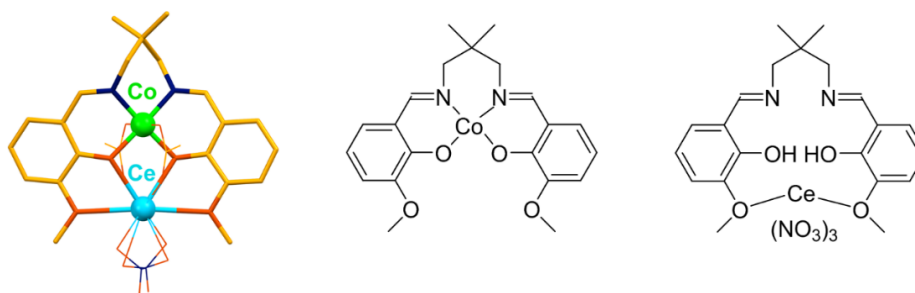


Fig. S6. Structures of the different salen complexes. The complexes were synthesized according to known literature procedures described before.

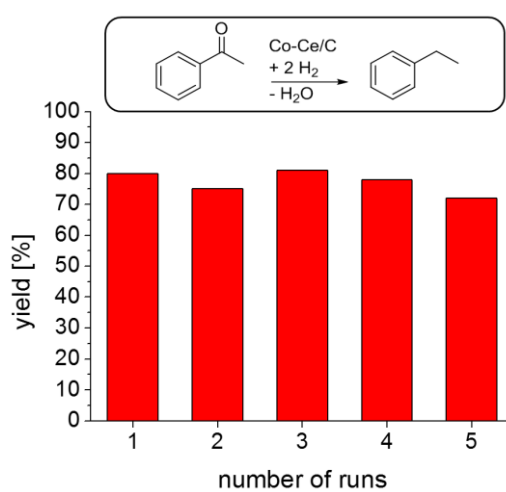
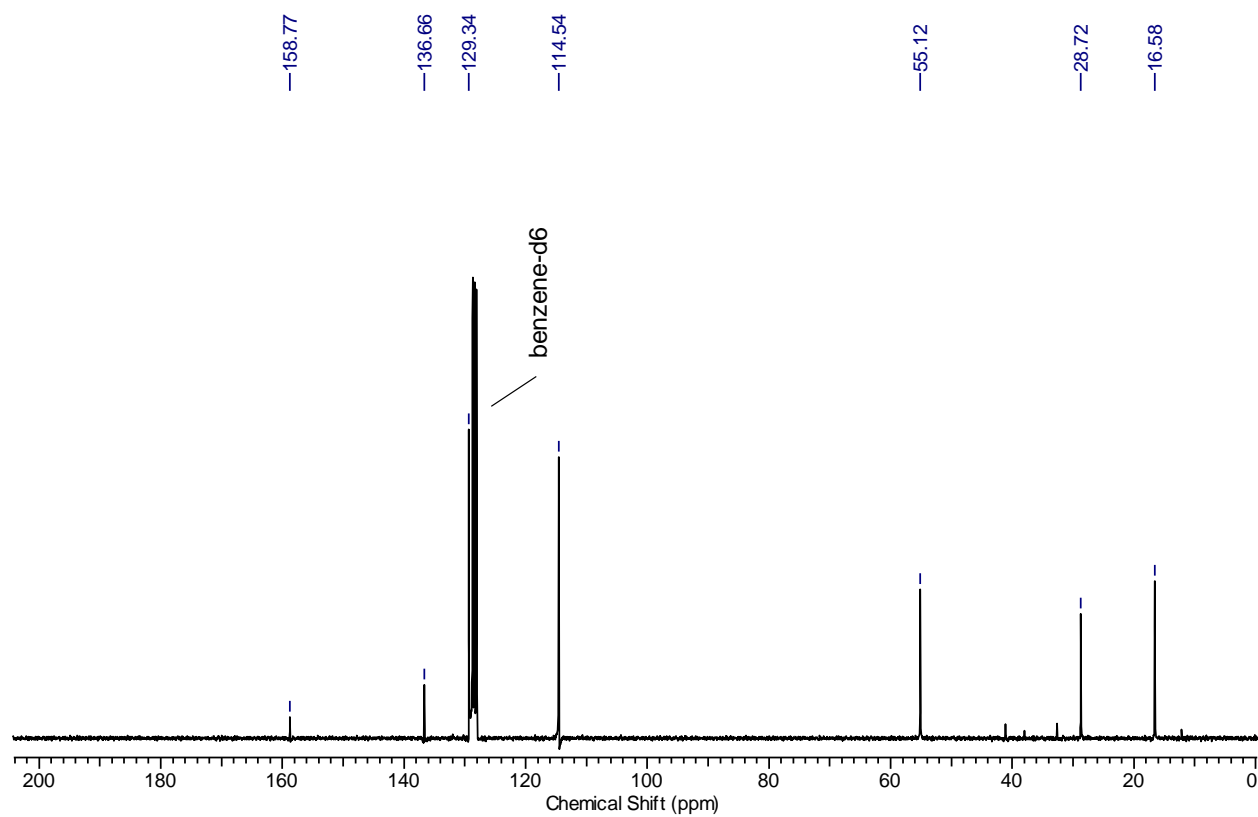
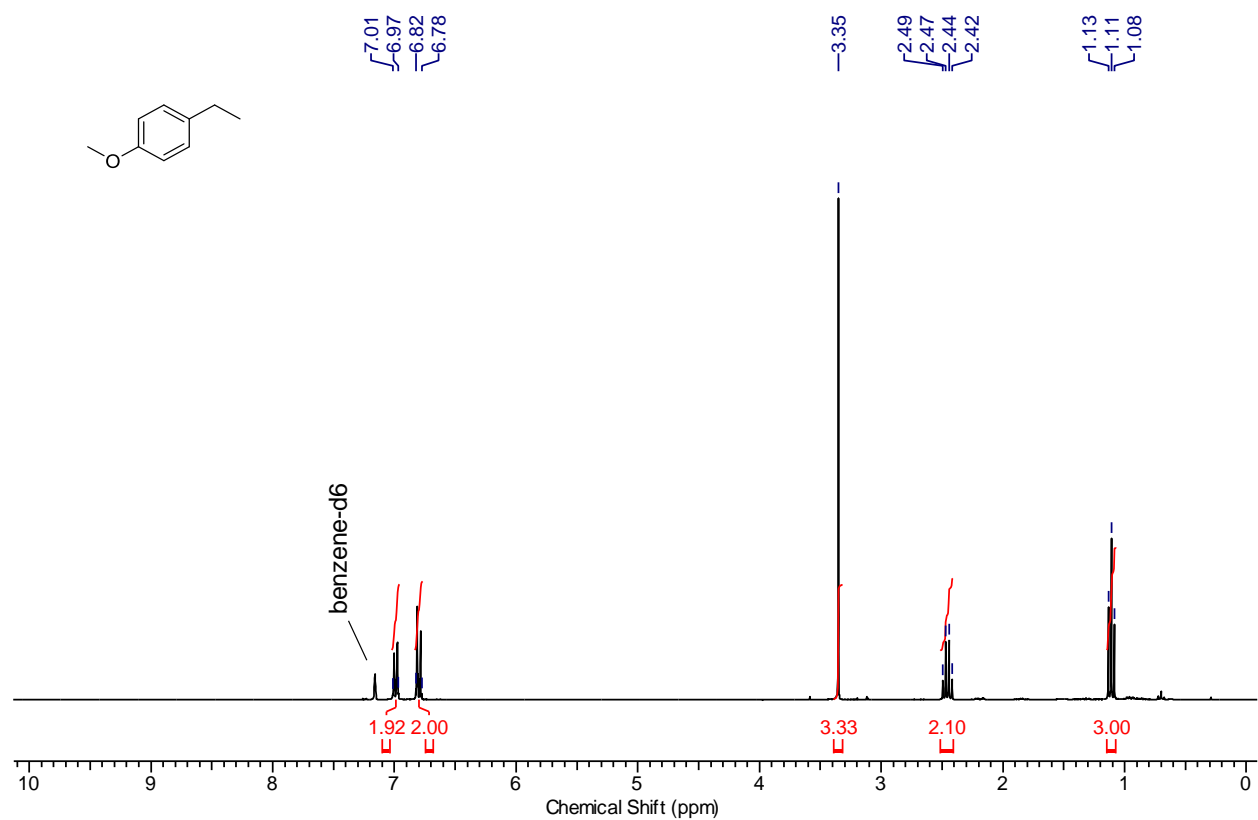
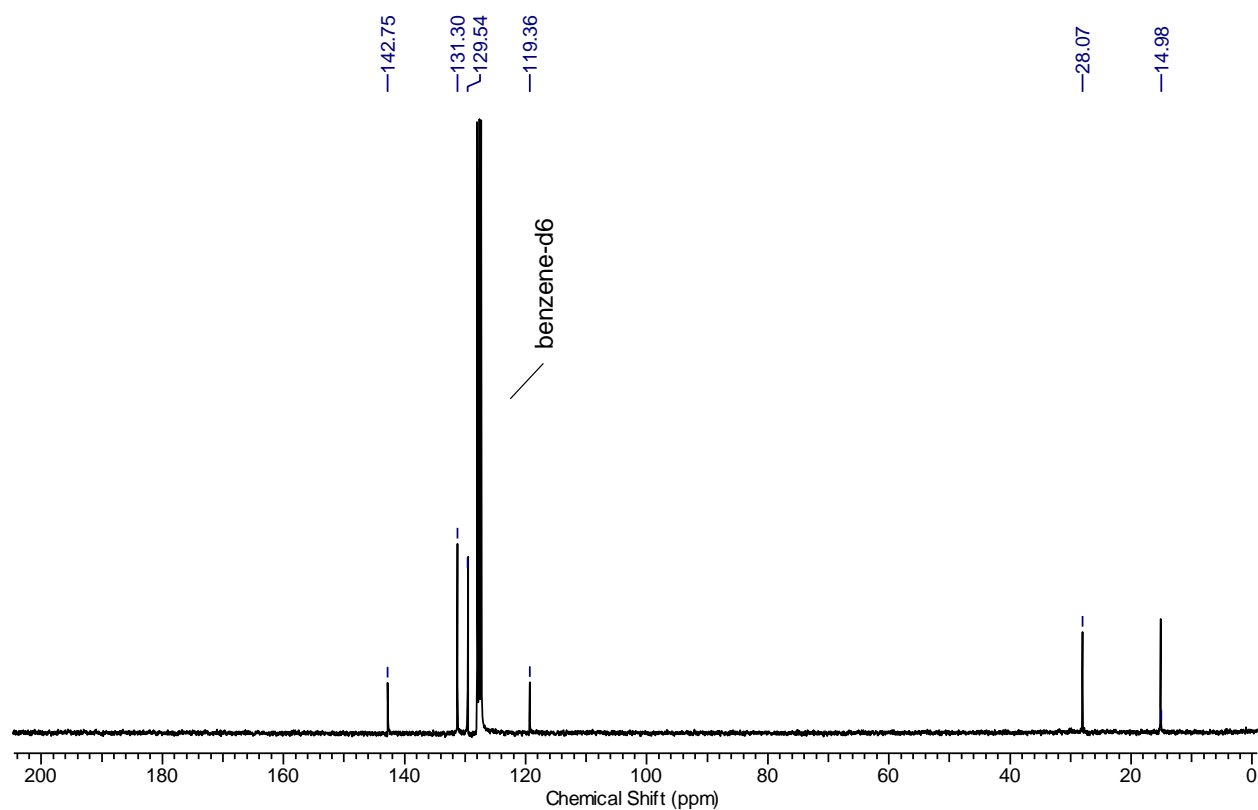
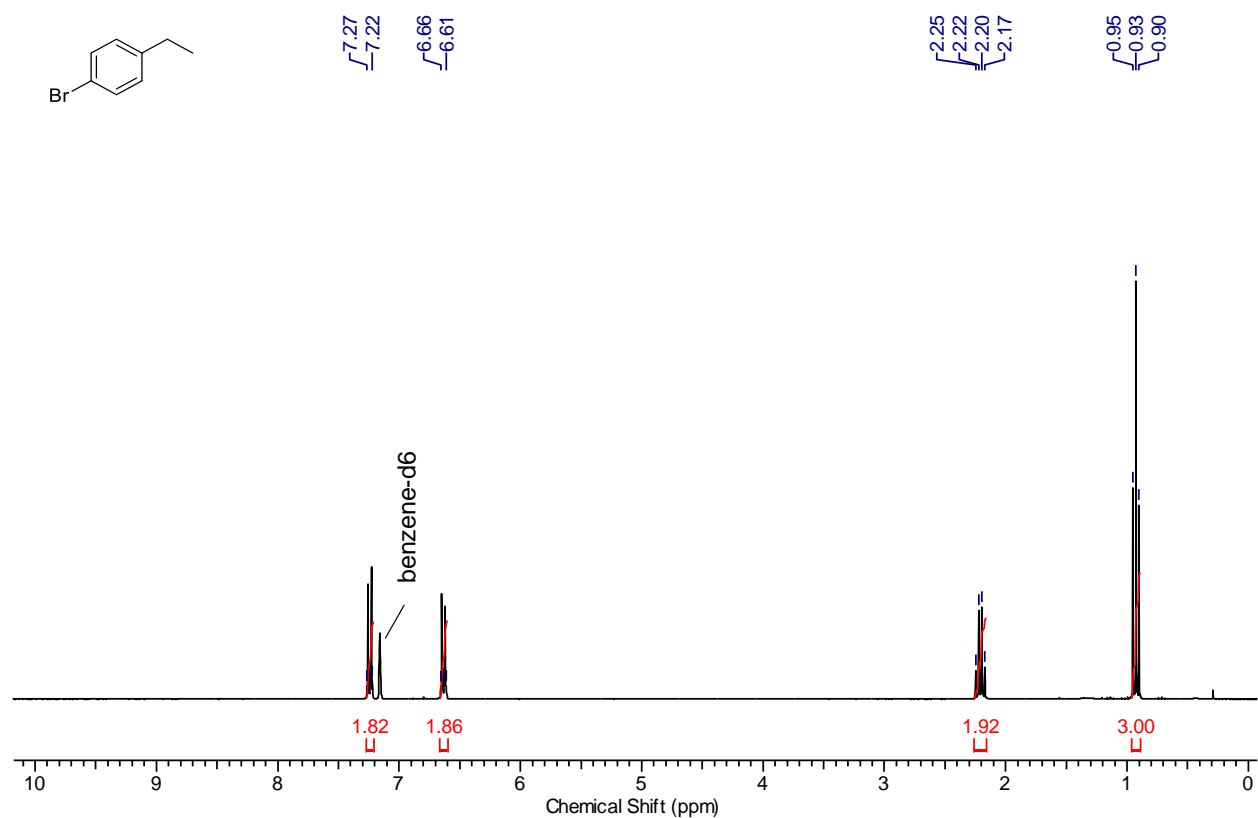
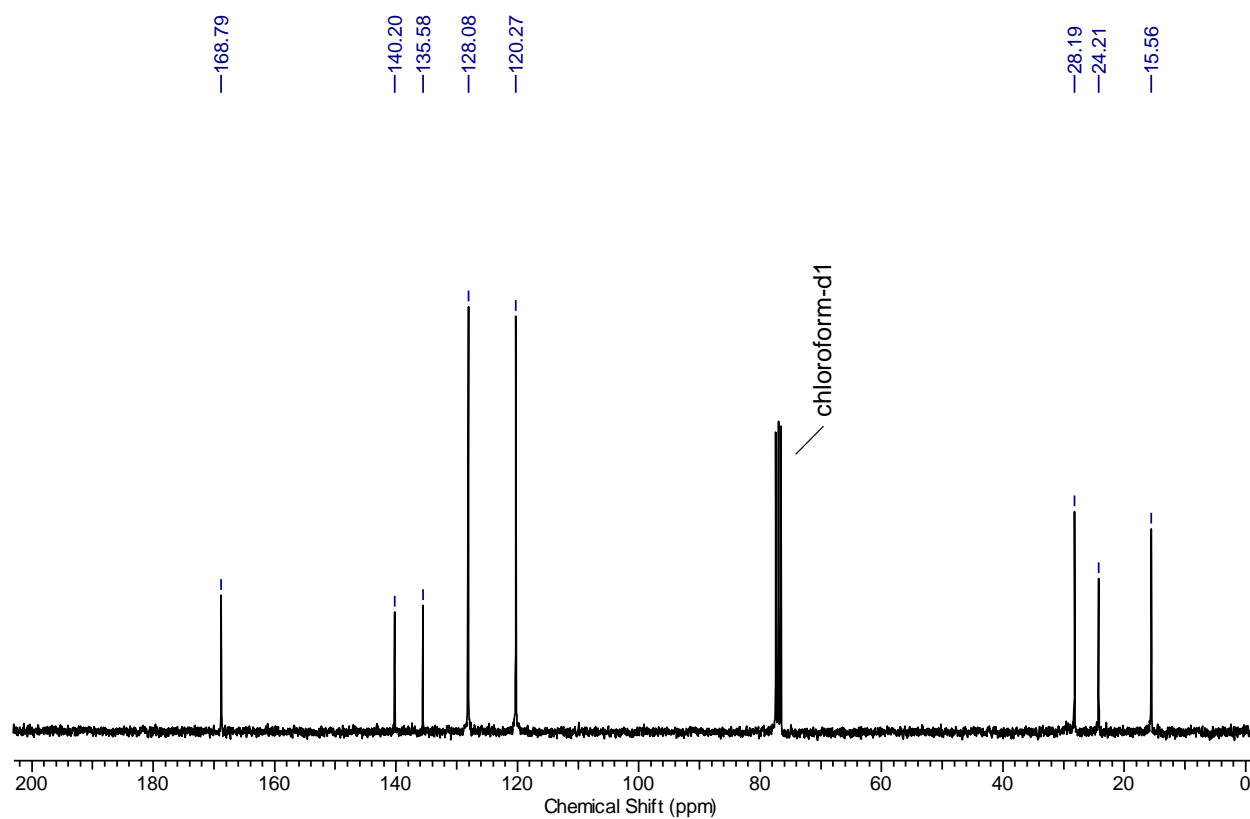
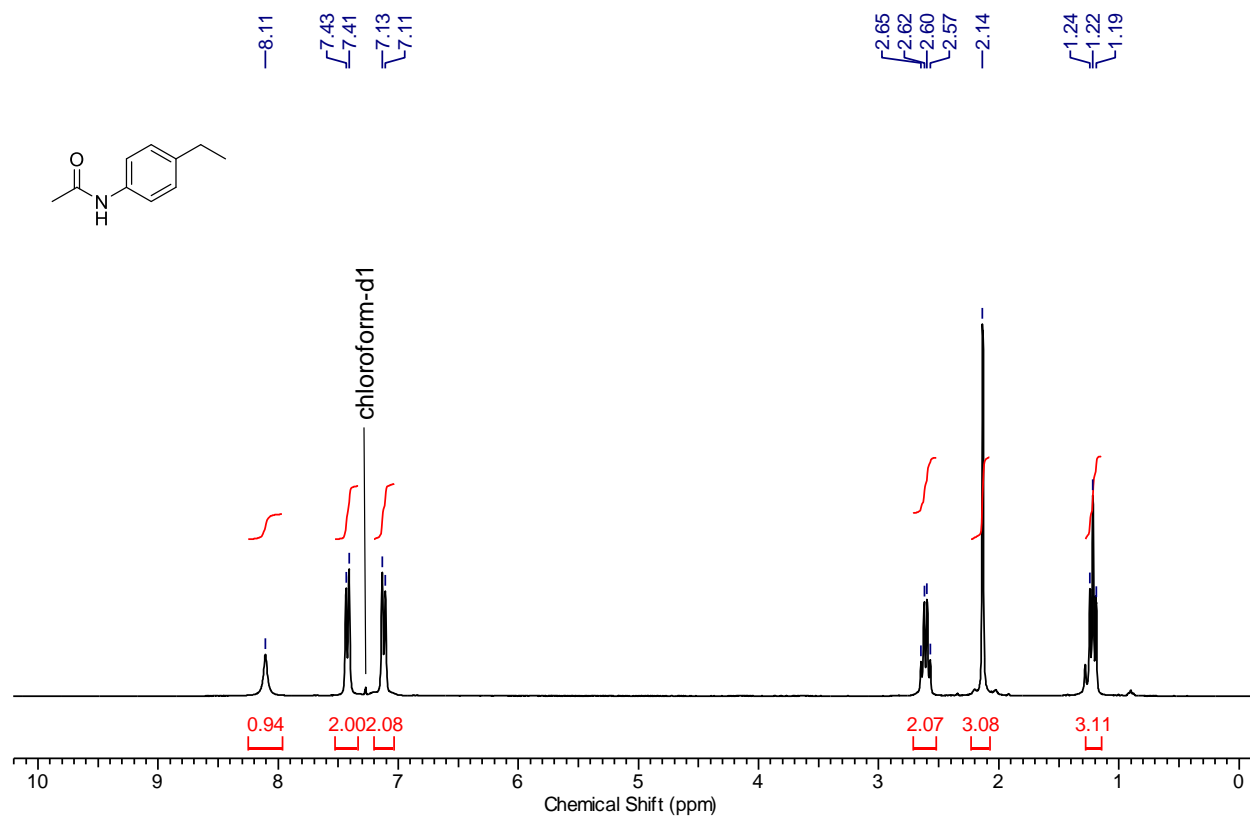


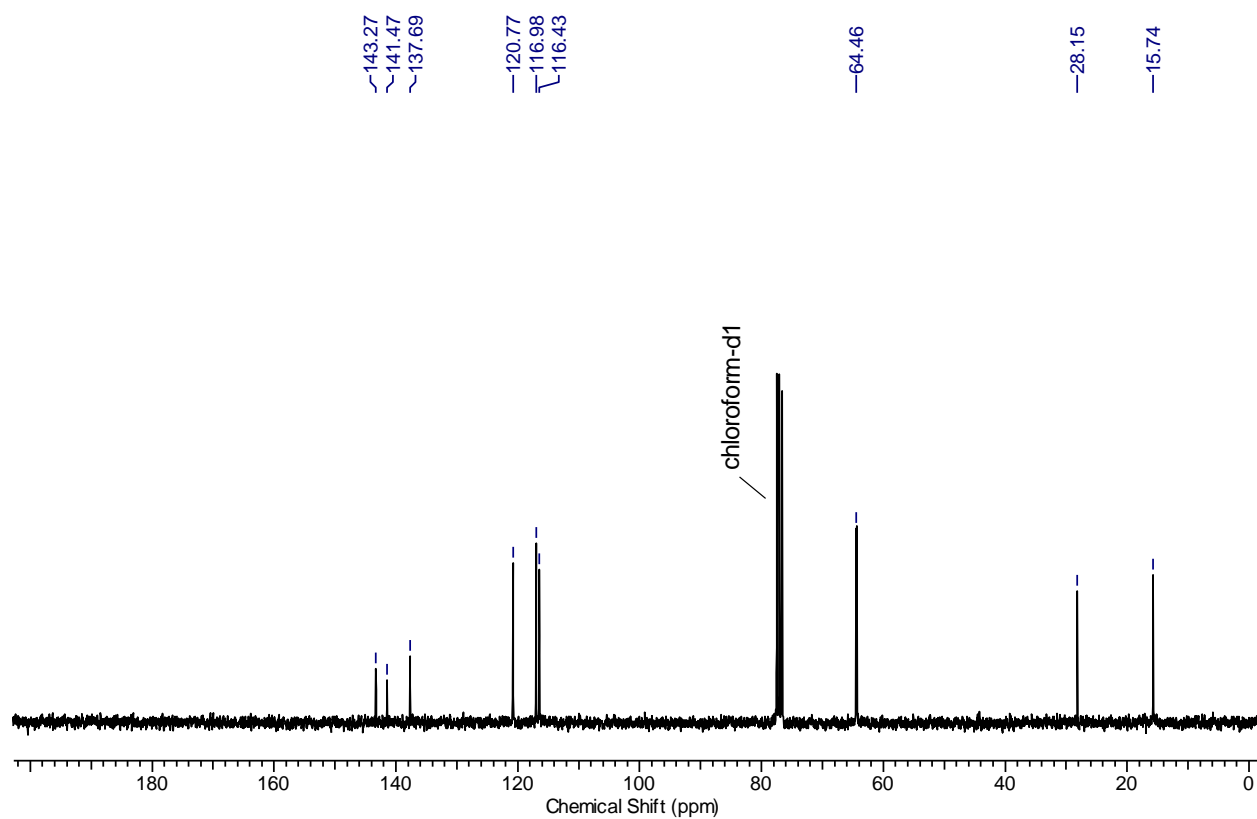
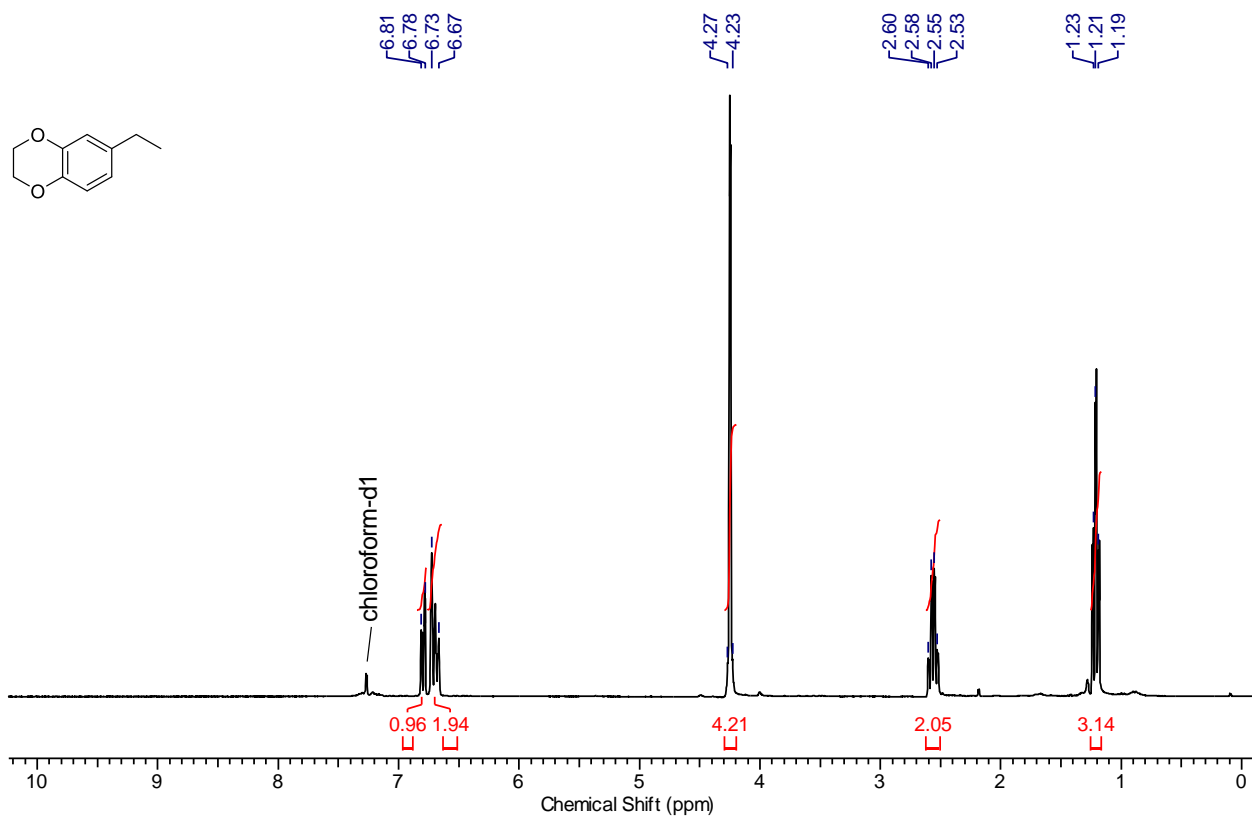
Fig. S7. Recycling study. The catalyst was reused in five consecutive runs without any remarkable decrease in catalytic activity. Reaction conditions: 0.5 mmol substrate, 15 mg catalyst (1.8 mol% Co, 1.6 mol% Ce), 100 °C, 4.0 MPa H₂, 3 ml methylcyclohexane, 20 h. Yields were determined by GC and GC-MS using n-dodecane as internal standard. The catalyst was separated using a magnet, washed and reused again.

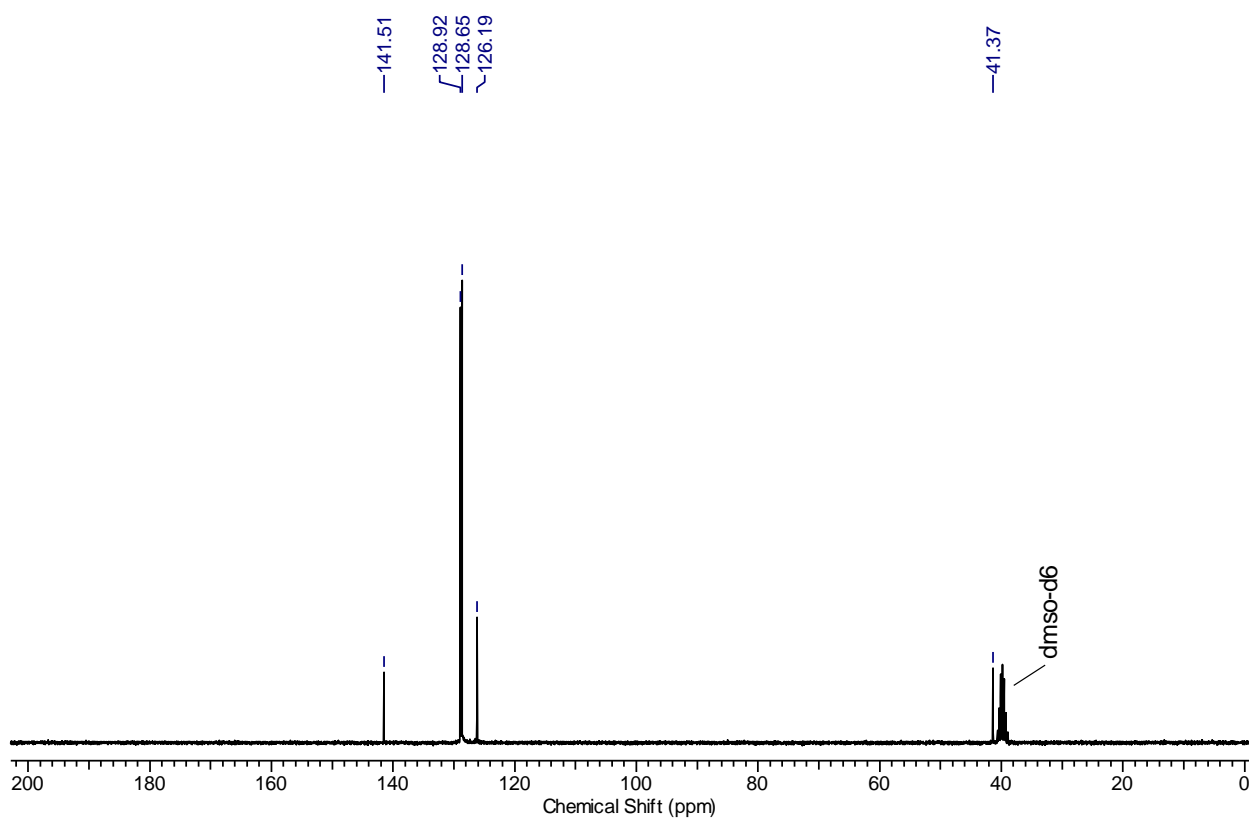
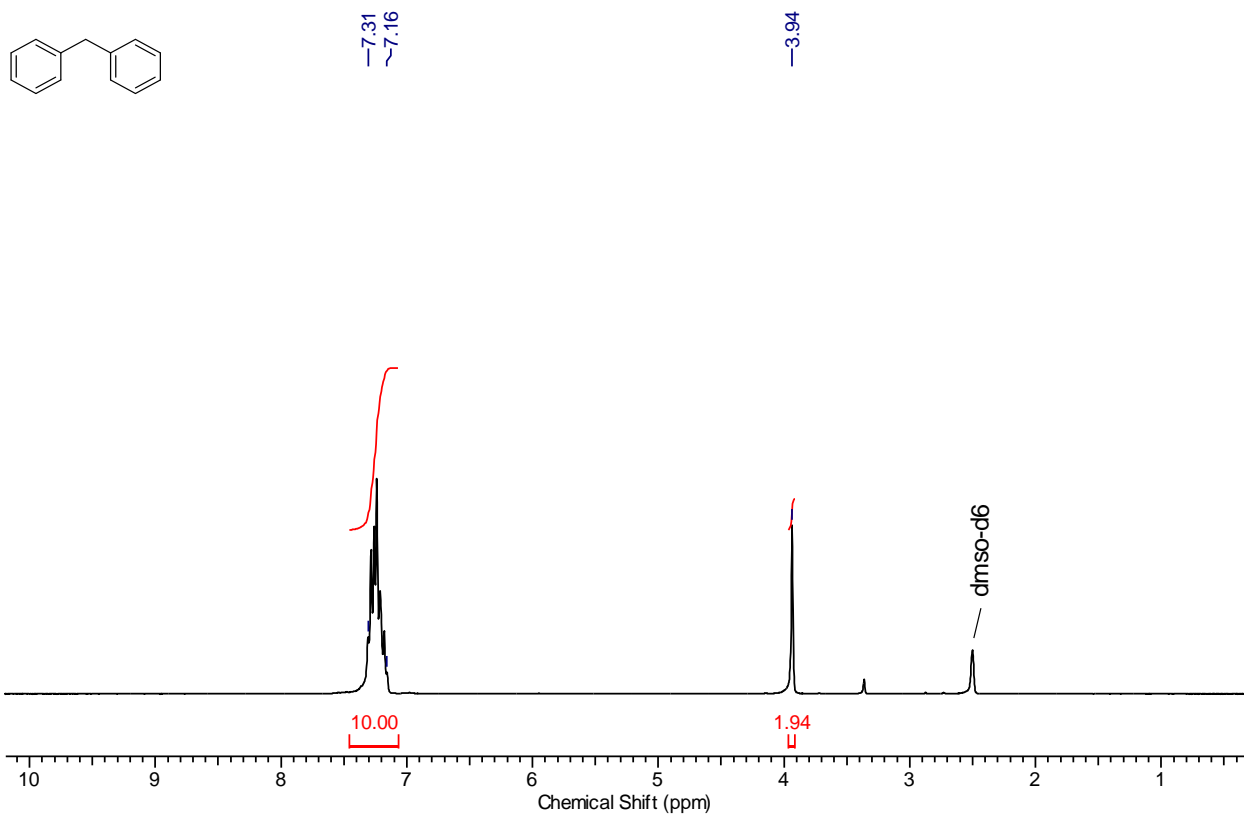
NMR spectra

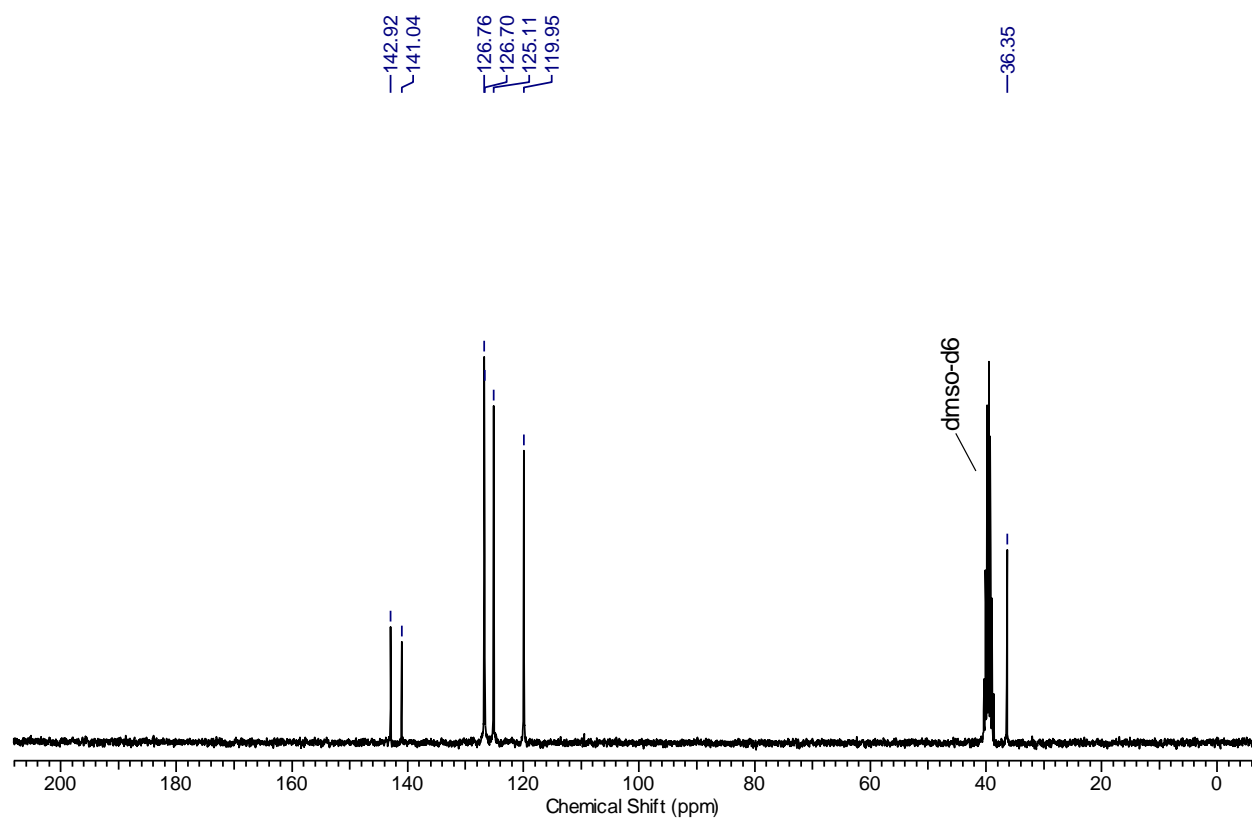
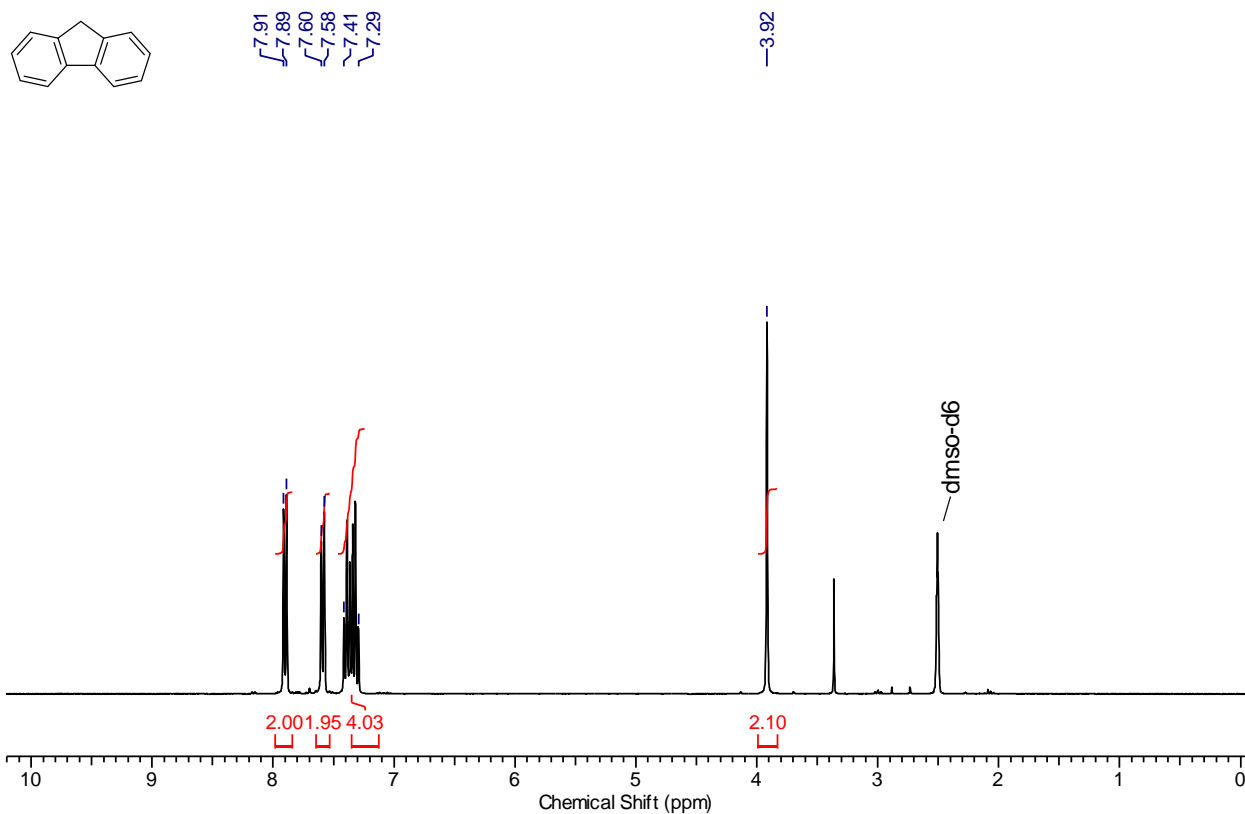


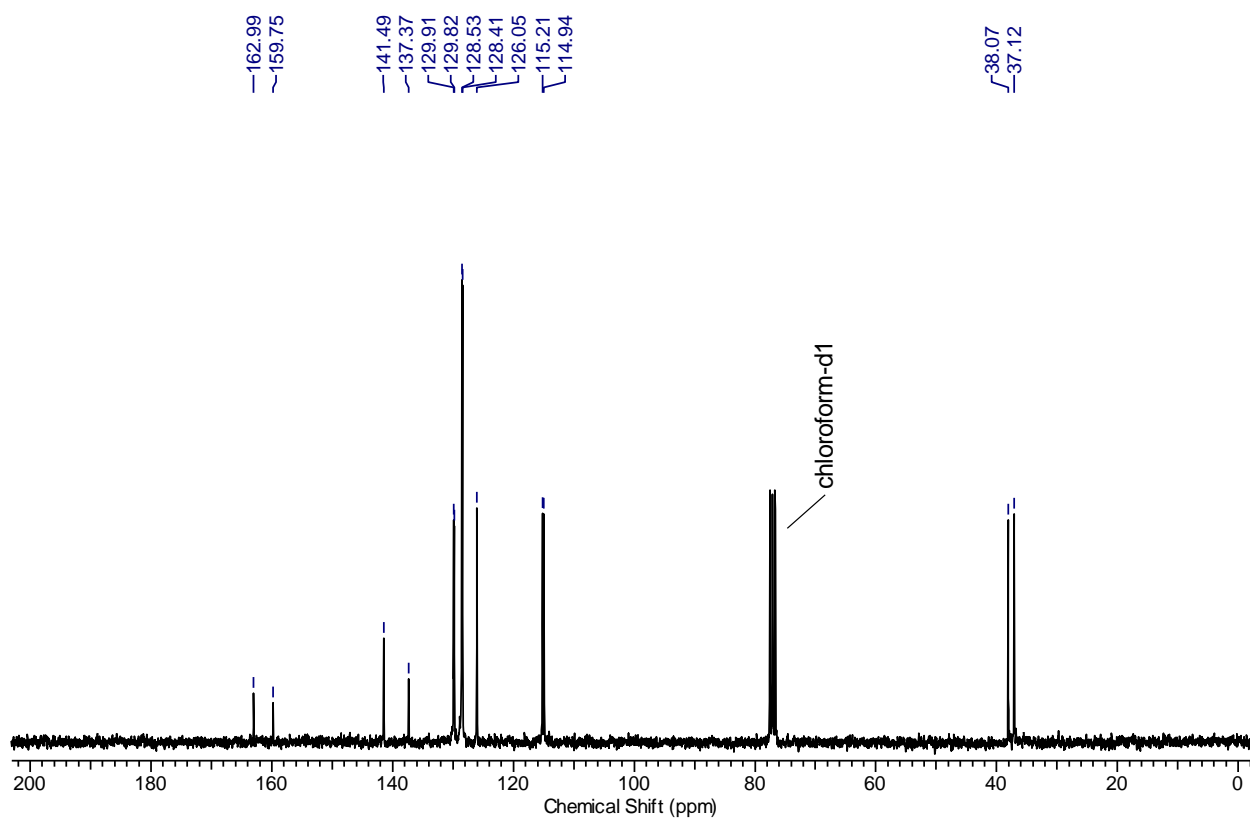
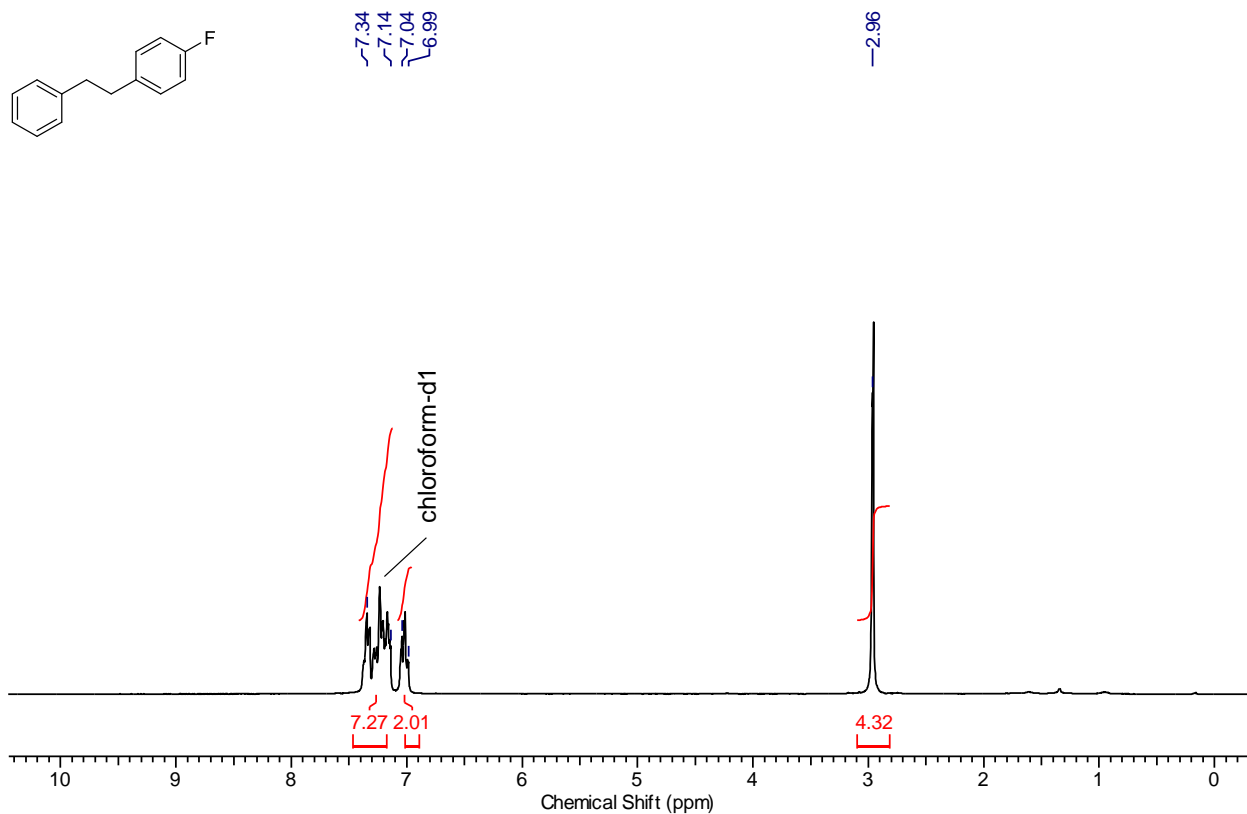


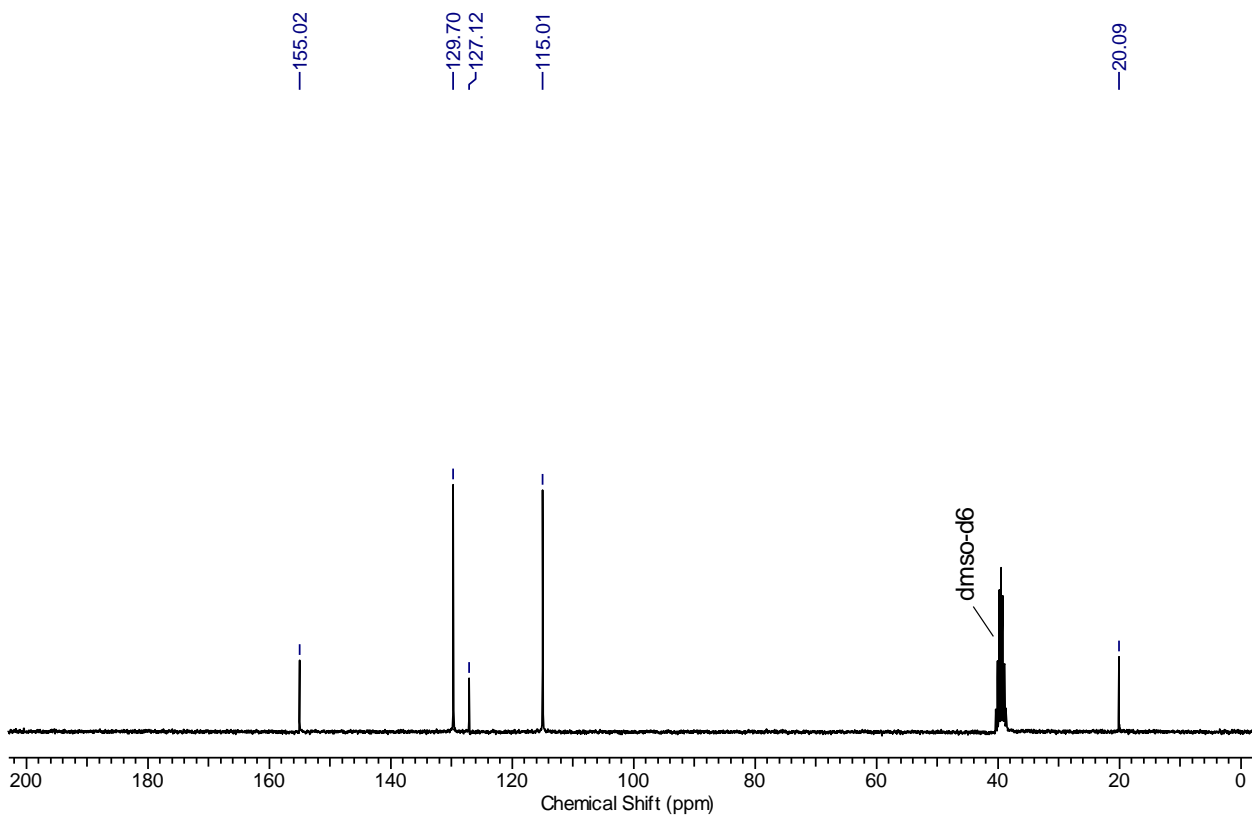
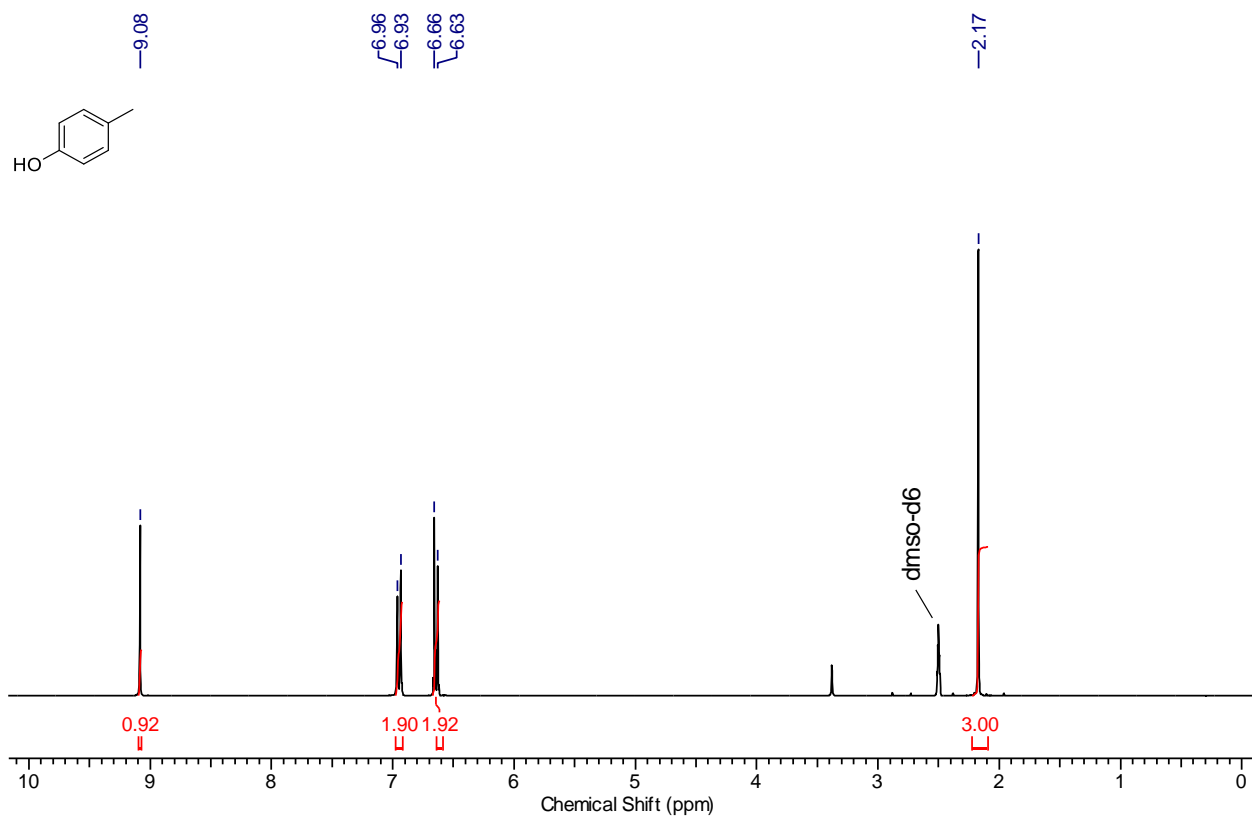


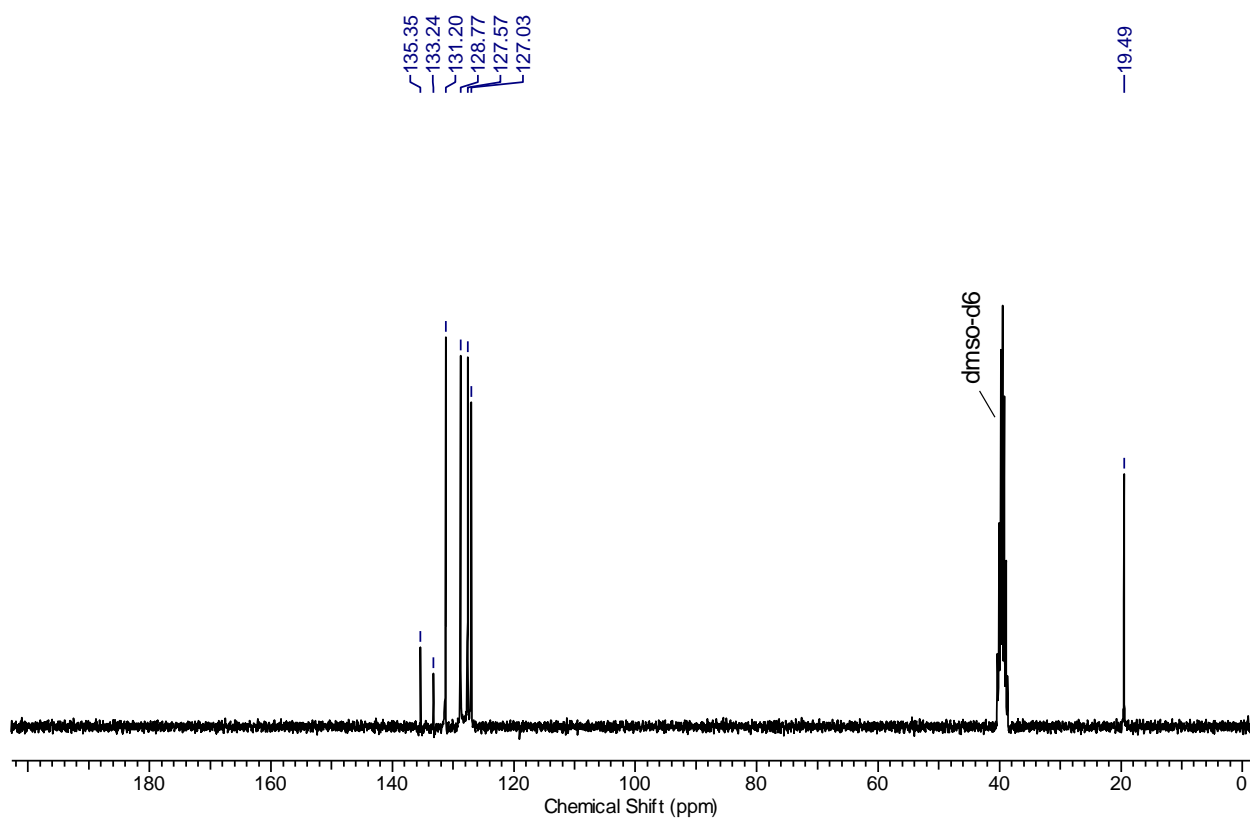
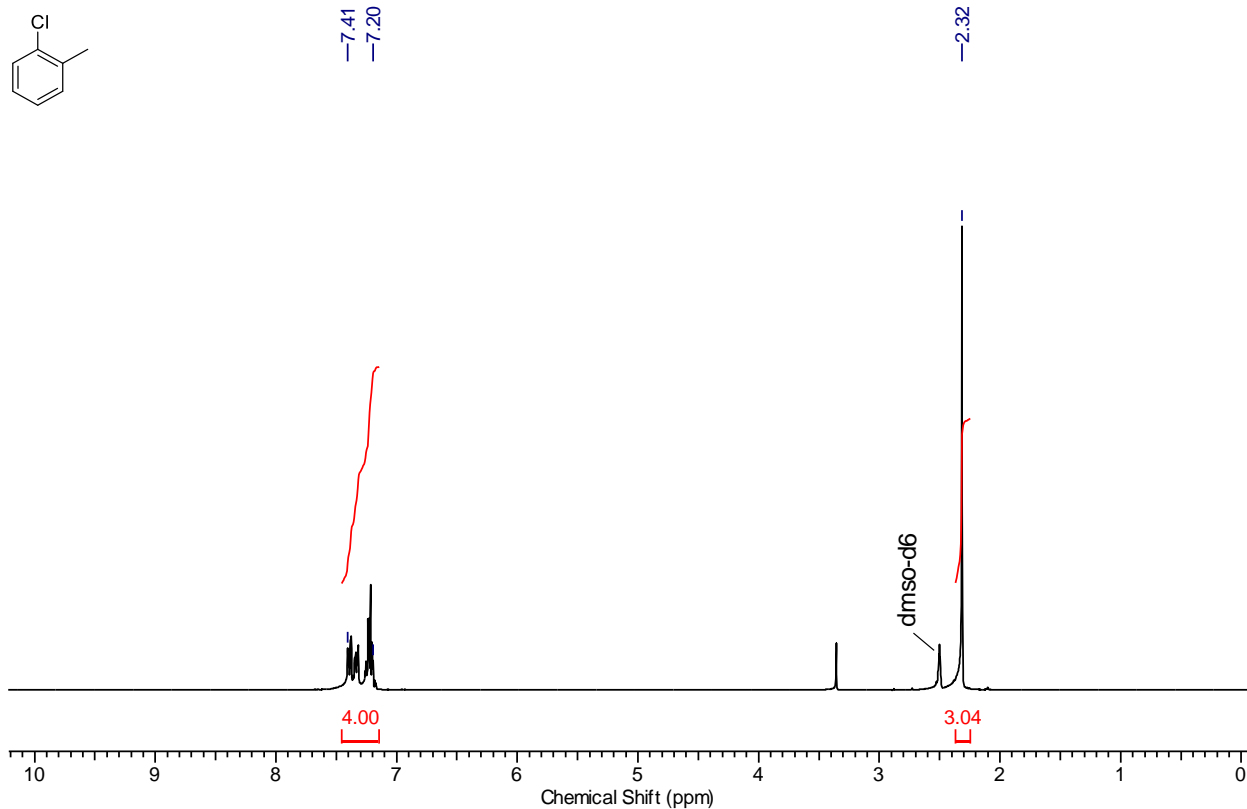


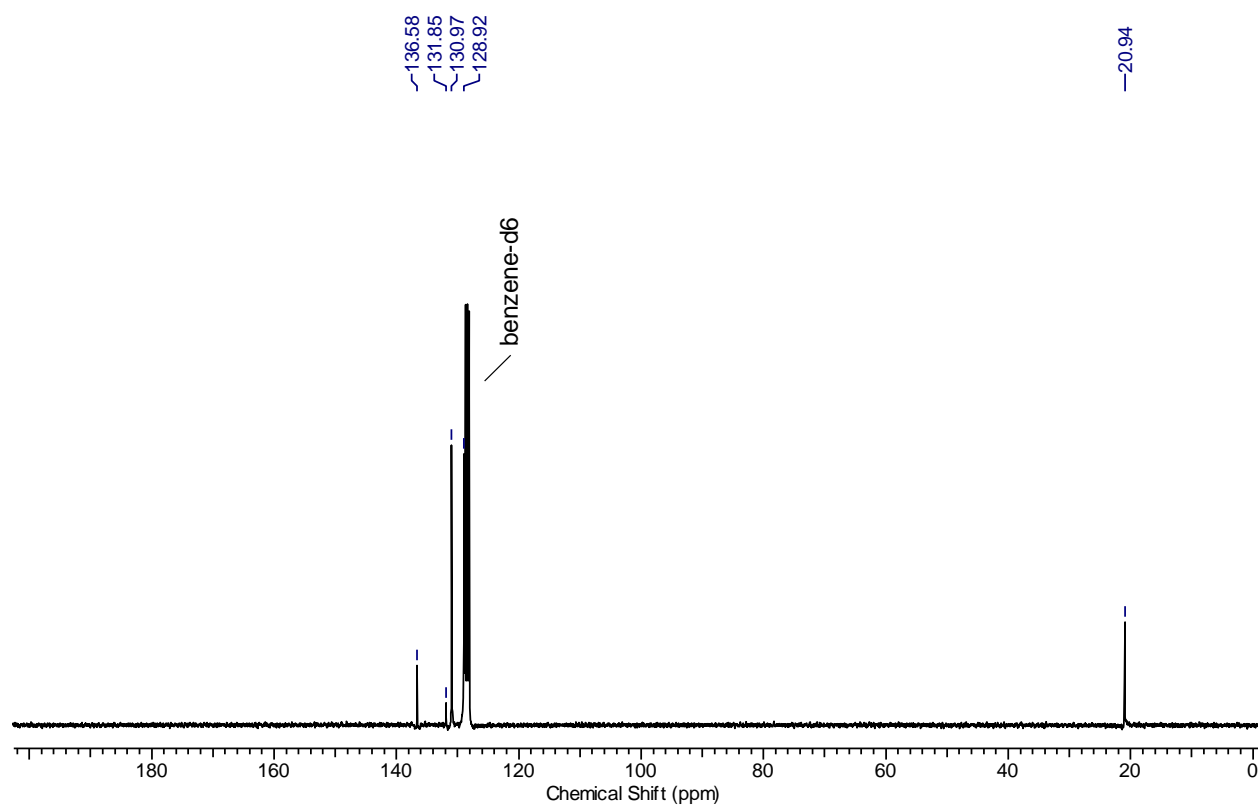
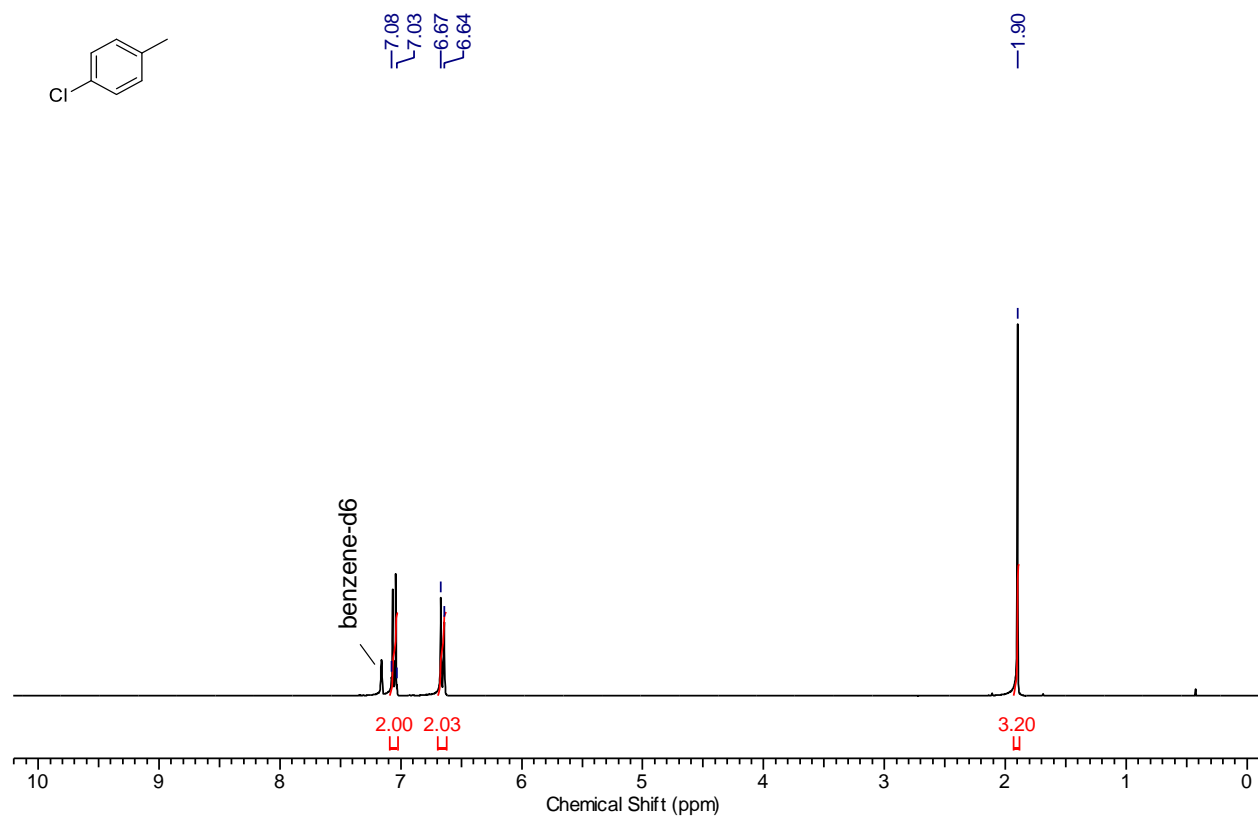


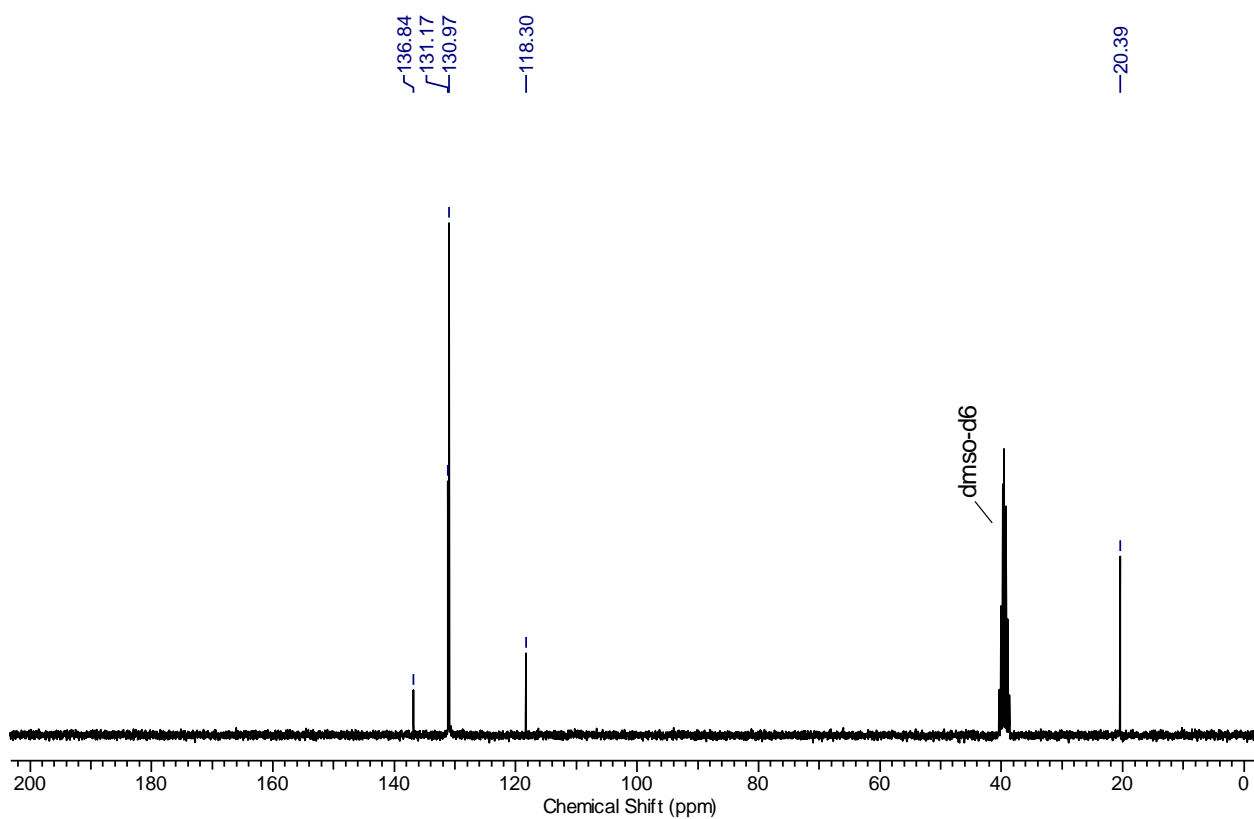
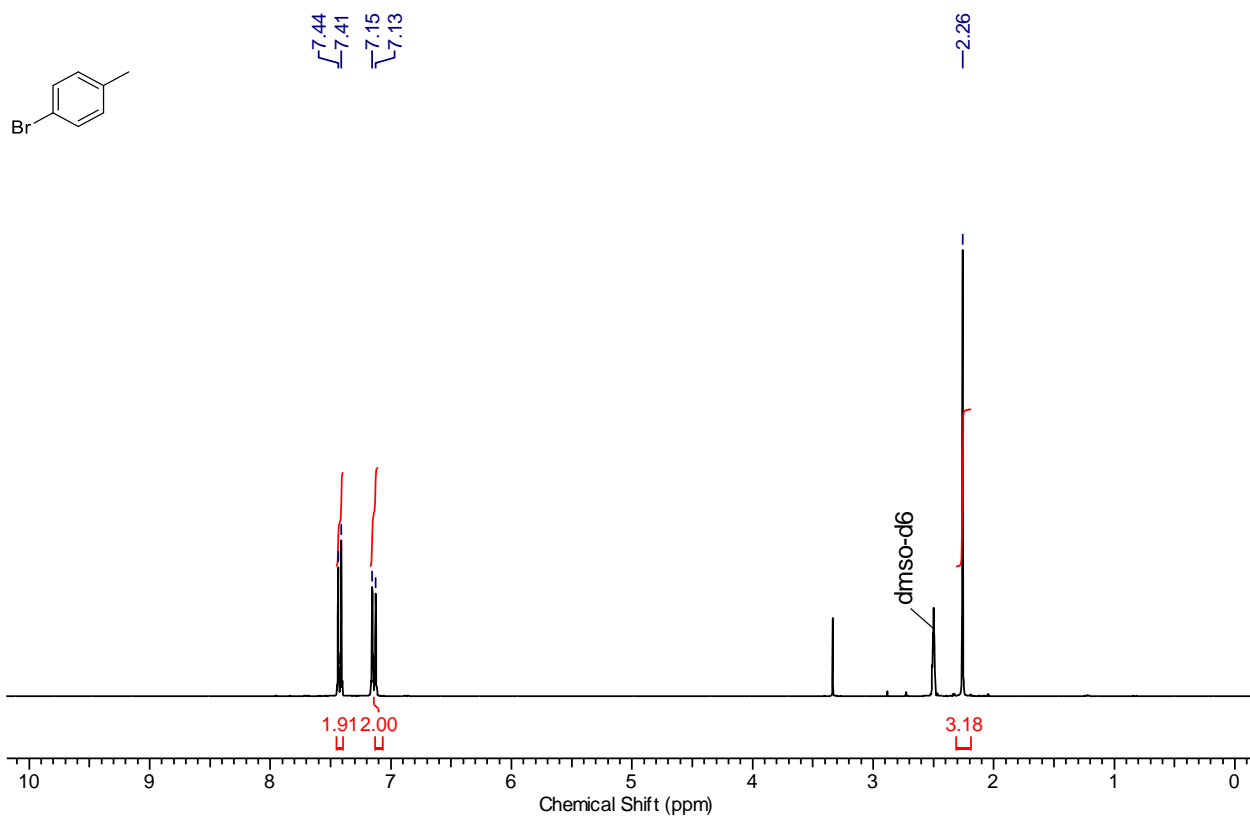


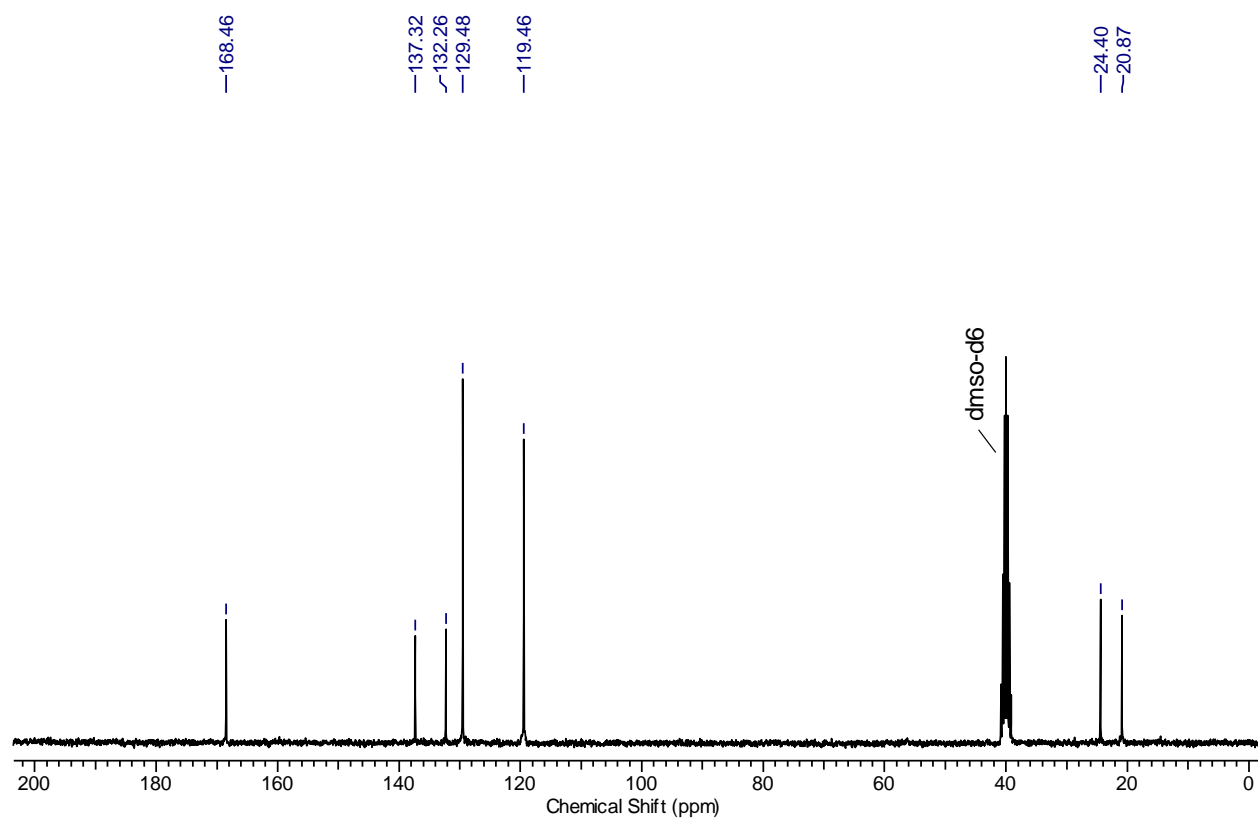
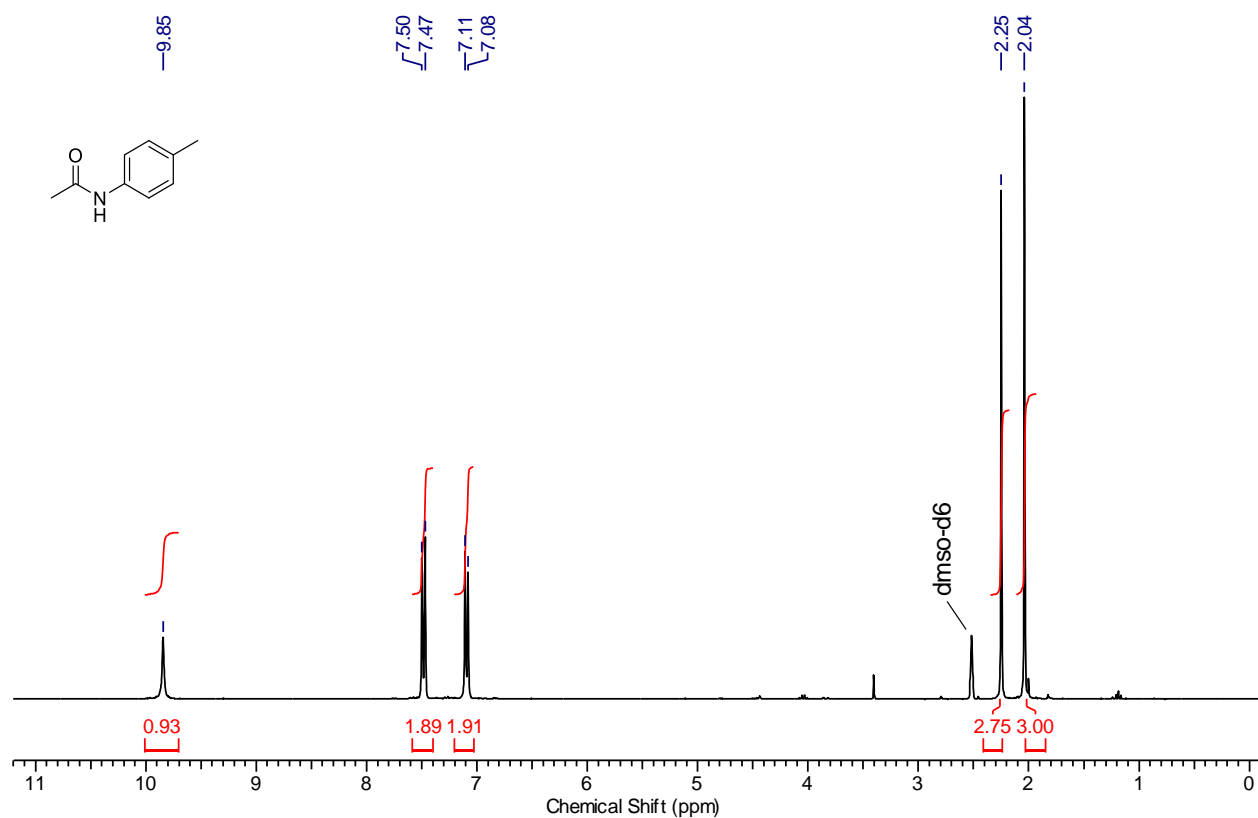


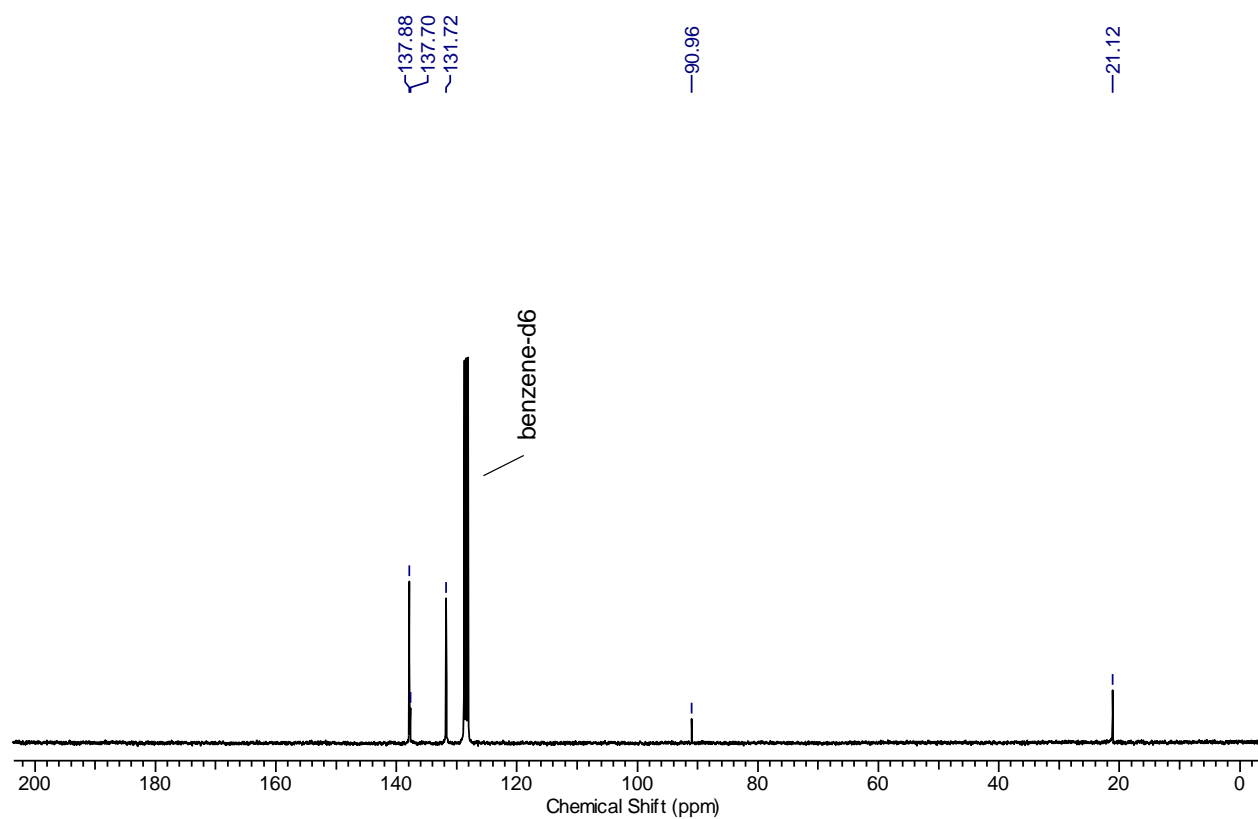
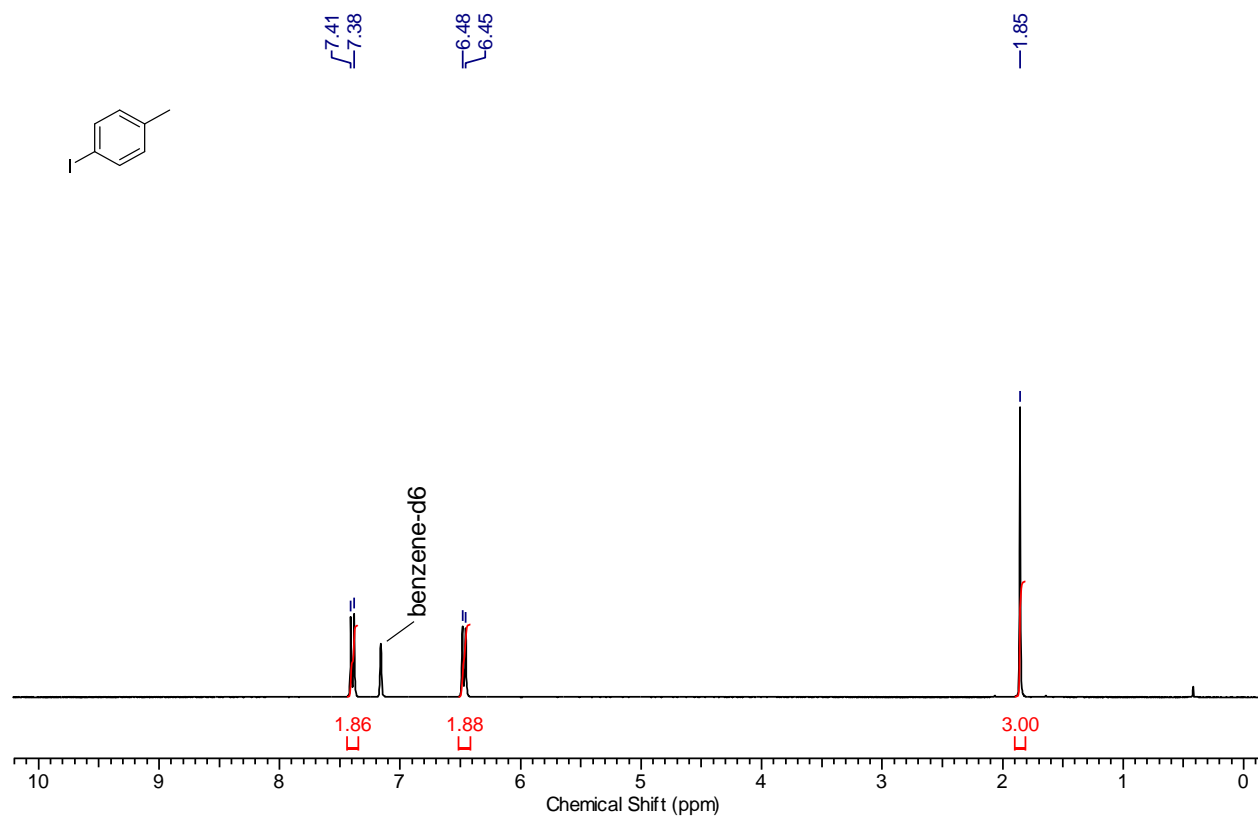


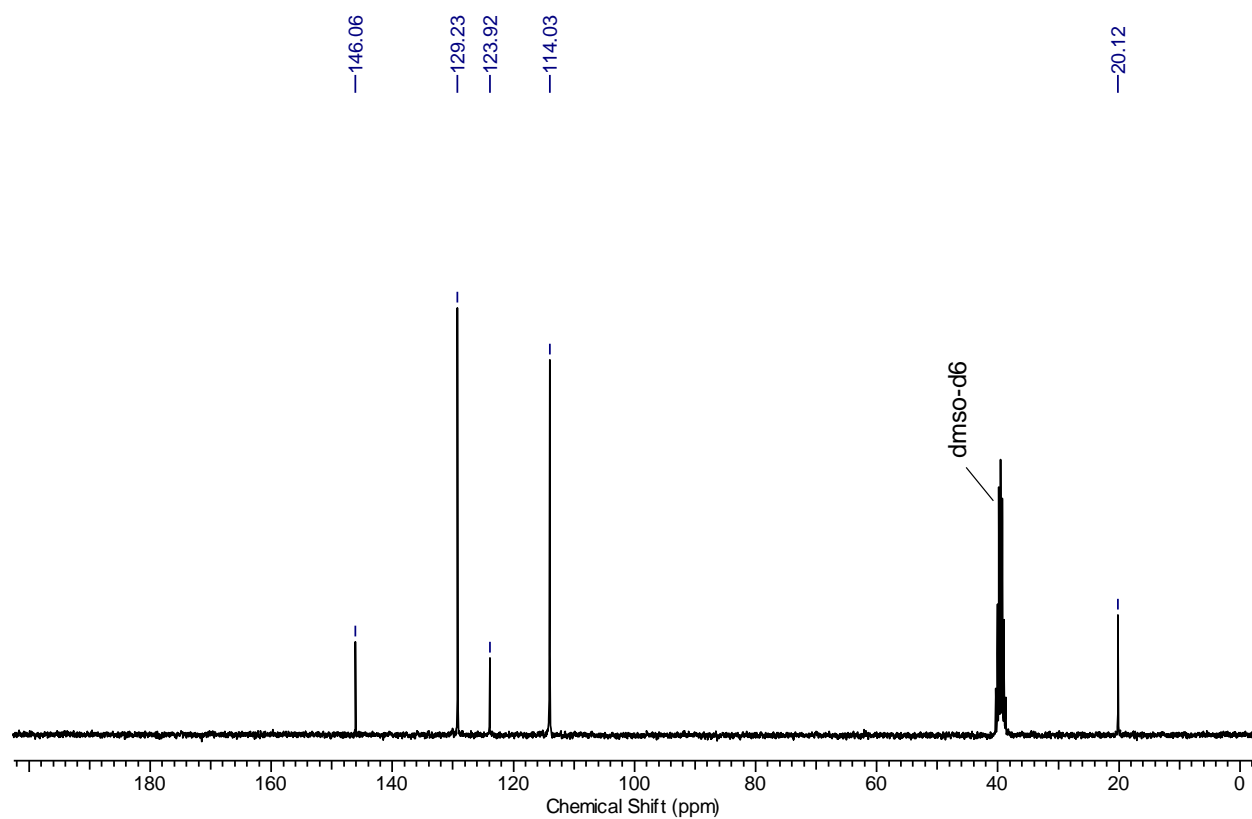
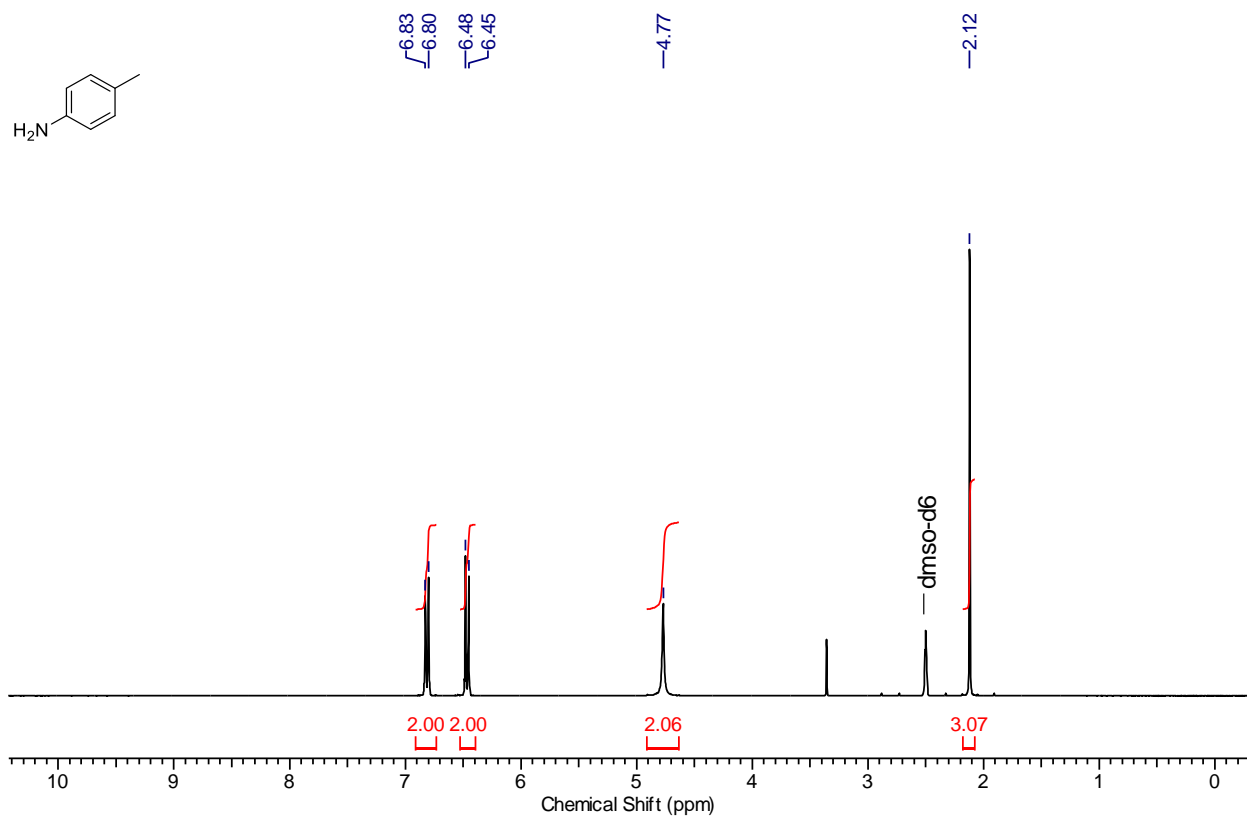


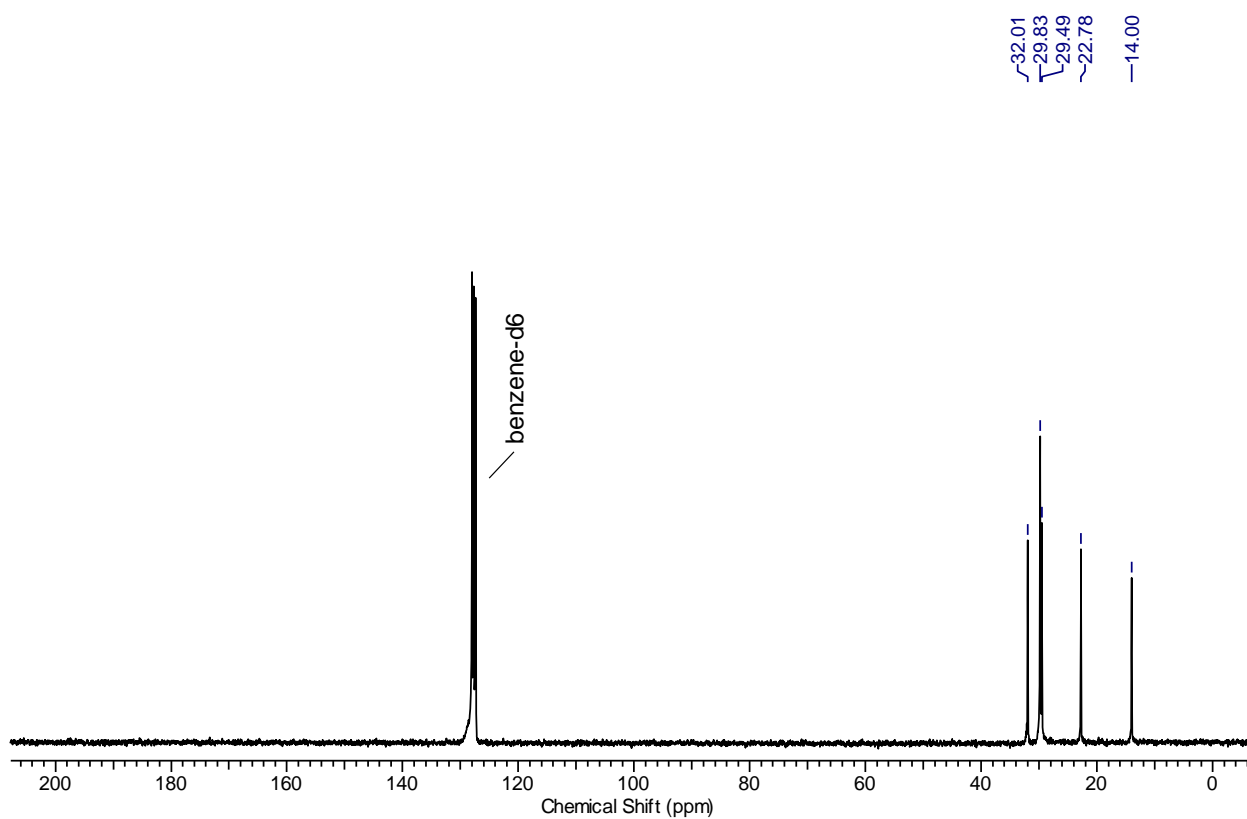
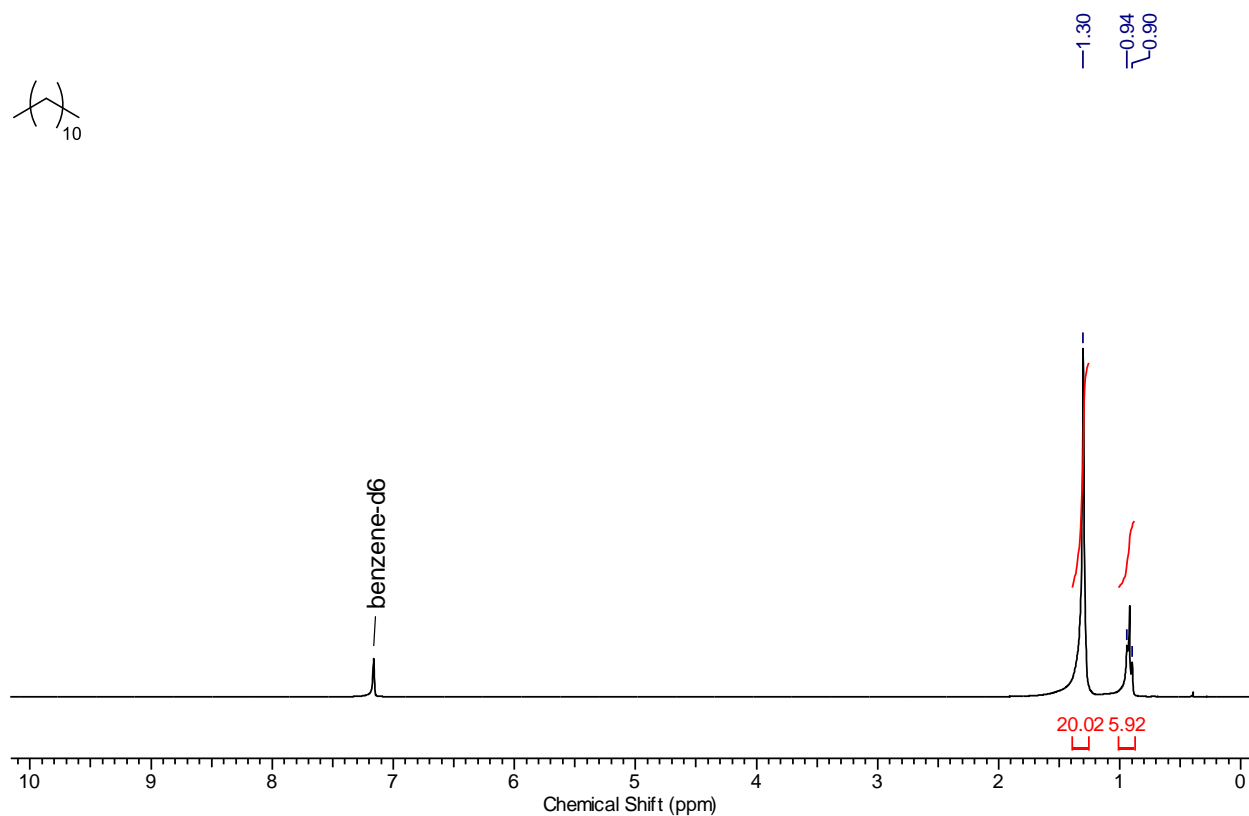


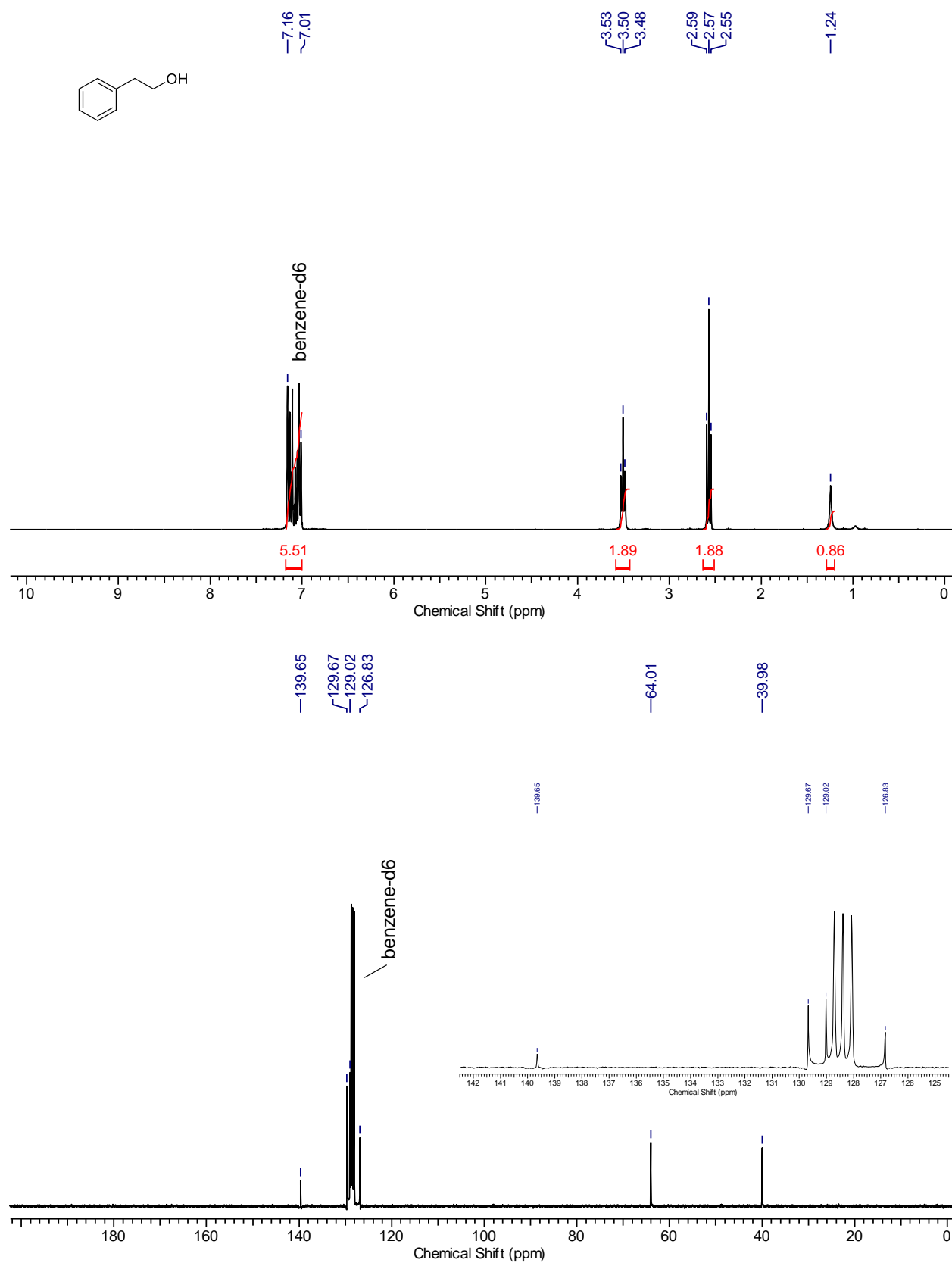


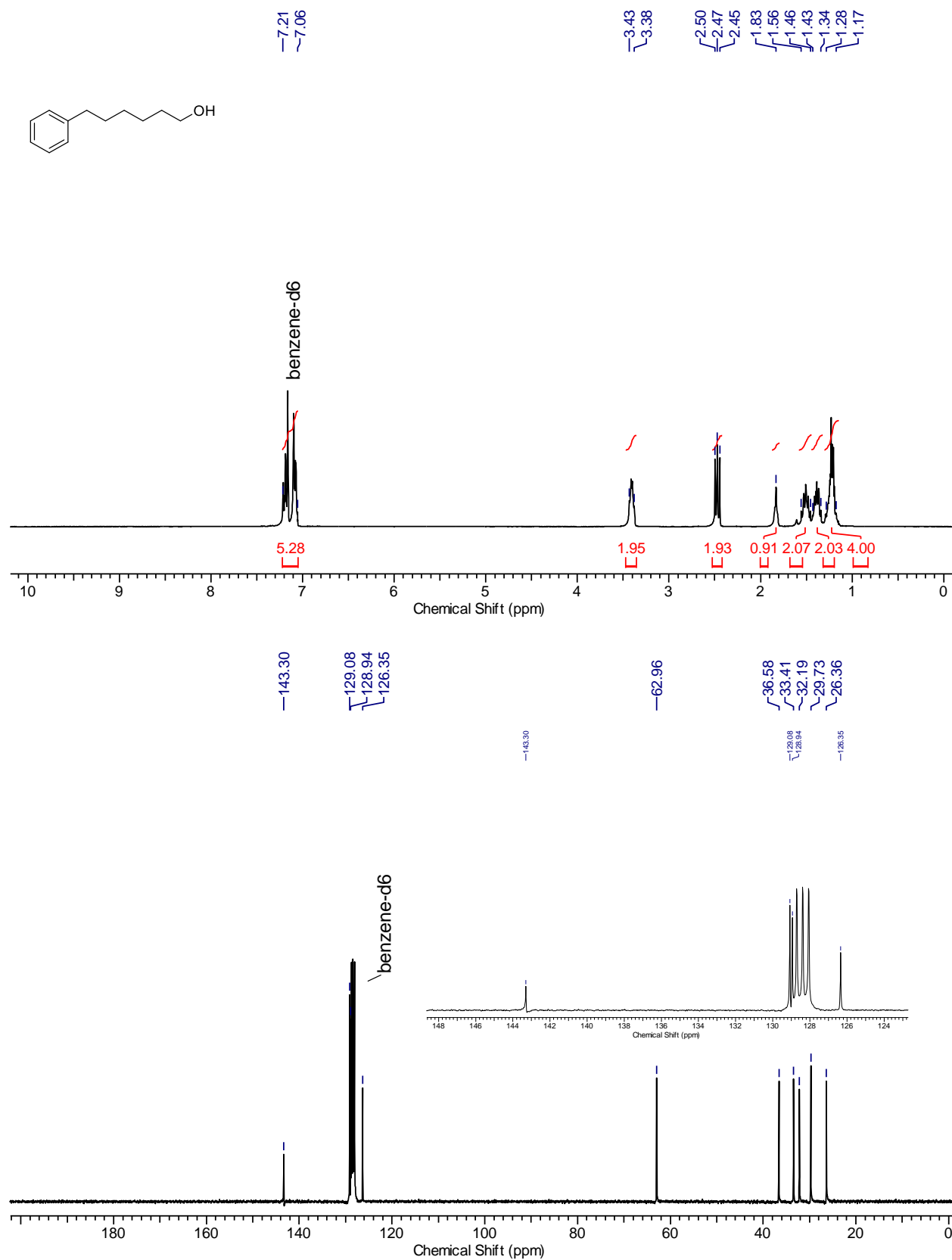


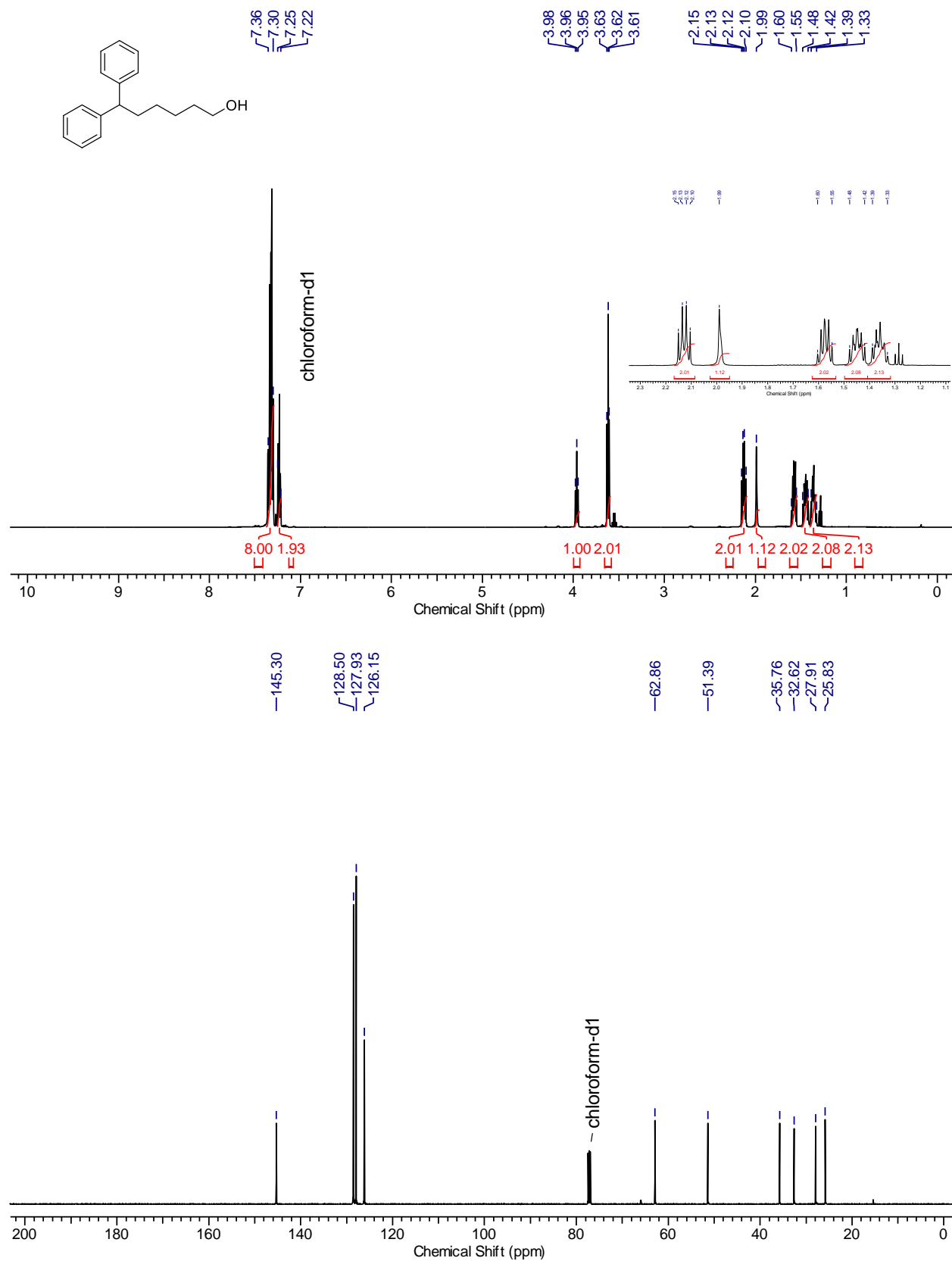


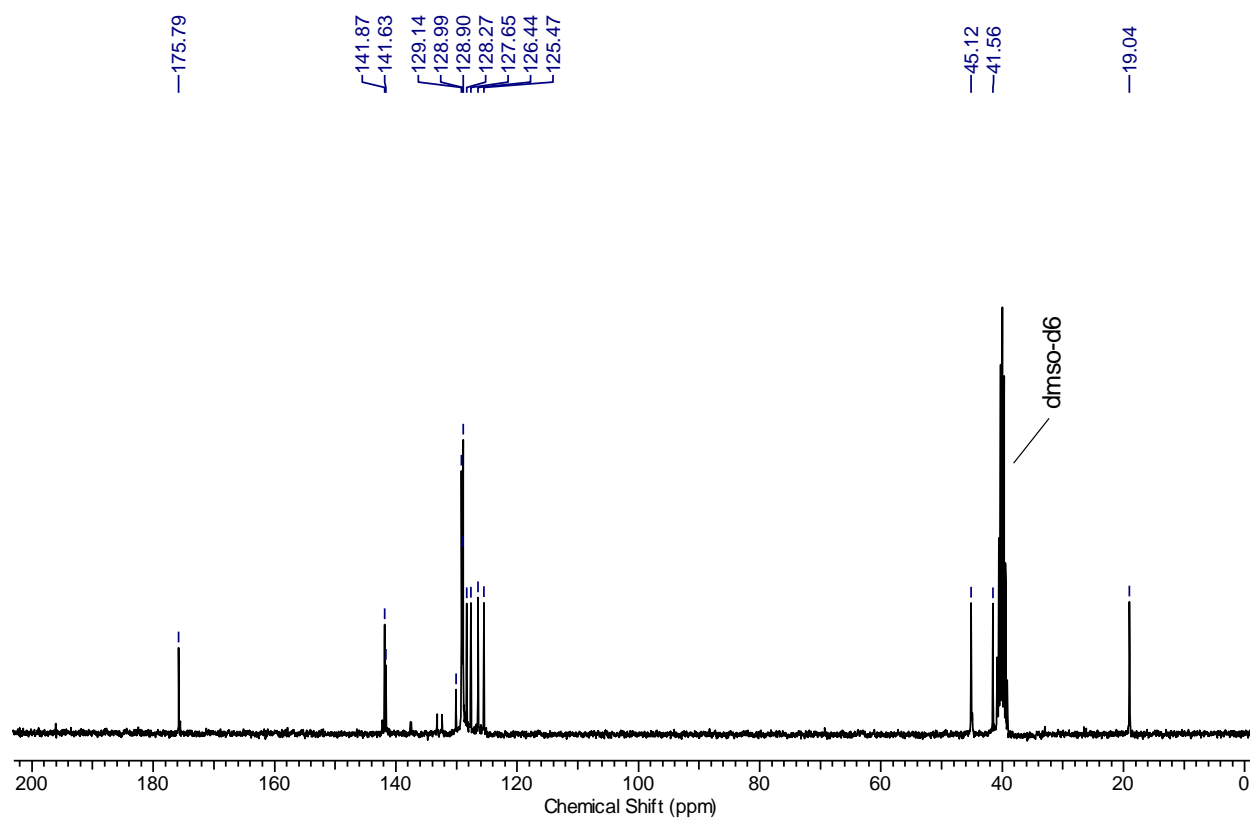
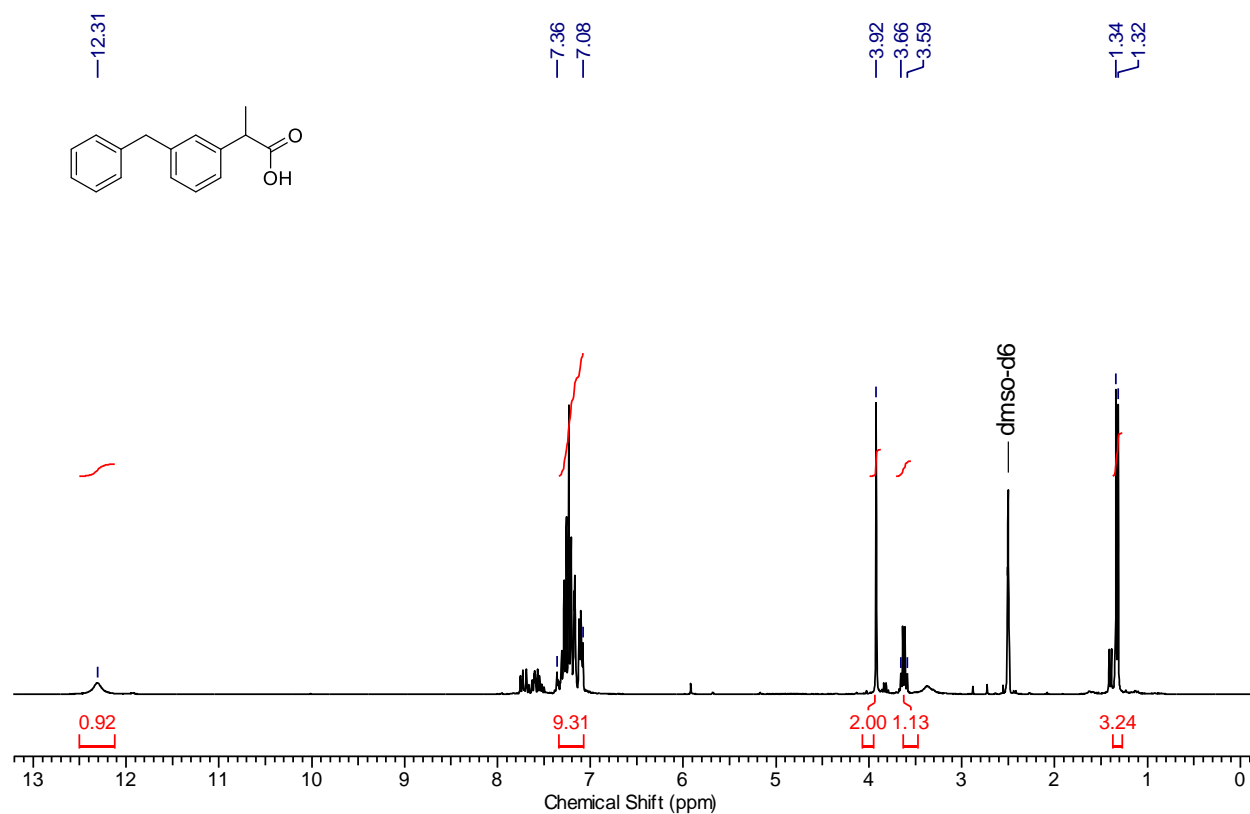


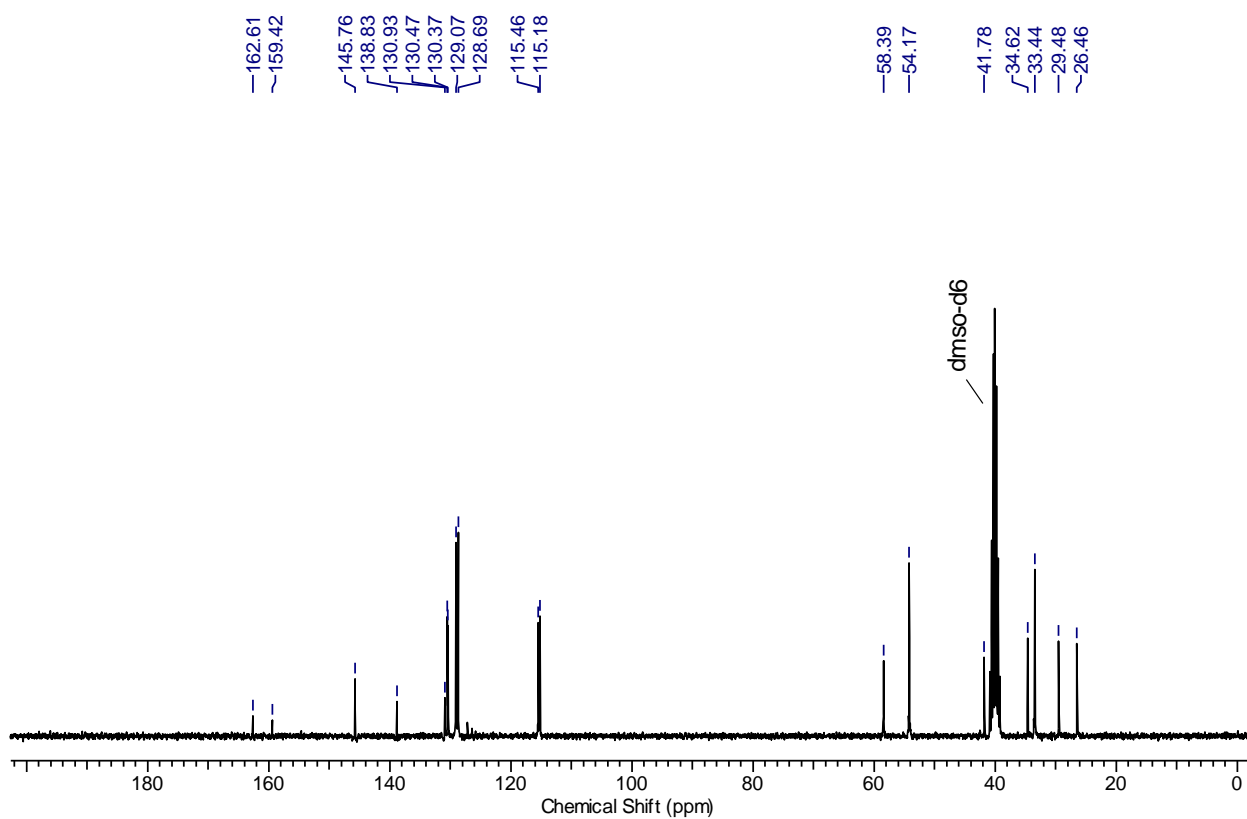
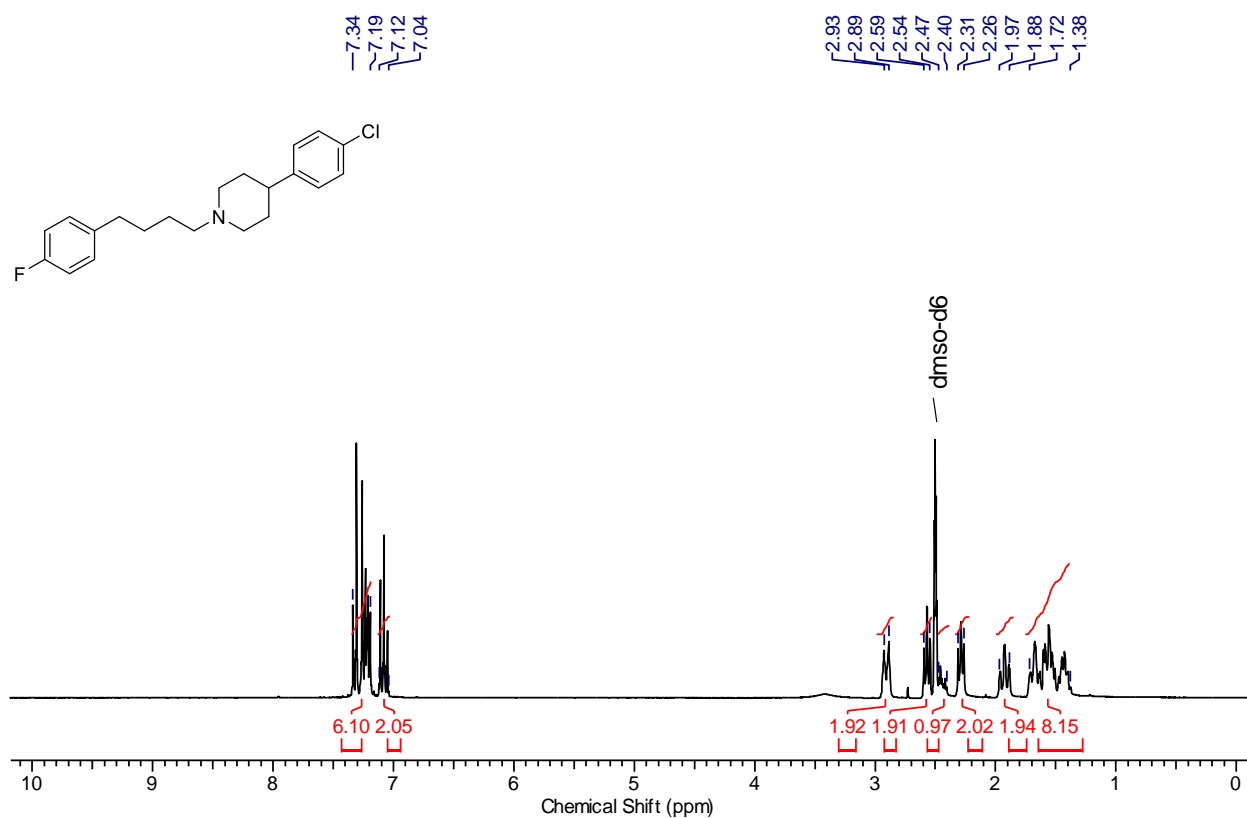


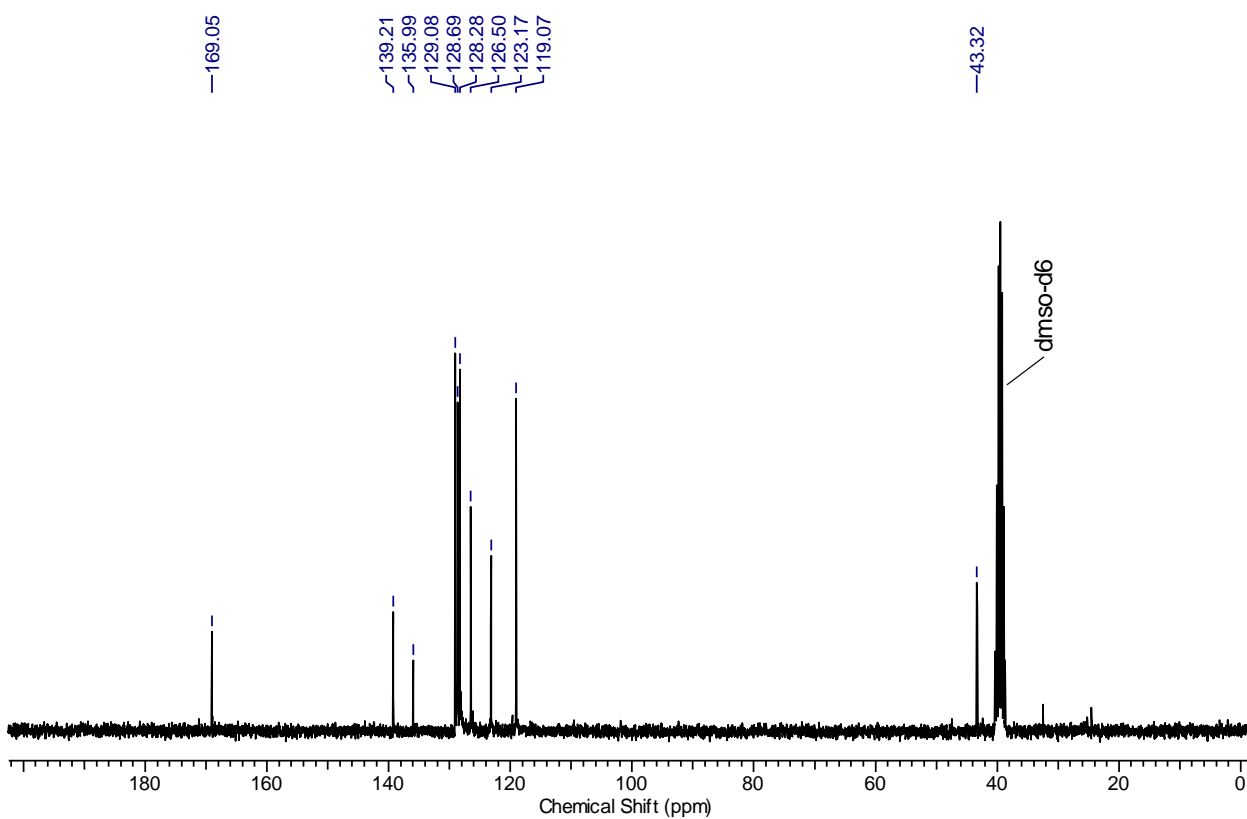
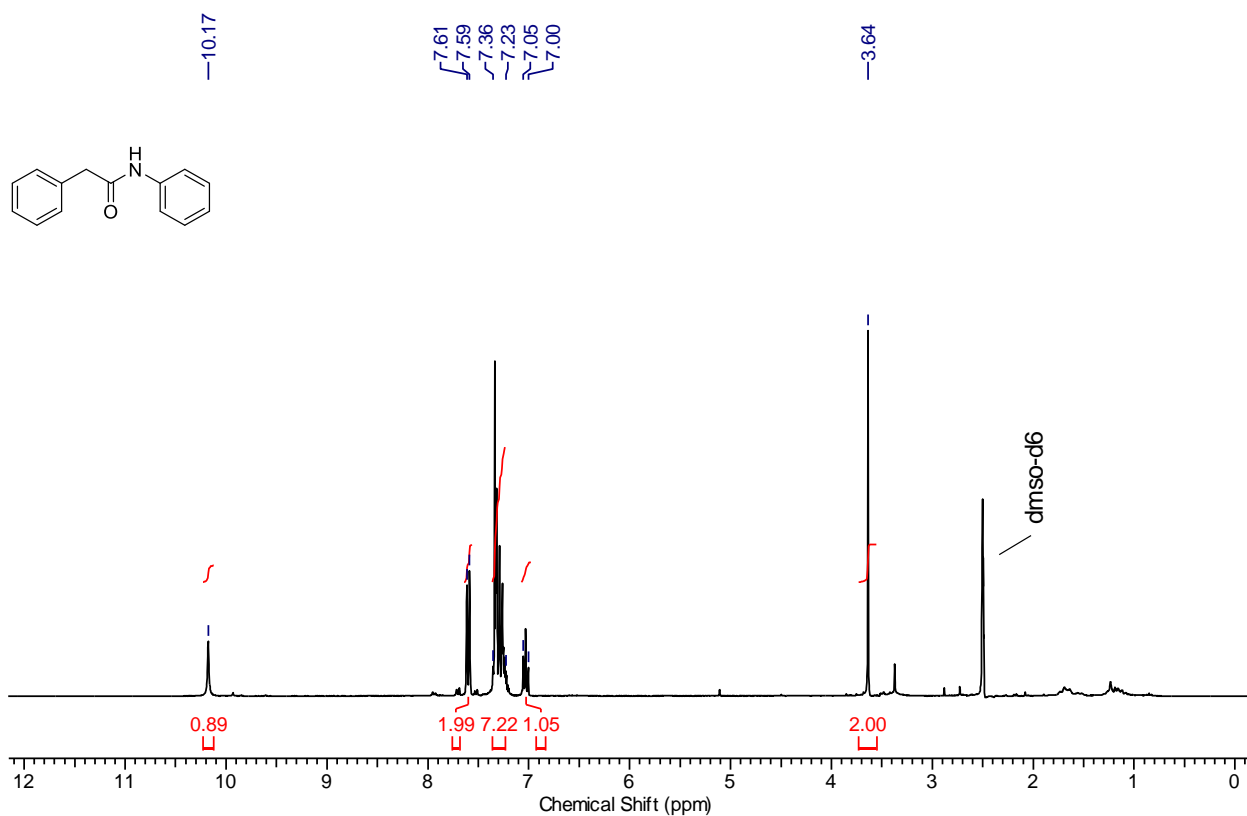


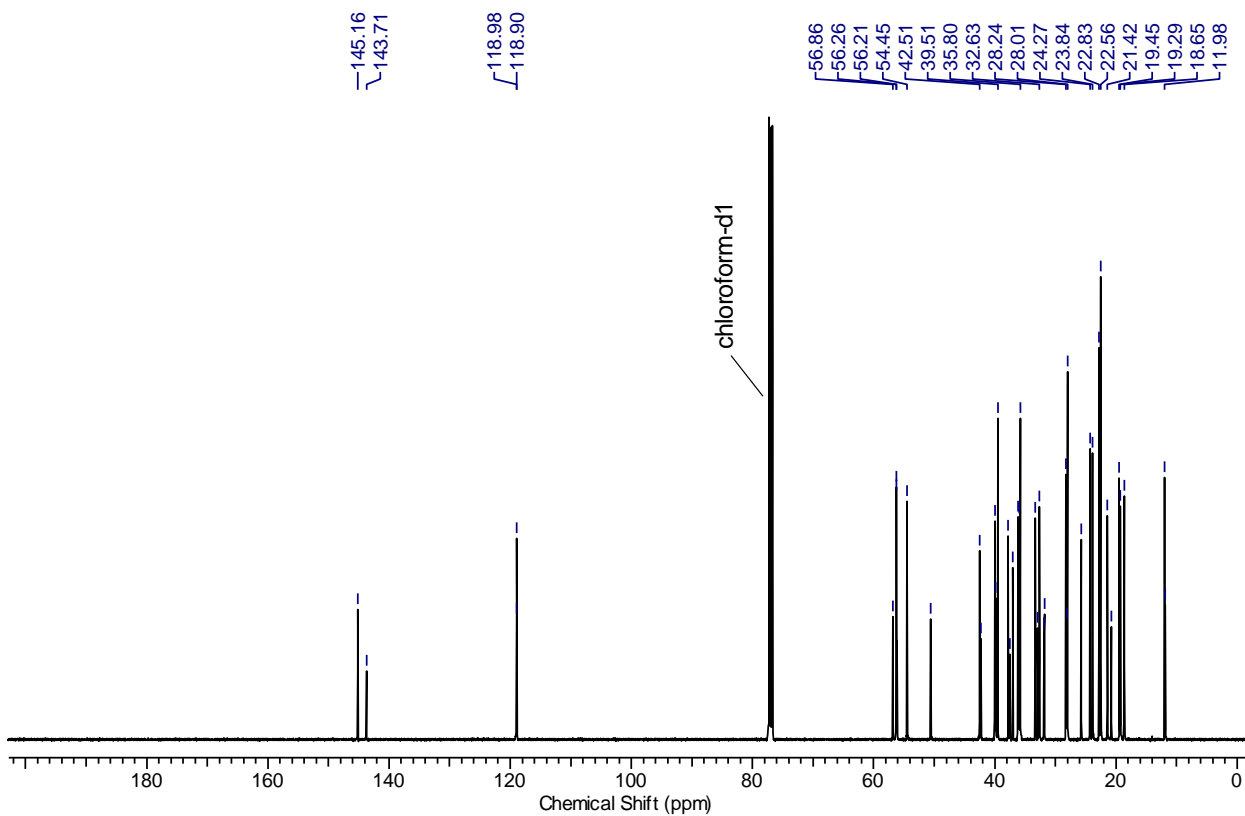
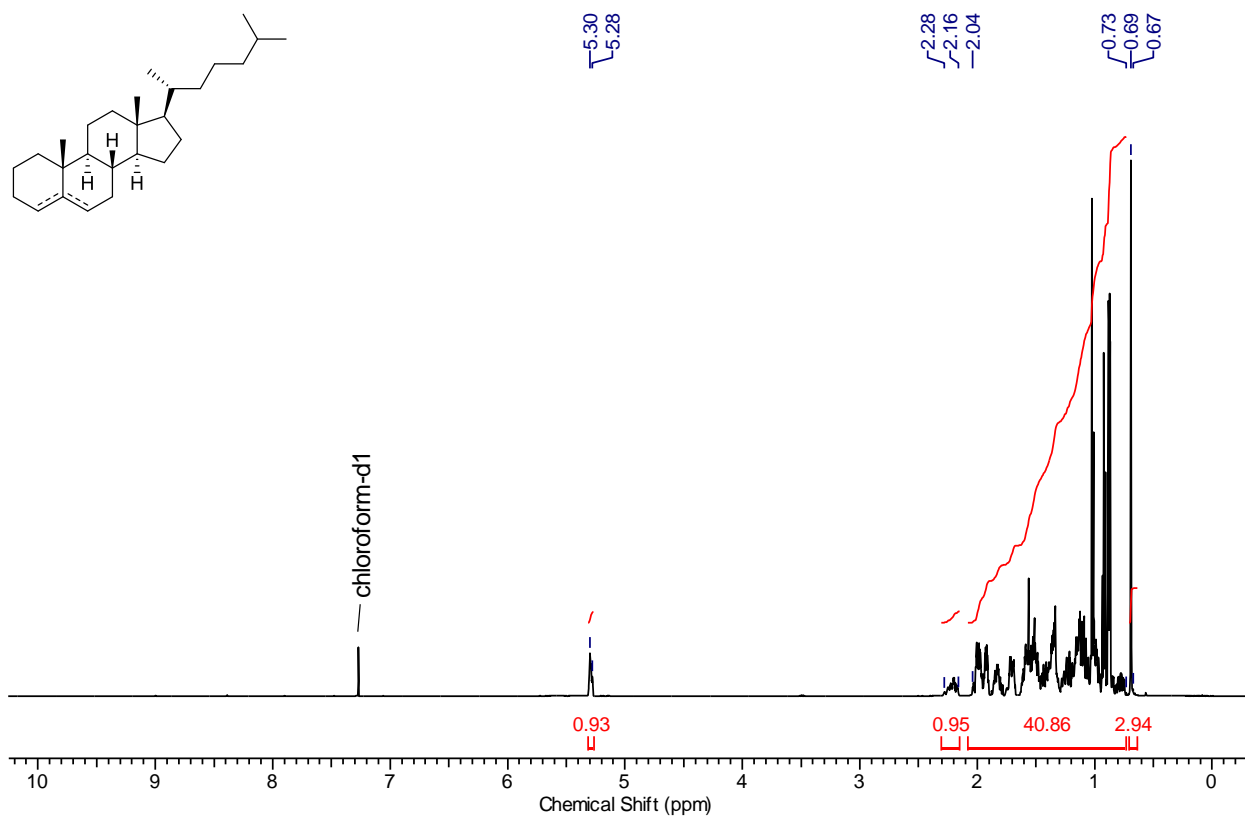












Supplementary references

- 1 J. S. Elias et al., Structure, bonding, and catalytic activity of monodisperse, transition-metal-substituted CeO₂ nanoparticles. *J. Am. Chem. Soc.* **136**, 17193–17200 (2014).
- 2 B. Morandi, B. Mariampillai, E. M. Carreira, Enantioselective cobalt-catalyzed preparation of trifluoromethyl-substituted cyclopropanes. *Angew. Chem. Int. Ed.* **50**, 1101–1104 (2011).
- 3 S.-B. Yang, F.-F. Gan, G.-J. Chen, P.-F. Xu, An efficient one-pot synthesis of ω -hydroxy ketones from lactones. *Synlett* **16**, 2532–2534 (2008).
- 4 E. Beche et al., Ce 3d XPS investigation of cerium oxides and mixed cerium oxide (Ce_xTi_yO_z). *Surf. Interface Anal.* **40**, 264–267 (2008)
- 5 Y. Lykhach et al., Counting electrons on supported nanoparticles. *Nat. Mater.* **15**, 284–288 (2016).

8 List of publications

The following publications were published or are submitted:

1. T. Schwob, R. Kempe, *Angew. Chem. Int. Ed.* **2016**, *55*, 15175.

“A Reusable Co Catalyst for the Selective Hydrogenation of Functionalized Nitroarenes and the Direct Synthesis of Imines and Benzimidazoles from Nitroarenes and Aldehydes”

2. D. Forberg, T. Schwob, M. Zaheer, M. Friedrich, N. Miyajima, R. Kempe, *Nat. Commun.* **2016**, *7*, 13201.

“Single-catalyst high-weight% hydrogen storage in an *N*-heterocycle synthesized from lignin hydrogenolysis products and ammonia”

3. D. Forberg, T. Schwob, R. Kempe, *Nat. Commun.* **2018**, *9*, 1751.

“Catalytic condensation for the formation of polycyclic heteroaromatic compounds”

4. T. Schwob, M. Ade, R. Kempe, submitted to *ChemSusChem* and out for review.

“A Co catalyst permits the direct hydrogenative synthesis of 1*H*-perimidines from a dinitroarene and an aldehyde”

Now published as:

T. Schwob, M. Ade, R. Kempe, *ChemSusChem* **2019**, *12*, 3013.

5. T. Schwob, P. Kunnas, N. de Jonge, C. Papp, H.-P. Steinrück, R. Kempe, submitted to *Sci. Adv.* and out for review.

“General and selective deoxygenation by hydrogen employing a reusable earth-abundant metal catalyst”

Now published as:

T. Schwob, P. Kunnas, N. de Jonge, C. Papp, H.-P. Steinrück, *Sci. Adv.* **2019**, *5*, eaav3680.

9 Acknowledgements

I would like to thank my academic supervisor,

Prof. Rhett Kempe,

for giving me the opportunity to work on this very interesting topic. I am grateful for his constant interest in the progress of the work and for the numerous scientific discussions.

I want to thank Dr. Christine Denner for the great supervision during the past years, the REM and EDX measurements and the constant support.

A great thank goes to all my lab-mates, Julia-Katharina Ewert, Daniel Forberg, Sonja Fehn, Stefan Schwarz, Gabriela Wietzel, Mirco Eckardt, Christoph Bäumlner, Mara Klarner, Leah Kaiser and Christina Thiersch for the trouble-free time and great support in lab.

Furthermore, I want to thank Prof. Niels de Jonge, Peter Kunnas, Dr. Christian Papp and Prof. Hans-Peter Steinrück for the great cooperation.

I want to thank all other members of the ACII group for the great time, interesting discussions and helpful practical advises: Toni Hille, Nicklas Deibl, Dr. Winfried Kretschmer, Dr. Torsten Irrgang, Andreas Gollwitzer, Thomas Dietel, Dominik Tilgner, Frederick Freitag, Fabian Kallmeier, Robin Fertig, Martin Schlagbauer, Alexander Goller and Patrick Wolff.

Special thanks to my students Simon Winterstein, Barbara Klausfelder and Mirco Ade, who were involved in several projects during their internships.

Moreover, I want to thank Anna-Maria Dietel, Heidi Maisel and Marlies Schilling for their assistance and support regarding administration matters and work in the lab.

My sincere thanks go to my family. None of this would have been possible without your constant motivation and support.

Very special thanks go to Katharina Cheimanoff for your enormous patience, and your never-ending support and love.

10 Declaration / Erklärung

(Eidesstattliche) Versicherungen und Erklärungen

(§ 8 Satz 2 Nr. 3 PromO Fakultät)

Hiermit versichere ich eidesstattlich, dass ich die Arbeit selbstständig verfasst und keine anderen als die von mir angegebenen Quellen und Hilfsmittel benutzt habe (vgl. Art 64 Abs. 1 Satz 6 BayHSchG).

(§ 8 Satz 2 Nr. 3 PromO Fakultät)

Hiermit erkläre ich, dass ich die Dissertation nicht bereits zur Erlangung eines akademischen Grades eingereicht habe und dass ich nicht bereits diese oder eine andere gleichartige Doktorprüfung endgültig nicht bestanden habe.

(§ 8 Satz 2 Nr. 4 PromO Fakultät)

Hiermit erkläre ich, dass ich Hilfe von gewerblichen Promotionsberatern bzw. -vermittlern oder ähnlichen Dienstleistern weder bisher in Anspruch genommen habe noch künftig in Anspruch nehmen werde.

(§ 8 Satz 2 Nr. 7 PromO Fakultät)

Hiermit erkläre ich mein Einverständnis, dass die elektronische Fassung der Dissertation unter Wahrung meiner Urheberrechte und des Datenschutzes einer gesonderten Überprüfung unterzogen werden kann.

(§ 8 Satz 2 Nr. 8 PromO Fakultät)

Hiermit erkläre ich mein Einverständnis, dass bei Verdacht wissenschaftlichen Fehlverhaltens Ermittlungen durch universitätsinterne Organe der wissenschaftlichen Selbstkontrolle stattfinden können.

.....

Ort, Datum, Unterschrift